Hysteretic Behaviour of Asymmetric Friction Connections (AFCs)

A thesis submitted in partial fulfilment of the requirements for the degree

of

Doctor of Philosophy in Civil Engineering

in

The University of Canterbury
Christchurch – New Zealand

by

Jose Christian Chanchi Golondrino

May 2019

This thesis is dedicated to my family

Abstract

Asymmetric Friction Connections (AFCs) are bolted connections used to dissipate seismic energy via friction. AFCs have been experimentally validated as seismic dissipaters for different steel structural systems. However, the AFC experimental validation has not considered the effects of: fire, corrosion, sliding surface treatments, bolt length variation, the use of non-metallic sliding surfaces such as brake pads, or bolt inclination during sliding. This thesis evaluates the above effects on the hysteretic behaviour of AFCs subject to reversed cyclic experimental testing under increasing displacements, and proposes simple models to quantify the average AFC strength considering these effects.

Experimental results showed that the average AFC strength reduced with increasing heating temperature and bolt length. Depending on the surface treatment, the average AFC strength was greater or less than the average AFC strength for standard steel surfaces. For AFCs subjected to a cyclic corrosion testing, the AFC strength increased in the initial sliding cycles while the corrosion product was removed and became almost constant approaching that of the non-corroded condition. As a result of bolt inclination, the lowest value of AFC strength was observed in the initial sliding cycles while the bolts were near vertical. However, the strength increased until the bolt reached its maximum inclination, after which the AFC strength became almost constant. For brake pads, the AFC strength decreased as the cycles increased until becoming constant when the brake pads reached their steady wear state.

Models proposed using the dry friction theory of Coulomb, and experimentally determined friction coefficients, represented the average experimental AFC strengths well considering the above effects.

Finally, AFC design recommendations are made based on the experimental results and models presented in this thesis.

UNIVERSITY OF CANTERBURY
Te Whare Wānanga o Waitaha
CHRISTCHURCH NEW ZEALAND

Deputy Vice-Chancellor's Office
Postgraduate Research Office

Co-Authorship Form

This form is to accompany the submission of any thesis that contains research reported in co-authored work that has been published, accepted for publication, or submitted for publication. A copy of this form should be included for each co-authored work that is included in the thesis. Completed forms should be included at the front (after the thesis abstract) of each copy of the thesis submitted for examination and library deposit.

I. Please indicate the chapter/section/pages of this thesis that are extracted from co-authored work and provide details of the publication or submission from the extract comes:

This thesis was organized in the papers format. Chapters and appendices comprising this thesis have been published, accepted for publication, or submitted for publication according to the details below. Topics of these chapters and appendices were developed as main component of the research associated to this thesis. Full details of the chapters and appendices are presented in the list of publications section on this thesis.

Chapter 1: "Asymmetric Friction Connections Post-Heating Behaviour"

Published in Journal of Constructional Steel Research - Elsevier

Chapter 2:"Surface Treatments and Corrosion Effects on the Hysteretic Behaviour of Asymmetric Friction Connections (AFCs) with High Hardness Steel Shims"

Published in Structures Journal - Elsevier

Chapter 3: "Hysteretic Behaviour of Asymmetric Friction Connections Using Brake Pads of D3923"

Published in Structures Journal - Elsevier

Chapter 4: Asymmetric Friction Connection Bolt Lever Arm Effects on Hysteretic Behaviour

Submitted to Journal of Earthquake Engineering

Chapter 5: Improved Bolt Flexural – Axial Force – Shear Force Interaction Model for Asymmetric Friction Connections (AFCs)

Published in Journal of Constructional Steel Research - Elsevier

Appendix A.1: Behaviour of Asymmetrical Friction Connections (AFCs) Using Different Shim Materials

Published in New Zealand Society for Earthquake Engineering Conference (NZSEE 2012)

Appendix A.2: Clamping Force Effects on the Behaviour of Asymmetrical Friction Connections (AFCs)

Published in 15th World Conference on Earthquake Engineering (WCEE 2012)

Appendix A.3: Velocity Effects on The Behaviour of Asymmetrical Friction Connections (AFCs)

Published in 8th International Conference on Behaviour of Steel Structures in Seismic Areas

Appendix A.4: Is the Asymmetrical Friction Connection (AFC) a Low Damage Dissipater?

Published in New Zealand Society for Earthquake Engineering Technical Conference (NZSEE 2015)

Appendix A.5: Hysteretic Behaviour of Symmetrical Friction Connections (SFCs) Using Different Steel Grade Shims

Published in the Pacific Structural Steel Conference (PSSC 2013)

Appendix A.6: Design Considerations for Braced Frames with Asymmetrical Friction Connections (AFCs)

Published in Behaviour of Steel Structures in Seismic Areas (STESSA 2012)

Appendix A.7: Low Damage Braces Using Asymmetrical Friction Connections (AFCs)

Published in New Zealand Society for Earthquake Engineering Conference (NZSEE 2014)

Appendix A.8: Methodology for Quantifying Seismic Sustainability of Steel Framed Structures

Published in Behaviour of Steel Structures in Seismic Areas (STESSA 2012)

Co-authors of the publications above were the supervisory team at University of Canterbury and at University of Auckland. This supervisory team is listed below:

Main Supervisor: Professor Gregory Mac Rae – University of Canterbury

Second Supervisor: Professor Geoffrey Chase – University of Canterbury

Supervisors: Professor Charles Clifton – University of Auckland

Professor Geoffrey Rodgers – University of Canterbury

Professor Allan Scott – University of Canterbury

Professor Anthony Abu – University of Canterbury

The Main Supervisor of this thesis, Professor Gregory Mac Rae is signing this form on behalf of the full supervisory team that co-authored whole publications listed above.

II. Please detail the nature and extent (%) of contribution by the candidate:

On each of the publications listed above, the candidate contributed about 80% on each of the activities listed below. The remaining 20% on each of the activities listed below corresponded to supervision and feedback from the co-authors.

1. Research planning
2. Experimental testing
3. Data processing
4. Results interpretation
5. Publication writing
6. Publication submission

Certification by Co-authors:

If there is more than one co-author then a single co-author can sign on behalf of all

The undersigned certifies that:

- The above statement correctly reflects the nature and extent of the PhD candidate's contribution to this co-authored work
- In cases where the candidate was the lead author of the co-authored work he or she wrote the text

Name: Gregory MacRae

Co-authors comments:

Yes. While the initial selection of the topic, definition of the problem and research methodology were suggested by the supervisory team, the student carried out the vast majority of the work adding significant intellectual contributions and modifications to the initial plans. Throughout the project the supervisory team often challenged the student and made suggestions as to how to improve the work. The vast majority of the work was conducted by the student, as described by the student.

Signature:

Date: 14 November 2018

Acknowledgements

I would like to thank to my supervisors, Professor Gregory MacRae, Professor Geoffrey Chase, Professor Geoffrey Rodgers, Professor Charles Clifton, Professor Allan Scott, and Professor Anthony Abu, for their invaluable strong support and advice during this research project. I would like to acknowledge funding from MBIE Natural Hazards Research Platform (NHRP), material donation from John Jones Steel Ltd., and my paid leave from Universidad Nacional de Colombia – Sede Manizales, for undertaking this research. I also would like thank to the Technicians in the University of Canterbury Structures Laboratory for their help on the experimental component of this research.

Table of Contents

List of Figures

List of Tables

List of publications

Publication	Title	Published in / Submitted to	Reference	Included in	Page
Journal papers	Asymmetric Friction Connections Post-Heating Behaviour	Published in Journal of Constructional Steel Research - Elsevier	[10]	Chapter 1	1
	Steel Building Friction Connection Seismic Performance – Corrosion Effects.	Published in Structures Journal - Elsevier	[11]	Chapter 2	32
	Hysteretic Behaviour of Asymmetric Friction Connections Using Brake Pads of D3923	Published in Structures Journal - Elsevier	[12]	Chapter 3	68
	Asymmetric Friction Connection Bolt Lever Arm Effects on Hysteretic Behaviour	Submitted to Journal of Earthquake Engineering	[13]	Chapter 4	106
	Asymmetric Friction Connection (AFC) design for seismic energy dissipation	Published in Journal of Constructional Steel Research - Elsevier	[14]	Chapter 5	143
Conference papers	Behaviour of Asymmetrical Friction Connections (AFCs) Using Different Shim Materials	Published in: New Zealand Society for Earthquake Engineering Conference (NZSEE 2012)	[15]	Appendix A.1	179
	Clamping Force Effects on the Behaviour of Asymmetrical Friction Connections (AFCs)	Published in: 15th World Conference on Earthquake Engineering (WCEE 2012)	[16]	Appendix A.2	187
	Velocity Effects on The Behaviour of Asymmetrical Friction Connections (AFCs)	Published in: 8th International Conference on Behaviour of Steel Structures in Seismic Areas	[17]	Appendix A.3	197
	Is the Asymmetrical Friction Connection (AFC) a Low Damage Dissipater?	Published in: New Zealand Society for Earthquake Engineering Technical Conference (NZSEE 2015)	[18]	Appendix A.4	206
	Hysteretic Behaviour of Symmetrical Friction Connections (SFCs) Using Different Steel Grade Shims	Published in: The Pacific Structural Steel Conference (PSSC 2013)	[19]	Appendix A.5	215
	Design Considerations for Braced Frames with Asymmetrical Friction Connections (AFCs)	Published in: Behaviour of Steel Structures in Seismic Areas (STESSA 2012)	[20]	Appendix A.6	223
	Low Damage Braces Using Asymmetrical Friction Connections (AFCs)	Published in: New Zealand Society for Earthquake Engineering Conference (NZSEE 2014)	[21]	Appendix A.7	230
	Methodology for Quantifying Seismic Sustainability of Steel Framed Structures	Published in: Behaviour of Steel Structures in Seismic Areas (STESSA 2012)	[22]	Appendix A.8	239

List of Appendices

Introduction

Asymmetric Friction Connections (AFCs) are bolted connections used to dissipate seismic energy via friction [1, 2]. AFCs are assembled with two thin plates termed shims placed at both sides of a slotted plate; the slotted plate and shims are clamped in-between a fixed plate and a floating plate termed cap plate by means of high strength bolts [1]. Energy is dissipated in AFCs when the slotted plate driven by an axial force overcomes the friction at the interfaces between the slotted plate and shims producing the sliding of the slotted plate [1]. The force producing the sliding of the slotted plate is termed AFC strength, and it is dependent on the friction at the sliding surfaces and on the bolt tension during the assembly (bolt proof load) [1].

AFCs were proposed when testing brass shims [1]. Results showed AFCs hysteresis loop is bilinear and dissimilar sliding surfaces may develop predictable stable hysteretic behaviour. Testing of beam – column joints equipped with AFCs using aluminum and Grade 300 steel shims showed hysteretic behavior of beam – column joints equipped with AFCs is bilinear, predictable and stable [1, 2].

The concept of the effect of dissimilar sliding surfaces on the stability of the hysteretic behaviour was experimentally validated when testing AFCs with slotted plates of Grade 300 steel and shims with Brinell hardness varying between 40BH – 400BH [3]. Results showed increasing the shims hardness increased the hysteresis loop stability and predictability of AFC strength. Given the benefits of high hardness shims on the hysteresis loop stability of AFCs, the use of Bisalloy 500 shims (Brinell hardness of 500BH) in AFCs with slotted plates

of Grade 300 steel were introduced [4]. Testing of these AFCs showed repeatable and very stable hysteretic performance with low degradation on the sliding surfaces.

Testing of AFCs with brass shims and Grade 8.8 bolts with bolt lever arm to bolt diameter ratios of 0.9 – 1.6 showed the AFC strength had a weak decreasing trend with increasing bolt length [1, 2]. Similar results were observed for Bisalloy 400 shims and Grade 8.8 bolts with bolt lever arm to bolt diameter ratios of 0.9 – 1.9 [5]. In these research works, the bolt lever arm was defined as the distance between the points, where the bolt shank bears on the cap plate and on the fixed plate, after bolt inclines, and while sliding of the slotted plate occurs. The decrease in AFC strength with increasing bolt length was attributed to loss of bolt tension due to interaction between the moment, shear and axial demands that bolts undergo while sliding of the slotted plate occurs (MPV interaction) [1, 2, 5].

Models to capture the decrease in AFC strength were proposed and termed MPV models [1, 5]. These models assume bolts yield during the assembly and ignore the bolt inclination during the sliding as well as any increase in bolt tension from the bolt inclination. Comparisons of these models to experimental AFC strength showed the predicted AFC strength tend to be a lower bound on the experimental AFC strength [1, 2, 5]. The variability of the experimental AFC strength is considered to result from variability in the installed bolt tension during the assembly, variability in the bolt ultimate strength, and variability in the sliding surface conditions [5]. To consider in AFC design these variables during the assembly, as well as the variability of the AFC strength due to degradation of the sliding surfaces, overstrength and understrength factors of 0.7 and 1.4 were proposed [6].

Applications of AFCs as seismic dissipaters in structural systems non-exposed to corrosive environments have been also experimentally validated [1, 2, 7, 8, 9]. These studies considered dissipation of AFCs at beam column joints [1, 2], at column bases [7, 8], and within braces [9]. Results showed:

i. Structural systems equipped with AFCs had stable and predictable hysteretic response,

ii. AFCs can successfully protect structural systems from yielding or damage when the structural system undergo large drifts, and

iii. Low damage was observed in the AFCs sliding interfaces, and yielding in AFCs bolts, which both may easily be replaced.

Research studies above show that efforts have been made to experimentally validate the application of AFCs as seismic dissipaters in low corrosive environments, with a limited range of bolt lengths, and with sliding surfaces capable to reproduce predictable and stable hysteretic response. However these studies did not describe:

i. Effects of high temperature, such as fire, on the AFC mechanical properties and hysteretic response,

ii. Possible surface treatments to delay corrosion in AFCs and their effect on the hysteretic response of these connections,

iii. Hysteretic response after AFCs have been significantly corroded,

iv. Possible non-metallic sliding surfaces that can be used, instead of metallic sliding surfaces which are likely to develop corrosion, and the hysteretic response of these non-metallic sliding surfaces,

v. The effect of the wide range of bolt lengths that may be used in practice, and that show the AFC strength decreasing trend with increasing bolt length as predicted by Khoo model [5],

vi. Implications of the bolt inclination during the sliding on the AFC strength, and a model to quantify these effects,

By addressing these needs, AFC design regulations can be improved, and design can be conducted with confidence allowing to use AFCs in different structural applications. For that reasons, in this thesis, experimental and theoretical research was undertaken on AFCs with Bisalloy 500 shims to address these needs and aiming to answer following questions:

i. What are the post-fire effects on the AFCs hysteretic behaviour and on the mechanical properties of AFCs components?

ii. What are the effects of using different surface treatments on the hysteretic behaviour of AFCs?

iii. What are the corrosion effects on the AFCs hysteretic behaviour and the corrosion mechanisms developed by AFCs?

iv. What is the hysteretic behaviour of AFCs using non-metallic sliding surfaces such as brake pads?

v. What are the effects of increasing bolt length on the hysteretic behaviour of AFCs?

vi. What are the effects of bolt inclination during sliding on the hysteretic behaviour of AFCs?

vii. Can a model be developed to quantify the average AFC strength considering the effects of fire, surface treatment, corrosion, non-metallic sliding surfaces, and different bolt lengths?

These seven questions are answered through the five chapters comprising this thesis. Content of these five chapters is described below:

i. Chapter 1 describes the hysteretic behaviour of AFCs after heating to temperatures of 150°C - 750°C. Effects of heating on the shim hardness and on the mechanical properties of bolts and plates are described. A simple model proposed to quantify the average AFC strength after heating is discussed.

ii. Chapter 2 describes the hysteretic behaviour of AFCs before and after accelerated corrosion testing. Four AFCs surface treatment were considered: cleaned surfaces, sweep blasted surfaces, alkyd coated surfaces, and zinc coated surfaces. Corrosive mechanisms developed by AFCs are described. A simple model proposed to quantify the average AFC strength before and after corrosion is discussed.

iii. Chapter 3 describes the hysteretic behaviour of AFCs using three configurations of non – metallic sliding surfaces made of bonded brake pads of non-asbestos material D3923. Mechanisms of degradation of brake pads and its effects on the development of AFC strength are described. A simple model proposed to quantify the average AFC strength for bonded brake pads of non-asbestos material D3923 is discussed.

iv. Chapter 4 describes the effects of increasing bolt length on the hysteretic performance of AFCs. Causes for loss bolt tension and causes for bolt flexural yielding in AFCs are described. Effects of the bolt inclination during the sliding on the development of AFC strength are discussed. Comparisons between the Khoo MPV model [5] and strength degradation experimentally observed when increasing bolt length are discussed.

v. Chapter 5 describes the development of a MPV model considering bolt inclination during sliding. Comparisons between experimental AFC strengths and predicted AFC strengths with the proposed MPV model are discussed. A parametric study showing the effects of the bolt inclination, bolt hole oversize, bolt ultimate strength, friction coefficient, and bolt thread location on the AFC strength are discussed.

Each chapter was written in journal paper format. To date two chapters have been already published and the other three chapters have been submitted for possible publication in different journals. This thesis also presents eight conferences papers in the Appendix. These conference papers were published in different conferences and topics of these conference papers are complementary to the main five chapters. Details of journal papers and conference papers are presented in the list of publications of this thesis. Given that thesis is in journal paper format, repetition of definitions, materials, methods, and references is unavoidable.

Chapter 1

Asymmetrical Friction Connections (AFCs) Post-Heating Behaviour

Chapter 1

"Asymmetric Friction Connections Post-Heating Behaviour"

Jose Christian Chanchi Golondrino [a, b,1*], Gregory Anthony MacRae[b,2], James Geoffrey Chase[c,3], Geoffrey William Rodgers[c,4], Anthony Kwabena Gyekye Abu[b,5], George Charles Clifton[d,6]

[a] Universidad Nacional de Colombia, Departamento de Ingeniería Civil, Manizales - Caldas 170004, Colombia.

[b] University of Canterbury, Department of Civil and Natural Resources Engineering, Private Bag 4800, Christchurch 8140, New Zealand.

[c] University of Canterbury, Department of Mechanical Engineering, Private Bag 4800, Christchurch 8140, New Zealand.

[d] The University of Auckland, Department of Civil & Environmental Engineering, Faculty of Engineering, Private Bag 92019, Auckland Mail Centre, Auckland 1142, New Zealand.

[1] jcchanchigo@unal.edu.co, [2]gregory.macrae@canterbury.ac.nz, [3]geoff.chase@canterbury.ac.nz, [4]geoff.rodgers@canterbury.ac.nz, [5]anthony.abu@canterbury.ac.nz, [6]c.clifton@auckland.ac.nz
[*]Corresponding author

Key Words: Asymmetric Friction Connection, Bisalloy 500 shim, Post-Heating Hysteretic Behaviour, Low damage dissipater.

ABSTRACT

Asymmetric Friction Connections (AFCs) are used to dissipate seismic energy in structural systems. However, after they have suffered heat or fire damage their performance has not been documented. In this paper, changes to the properties and hysteretic behaviour of 18 AFCs with Bisalloy 500 shims, 2 M16 Grade 8.8 galvanized bolts, and Grade 300 steel plates after heating are described. The AFCs heating is conducted to between 150°C - 750°C, cooled to room temperature, and then quasi-statically tested. It was found that while the hardness, the modulus of elasticity and the ultimate tensile strength of Grade 300 steel plates underwent

only minor reductions as a result of the heating, significant reductions in hardness were recorded for Bisalloy 500 shims heated above 300°C. Also, the ultimate tensile strength and modulus of elasticity of the Grade 8.8 galvanized bolts were significantly reduced when heated above 400°C and 600°C, respectively. The stability of the hysteresis loops decreased when the connection was heated above 150°C. In general, the AFC strength decreases as the ratio of shim hardness to slotted plate hardness decreases. Thus, since increasing temperature decreases the shim hardness so the AFC performance degrades. Based on these concepts, a model to quantify the maximum and minimum likely AFC strength after heating is proposed based on Coulomb dry friction theory.

I. INTRODUCTION

AFCs are friction bolted connections used to dissipate seismic energy. AFCs can be assembled using three Grade 300 steel plates, two thin plates termed shims made of high hardness materials such as Bisalloy 400 or Bisalloy 500, and high strength structural bolts such as Grade 8.8 bolts. AFCs dissipate energy via friction when a slotted plate is forced to slide over the shims [1.1, 1.2, 1.3]. The sliding force of the resulting approximately square hysteresis loop is termed the AFC strength, and quasi-static testing has shown it may be almost constant [1.1]. AFCs can be used as seismic dissipaters in moment resistant frames at the beam column joint, or in braced frames [1.1, 1.3, 1.4]. Since there is a possibility that AFCs may be subjected to significant heating events, such as fire, this may affect the connection components properties and AFC performance. Currently, there is no reported study of these effects, which affect the decision of what, if anything, should be replaced. Some evidence that a heating event may compromise the performance of AFCs is based on the reduction in tensile strength, shear strength, and hardness that Grade 8.8 bolts underwent when loaded in tension and heated to temperatures above 500°C [1.5], and when loaded in double shear and heated to temperatures above 500°C [1.5]. Evidence of the possible effect of heating on the performance of AFCs is also based on the reduction in tensile strength and shear strength of isolated high strength bolts after being heated to temperatures above 400°C - 500°C, and on the significant loss of strength of friction connections as a result of the loss of installed bolt tension (relaxation effect) during heating and cooling to temperatures above 400°C [1.6, 1.7]. In addition to the bolts, there is concern that the properties of tempered Bisalloy 500 shim plate, Grade 300 steel plate, and sliding interfaces may change. For confidence to be obtained that AFC connections will behave well after a significant heating

event, such as fire or even due to excessive sliding, there is a need to understand and characterize this behaviour. To address these needs, this paper seeks answers to following questions:

i. How do AFC connection component properties change due to heating?

ii. How does the hysteresis loop change after AFCs have been heated?

iii. How does the effective friction coefficient of AFCs change due to heat?

iv. What is the strength degradation of AFCs after AFCs have been heated?

v. Can the strength of AFCs after being subjected to a heating regime be easily characterised?

II. MATERIALS AND METHODS

2.1 AFC devices

A total of 21 AFCs were assembled using Bisalloy 500 shims of 6mm thickness, and Grade 300 steel plates of 20mm thickness for the fixed, slotted, and cap plates. They were clamped using 2 M16 Grade 8.8 structural galvanized bolts of 110mm length with unthreaded length of 72mm and threaded length of 38mm. Bolts were assembled using a structural washer of 4mm thickness, a flat washer of 4mm thickness, and a single Belleville washer of 2.5mm at the fully squashed condition, as shown in Figure 1.1.

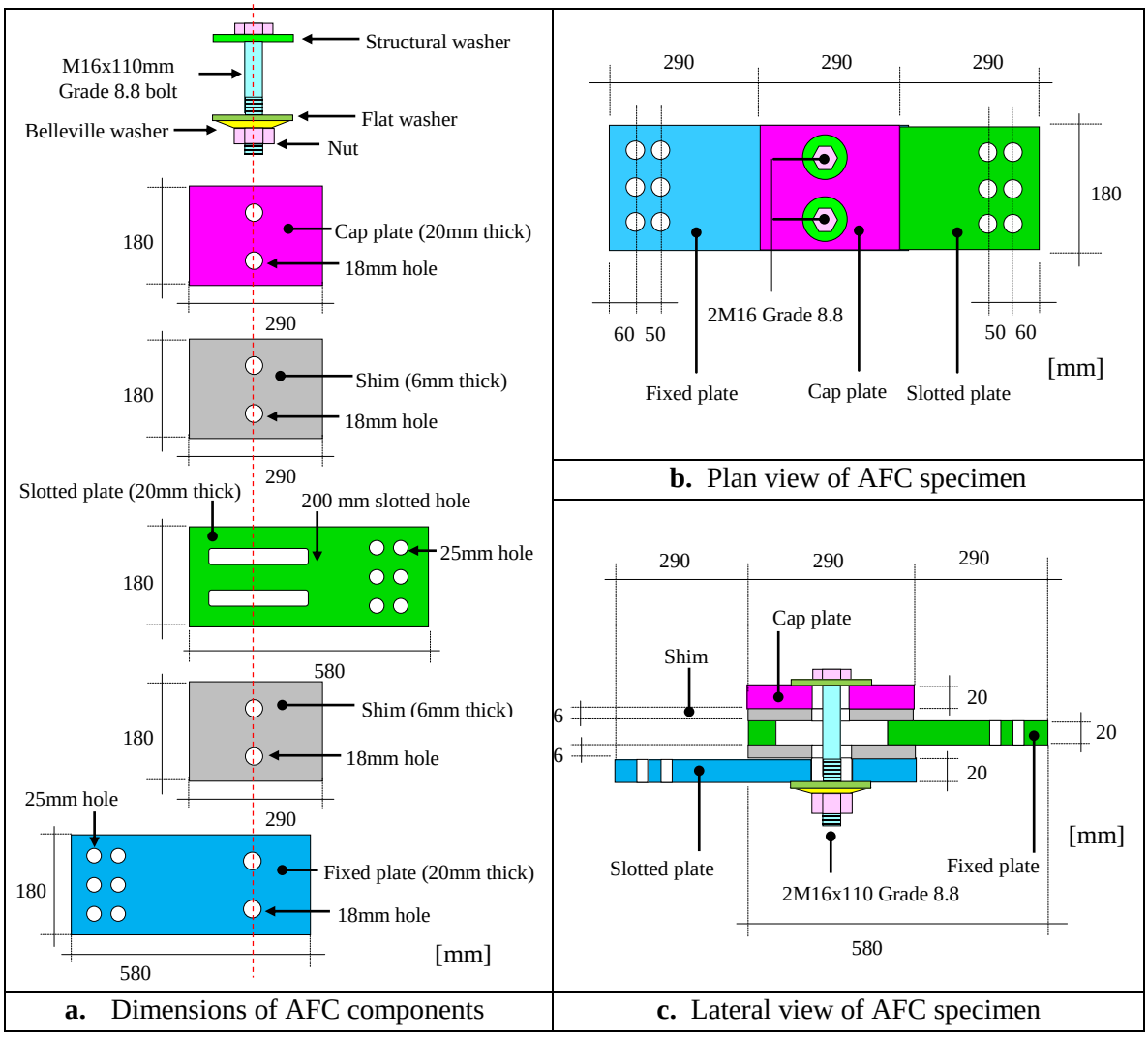

a. Dimensions of AFC components

b. Plan view of AFC specimen

c. Lateral view of AFC specimen

Figure 1.1. Dimensions of AFC components, plan and lateral view of AFCs assembly (Not to scale).

Belleville washers were used to reduce the variation of the clamping force on the bolts due to degradation of the sliding surfaces [1.1]. The bolt grip length of 82.5mm was calculated as 3 x 20mm for the plates, plus 2 x 6mm for the shims, plus 4.0mm for the structural washer, 4.0mm for the flat washer, and 2.5mm for the flattened Belleville washer.

2.2 Assembling of AFCs

AFCs were assembled by tensioning bolts in the clamped zone of the connection up to the proof load of 95kN for a Grade 8.8 M16 bolt using the torque control method. In this method, a bolt is gradually tensioned to a torque that develops an axial elongation equivalent to the computed elongation that the bolt develops when it reaches the proof load in axial tensile testing, ignoring bolt torsion. This torque is termed proof load torque, and the elongation of the bolt, when it reaches the proof load in axial tensile testing, was termed proof load elongation.

The proof load elongation of 0.21mm, which occurred over the grip length, was read from an axial tensile testing relationship from 3 bolts using the proof load value, as shown in Figure 1.2a. The proof load torque of 270N-m was assessed as the average of the maximum and minimum torques read from a torque - induced bolt elongation relationship for 3 bolts using the proof load elongation value, as shown in Figure 1.2b. Here, the bolt grip length was 82.5mm.

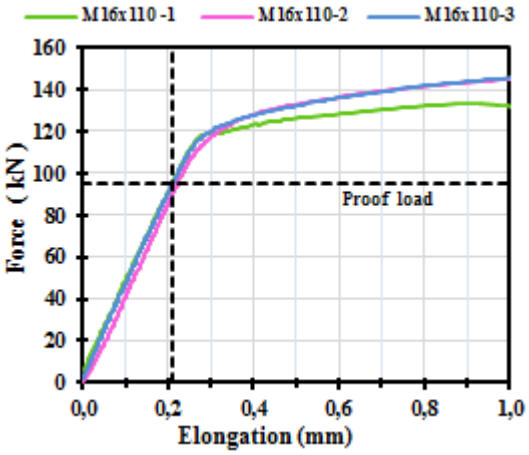

a. Axial tensile testing relationship

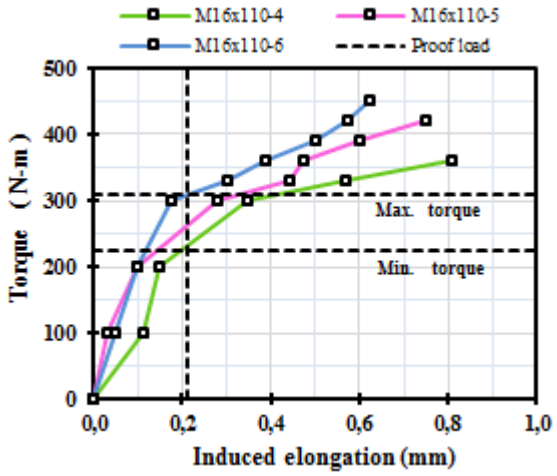

b. Torque – Induced bolt elongation relationship

Figure 1.2. Assembling relationships of AFCs with M16 x 110 Grade 8.8 bolts with grip length of 82.5mm

2.3 Heating of AFCs

The 21 AFCs were divided into 7 groups, with three in each group. Six groups of three AFCs were heated at target temperatures of 150°C, 300°C, 400°C, 500°C, 600°C, and 750°C, respectively. The remaining group of three AFCs were kept at room temperature (i.e. 20°C) as a control. AFCs were heated in an electric furnace with temperature control. Each AFC was placed horizontally in the heating chamber of the furnace. AFCs were placed onto the supports 850mm apart located at both ends of the furnace, as shown in Figure 1.3a. In this setup AFCs were only under the action of their own weight and the heat, and could freely elongate under the action of the heat. The plates in the AFC clamped zone were instrumented with four thermocouples. Two thermocouples were placed in holes drilled at the heads of the bolts, and two thermocouples were placed in holes drilled at the lateral sides of the clamped zone of the slotted plate, as shown in Figure 1.3a.

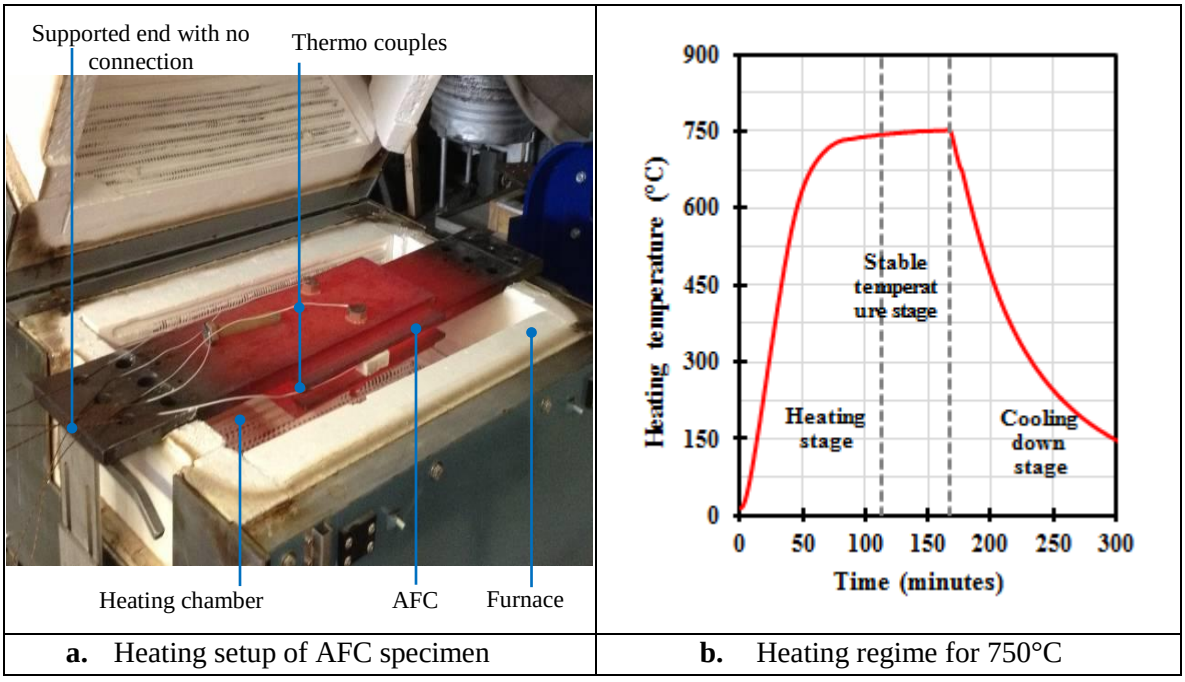

a. Heating setup of AFC specimen

b. Heating regime for 750°C

Figure 1.3. AFC heating setup and heating regime

The heating regime comprised three stages, as shown in Figure 1.3b. In the first "heating" stage, the furnace temperature is increased from room temperature up to the target temperature at an approximate rate of 10°C/min. During the second "stable temperature" stage the target temperature is held constant for 45 minutes. The "cooling down" stage is the third and final stage, where the AFC is cooled up to room temperature by opening the furnace and allowing the specimen to be in contact with air via free convection. This heating regime mimics the temperature - time curve for fire events in buildings. The three stages of the heating regime match with the three stages of fire events in buildings, which are fire growth, fully developed fire, and fire decay [1.8]. The maximum target temperature in the "stable temperature" stage of the heating regime (i.e. 750°C) was chosen from the range of the average temperatures measured in the fully develop fire stage for fire events in buildings (i.e. 700°C - 1200°C) [1.8]. The duration of the "stable temperature" stage of the heating regime

(i.e. 45min) was adopted from the time range considered as usual for firefighters to gain entry and begin firefighting operations in a building during a fire event (i.e. 30min – 180min) [1.8].

2.4 Quasi-static testing of AFCs

AFCs were quasi-statically tested after heating and cooling. Quasi-static testing was performed using a shaking table to provide a strictly horizontal input at the required force levels; thus, minimizing prying effects that reduce AFC strength [1.9, 1.10]. The test setup comprised a fixed bracket attached to a reaction frame bolted to a reaction floor, and a moving bracket attached to a reaction frame bolted to a shaking table. AFCs were connected using 6 Grade 8.8 M24 bolts at each end. A load cell was placed between the fixed bracket and reaction frame, and a potentiometer was placed across the connection. Details are shown in Figure 1.4a.

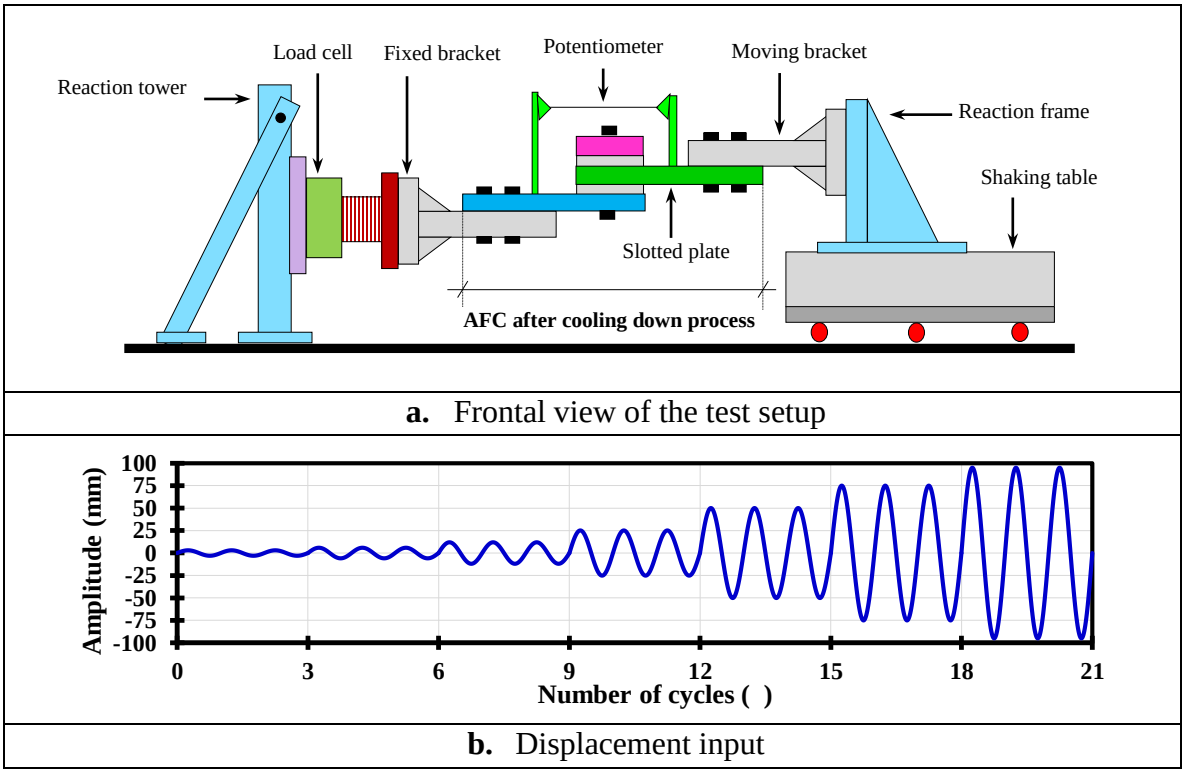

Figure 1.4. Setup of AFC specimens and displacement input (Not to scale)

Figure 1.4b shows the displacement input comprising 21 sinusoidal cycles with a maximum velocity of 10mm/s and amplitudes varying from 0 to ±95mm. This amplitude is 95% of the full 200mm slot length. The peak velocity of 10mm/s at each amplitude is slow enough to minimise velocity dependence effects [1.3]. Each AFC specimen was subjected to two runs of this displacement regime with no bolt re-tensioning. Between the first and second run, 30 minutes were allocated to allow the test specimen to cool to room temperature, eliminating the effects of heating due to friction between runs. The shaking table was used in the AFC testing as the inputs were more than quasi-static (i.e. peak velocity of 10mm/s) and the shaking table can provide this force. It also reused an experimental setup used in prior works with AFCs, which had proven effective [1.3].

2.5 Tensile and hardness testing of the heated connection components

The 21 AFCs were disassembled after heating and quasi-static testing. Brinell hardness tests were conducted on the disassembled AFC plates. Axial tensile testing of 21 Grade 300 steel coupons machined from the slotted plates, and on 21 M16 Grade 8.8 galvanized bolts obtained from the 21 disassembled AFCs was conducted in an Avery universal testing machine. Elongations of the coupons and bolts during axial testing were recorded with an extensometer attached to the testing specimens. The extensometer recorded the elongations of the Grade 300 steel coupons over a length of 55mm, and for the M16 Grade 8.8 galvanized bolts over a length of 82.5mm that correspond to the bolt grip length used to assemble AFCs. Figure 1.5 shows examples of the slotted plate coupons and bolts obtained from the disassembled AFCs.

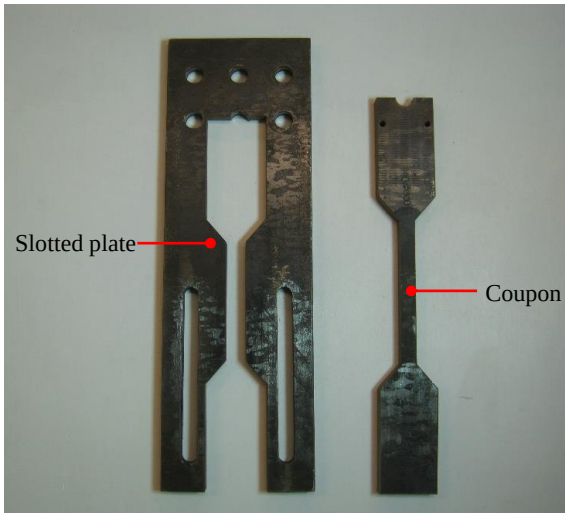

a. Slotted plate coupon from disassembled AFCs

b. Bolts from disassembled AFCs

Figure 1.5. Tensile testing samples from disassembled AFCs.

2.6 Assessment of the experimental residual AFC strength

The experimental AFC strength, *Sa*, at a given hysteresis loop amplitude can be assessed by reading the force values at the four corners and at the two zero displacement points of the hysteresis loop, as shown in Figure 1.6.

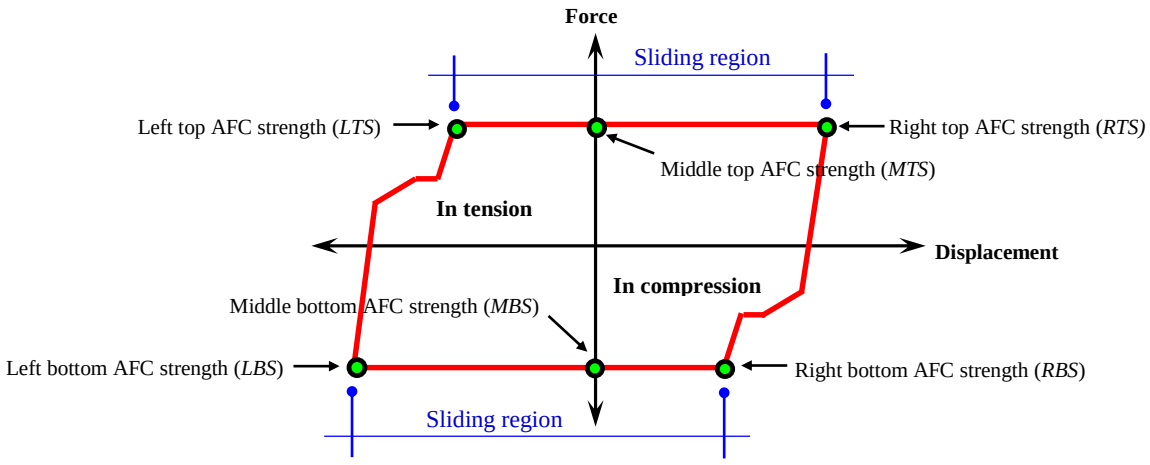

Figure 1.6. Assessment points of experimental AFC strength at a given hysteresis loop amplitude

The experimental AFC strength, *Sa*, can be also assessed as the average absolute value of the tension and compression sliding regions of the hysteresis loop according to Equation 1.1, where, *LTS*, *MTS*, and *RTS* are the experimental AFC strengths at the tension sliding region of the hysteresis loop, and *LBS*, *MBS*, and *RBS* are the experimental AFC strengths at the compression sliding region of the hysteresis loop, as shown in Figure 1.6.

$$Sa = \left[\frac{\left(LTS + MTS + RTS\right) + \left|LBS + MBS + RBS\right|}{6} \right] \quad (1.1)$$

2.7 Assessment of the effective friction coefficient at room temperature

The effective friction coefficient at room temperature, μe, can be assessed according to Equation 1.2 following the dry friction theory of Coulomb as function of the clamping force, F_{proof}, induced by each of the *n* bolts acting over the *m* interfaces on the clamped zone, and the measured AFC strength, *S* [1.11]. This friction coefficient is termed effective because the clamping force is not constant and there may be variation due to the degradation of the sliding surfaces of AFCs, any surface coating [1.3], and materials used [1.12].

$$\mu e = \frac{S}{m \times n \times F_{proof}} \quad (1.2)$$

2.8 Assessment of strength degradation

Strength degradation is defined as the reduction in the average AFC strength from the first run to the second run of the displacement input according to Equation 1.3, where, *SD*, is the strength degradation, $Sa_{\ second\ run}$ and $Sa_{first\ run}$, are the experimental AFC strength for the first run and second run, respectively [1.3].

$$SD = \left[1 - \left(\frac{Sa_{second\ \ run}}{Sa_{\ first\, run}}\right)\right] \times 100\% \qquad (1.3)$$

III. RESULTS AND ANALYSIS

3.1 Heating Effects on Bisalloy 500 Shims and Grade 300 Steel Plates Hardness

For Bisalloy 500 shims, hardness reduces at a low rate of 0.08BH/°C for heating temperatures below 300°C, and faster at a rate of 0.59 BH/°C for heating temperatures of 300°C - 750°C, as shown in Figure 1.7a. For Grade 300 steel plates, there is negligible reduction with heating temperature. Figure 1.7a show that the minimum and maximum variability for both the Bisalloy 500 shim hardness and the Grade 300 steel hardness occurred at room temperature and at heating temperature of 600°C, respectively.

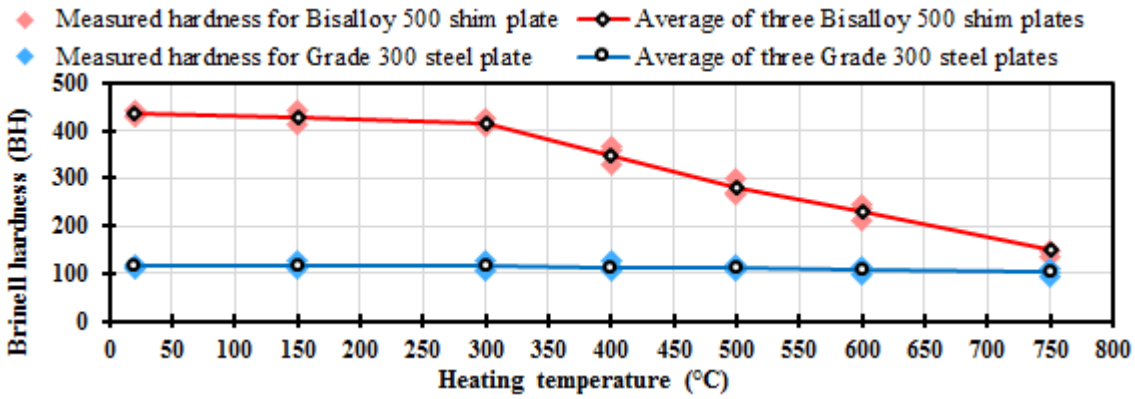

a. Brinell hardness of Bisalloy 500 shims and Grade 300 steel plates

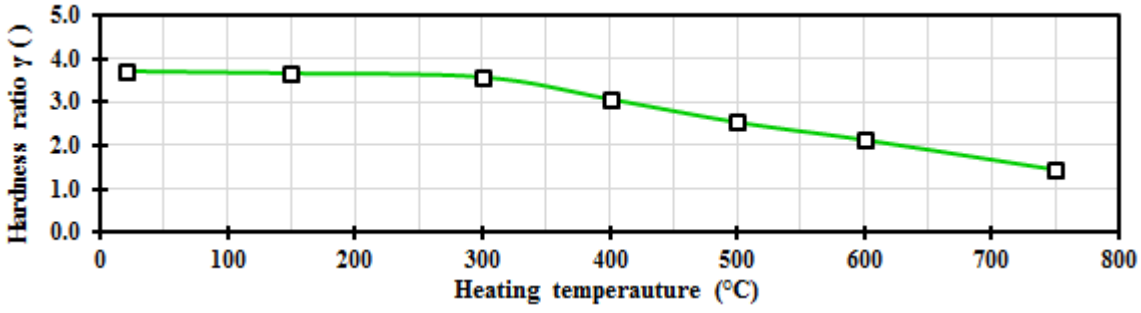

b. Hardness ratio γ

Figure 1.7. Brinell hardness of Bisalloy 500 shims, Brinell hardness of Grade 300 steel plates, and hardness ratio at room temperature, and after AFC have been heated, cooled and quasi – statically tested.

The minimum and maximum variability of the hardness values respect to the average calculated from three experimental values were of 1% - 3% and 6% - 9% for Bisalloy 500 shims plates, respectively, and of 1% - 2% and 5% - 8% for Grade 300 steel plates, respectively. The hardness ratio, γ, defined as the ratio of the hardness of the Bisalloy 500 shims to the hardness of the Grade 300 steel plates, as shown in Figure 1.7b, follows the shape of the Bisalloy 500 shims hardness curve in Figure 1.6b, with values of 3.71 – 1.45. It is interesting to note that the maximum hardness is less than the value of 500BH expected for Bisalloy 500 shims. The reason for the Bisalloy 500 shim hardness decrease with heating temperatures above 300°C may be due to its heat treatment. This decrease in hardness of AFC shims heated above 300°C, which may be from fire or friction, indicates that they need to be replaced, but not the steel plate, to reinstate the AFC performance.

3.2 Heating Effects on Grade 300 Steel Plates and Bolt Stiffness and Strength

Figure 1.8 shows the monotonic stress and strain curve results, and properties for Grade 300 steel plates and M16 Grade 8.8 galvanized bolts. For heating temperatures of 600°C, the ultimate strength, yielding strength, and elastic modulus of Grade 300 steel plates are reduced up to 3.5%, 5.1%, and 6.0%, of the room temperature values, respectively. For heating temperatures of 750°C these properties are reduced up to 7.7%, 16.2%, and 12.5%, respectively. The ultimate strength of Grade 8.8 bolts for heating temperatures of 400°C is reduced up to 1.3% of the ultimate strength at room temperature, and up to 49.9% for heating temperatures of 750°C. The elastic modulus, for heating temperatures of 600°C is reduced up to 3.1% of the elastic modulus at room temperature, and up to 27.9% for heating temperatures of 750°C. Since the ultimate strength, yielding strength, and elastic modulus

of Grade 300 steel plates did not change significantly (i.e. less than 16.2%) up to 750°C, they may be reusable after a major event. In contrast, for Grade 8.8 bolts heated above 400°C, they should be replaced in order to reinstate the AFC performance. According to the results above, for reusing Grade 300 steel plates and for not changing Grade 8.8 after a fire event, it is recommended a maximum acceptable change in mechanical properties of 15%, which corresponds to that observed in both cases for heating temperatures below 400°C.

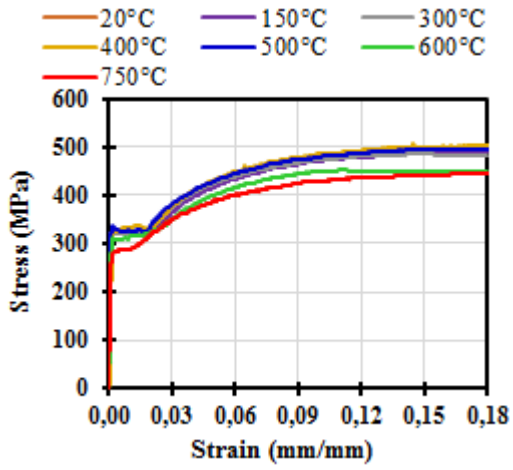

a. Monotonic stress and strain curves of a set of 7 Grade 300 steel coupons

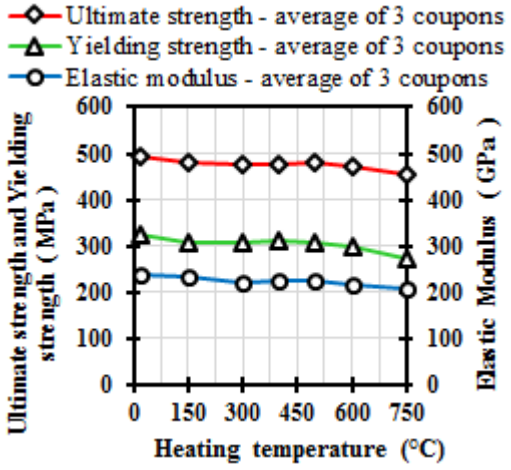

b. Ultimate strength modulus of elasticity, and yielding strength of Grade 300 steel coupons

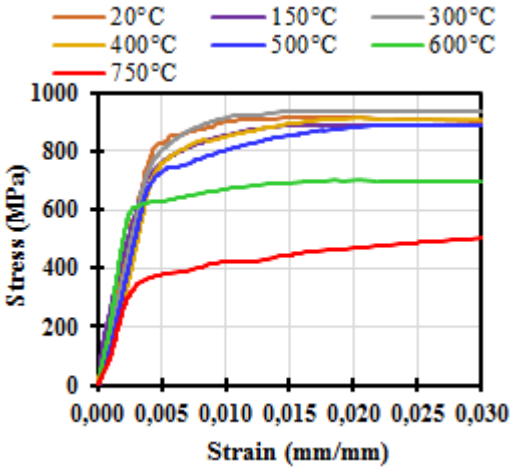

c. Monotonic stress and strain curves of a set of seven M16 Grade 8.8 galvanized bolts

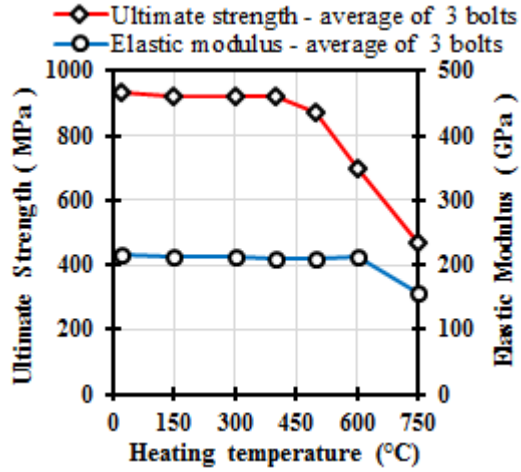

d. Ultimate strength and elastic modulus of M16 Grade 8.8 galvanized bolts

Figure 1.8. Properties of Grade 300 steel coupons and M16 Grade 8.8 galvanized bolts in AFCs at room temperature, and in AFCs after heating, cooling and quasi-static testing.

Results in this section were obtained from AFCs under the action of their own weight and the heat, and allowing AFCs freely elongate under the action of the heat. In Practice, AFCs are assembled in structural elements that generate some restriction on the expansion of the AFC, and that carry vertical loads additional to the own weight. For that reason, additional research needs to be conducted to quantify effects such as permanent deformations resulting from the combined action of heat, extra vertical load, and restriction on the expansion that could modify the results reported in this section.

3.3 Effects of heating on the hysteresis loop of AFCs

Figure 1.9 shows hysteresis loops and hardness ratios obtained from AFCs at room temperature, and from AFCs after heating and cooling. The shape of the hysteresis loop and the average AFC strength, *Sa*, as defined by Equation 1.1 in Section 2.7 vary as the heating temperature and the hardness ratio vary. Lack of variation in the hysteresis loop shape and in the average AFC strength is referred to here as hysteresis loop stability. For heating temperatures below 300°C, where the hardness ratio is almost constant, hysteresis loops are stable and the average AFC strength is almost constant. It can be also seen in Figures 1.9a – c that the AFC strength is constant for both positive (tension) and negative (compression) displacements up to 25mm. However, for displacement amplitudes greater than 25mm, the AFC strength for positive (tension) displacements is greater than that for negative (compression) displacements. That is because during positive (tension) displacements the AFC increases in length due to the slotted plate displacement, which increases the slotted plate rotation due to the asymmetry of the AFC, thus making the slotted plate pry on the fixed plate. As a result of the prying forces developed between the slotted plate and the fixed plate the AFC strength increases. For heating

temperatures between 300°C and 750°C, where the hardness ratio reduces from 3.6 to 1.5, hysteresis loop stability reduces, and the average AFC strength may reduce or increase.

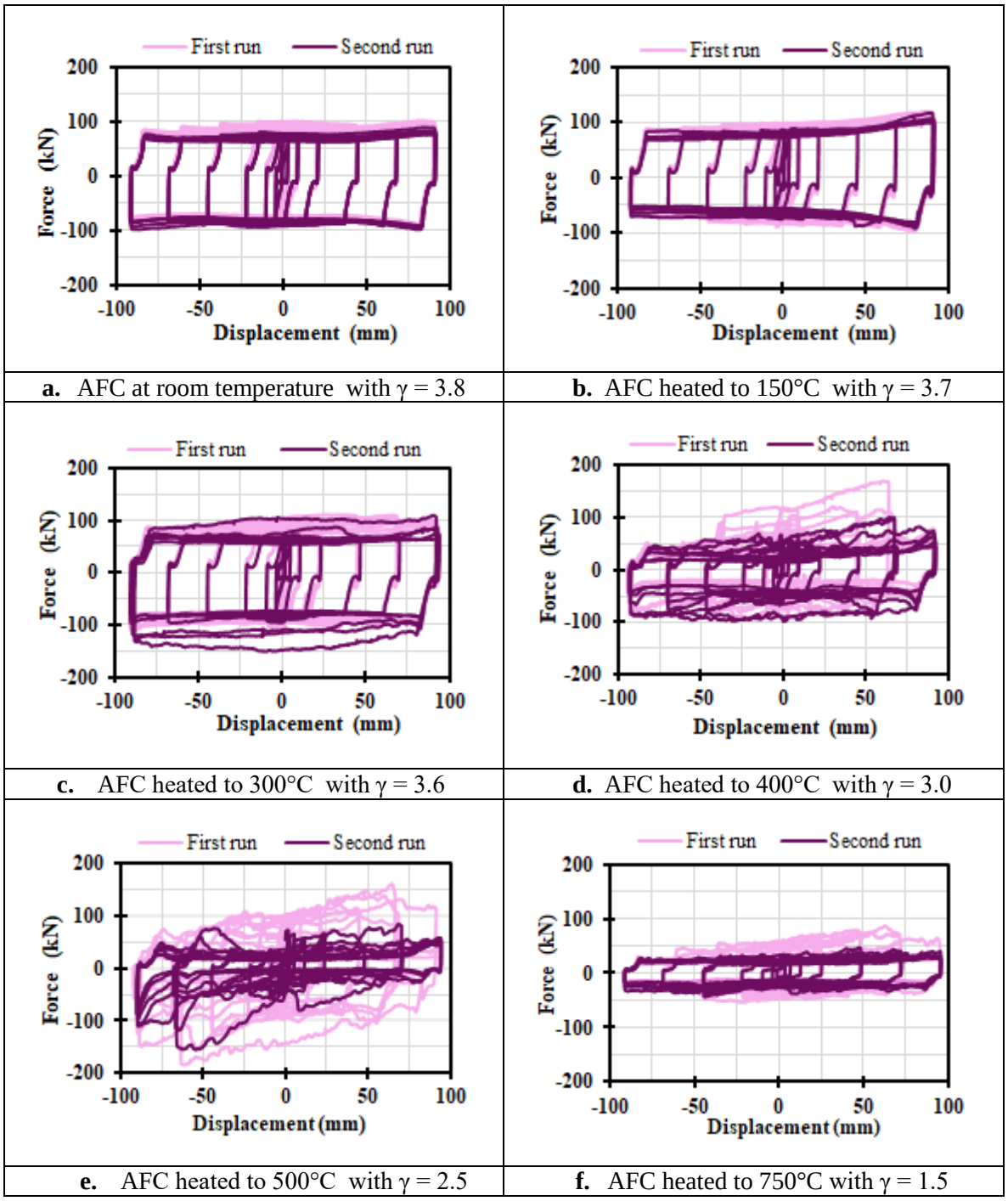

a. AFC at room temperature with $\gamma = 3.8$ | **b.** AFC heated to 150°C with $\gamma = 3.7$

c. AFC heated to 300°C with $\gamma = 3.6$ | **d.** AFC heated to 400°C with $\gamma = 3.0$

e. AFC heated to 500°C with $\gamma = 2.5$ | **f.** AFC heated to 750°C with $\gamma = 1.5$

Figure 1.9. Hysteresis loop and hardness ratio, γ, of AFCs at room temperature and AFCs after heating and cooling.

Variations in hysteresis loop stability and in the average AFC strength with the heating temperature are related to the type of sliding mechanism the AFCs develop according to the hardness ratio. For hardness ratios around 3.7, AFCs develop an adhesive sliding mechanism, where the sliding surfaces degrade with particles that either adhere to the sliding surfaces or become loose as debris producing minor changes on the bolt tension. This behaviour helps maintain hysteresis loop stability and the average AFC strength almost constant. For hardness ratios between 3.6 and 1.5, AFCs develop an abrasive sliding mechanism, where the sliding surfaces degrade with particles that abrade the sliding surfaces and become loose as debris producing increments and reductions in bolt tension as the particles slide, thus reducing the hysteresis loop stability, and increasing or decreasing the average AFC strength. Both sliding mechanism described above are dependent not only on the variation of Bisalloy 500 shim hardness but also on the variation of bolt mechanical properties. The contribution of each of these two effects on the sliding mechanism is difficult to quantify, since both effects act simultaneously as the sliding of the slotted plate is developed. These results mimic some of those seen in corrosion testing, coating testing, and in testing of AFCs with Grade 300 steel shims, where different behaviours depend on how the plates degrade [1.3, 1.12].

During the first and second runs, the external perimeter of sliding interfaces of all tested AFCs heated up to 30°C - 40°C due to friction. Since this temperature is much lower than 300°C, it is unlikely that heating due to friction reduced the hardness of the Bisalloy 500 shims, and therefore it did not influence the hardness ratio, or the AFC hysteretic performance shown in Figure 1.9. After the second run, AFCs were dismantled for describing the sliding surfaces. For AFCs heated below 300°C, the sliding surfaces were

characterized by slightly worn areas at both sides of the slotted holes. These slightly worn areas on the sliding surfaces are due to the adhesive sliding mechanism described above. For AFCs heated between 300°C and 750°C, the sliding surfaces were characterized by scratched areas at both sides of the slotted holes, and that increased in size with the heating temperature. These scratched areas on the sliding surfaces are due to the abrasive sliding mechanism described above.

3.4 Effect of heating on effective friction coefficient and strength degradation

Figure 1.10 shows the effective friction coefficient, μe, assessed with Equation 1.2 in both runs for AFCs at room temperature, and for AFCs after heating and cooling. In Equation 1.2, AFC strength, S, was calculated as the average of the AFC strength assessed as defined in Section 2.7 for 3 AFCs in each group, a number of bolts, m, of 2, and number of shear planes, n, of 2 and a bolt proof load, F_{proof}, of 95kN. It can be seen in Figure 1.9 that μe varies as the heating temperature increases in both runs of the displacement input. Also, regardless of the heating temperature μe in the first run is greater than μe in the second run, and that for both runs μe also varies with the hysteresis loop amplitude.

For heating temperatures below 150°C, μe has no major changes compared with μe at room temperature, and varies in the ranges of 0.17 – 0.23 and 0.16 – 0.21 for the first run and second run, respectively. For heating temperatures above 150°C, μe may increase or reduce with respect to μe at room temperature, and varies in the ranges of 0.11 – 0.24 and 0.03 – 0.16 for the first run and second run, respectively. Values of μe for heating temperatures below 150°C are consistent with values reported for AFCs with Bisalloy 500 shims quasi-statically tested at room temperature [1.3, 1.12].

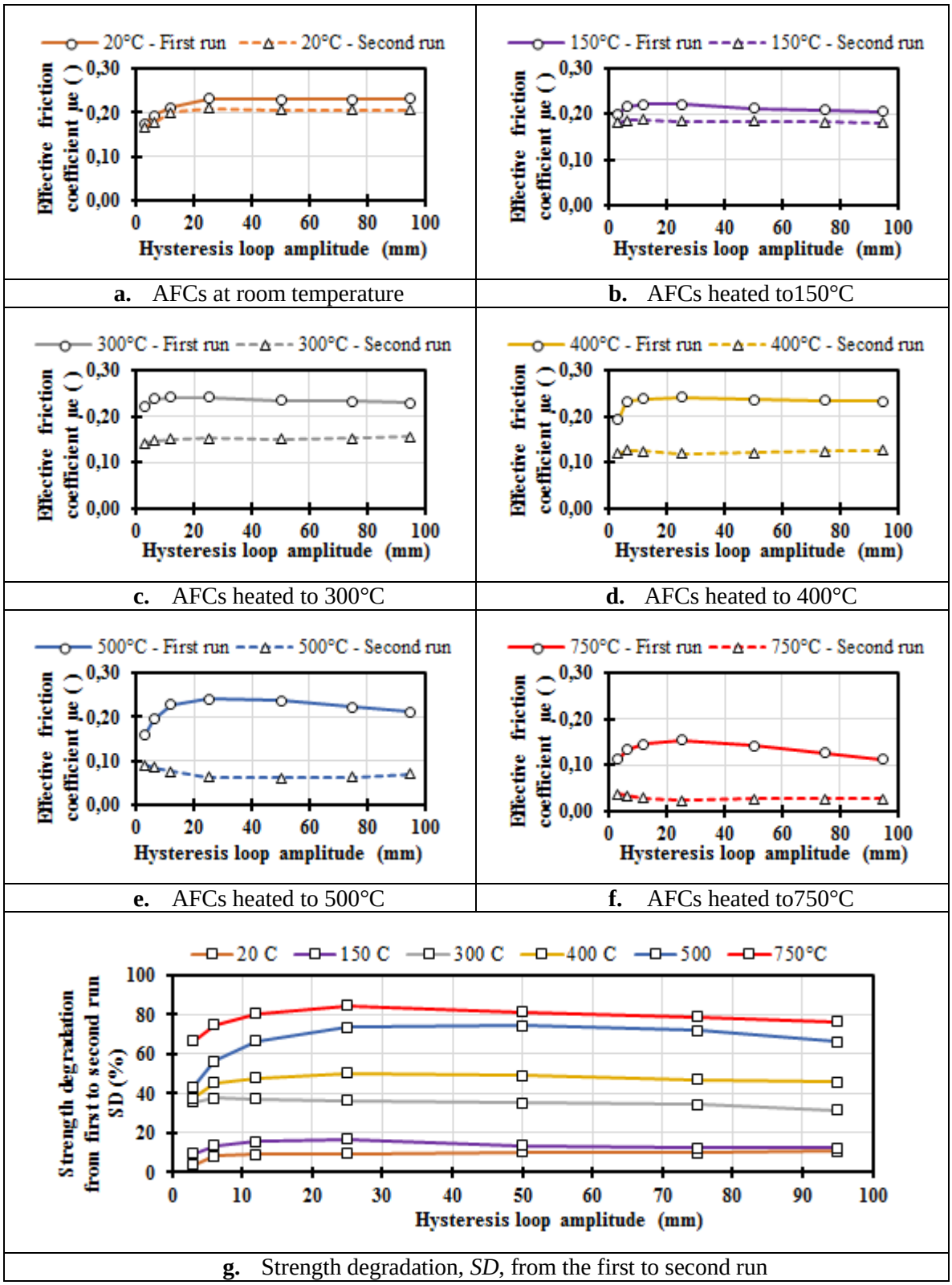

Figure 1.10. *μe*, and *SD*, in AFCs at room temperature, and in AFCs after heating and cooling.

Figure 1.10g shows the strength degradation, *SD*, assessed with Equation 1.3 at hysteresis loop amplitudes of 3mm - 95mm and using μe presented in Figures 1.10a - f. It shows that *SD* increases with the heating temperature, implying greater degradation. In Figure 1.10g, low strength degradations up to 4% - 17% are observed for AFCs at room temperature and for AFCs heated up to 150°C. In contrast, significant strength degradations up to 35% - 85% are observed for AFCs heated to 300°C - 750°C. Hence, heating temperature can significantly degrade AFC performance.

IV. MODEL OF AFC STRENGTH CONSIDERING HEATING EFFECTS

The average AFC residual strength, *RS*, is defined as the AFC strength after an AFC has been heated and cooled to room temperature. It can be computed as the AFC strength at room temperature, *S*, multiplied by a non-dimensional "heating factor", K_T, according to Equation 1.4.

$RS = K_T \times S$	(1.4)
$K_T = \begin{bmatrix} 1.0 & T \le 300^{o}C \\ 1.2963 - (0.0009877 \times T) & T \rangle 300^{o}C \end{bmatrix}$	(1.5)

To obtain the heating factor, K_T, a bilinear trend was fitted on the average effective friction coefficients obtained from the maximum and minimum effective friction coefficients for the first run, μe, in Figure 1.10 for AFCs at room temperature, and for AFCs after heating to 150°C - 750°C, as shown in Figure 1.11a. The heating factor, K_T, was obtained by normalizing the bilinear trend by the average effective friction coefficient at room temperature of 0.215, as shown in Figure 1.11b**.** The average effective friction coefficient at room temperature was obtained as the average across the full hysteresis loop amplitudes of

the effective friction coefficients recorded for the first run of AFCs at room temperature in Figure 1.10a. The heating factor K_T as function of the heating temperature T in °C is defined in Equation 1.5.

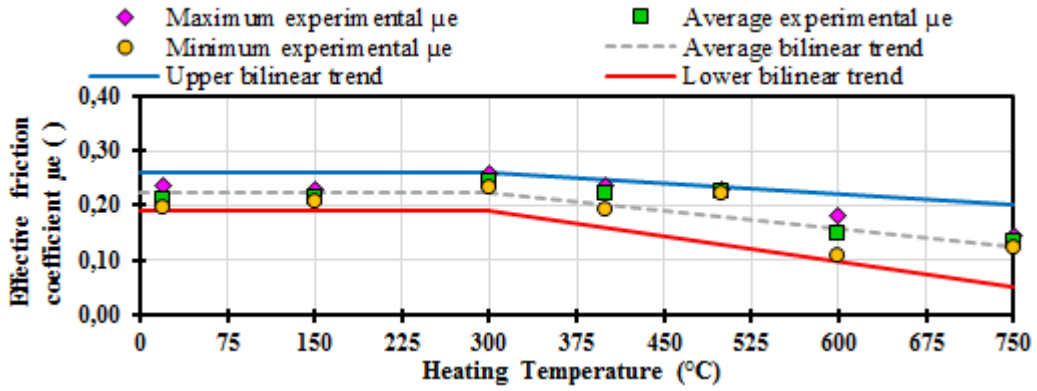

a. Variation of the maximum and minimum effective friction coefficient, μe, with heating temperature.

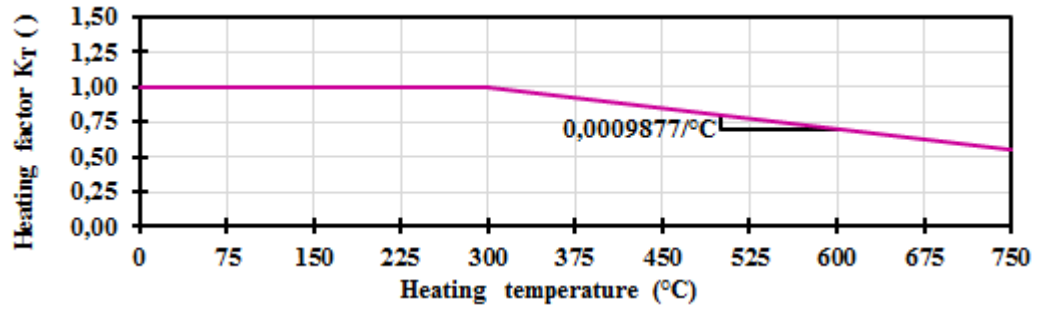

b. Variation of the heating factor, K_T, with heating temperature.

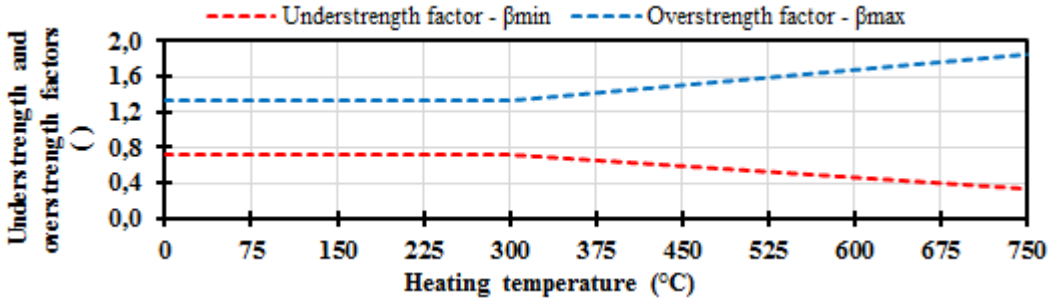

c. Variation of overstrength, β_{max}, and understrength, β_{min}, factors with heating temperature

Figure 1.11. Variation of the minimum and maximum effective friction coefficients μe, of the understrength factor, β_{min}, of the overstrengh factor, β_{max}; and of the heating factor K_T with heating temperature.

Maximum and minimum likely first run residual AFC strengths considering temperature, $RS_{max,}$ and, RS_{min}, are obtained by multiplying the average residual strength considering temperature, RS, by overstrength, β_{max}, and understrength, β_{min}, non-dimensional factors, according to Equations 1.6 and 1.7.

$RS_{\min} = \beta_{\min} \times RS$	(1.6)
$RS_{\max} = \beta_{\max} \times RS$	(1.7)

To obtain the understrength and overstrength factors, β_{min} and β_{max}, lower and an upper bilinear trends were first fitted to envelope the effective friction coefficients, μe, in Figure 1.11a. The understrength factor, β_{min}, was obtained by multiplying the lower bilinear trend normalized by the effective friction coefficient at room temperature by 0.85. The overstrength factor, β_{max}, was obtained by multiplying the upper bilinear trend normalized by the effective friction coefficient at room temperature by 1.15. These values of 1.15 and 0.85 used to obtain the overstrength and understrength factors were calculated from Figure 1.11a at room temperature. The value of 1.15 was calculated as the ratio between the maximum effective friction coefficient and the average effective friction coefficient. The value of 0.85 was calculated as the ratio between the minimum effective friction coefficient and the average effective friction coefficient. Trends for β_{min} and β_{max}, as function of the heating temperature, T, in °C are therefore given by Equation 1.8 and Equation 1.9.

$\beta_{\min} = \begin{bmatrix} 0.72 & T \le 300^{o}C \\ 0.969 - (0.000839 \times T) & T \rangle 300^{o}C \end{bmatrix}$	(1.8)

$$\beta_{\max} = \begin{bmatrix} 1.33 & T \le 300^{o}C \\ 0.988 + (0.001136 \times T) & T \rangle 300^{o}C \end{bmatrix} \quad (1.9)$$

It is noted that for heating temperatures below 300°C, β_{min} and β_{max}, are consistent with values in current practice of 0.70 and 1.4 for AFCs with Bisalloy 500 shims quasi-statically tested at room temperature [1.13].

V. EXPERIMENTAL AND PREDICTED AFC STRENGTH COMPARISONS

Figure 1.12 compares the 294 experimental AFC strengths with lines representing the maximum residual strength, RS_{max}, the average residual strength, RS, and the minimum residual strength, RS_{min}, considering temperature according to equations above. The 294 experimental AFC strengths correspond to 42 AFC strengths at room temperature and 42 AFC strengths at each of the 6 heating temperatures of 150°C, 300°C, 400°C, 500°C, 600°C and 750°C. The 42 experimental values at each heating temperature resulted from assessing the AFC strength using the methodology described in Section 2.7 at hysteresis loop amplitudes of 3mm, 6mm, 12mm, 25mm, 50mm, 75mm and 95mm in 3 AFCs.

The maximum and minimum theoretical AFC strengths in Figure 1.12 were predicted with Equations 1.6 and 1.7, respectively, considering the number of shear planes, m = 2, the number of bolts n = 2, the proof load F_{proof} = 95kN, and the effective friction coefficient at room temperature μe = 0.225. The heating factor, K_T, the understrength factor, β_{min}, and the overstrength factor, β_{max}, were determined with Equations 1.5, 1.8, and 1.9, respectively, using the appropriate heating temperature.

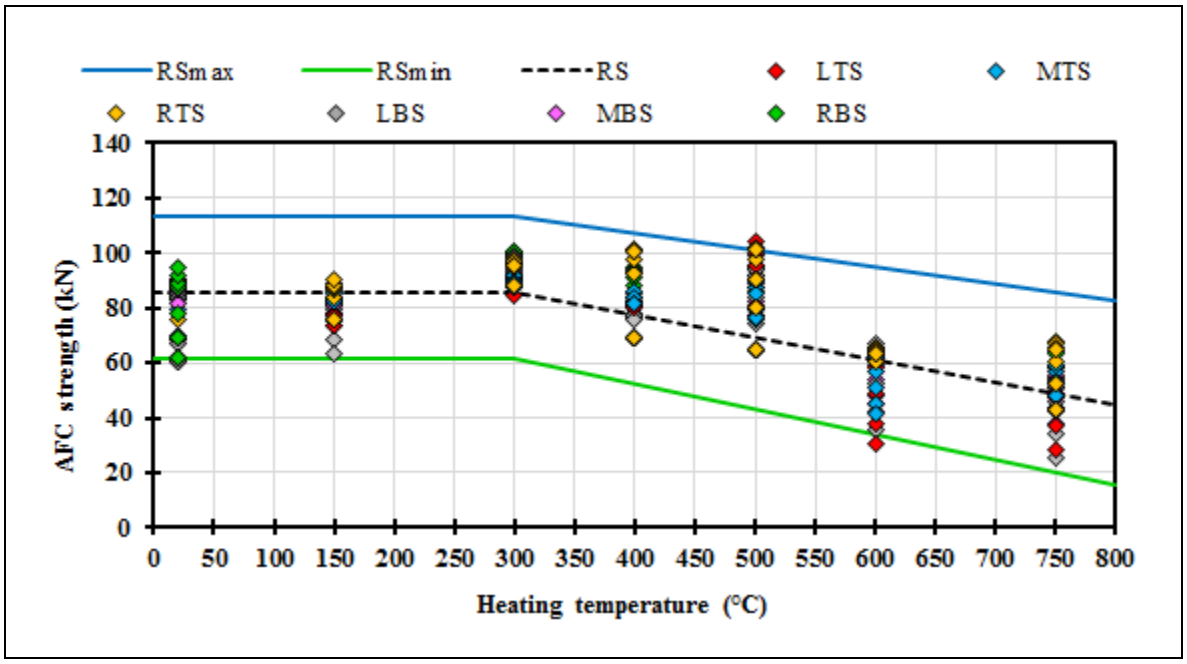

Figure 1.12. Comparison between experimental AFC strength and predicted AFC strength for AFCs at room temperature and for AFCs after heating and cooling.

It can be seen in Figure 1.12 that out of the 294 experimental AFC strength values only 5 experimental AFC strength values (1.7%) were not enclosed by the area delimited by the maximum and minimum theoretical AFC strengths. Thus, the maximum and minimum theoretical AFC strengths enveloped 98.3% of the experimental AFC strength values. It can also be seen that by considering a linear trend on the expressions that define the maximum and minimum theoretical AFC strengths, a conservative approach can be made at predicting AFC strength. For this reason, the theoretical model presented to predict the minimum and maximum AFC strengths after have heating and cooling can be considered simple and conservative.

CONCLUSIONS

This paper describes the effects of subjecting AFCs with Bisalloy 500 shims to a heating regime with temperatures of 20°C-750°C. It was shown that:

i. The Brinell hardness for Grade 300 steel plates did not change significantly with heating temperature up to 750°C. For the Bisalloy 500 shims after a temperature of 300°C the hardness dropped by 63.9% at 750°C. The ultimate strength, the yielding strength, and the elastic modulus of Grade 300 steel plates reduced up to 7.7%, 16.2%, and 12.5%, respectively at 750°C. The ultimate strength of Grade 8.8 galvanized bolts, reduced up to 1.3% for heating temperatures below 400°C, and reduced up to 49.9% for heating temperatures of 750°C. The elastic modulus of Grade 8.8 galvanized bolts, reduced up to 3.1% for heating temperatures below 600°C, and reduce up to 27.9% for heating temperatures of 750°C.

ii. The hysteresis loop stability for AFCs heated below 300°C was stable and the AFC strength was almost constant. For AFC heated to 750°C the hysteresis loop stability decreased and the AFC strength in some cases increased or decreased. Reasons for these were attributed to the degradation mechanism.

iii. For heating temperatures below 150°C the effective friction coefficient was almost constant varying between 0.17 – 0.23 and 0.16 – 0.21 for the first run and second run of the displacement input, respectively. For heating temperatures of 150°C - 750°C the effective friction coefficient increased or reduced and varied between 0.11 – 0.24 and 0.03 – 0.16 for the first run and second run of the displacement input, respectively.

iv. Strength degradation from the first to the second run of the displacement input was 4% - 17% were reported for AFCs heated to 150°C, and 35% - 85% for AFCs heated to 750°C.

v. For AFCs similar to those tested, the strength considering heating can be estimated. The average estimation, using the dry friction theory of Coulomb, results in an effective friction coefficient of 0.22. This is multiplied by an empirically derived non-dimensional heating factor. The maximum and minimum likely AFC strengths can also be obtained by factoring the average AFC strengths using factors derived indicating overstrength and understrength limits.

ACKNOWLEDGEMENTS

The authors would like to acknowledge funding from MBIE Natural Hazards Research Platform (NHRP), and material donation from John Jones Steel Ltd., for undertaking this research. All opinions expressed remain those of the authors.

REFERENCES

[1.1] Khoo, H.H., Clifton, C., Butterworth, J., MacRae, G. and Ferguson, G. (2011). *Influence of steel shim hardness on the Sliding Hinge Joint.* Journal of Constructional Steel Research. Vol 72, May 2012, p 119 – 129. https://doi.org/10.1016/j.jcsr.2011.11.009

[1.2] Clifton, G.C. (2005). Semi-Rigid Joints for Moments Resisting Steel Framed Seismic Resisting Systems. *Published PhD Thesis, Department of Civil and Environmental Engineering.* University of Auckland – New Zealand.

[1.3] Rodgers, GW, Chase, JG, Causse, R, Chanchi Golondrino, J and MacRae, GA (2017). *Performance and Degradation of Sliding Steel Friction Connections: Impact of Velocity, Corrosion Coating and Shim Material*. Engineering Structures. Vol. 141, pp. 292–302. ISSN: 0141-0296. https://doi.org/10.1016/j.engstruct.2017.02.070.

[1.4] MacRae, G.A., Clifton, C.G., MacKinven, H., Mago, N., Butterworth, J., Pampanin, S. (2010). *The Sliding Hinge Joint Moment Connection*. Bulletin of the New Zealand Society for Earthquake Engineering. Vol 43, Issue 3, pp. 202-212.

[1.5] Kirby, B. R. (1995). *The Behaviour of High – Strength Grade 8.8 Bolts in Fire*. Journal of Construction Steel Research, Vol.33 (1-2), pp. 3-38. https://doi.org/10.1016/0143-974X(94)00013-8.

[1.6] Sakumoto, Y., Keira, K, Furumura, F. & Ave, T. (1993). *Test of Fire Resistant Bolts and Joints*. Journal of Structural Engineering ASCE, Vol.119 (11), pp. 3131-3150. https://doi.org/10.1061/(ASCE)0733-9445(1993)119:11(3131)

[1.7] Yu, L. (2006). *Behaviour of Bolted Connection During and After a Fire.* Unpublished PhD Thesis, Faculty of Engineering. University of Texas – United States.

[1.8] Karlsson, B and Quintiere, JG (2000). *Enclosure Fire Dynamics*. CRC press LLC, Florida – United States.

[1.9] Borzouie, J, Chase, JG, MacRae, GA and Rodgers, GW (2015). *Experimental Studies on Cyclic Performance of Column Base Weak Axis Aligned Asymmetric Friction Connection*. Journal of Constructional and Steel Research (JCSR), Vol 112, pp. 252-262. https://doi.org/10.1016/j.jcsr.2015.05.007

[1.10] Borzouie, J, Chase, JG, MacRae, GA, Rodgers, GW and Clifton, C (2016). *Experimental Studies on Cyclic Performance of Column Base Strong Axis Aligned Asymmetric Friction Connections*. ASCE J. Structural Engineering, Vol 142(1), Article 04015078, 10-pages. ISSN: 0733-9445. https://doi.org/10.1061/(ASCE)ST.1943-541X.0001327

[1.11] Khoo, H.H., Clifton, G.C., MacRae, G.A., Zhou, H., and Ramhormozian, S. (2014). *Proposed design models for the asymmetric friction connection*. Earthquake and Structural Dynamics Journal. Vol 44, Issue 8, pp. 1309-1324. https://doi.org/10.1002/eqe.2520

[1.12] Rodgers, GW, Mesnil, O, Chanchi Golondrino, J, MacRae, GA and Chase, JG (2014). *Generalised nonlinear modeling of unstable stick-slip force reduction effects in friction energy dissipation devices*. Bulletin of the New Zealand Society for Earthquake Engineering, Vol 47(3), pp. 217-223, ISSN No. 1174-9857.

[1.13] MacRae, G.A., and Clifton, C.G. (2015). *Research on Seismic Performance of Steel Structures*. Steel Innovation Conference 2015. September 3-4, 2015, Auckland, New Zealand.

Chapter 2

Surface Treatments and Corrosion Effects on the Hysteretic Behaviour of Asymmetric Friction Connections (AFCs) with High Hardness Steel Shims

Chapter 2

"Surface Treatments and Corrosion Effects on the Hysteretic Behaviour of Asymmetric Friction Connections (AFCs) with High Hardness Steel Shims"

Jose Christian Chanchi Golondrino [a, b,1*], Gregory Anthony MacRae[b,2], James Geoffrey Chase[c,3], Geoffrey William Rodgers[c,4], Allan Charles Nye Scott [b,5], George Charles Clifton[d,6]

[a] Universidad Nacional de Colombia, Departamento de Ingeniería Civil, Manizales 170004, Colombia.

[b] University of Canterbury, Department of Civil and Natural Resources Engineering, Private Bag 4800, Christchurch 8140, New Zealand.

[c] University of Canterbury, Department of Mechanical Engineering, Private Bag 4800, Christchurch 8140, New Zealand.

[d] The University of Auckland, Department of Civil & Environmental Engineering, Faculty of Engineering, Private Bag 92019, Auckland Mail Centre, Auckland 1142, New Zealand.

[1] jcchanchigo@unal.edu.co, [2]gregory.macrae@canterbury.ac.nz, [3]geoff.chase@canterbury.ac.nz, [4]geoff.rodgers@canterbury.ac.nz, [5]allan.scott@canterbury.ac.nz, [6]c.clifton@auckland.ac.nz

[*]Corresponding author

Key words: Steel building connection, Friction connections, Low damage dissipaters, Corrosion, Surface treatment.

ABSTRACT

Asymmetric Friction Connections (AFCs) dissipate energy in structural systems. Surface treatments and severe corrosion effects on AFC strength, and the corrosion mechanism of AFCs have not been explained yet. A total of 12 AFCs were surface treated, exposed to a severe corrosive regime, and cyclically loaded. Surface treatments, such as cleaned, sweep blasted, alkyd coated, and zinc coated surfaces were considered. AFC strength and the stability of the hysteresis loop of the connection were sensitive to both surface treatment and corrosion. AFCs developed general, crevice, and filiform corrosion not only at the external

surfaces, but also at the internal clamped surfaces for some surface treatments. As a result of corrosion, connection strength increased at the initial sliding cycles up to 100%, 120%, 130%, and 50% for cleaned, sweep blasted, alkyd coated, and zinc coated surfaces, respectively. After the corrosive product is removed by the sliding of the slotted plate, the connection strength returned to approximately the strength of the non-corroded connections. These results were used to propose a model to predict the maximum and minimum likely AFC strengths when plate surfaces of the plates are treated, and when these four surface treatments are severely corroded. The experimental results, and resulting model, provide significant insight and design tools for the practical use of AFCs in design.

I. INTRODUCTION

AFCs are friction bolted connections used to dissipate seismic energy. AFCs can be assembled using three Grade 300 steel plates, two thin plates termed shims made of high hardness materials, such as Bisalloy 400 or Bisalloy 500, and high strength structural bolts, such as Grade 8.8 bolts. AFCs dissipate energy via friction when a slotted plate is forced to slide over the shims [2.1, 2.2, 2.3]. The sliding force of the resulting approximately square hysteresis loop is termed the AFC strength, and quasi-static testing has shown it may be almost constant [2.1]. AFCs can be used as seismic dissipaters in moment resistant frames at the beam column joint, or in braced frames [2.1, 2.3, 2.4].

Applications of AFCs have been restricted to structural systems located in interior environments or environments where atmospheric conditions will not corrode AFC components, or AFCs without surface treatment on the sliding interfaces [2.2]. In particular, there is no robust experimental data describing the effect of severe corrosion on the hysteretic

behaviour of AFCs. There are also no experimental studies examining how AFC surface treatments under severe corrosion modifies AFC hysteretic behaviour. Some evidence that surface treatments and corrosion compromise the performance of AFCs is based on the reduction in hysteresis loop stability and strength observed in AFCs with treated surfaces and cyclically tested after a preliminary corrosion testing [2.3]. However, the AFCs in this study were not severely corroded. To date there is no study describing:

i. The types of corrosion and corrosion mechanism developed in AFCs with different surface treatments when exposed to a severe corrosive environment.
ii. The effects of surface treatment and severe corrosive environments on AFC strength, friction coefficient, and hysteretic performance.
iii. A simple model to assess the AFC strength considering the effects of surface treatment and severe corrosive environment.

There is a need to understand and characterize this behaviour. To address these needs, this paper seeks answers to following questions:

i. What types of corrosion develop in AFCs with different surface treatments under a severe corrosive regime?
ii. What is the corrosion mechanism of AFCs with different surface treatments, and what is the most efficient surface treatment to protect AFCs under a severe corrosive regime?
iii. What are the effects of different surface treatments on the hysteretic behaviour of AFCs?
iv. What are the effects of a severe corrosion regime on the hysteretic behaviour of AFCs with different surface treatments?
v. What are the effects of surface treatments and severe corrosion on the effective friction coefficient of AFCs?

vi. Is there a simple model to assess AFC strength considering the effects of different surface treatments and corrosion?

II. MATERIALS AND METHODS

2.1 AFC dimensions

Two types of AFC specimens were assembled: AFCs joints and full scale AFCs. AFC joints were used for describing the effects of corrosion on bolts and sliding surfaces after AFC joints were subjected to accelerated corrosion conditions. Full scale AFCs were used for assessing the hysteretic behaviour after full scale AFCs were subjected to accelerated corrosion conditions. For both, AFC joints and full scale AFCs, the corrosion rate achieved during the corrosion testing was assessed.

Both AFC specimens were assembled using Bisalloy 500 shims of 6mm thickness, and Grade 300 steel plates of 20mm thickness for the fixed, slotted, and cap plates. They were clamped using 2 M16 Grade 8.8 structural galvanized bolts of 110mm length with unthreaded length of 72mm and threaded length of 38mm. Bolts were assembled using a structural washer of 4mm thickness, a flat washer of 4mm thickness, and a single Belleville washer of 2.5mm at the fully squashed condition, as shown in Figures 2.1a-e. Belleville washers were used to reduce the variation of the clamping force on the bolts due to degradation of the sliding surfaces [2.1]. In both configurations, the slotted plate has a slot length of 220mm and a bolt grip length of 82.5mm. The bolt grip length was calculated as 3 x 20mm for the plates, plus 2 x 6mm for the shims, plus 4.0mm for the structural washer, 4.0mm for the flat washer, and 2.5mm for the flattened Belleville washer.

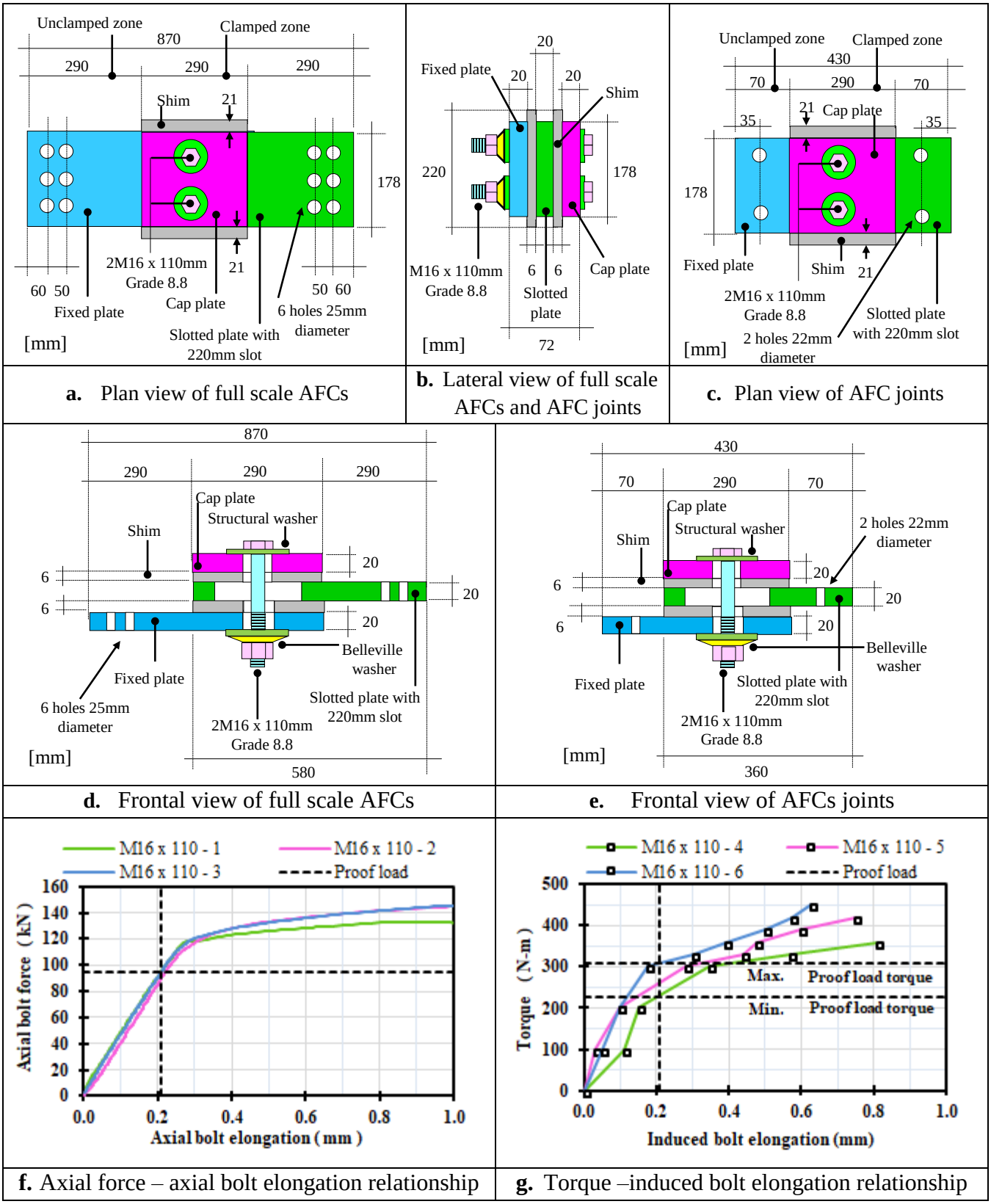

a. Plan view of full scale AFCs

b. Lateral view of full scale AFCs and AFC joints

c. Plan view of AFC joints

d. Frontal view of full scale AFCs

e. Frontal view of AFCs joints

f. Axial force – axial bolt elongation relationship

g. Torque –induced bolt elongation relationship

Figure 2.1. Dimensions of full scale AFCs and AFCs joints, and assembly relationships (Not to scale)

Both AFC specimens comprised one clamped zone and two unclamped zones. The clamped zone is defined as the zone carrying the compression induced by the 2 M16 Grade 8.8 galvanized bolts. This clamped zone has same dimensions for both configurations, as shown in Figures 2.1a-e, since the interest of this research is describing the behaviour of this zone during the corrosion testing, and the effects of corrosion in the hysteretic behaviour of this zone. The unclamped zones are defined as the zones of the fixed and slotted plate free of the compression induced by the 2 M16 Grade 8.8 galvanized bolts, and that are located beside the cap plate. The unclamped zones for full scale AFCs are used to allow the slotted plate to slide across one half of the slot length during the quasi-static testing, and for AFC joints, these zones are only used for manipulating the samples during the corrosion testing. For that reason, the unclamped zones of the AFC joints and full scale AFCs have the same width, but the length of the unclamped zone of the AFC joints is 24.1% of the length of the unclamped zone of the full scale AFCs, as shown in Figures 2.1a-e.

2.2 Surface treatments

Prior to assembly the AFC joints and the full scale AFCs, the entire surfaces of the fixed plate, of the slotted plate, the cap plate, and the shims were treated. Treatment was not applied to bolt holes. Surface treatments include: cleaned surfaces, sweep blasted surfaces, alkyd coated surfaces, and zinc coated surfaces. These surface treatments are described in Table 2.1. Table 2.1 also presents for each surface treatment, the AFC specimen initial mass, W, and the AFC specimen external area, A. The AFC specimen initial mass, W, is defined as the mass of an AFC specimen before corrosion. It was calculated as the average of the mass obtained experimentally for 3 AFC specimens after surface treatment was applied and assembly was undertaken. The AFC specimen external area, A, is defined as the area of an

AFC specimen that can be exposed to the corrosive agent during the corrosion testing, and it considers the plan, lateral, and frontal areas of the AFC specimen plates presented in Figures 2.1a – e ignoring the bolts and washers at the clamped zone. The AFC specimen external area, *A*, was calculated as twice the lateral area plus twice the frontal area ignoring the bolt holes and the slot, and plus twice the plan area considering the bolt holes at the unclamped zones, ignoring the bolt holes at the clamped zone, and considering four times the plan area of the shims at both sides of the clamped zone.

Table 2.1 Description of surface treatments applied on full scale AFCs and AFCs joints, and AFC joints initial mass and external area

Surface treatment	**Dry Film Thickness** **DFT microns**	**Surface treatment description**	**AFC joint initial mass** **W grams**	**AFC joint external area** **A cm^2**	**Full scale AFC initial mass** **W grams**	**Full scale AFC external area** **A cm^2**
Cleaned	Not applicable	Removing impurities over all surfaces of plates and shims by means of a rubbing the surfaces with rag impregnated of thin layer of acetone	31854.0	2727.6	43352.0	4441.5
Sweep blasted	40	Blasting all surfaces of plates and shims with Ilmenite sand with a size of 150microns - 180microns as defined by [2.5].	31849.0	2727.6	43420.0	4441.5
Coated with alkyd	40	Application of Alkyd Primer over all surfaces of plates and shims as defined by [2.6].	31967.0	2727.6	43552.0	4441.5
Coated with zinc	75	Application of inorganic Zinc Silicate over all surfaces of plates and shims as defined by [2.6].	31911.0	2727.6	43408.0	4441.5

2.3 AFC assembly

A total of 12 full scale AFCs and 12 AFC joints were assembled and divided into 4 groups of 3 specimens each. The 4 groups of full scale AFCs and 4 groups of AFC joints matched

with the 4 types of the surface treatment defined in Table 2.1. Full scale AFCs and AFCs joints were assembled by tensioning bolts in the clamped zone of the specimen up to the proof load of 95kN for a Grade 8.8 M16 bolt using the torque control method. In this method, a bolt is gradually tensioned to a torque that develops an axial elongation equivalent to the elongation that the bolt develops when it reaches the proof load in axial tensile testing. This torque is termed proof load torque, and the elongation of the bolt, when it reaches the proof load in axial tensile testing, is termed proof load elongation.

The proof load elongation of 0.21mm, which occurred over the grip length of 82.5mm, was read from an axial tensile testing relationship from 3 bolts using the proof load value, as shown in Figure 2.1f. The proof load torque of 270N-m was assessed as the average of the maximum and minimum torques read from a torque - induced bolt elongation relationship for 3 bolts using the proof load elongation value, as shown in Figure 2.1g.

2.4 Corrosion testing

Full scale AFCs and AFC joints were subjected to an accelerated cyclic corrosion regime capable of producing an equivalent uniform corrosion rate greater than 80μm/year, which represents the minimum corrosion rate exhibited by mild steel in a very high corrosive environment based on site corrosion studies [2.6]. The accelerated corrosive regime comprised 120 cycles with a duration per cycle of 1 day. Each cycle comprises two stages: i) an immersion stage with a duration of 12 hours, where AFC specimens were immersed in a salt water solution at 40°C with a salt concentration of 3.5% and an oxygen concentration of approximately 5.7mg/lt, as shown in Figure 2.2a; and ii) a steaming stage with a duration of 12 hours, where the AFC specimens were exposed to steam at 40°C produced from heating

the salt water solution used in the immersion stage, as shown in Figure 2.2a. Every 10 cycles, the salt water solution was changed, the AFC specimens were cleaned with a clean water blaster to remove any of the corrosive product, and the mass of the AFC specimens was determined after water cleaning.

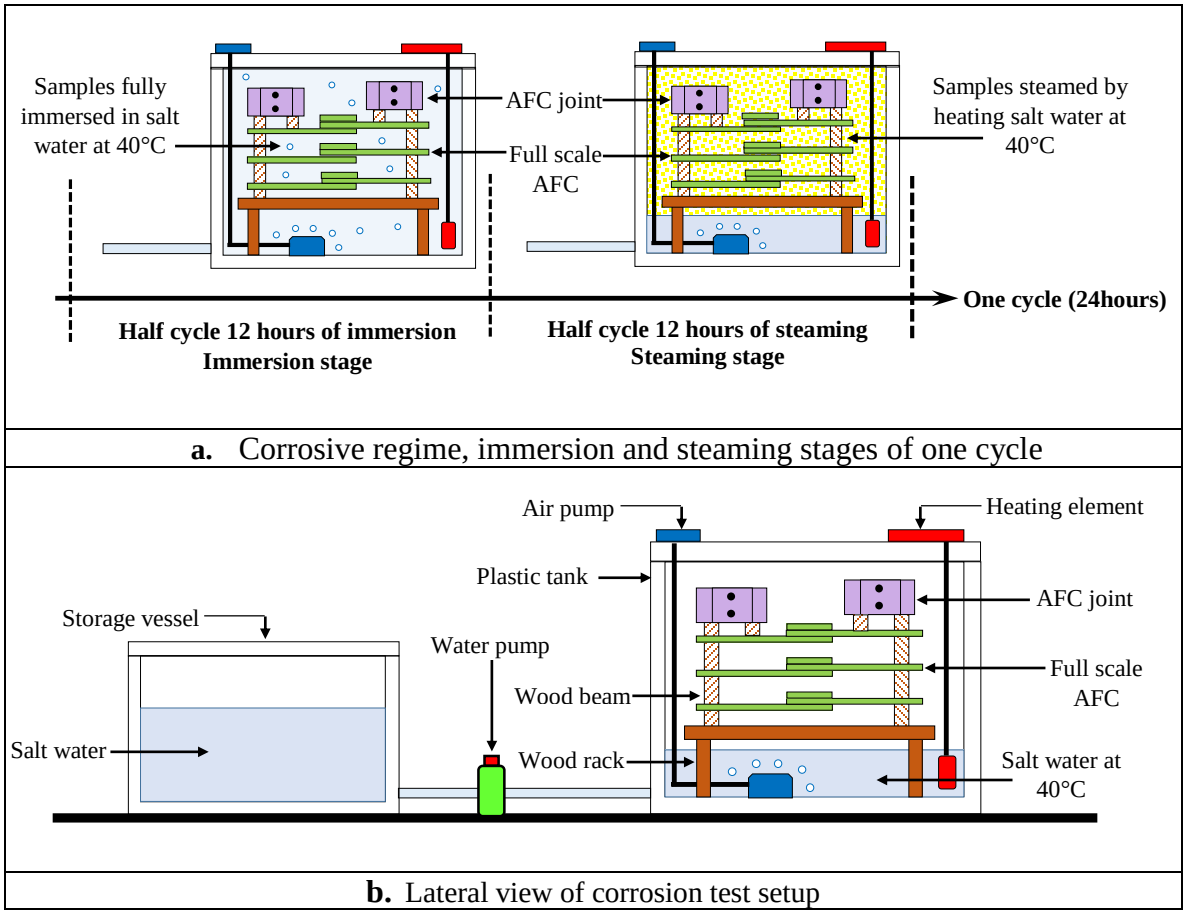

a. Corrosive regime, immersion and steaming stages of one cycle

b. Lateral view of corrosion test setup

Figure 2.2. Corrosion test setup and corrosive regime for full scale AFCs and AFCs joints (Not to scale)

The corrosion test setup comprised a plastic tank equipped with a heating element with a digital temperature controller for heating the salt water solution, an air pump for injecting air to the salt water solution, and a storage vessel equipped with a water pump for filling or draining the salt water solution of the plastic tank. This system is shown in Figure 2.2b. AFC specimens were placed in the two top vertical thirds of the plastic tank depth supported on a

wood rack, and separated vertically and horizontally to allow each AFC specimen to develop its own corrosion mechanism, as also shown in Figure 2.2b. The corrosion test set up as well as the accelerated corrosive regime described above were proposed using as reference the corrosion testing procedures defined by ASTM G31 [2.7] and ASTM G60 [2.8].

2.5 Quasi-static testing

Quasi–static testing was undertaken in full scale AFCs with surface treatment after assembly, and in full scale AFCs with surface treatment and corrosion after drying at room temperature over 30 days until reaching constant mass. This approach ensures the sliding surfaces of the full scale AFCs were dried. Full scale AFCs were quasi-statically tested using a shake table to provide a strictly horizontal input at the required force level, thus minimizing prying effects that reduce AFC strength [2.9, 2.10]. The test setup comprised a fixed bracket attached to a reaction frame bolted to a reaction floor, and a moving bracket attached to a reaction frame bolted to a shaking table. Full scale AFCs were connected using 6 M24 Grade 8.8 bolts at each end. A load cell was placed between the fixed bracket and the reaction frame, and a potentiometer was placed across the connection stroke. Details are shown in Figure 2.3a.

The displacement inputs are defined in Figure 2.3b and comprise 21 sinusoidal cycles with a maximum velocity of 10mm/s and amplitudes varying from 0 to ± 95mm. This amplitude is 95% of the full 220mm slot length. The peak velocity of 10mm/s is slow enough to minimise velocity dependent effects [2.3]. Each AFC was run twice with no bolt re-tensioning and with a 30-minute break for cooling the AFC; thus, removing the friction heat from the first run.

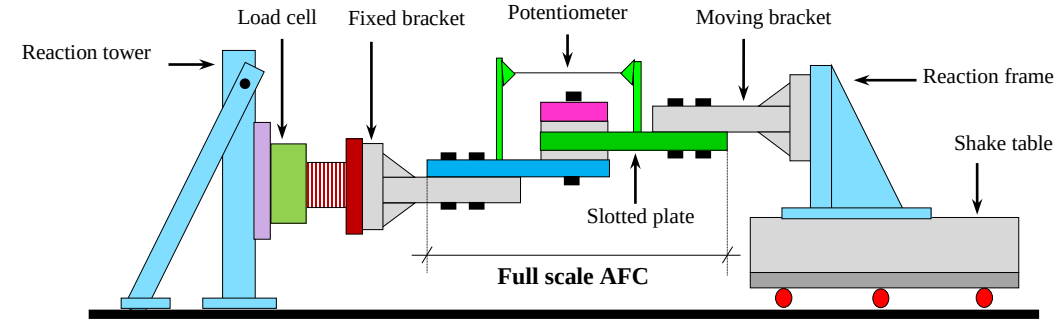

a. Frontal view of the test setup

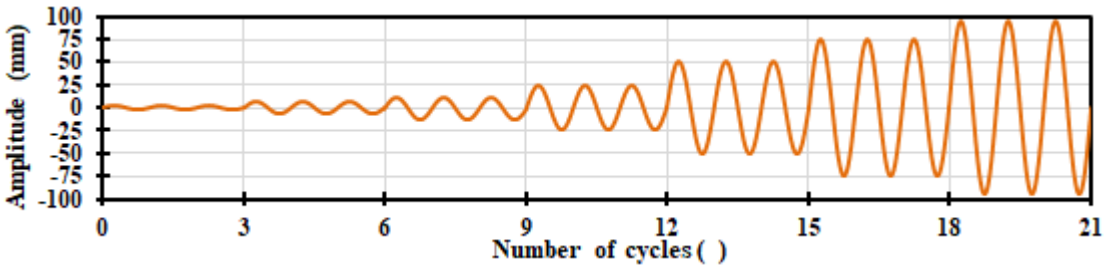

b. Displacement input

Figure 2.3. Setup of AFCs and displacement input (Not to scale)

2.6 Assessment of corrosion rate in AFCs

The corrosion rate, *CR*, was calculated from the mass loss of the AFC specimens subject to accelerated corrosion conditions. The corrosion rate is expressed in micrometres per year (µm/year) and it can be determined [2.7]:

$$CR = 36500 \times \frac{W \times P}{A \times T \times D} \quad (2.1)$$

Where W is the initial mass of the AFC specimen in grams, P is the mass loss expressed as percentage of the initial mass of the AFC specimen and that varies between 0% and 100%, A is the external area of the AFC specimen in cm^2, T is the time of duration of the corrosive regime in days or cycles (note that 1cycle = 1day), and D is the density of the material of the AFC specimen in gr/cm^3.

2.7 Assessment of equivalent real corrosion exposure time

The equivalent real corrosion time, *Tr*, is defined as the time in years that would be required for the AFC specimens to develop the minimum design corrosion penetration in a very high corrosive environment (45μm/year) [2.11]. The equivalent corrosion time, *Tr*, in years can thus be determined:

$$Tr = 100 \times \left[\frac{W \times P}{A \times D \times 45} \right] \quad (2.2)$$

Where *W* is the initial mass of the AFC specimen in grams, *P* is the mass loss expressed as percentage of the initial mass of the AFC specimen and that varies between 0% and 100%, *A* is the external area of the AFC specimen in cm^2, *D* is the density of the material of the AFC specimen in gr/cm^3, and *45* is the minimum design corrosion rate defined for mild steel in a very high corrosive environment in μm/year [2.11]. It should be noted that in Equation 2.2 the equivalent real corrosion time, *Tr*, is calculated with the minimum design corrosion rate for mild steel, since there is not available experimental information for the minimum design corrosion rates for surface treatments such as sweep blasted surfaces, alkyd coated surfaces, and zinc coated surfaces.

2.8 Assessment of experimental AFC strength

The experimental AFC strength, *S*, of a full scale AFC at a given hysteresis loop amplitude was assessed by reading the force values at the four corners and at the two zero displacement points of the hysteresis loop, as shown in Figure 2.4.

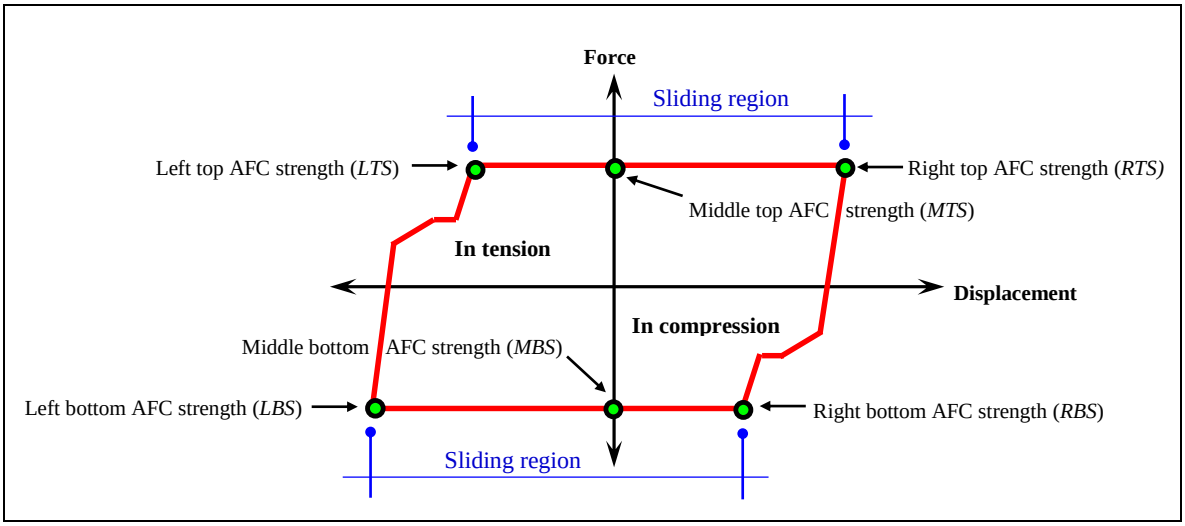

Figure 2.4. Assessment points of experimental AFC strength at a given hysteresis loop amplitude

The average experimental AFC strength, *Sa*, was assessed as the average absolute value of the tension and compression sliding regions of the hysteresis loop, and it is defined:

$$Sa = \left[\frac{\left(LTS + MTS + RTS\right) + \left|LBS + MBS + RBS\right|}{6} \right] \quad (2.3)$$

Where, *LTS*, *MTS*, and *RTS* are the experimental AFC strengths at the tension sliding region of the hysteresis loop, and *LBS*, *MBS*, and *RBS* are the experimental AFC strengths at the compression sliding region of the hysteresis loop, as shown in Figure 2.4.

2.9 Assessment of the effective friction coefficient

The effective friction coefficient is a non-dimensional factor defined as the ratio between the AFC strength and the total clamping force induced by the bolts on the AFC [2.12]. This friction coefficient is termed effective because it is not constant due to any degradation of the AFC sliding surfaces, any surface coating [2.3], and the materials used [2.13]. For ease,

it is evaluated by considering that the clamping force remains constant regardless of any degradation of the sliding surfaces. The effective friction coefficient, μ_e, can thus be determined:

$$\mu_e = \frac{Sa}{m \times n \times F_{proof}} \quad (2.4)$$

Where, *Sa* is the average experimental AFC strength as defined in Section 2.8 and calculated with Equation 2.3, *m* is the number of bolts, *n* is the number of shear planes, and F_{proof} is the proof load per bolt.

2.10 Assessment of the hysteresis loop stability

The hysteresis loop stability is defined as how repetitive is the shape of the hysteresis loop as the displacement amplitude increases. It is assessed qualitatively. The hysteresis loop is termed stable when the loop shape is repeated with the hysteresis loop amplitude, and unstable when the loop shape is not repeated with the hysteresis loop amplitude.

III. RESULTS AND ANALYSIS

3.1 Types of corrosion developed in AFCs specimens

General corrosion, defined as the uniform loss of mass accompanied by the uniform presence of corrosion product and surface deterioration from smooth to very rough, was developed in AFC specimens with the four surface treatments, as shown in Figure 2.5. In the present investigation, the general corrosion also includes shallow pits, which were observed over the surface of the AFC specimens. At the external surface of AFC specimens, general corrosion was significantly developed across the full surfaces of the four surface treatments, and the

greatest general corrosion was developed by AFCs with cleaned, and sweep blasted surfaces, and the lowest by AFCs with zinc coated surfaces, as shown in Figure 2.5. At the internal surfaces of AFC specimens, the corrosion process was likely that of crevice corrosion but had the same general appearance as the external corroded surfaces. Some corrosion was observed across the full internal surfaces of AFC specimens with cleaned and sweep blasted surfaces, and only limited corrosion initiating from the edges to internal regions of the internal surfaces in AFC specimens with alkyd and zinc coatings, as shown in Figure 2.5.

Filiform corrosion, defined as the coating deterioration due to grow of white fine filaments in a random pattern that turned the coating in a light rusty veined surface with no major changes in smoothness or mass [2.14], was developed in AFC specimens with sweep blasted, alkyd coating, and zinc coating treatments, as shown in Figure 2.5. Filiform corrosion was developed prior to general corrosion, and it first developed on the external surfaces and then on the internal surfaces of AFC specimens, as shown in Figures 2.5c - d.

Galvanized bolts developed first filiform corrosion and then general corrosion from the external to the internal surfaces of the AFC specimens, as shown in Figure 2.5. Greatest general corrosion was developed in bolts of AFCs with alkyd and zinc coated surfaces, as shown in Figures 2.5c - d.

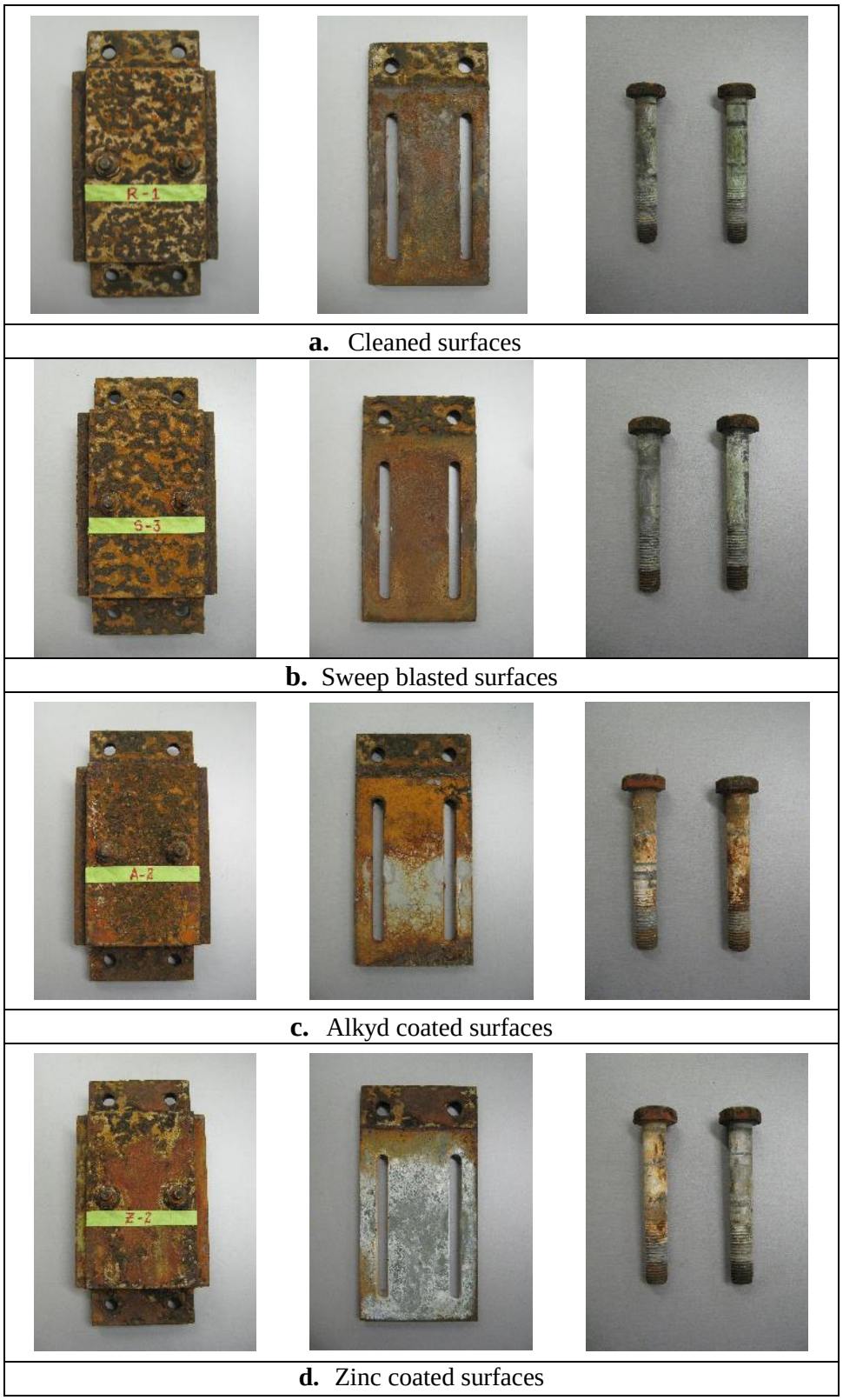

a. Cleaned surfaces

b. Sweep blasted surfaces

c. Alkyd coated surfaces

d. Zinc coated surfaces

Figure 2.5. AFC joint and slotted plate with the four surface treatments and Grade 8.8 galvanized bolts after corrosion testing

3.2 Corrosive mechanism of AFCs

Figure 2.6 shows the average corrosion rate and the average mass loss for 3 AFC joints, and for 3 full scale AFCs exhibited by each of the four surface treatments during the corrosion testing. Corrosion rates were assessed with Equation 2.1 using a material density, *D*, of 7.85gr/cm^3, the percentages of mass loss, *P*, and the exposure times, *T*, indicated in Figure 2.6b, and the external areas, *A*, and the initial masses, *W*, indicated in Table 2.1. In Figure 2.6 the mass loss percentage and the corrosion rate for full scale AFCs are only presented for the second half of the corrosion testing, since the cleaning and mass control process defined in Section 2.4 were undertaken for these specimens only on this period in order to check if by the end of the corrosion testing, full scale AFCs and AFC joints would develop the same corrosion mechanisms.

Two types of corrosive mechanisms can be observed in Figure 2.6 according to the surface treatment:

i. For AFC joints with cleaned surface treatment, the corrosion rate increased almost linearly as the corrosive cycles increase, as shown in Figure 2.6a. This linearly increasing corrosion rate implies a parabolic decreasing mass with time as shown in Figure 2.6b. This corrosive mechanism is based on mass loss produced by general corrosion, which is activated at the initial corrosive cycles due to absence of a coating barrier that protects AFC joint surfaces from corrosive deterioration. This mechanism is similar to that developed for full scale AFCs, since the mass loss percentage and the corrosion rate trends exhibited for full scale AFCs had the same trend as those exhibited by AFC joints, as shown in Figures 2.6a - b. Figures 2.6 shows AFC joints and full scale AFCs with cleaned surface treatment

underwent after 120 corrosive cycles a resulting total corrosion rate of 974.5μm/year and 848.3μm/year, for a total mass loss respect to the initial mass of 2.15% and 2.24%, respectively. The corrosion rates for AFC joints and full-scale AFCs with cleaned treatment correspond to an equivalent real corrosion exposure time, *Tr*, of 6.2 – 7.1years. Here, the equivalent real corrosion exposure time, *Tr*, was assessed according to Section 2.7 using the mass losses described above, a material density, *D*, of 7.85gr/cm^3, the external areas, *A*, and the initial masses, *W*, indicated in Table 2.1.

ii. For AFC joints with sweep blasted, alkyd coated, and zinc coated treatments, the corrosion rate is null for certain amount of corrosion cycles, and then it increased almost linearly as the corrosive cycles increase, as shown in Figure 2.6a. This corrosive mechanism keeps AFC joint mass almost constant for a certain number of cycles due to the development of filiform corrosion. However, subsequently, mass loss is activated due to general corrosion and it increased almost parabolic. This mechanism is similar to that developed for full scale AFCs, since the mass loss percentage and the corrosion rate trends exhibited for full scale AFCs had the same trend as those exhibited by AFC joints, as shown in Figures 2.6a. Figure 2.6b shows activation of mass loss occurred after 20, 40, and 110 corrosive cycles, and after 120 corrosive cycles, for AFC joints mass losses respect to the initial masses were 2.05, 1.06, 0.25%, and for full scale AFCs were 1.86, 0.94, 0.16%, for sweep blasted, alkyd coated, and zinc coated treatments, respectively. Figure 2.6a shows after 120 corrosive cycles, AFC joints underwent resulting total corrosion rates of 933.8, 482.3, 111.8μm/year, and full scale AFCs underwent resulting corrosion rates of 705.2, 357.7, 61.4μm/year, for sweep blasted, alkyd coated, and zinc coated treatments, respectively. These corrosion rates for AFC joints and full scale AFCs with sweep blasted, alkyd coated and zinc coated

surfaces correspond to an equivalent real exposure corrosion times, *Tr*, of 5.1 – 6.8, 2.6 – 3.5, and 0.4 – 0.8years, respectively. Here, the equivalent real exposure corrosion time, *Tr*, was assessed according to Section 2.7 using the mass losses described above, a material density, *D*, of 7.85gr/cm^3, the external areas, *A*, and the initial masses, *W*, indicated in Table 2.1.

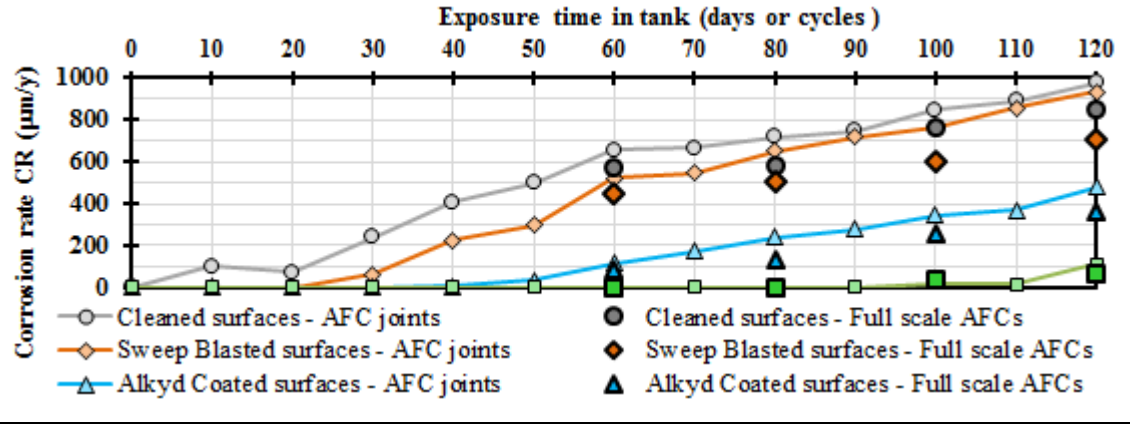

a. Corrosion rates during corrosion testing of AFCs joints with four surface treatments

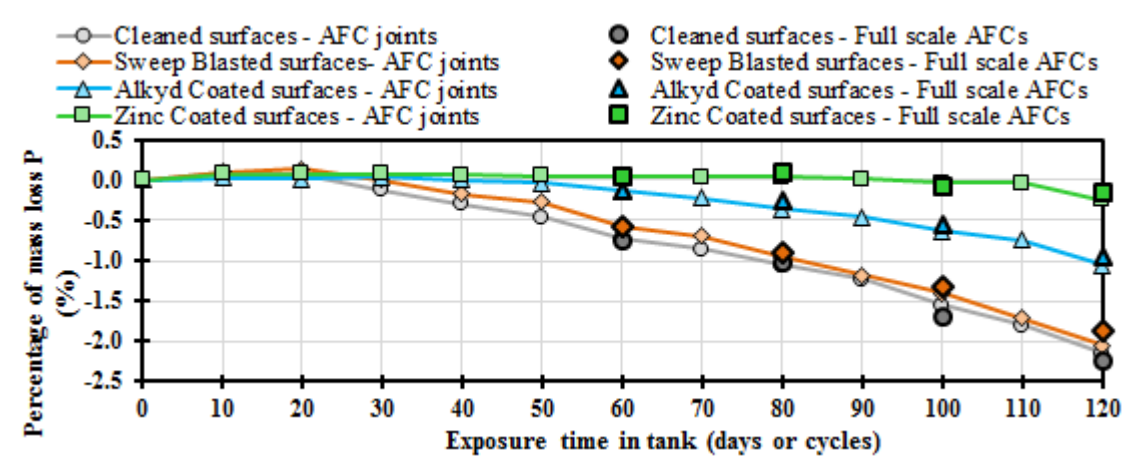

b. Mass loss during corrosion testing of AFCs joints with four surface treatments

Figure 2.6. Mass loss and corrosion rates recorded during corrosion testing for AFCs joints with four surface treatments

In the results described above, differences in percentage of mass loss and corrosion rate between the AFC joints and full scale AFCs are attributed to not undertaking the cleaning process defined in Section 2.4 in full scale AFCs during the first half of the corrosion testing,

which slightly delayed the development of the corrosive mechanism in these specimens. It should be also noted that undertaking the cleaning process every 10 cycles resulted in a higher measured rate of corrosion that would occur if the corrosion product was not removed and the AFC specimens were allowed to reach steady state corrosion conditions. From the results described, it can be stated that AFCs with cleaning and sweep blasted surface treatments exposed to a high corrosive environment can undergo significant corrosion rates. Surface treatments such as alkyd coated and zinc coated surfaces can be used to delay corrosive effects. Finally, the most effective surface treatment is zinc coated surfaces.

3.3 Effects of surface treatments on AFC hysteresis loop

Figure 2.7 compares hysteresis loops of full scale AFCs before corrosion with cleaned surfaces with hysteresis loop of full scale AFCs before corrosion with sweep blasted, alkyd coated and zinc coated surfaces. Figure 2.7 shows the average AFC strength as defined in Section 2.8 may change, and hysteresis loop stability as defined in Section 2.10 may reduce depending on the type of surface treatment.

For sweep blasted surfaces, the hysteresis loop stability decreased in both runs, and the average AFC strength increased by 15% and 10% for the first and second run, respectively, when compared with the stability and the average AFC strength for cleaned surfaces, as shown in Figure 2.7a. The reduction in hysteresis loop stability for sweep blasted surfaces when compared with cleaned surfaces can be seen on the repeatability of the AFC strength. While for cleaned surfaces the AFC strength is almost constant for whole cycles per run, for sweep blasted surfaces the AFC strength reduces as the cycles increase per run. These changes on the hysteresis loop stability and on the AFC strength for sweep blasted surfaces are attributed to the generation of a non-uniform surface roughness on the sliding surfaces

during the sweep blasting procedure, which increases the friction coefficient and develops a non-uniform mechanism of sliding surfaces degradation.

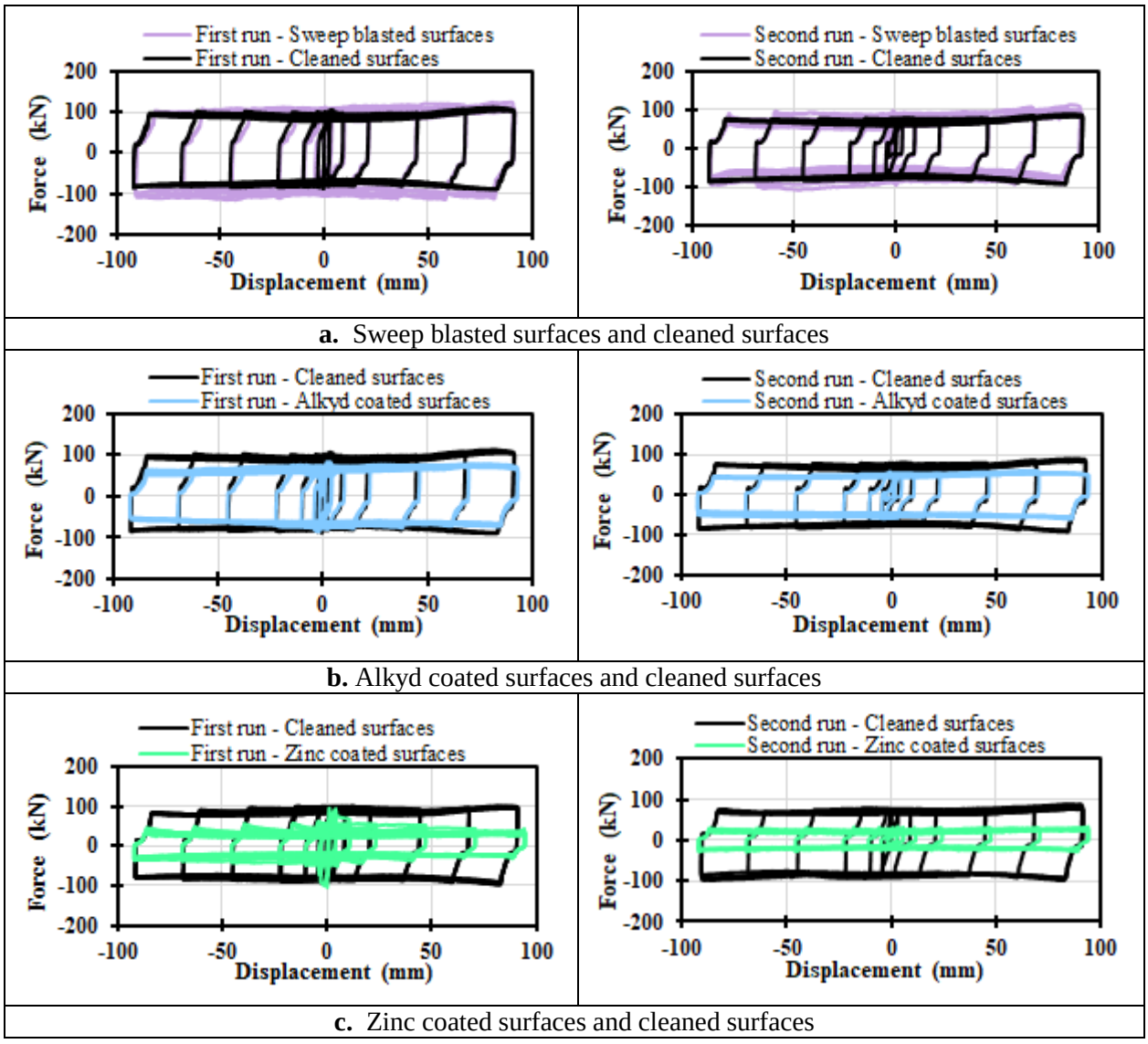

a. Sweep blasted surfaces and cleaned surfaces

b. Alkyd coated surfaces and cleaned surfaces

c. Zinc coated surfaces and cleaned surfaces

Figure 2.7. Hysteresis loop of full scale AFCs with four surface treatments before corrosion

Figures 2.7 b – c show for alkyd coated surfaces and zinc coated surfaces the hysteresis loop stability reduced in the first run, and it did not change in the second run, when compared with cleaned surfaces. That is because in the first run, while for cleaned surfaces the AFC strength is almost constant, for both, alkyd coated and zinc coated surfaces the AFC strength

decreased after the initial sliding cycles and then the AFC strength became almost constant, as shown in Figures 2.7b - c. The average AFC strength reduced for alkyd coated and zinc coated surfaces in the first run by 29% and 62%, respectively, and for the second run by 34% and 70%, respectively, as shown in Figures 2.7b - c. These reductions on the average AFC strength for alkyd coated and zinc coated surfaces are attributed to loss of bolt tension that occur when the coating at the sliding surfaces is either degraded or removed as the slotted plate slides. Once the degraded and removed coating particles are dragged and pushed out of the connection clamped zone, the connection plates move inwards reducing the bolt elongation and therefore reducing the bolt tension.

3.4 Effects of corrosion on AFC hysteresis loop

Figure 2.8 compares the hysteresis loop of the full scale AFCs after the corrosion testing to those before corrosion testing for the four surface treatments. For the four surface treatments, after corrosion, the overall hysteresis loop stability as defined in Section 2.10 decreased slightly, as shown in Figure 2.8. Also, for the four surface treatments, after corrosion, the AFC strength increased significantly in the initial sliding cycles. However, after the initial sliding cycles AFC strength decreased to an almost constant value approaching the AFC strength developed in the non-corroded condition, as shown in Figure 2.8. While for corroded cleaned and sweep blasted surfaces the almost stable AFC strength reduced with respect to the non-corroded case, for corroded alkyd coated and zinc coated surfaces it increased. Maximum increments in AFC strength in the initial sliding cycles with respect to average AFC strength in the non-corroded condition of 100%, 120%, 130%, and 50% were developed for the corroded cleaned, sweep blasted, alkyd coated, and zinc coated surfaces, respectively, as shown in Figure 2.8.

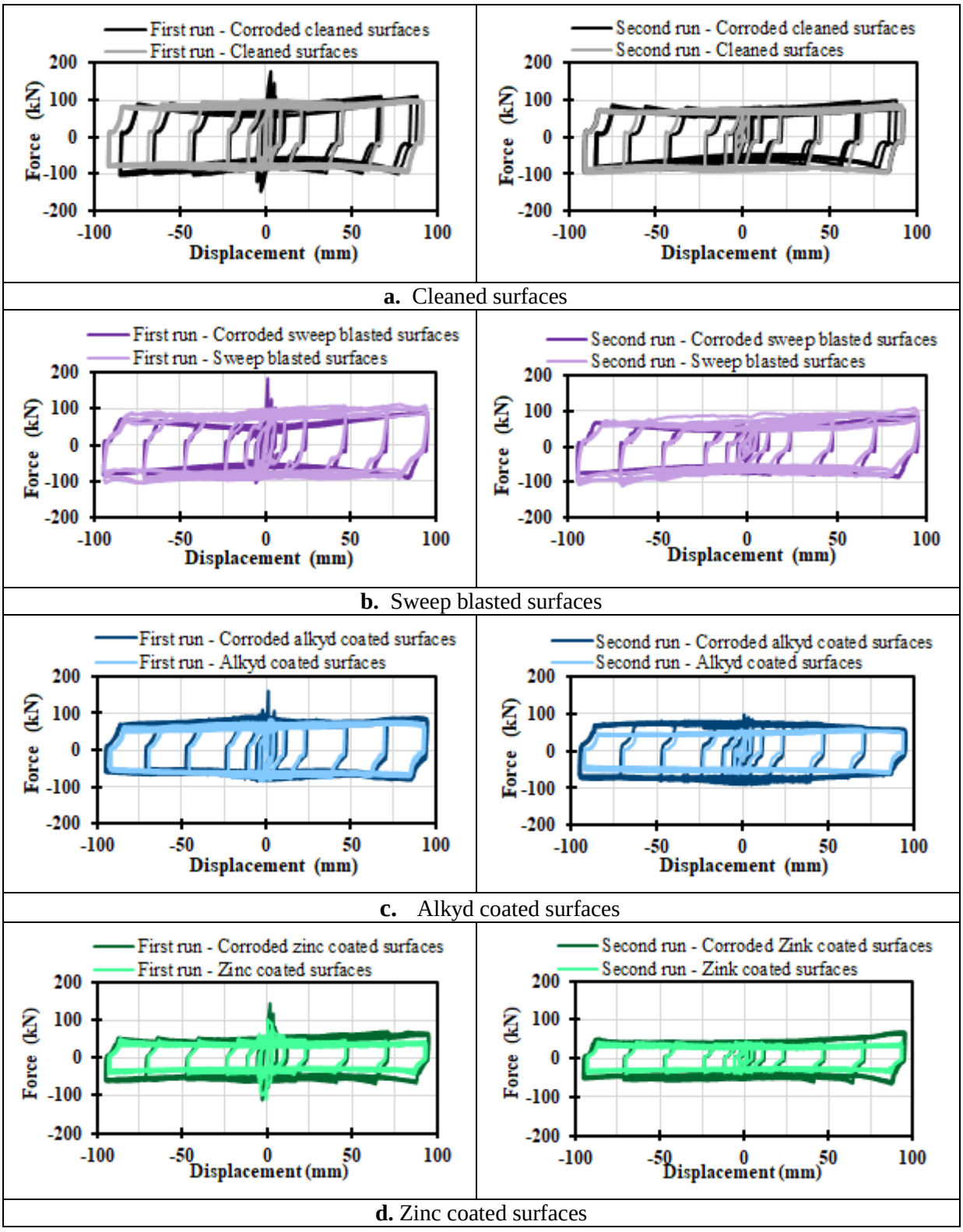

Figure 2.8. Hysteresis loops of full scale AFCs with four different surface treatments after and before corrosion testing

The increased AFC strength in the initial sliding cycles can be interpreted as the force required to activate the sliding of the slotted plate to break free of corrosion product deposited at the external perimeter of the sliding interfaces. The reduction in hysteresis loop stability of the corroded AFCs is attributed to the gain in roughness of the sliding surfaces as result of the corrosion product developed at the internal clamped sliding surfaces. Reductions in the stable AFC strength by corroded AFCs with cleaned and sweep blasted surfaces are attributed to losses of bolt tension presented when the plates moved inwards after the internal clamped sliding surfaces lose mass as a result of uniform corrosion. Increments in the stable AFC strength by corroded AFCs with alkyd and zinc coated surfaces are attributed to increments in bolt tension presented when the plates moved outwards as the corroded product is built at the internal clamped surfaces as a result of filiform corrosion.

3.5 Effects of surface treatments and corrosion on the effective friction coefficient of AFCs

The effective friction coefficient, μe, for full scale AFCs with the four surface treatments before and after corrosion are shown in Figure 2.9. The effective friction coefficient before and after corrosion were assessed at hysteresis loop amplitudes of 3mm, 6mm, 12mm, 25mm, 50mm, 75mm, and 95mm using Equation 2.4 considering $m = 2$, $n = 2$, $F_{proof} = 95$ kN, and Sa calculated as the average of 3 full scale AFCs, where for each AFC, Sa was assessed using Equation 2.3 according to the methodology described in Section 2.8.

Figures 2.9a -d shows μe before corrosion is dependent on the surface treatment. For the four surface treatments, μe varies with the hysteresis loop amplitude, for hysteresis loop amplitudes less than 20mm, but is almost constant for hysteresis loop amplitudes greater than 20mm. In the first run, cleaned, sweep blasted, alkyd coated, and zinc coated surfaces

exhibited values of μe of 0.20 - 0.22, 0.20 - 0.25, 0.18 - 0.20, and 0.10 - 0.24, respectively, and in the second run μe reduced to 0.19 - 0.21, 0.17 - 0.21, 0.14 - 0.15, and 0.07 - 0.08, respectively, as shown in Figures 2.9a - d. These values and Figures 2.9a - d show that by sweep blasting AFC surfaces μe increases slightly for the first run and reduces slightly for the second run, and by coating with alkyd and zinc, μe reduces for both runs. The greatest reductions in μe correspond to zinc coated surfaces. These values also show μe reduces from the first to the second run due to loss of bolt tension linked to degradation of sliding surfaces.

Figure 2.9e - h shows how μe depends on corrosion. For the four surface treatments, in the first run for hysteresis loop amplitudes smaller than 6mm, μe exhibited by corroded AFCs was greater than μe exhibited by AFCs with no corrosion. These increased values of μe for corroded AFCs respect with μe for non-corroded AFCs correspond to the increased AFC strength developed by the connection when removing the corrosion product to activate the sliding mechanism of the slotted plate as described in Section 3.4. For hysteresis loops amplitudes greater than 6mm in the first run, and for whole hysteresis loop amplitudes in the second run, while corroded AFCs with cleaned, and alkyd coated surfaces exhibited μe values near to μe values exhibited by AFCs with no corrosion, corroded AFCs with sweep blasted surfaces and zinc coated surfaces exhibited μe values lower and greater than μe values exhibited by AFCs with no corrosion, respectively, as shown in Figures 2.9e – h.

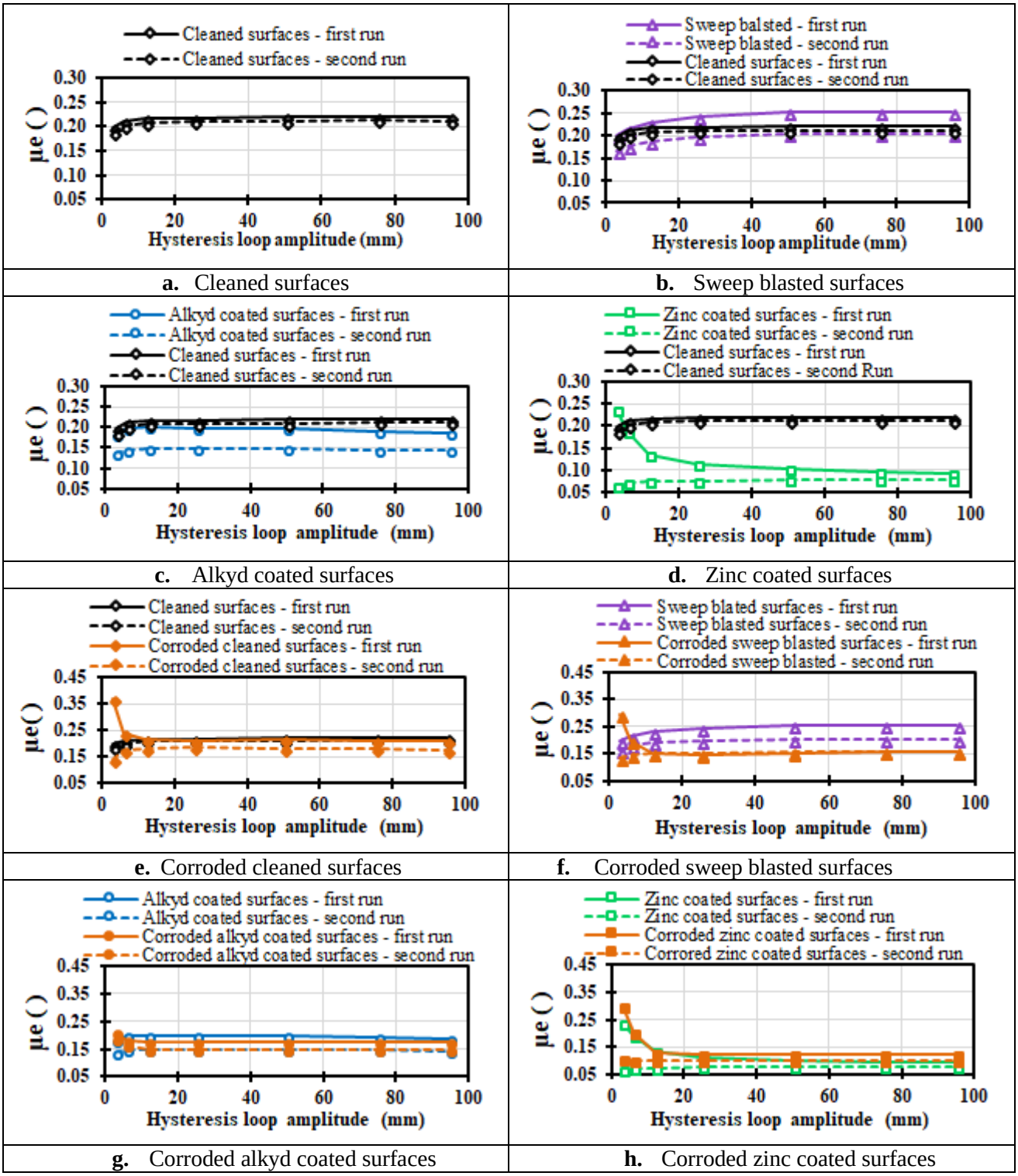

a. Cleaned surfaces | **b.** Sweep blasted surfaces

c. Alkyd coated surfaces | **d.** Zinc coated surfaces

e. Corroded cleaned surfaces | **f.** Corroded sweep blasted surfaces

g. Corroded alkyd coated surfaces | **h.** Corroded zinc coated surfaces

Figure 2.9. Effective friction coefficient, μe, of full scale AFCs with four different surface treatments before and after corrosion testing

Figures 2.9e -h also show that the greatest increase and the greatest reduction in μe due to corrosion were exhibited by AFCs with cleaned and sweep blasted surfaces, respectively. The greatest increase in μe was exhibited by AFCs with cleaned surfaces, since this surface treatment developed the greatest corrosion rate, thus requiring the greatest force to remove the corrosion product at the external surfaces for activating the sliding mechanism of the slotted plate, and therefore producing the greatest increase in μe. The greatest reduction in μe was exhibited by AFCs with sweep blasted surfaces, since this surface treatment developed the greatest corrosion at the sliding surfaces, thus producing the greatest loss of bolt tension when the slotted plate removed simultaneously corrosion product at the sliding surfaces and surface treatment, and therefore producing the greatest reduction in μe.

In the first run, after corrosion, cleaned, sweep blasted, alkyd coated, and zinc coated surfaces exhibited values of μe of 0.21 - 0.37, 0.15 - 0.29, 0.17 - 0.21, and 0.12 - 0.30, respectively, and in the second run μe reduced to 0.14 - 0.19, 0.13 - 0.16, 0.15 - 0.19, and 0.10 - 0.11, respectively, as shown in Figures 2.9e -h. Reductions in μe from the first to the second run are due to removal of corrosion product and degradation at the sliding surface during the sliding of the slotted plate and that produced loss of bolt tension.

IV. MODEL OF AFC STRENGTH CONSIDERING SURFACE TREATMENTS IN THE CORRODED AND NON-CORRODED CONDITION

The average AFC strength for the first run considering surface treatments effects, *Sa*, is modelled using the dry friction theory of Coulomb, and it is defined:

$Sa = m \times n \times F_{proof} \times \mu e_a$	(2.5)

Where, m is the number of sliding interfaces, n is the number of bolts, F_{proof} is the proof load per bolt, and μe_a is the average effective friction coefficient. For the four surface treatments, μe_a was assessed as the average of the effective friction coefficients in Figures 2.9a - d for the first run at hysteresis loop amplitudes of 3mm, 6mm, 12mm, 25mm, 50mm, 75mm, and 95mm. Values of μe_a are presented in Table 2.2, and these values can be used to assess *Sa* for the four surface treatments in the non-corroded and corroded condition using Equation 2.5.

Table 2.2. Average effective friction coefficients, overstrength and understrength factors for four different surface treatments in the corroded and non-corroded condition

Surface treatment	Non – Corroded condition			Corroded condition		
	μe_a	γ	β	γ	β	
	(0-95) mm*	(0-95) mm*	(0-95) mm*	(0-95) mm*	(0-6) mm*	(6-95) mm*
Cleaned surfaces	0.21	0.66	1.28	0.61	2.21	1.28
Sweep Blasted surfaces	0.23	0.65	1.32	0.37	1.35	1.07
Alkyd coated surfaces	0.19	0.72	1.28	0.38	1.23	1.07
Zinc coated surfaces	0.14	0.38	1.79	0.61	2.28	1.33

***** Hysteresis loop amplitude

To consider accuracy on tensioning bolts up to the proof load during assembly, cleanness of sliding surfaces during assembly, and variation of the effective friction with the hysteresis loop amplitude in the corroded and non – corroded condition, an understrength factor, γ, and an overstrength factor, β, were defined. These factors are used to account the minimum and maximum likely *Sa* termed understrength, Sa_{min}, and overstrength, Sa_{max}, respectively, and for the four surface treatments in the non-corroded and corroded condition they are defined:

$$Sa_{min} = \gamma \times m \times n \times F_{proof} \times \mu e_a \qquad (2.6)$$

$Sa_{max} = \beta \times m \times n \times F_{proof} \times \mu e_a$	(2.7)

Values of γ and β for the four surface treatments are defined in Table 2.2. At the non-corroded condition, values of γ and β do not vary with the hysteresis loop amplitude. At the corroded condition, values of γ and β were defined for hysteresis loop amplitudes less than 6mm and greater than 6mm, to model the increased AFC strength observed at the initial sliding cycles, and the almost constant AFC strength observed after the corrosion product is removed after the initial sliding cycles, respectively. It should be noted that the increased forces at the initial sliding cycles resulting from corrosion are independent from the hysteresis loop amplitude. This means for small or significant hysteresis loop amplitudes at the initial sliding cycles for corroded AFCs, the increased forces and proposed values of γ and β will be the same. Values of γ and β in the corroded condition, are applicable to the case when AFCs are exposed to a severe corrosive environment as that one described by AS/NZS 2312 [2.6]. Values of γ and β in Table 2.2 were obtained as the ratio between the lowest experimental AFC strength and the average experimental AFC strength in the case of γ, and as the ratio between the greatest experimental AFC strength and the average experimental AFC strengths in the case of β. The lowest, average, and greatest experimental AFC strengths, were determined from the AFC strengths assessed at hysteresis loop amplitudes of 3mm, 6mm, 12mm, 25mm, 50mm, 75mm, and 95mm using the methodology described in Section 2.8, for 3 full scale AFCs at each surface treatment, and in the corroded and non- corroded conditions.

Figure 2.10 shows for each surface treatment in the non-corroded and corroded condition a comparison between 126 experimental AFC strengths and the predicted average theoretical AFC strength, the understrength, and the overstrength.

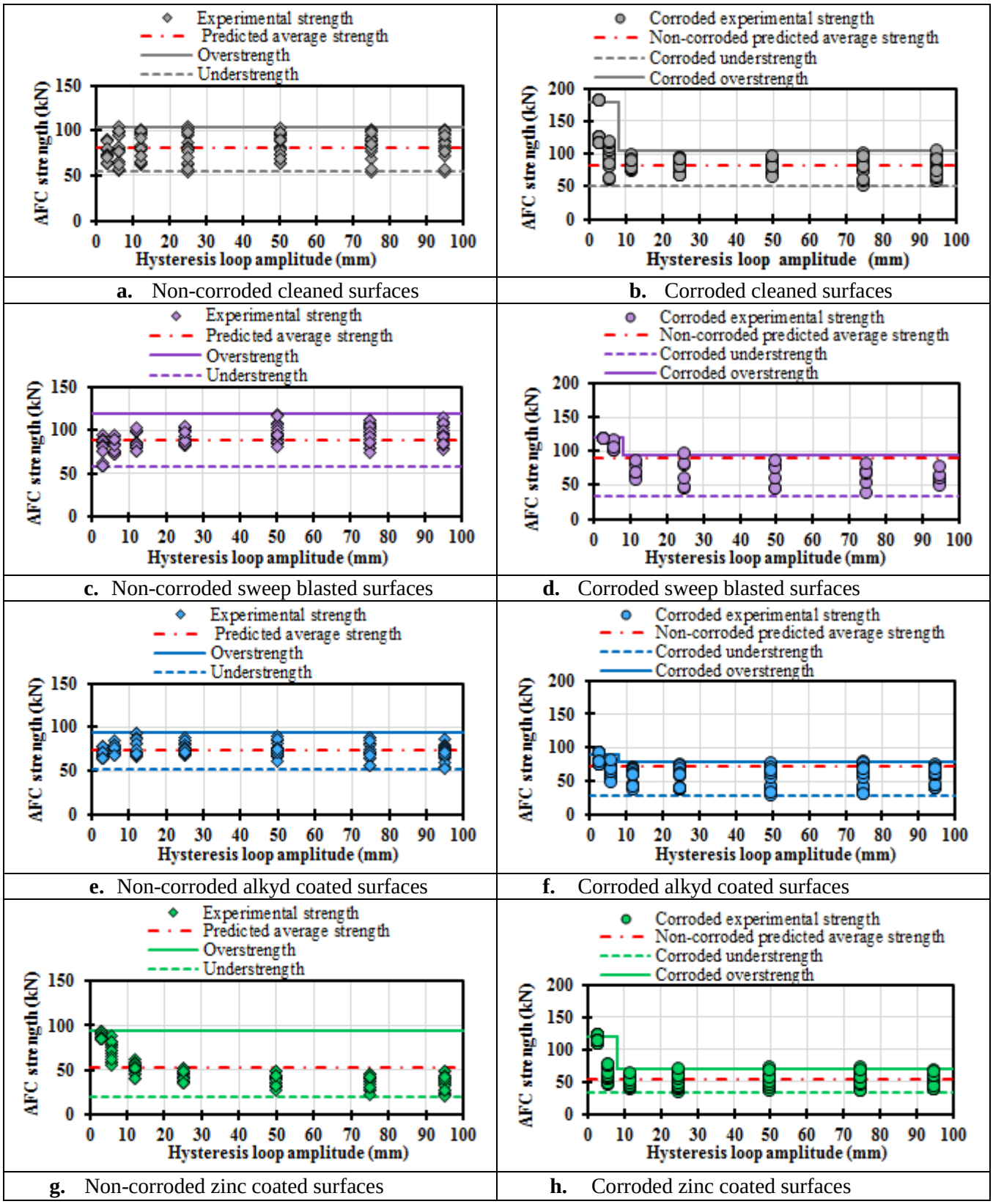

Figure 2.10. Comparison between AFC strength model and experimental AFC strength before and after corrosion for four surface treatments.

In Figure 2.10 the 126 experimental AFC strengths at each surface treatment in the non-corroded and corroded conditions were assessed from 3 full scale AFCs; thus 42 experimental AFC strengths correspond to each full-scale AFC. For each full scale AFC, 6 experimental AFC strength were assessed at each of the hysteresis loop amplitudes of 3mm, 6mm, 12mm, 25mm, 50mm, 75mm and 95mm following the methodology described in Section 2.8. In Figure 2.10, in the corroded conditions, the greatest values at hysteresis loop amplitudes less than 6mm correspond to the increased AFC strength required for removing the corroded product at the external surfaces to activate the sliding mechanism of the slotted plate. The average theoretical AFC strength, the understrength, and the overstrength were predicted using Equations 2.5 – 2.7 using $m = 2$, $n = 2$, $F_{proof} = 95$kN, and values of $\mu e_a, \gamma$, and β defined in Table 2.2.

Figure 2.10 shows for each surface treatment in the non-corroded and corroded conditions, the overstrength and understrength envelope 100% of the experimental strengths. This outcome shows the proposed model to predict the AFC strength considering surface treatments and corrosion is simple and accurate, and it should be used for design considerations.

CONCLUSIONS

This paper describes the effects of surface treatment and corrosion on the hysteretic behaviour of AFCs with Bisalloy 500 shims. It was shown that:

i. AFCs developed general, crevice, and filiform corrosion. AFCs with cleaned and sweep blasted surfaces developed general corrosion on the external surfaces and crevice corrosion with the same appearance of general corrosion on the internal surfaces. AFCs with alkyd coated and zinc coated surfaces developed general corrosion on the external surfaces and filiform corrosion on the internal surfaces.

ii. In AFCs with cleaned surfaces the corrosion rate increased almost linearly and the mass loss increased parabolically with corrosive cycles. In AFCs with sweep blasted, alkyd coated, and zinc coated surfaces, the corrosion rate and mass loss are activated after certain number of cycles, and then the corrosion rate increased almost linearly and the mass loss increased parabolically with corrosive cycles. The most effective surface treatment to delay the corrosion attack is zinc coated surfaces.

iii. Hysteresis loop shape does not change with surface treatment. In AFCs with sweep blasted surfaces the hysteresis loop stability decreased and the average AFC strength increased. In AFCs with alkyd coated and zinc coated surfaces, the stability of the hysteresis loop did not decrease, and the average AFC strength reduced.

iv. Hysteresis loop shape does not change with corrosion except for the increased AFC strength at the initial sliding cycles. However, the hysteresis loop stability decreased slightly. Regardless of the surface treatment, as a result of corrosion, AFC strength increased significantly in the initial sliding cycles, and after the initial sliding cycles AFC strength decreased to an almost constant value approaching the AFC strength developed in the non-corroded condition.

v. The effective friction coefficient changed with surface treatment and corrosion. The effective friction coefficient increased for AFC with sweep blasted surfaces, and reduced for AFCs with alkyd coated and zinc coated surfaces. The greatest reductions in effective friction coefficient occurred for AFCs with zinc coated surfaces. Regardless of the surface treatment, due to corrosion, the effective friction coefficient increased significantly at the initial sliding cycles, and after the initial sliding cycles, it decreased to a value approaching the value in the non-corroded condition.

vi. The average AFC strength in the non-corroded condition for different surface treatments is expressed as function of the average effective friction coefficient and the total bolt proof load on the AFC. The maximum and minimum likely AFC strengths in the corroded and non-corroded conditions for different surface treatments can be assessed as the average AFC strength in the non-corroded condition factored by overstrength and understrength factors. The overstrength and understrength factors were experimentally determined, and range from 0.37 to 2.28 considering the increased AFC strength at the initial sliding cycles.

ACKNOWLEDGEMENTS

The authors would like to acknowledge funding from MBIE Natural Hazards Research Platform (NHRP), and material donation from John Jones Steel Ltd., for undertaking this research. All opinions expressed remain those of the authors.

REFERENCES

[2.1] Khoo HH, Clifton C, Butterworth J, MacRae G, Ferguson G (2011). *Influence of steel shim hardness on the Sliding Hinge Joint Performance.* Journal of Constructional Steel Research. Vol 72, May 2012, pp. 119 – 129. https://doi.org/10.1016/j.jcsr.2011.11.009

[2.2] Clifton GC (2005). *Semi-Rigid Joints for Moments Resisting Steel Framed Seismic Resisting Systems*. Published PhD Thesis, Department of Civil and Environmental Engineering. University of Auckland – New Zealand.

[2.3] Rodgers GW, Chase JG, Causse R, Chanchi Golondrino JC, MacRae GA (2017). *Performance and Degradation of Sliding Steel Friction Connections: Impact of Velocity, Corrosion, Coating and Shim Material*. Engineering Structures, Vol. 141, pp. 292–302. ISSN: 0141-0296. https://doi.org/10.1016/j.engstruct.2017.02.070

[2.4] MacRae GA, Clifton CG, MacKinven H, Mago N, Butterworth J, Pampanin S (2010). *The Sliding Hinge Joint Moment Connection*. Bulletin of the New Zealand Society for Earthquake Engineering. Vol 43, Issue 3, pp. 202-212.

[2.5] Standards Australia/Standards New Zealand (2006). AS/NZS 4680. *Hot-dip galvanized (zinc) coatings on fabricated ferrous articles*. New Zealand.

[2.6] Standards Australia/Standards New Zealand (2014). AS/NZS 2312. *Guide to the protection of structural steel against atmospheric corrosion by the use of protective coatings*. New Zealand.

[2.7] ASTM International (2012). ASTM G31. *Standard guide for laboratory immersion corrosion testing of metals*. United States of America.

[2.8] ASTM International (2018). ASTM G60. *Standard practice for conducting cyclic humidity exposures*. United States of America.

[2.9] Borzouie J, Chase JG, MacRae GA, Rodgers GW (2015). *Experimental Studies on Cyclic Performance of Column Base Weak Axis Aligned Asymmetric Friction Connection*. Journal of Constructional and Steel Research (JCSR), Vol 112, pp. 252-262. https://doi.org/10.1016/j.jcsr.2015.05.007

[2.10] Borzouie J, Chase JG, MacRae GA, Rodgers GW, Clifton C (2016). *Experimental Studies on Cyclic Performance of Column Base Strong Axis Aligned Asymmetric Friction Connections*. ASCE J. Structural Engineering, Vol 142(1), 10-pages. https://doi.org/10.1061/(ASCE)ST.1943-541X.0001327

[2.11] Sarraf, E., R., Clifton, C., Mandeno, W. (2010). *HERA Report R4-133: New Zealand Steelwork Corrosion and Coatings Guide*. New Zealand Heavy Engineering Research Association. Manukau City - New Zealand.

[2.12] Khoo HH, Clifton GC, MacRae GA, Zhou H, Ramhormozian S (2014). *Proposed design models for the asymmetric friction connection*. Earthquake and Structural Dynamics Journal. Vol 44, Issue 8, pp. 1309-1324. https://doi.org/10.1002/eqe.2520

[2.13] Rodgers GW, Mesnil O, Chanchi Golondrino JC, MacRae GA, Chase JG (2014). *Generalised nonlinear modeling of unstable stick-slip force reduction effects in friction energy dissipation devices*. NZSEE Bulletin, Vol 47(3), pp. 217-223.

[2.14] Buchheit RG (2012). *Corrosion resistant coatings and paints.* In: Kuts, M. (editor). Handbook of Environmental Degradation of Materials, 2nd edition. Elsevier, pp. 539 – 568. https://doi.org/10.1016/B978-1-4377-3455-3.00018-3

Chapter 3

Hysteretic Behaviour of Asymmetrical Friction Connections (AFCs) Using Brake Pads of D3923

Chapter 3

"Hysteretic Behaviour of Asymmetric Friction Connections Using Brake Pads of D3923"

Jose Christian Chanchi Golondrino [a, b,1*], Gregory Anthony MacRae[b,2], James Geoffrey Chase[c,3], Geoffrey William Rodgers[c,4], George Charles Clifton[d,5]

[a] Universidad Nacional de Colombia, Departamento de Ingeniería Civil, Manizales - Caldas 170004, Colombia.

[b] University of Canterbury, Department of Civil and Natural Resources Engineering, Private Bag 4800, Christchurch 8140, New Zealand.

[c] University of Canterbury, Department of Mechanical Engineering, Private Bag 4800, Christchurch 8140, New Zealand.

[d] The University of Auckland, Department of Civil & Environmental Engineering, Faculty of Engineering, Private Bag 92019, Auckland Mail Centre, Auckland 1142, New Zealand.

[1] jcchanchigo@unal.edu.co, [2]gregory.macrae@canterbury.ac.nz, [3]geoff.chase@canterbury.ac.nz, [4]geoff.rodgers@canterbury.ac.nz, [5]c.clifton@auckland.ac.nz
[*]Corresponding author

Key Words: Asymmetric Friction Connection, Non- asbestos brake pad, D3923, Friction on non-metallic surface, Low damage dissipater.

ABSTRACT:

Asymmetric Friction Connections (AFCs) can provide stable hysteretic behaviour to dissipate seismic energy. However, the metallic sliding surfaces used in such AFCs may develop metal to metal corrosion compromising performance and their frictional resistance may be low. Non-metallic sliding surfaces should therefore be considered. The quasi-static testing performance of 12 AFCs using bonded non-asbestos D3923 brake pads on the sliding surfaces is evaluated. Three configurations of brake pads bonded on the sliding surfaces of the cap and fixed plates were considered: i) brake pads bonded over the full sliding surfaces (A), ii) strips of brake pads bonded beside the bolt holes (B), and iii) full recessed brake pad with strips beside the

bolt holes (C). The greatest AFC strength occurred in the initial sliding cycles, and became constant after the brake pad reached a steady wear state, at which time the hysteresis loop became symmetric, stable, and predictable. For the A, B, and C brake pad configurations, the steady wear state effective friction coefficient varied between 0.12 - 0.17, 0.10 - 0.14, and 0.12 – 0.17, respectively, with the average values being 0.15, 0.12, and 0.15. The peak values, obtained in the initial sliding cycles were 1.7, 2.2, and 1.9 times these average values, while the lower bound values, obtained after many sliding cycles were 0.71, 0.71, and 0.70 times these average values. The recessed brake pad Configuration C is the preferred configuration since it had the highest steady wear state friction coefficient and the least degradation. Configuration A could be also used in practice, given that this configuration is easy to assemble and hysteretic behaviour is close to that shown by Configuration C.

INTRODUCTION

AFCs are friction bolted connections used as seismic dissipaters, in moment resistant frames (at the beam-column joint or at the column base connection), in braces of braced frames [3.1 – 3.6], or elsewhere. AFCs are typically assembled using three Grade 300 flat steel elements such as plates or I section flanges. Two thin high hardness plates (termed shims) and high strength structural bolts provide sliding surfaces and normal clamping force. AFCs are assembled by tightening bolts up to the proof load. They dissipate energy via friction between the slotted plate and the shims [3.2, 3.3].

AFC strength from quasi-static testing is generally constant over a large displacement range. This strength is not sensitive to the bolt tightening force, as long as the bolt tightening force is greater than the proof load [3.2, 3.3]. Experimental studies showed while AFCs with bolts

tensioned below the proof load had a noticeable variability on the AFC strength, AFCs with bolts tensioned above the proof load had constant AFC strength [3.4]. It should be noted that only minor increments on the AFC strength can be achieved by tensioning bolts above the proof load [3.4] AFC strength reduces when AFCs are cyclically loaded due to loss of bolt tension occurring when bolts yield as a result of prying inputs [3.5, 3.6] and/or moment – axial – shear (MPV) interaction [3.3, 3.7, 3.8]. This latter occurs when the bolts rotate, bear on the cap plate and on the fixed plate, and bend in double curvature, as shown in Figure 3.1. In this figure, bolts are subjected to an axial tension, N^*, termed bolt axial tension during the sliding, and that corresponds to the difference between the bolt axial tension resulting from the AFC assembly and the loss of bolt axial tension due to MPV interaction.

AFCs have been experimentally developed and validated using different metallic sliding surfaces [3.1]. The steady AFC strength normalized by the bolt proof load per bolt on each sliding interface, termed the effective friction coefficient, for the preferred metallic shims, such as high hardness Bisalloy shims, is generally between 0.17 - 0.25 [3.1, 3.2, 3.8, 3.10]. This value can vary with coating [3.1], and material [3.9, 3.10].

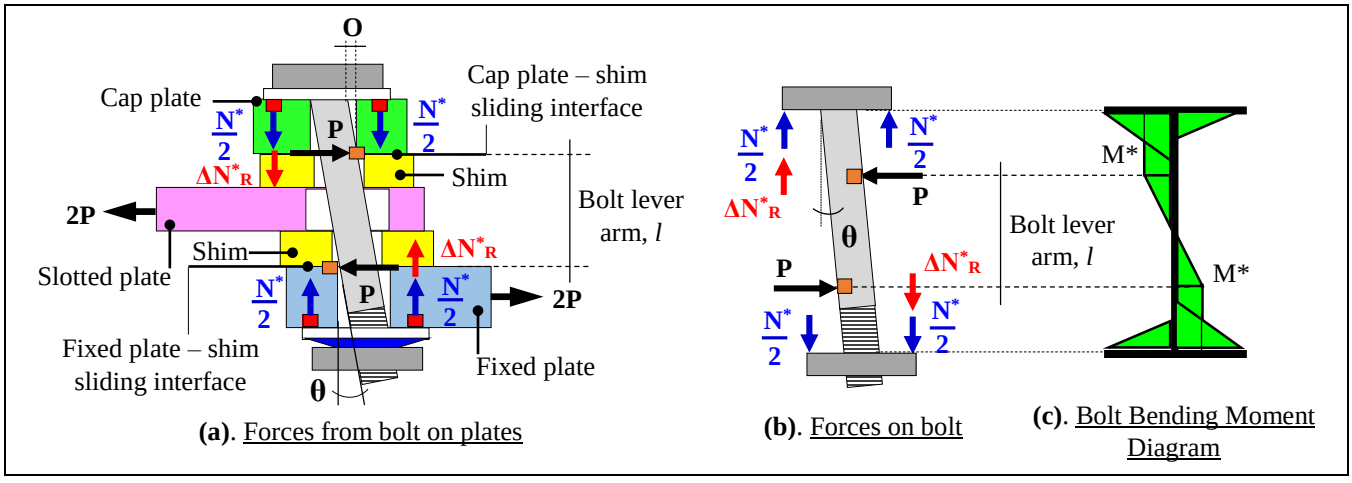

Figure 3.1. Forces on AFCs during sliding of slotted plate, idealized bolt deformation, and bolt bending moment diagram in MPV model [3.3, 3.7, 3.8] (Not to scale)

Studies in symmetrical friction connections (SFCs) used for energy dissipation purposes showed hysteretic performance became non-stable and unpredictable when using clean mill scale steel or metalized sliding surfaces [3.11 – 3.14]. These studies also showed by using dissimilar metallic materials at the sliding surfaces, SFC hysteretic performance became more stable and predictable [3.11 – 3.12]. Studies in AFCs confirmed using dissimilar metallic sliding surfaces improve the stability and predictability of hysteretic performance, and stable and predictable hysteretic performance can be achieved by using metallic sliding interfaces of Grade 300 steel – high hardness shims [3.2]. However, recent studies in AFCs have shown metallic sliding surfaces of Grade 300 steel – high hardness shims may degrade when exposed to corrosive environments, reducing the stability and predictability of hysteretic performance [3.1]. For that reason, there is a need to consider non–metallic sliding surfaces, which may be unaffected by corrosion and also may generate more stable, predictable AFC hysteretic performance. One possible non-metallic sliding surface experimentally explored are brake pads [3.13 – 3.17]. While some of these experimental results showed perfectly rectangular, stable, low degradation hysteretic behaviour using brake pads in Grade 300 mild steel symmetric friction configurations [3.13, 3.14, 3.16, 3.17], others indicated increased forces in the initial sliding cycles or strength reduction due to brake pad degradation [3.14]. To date, there is no experimental research describing the hysteretic behaviour of AFCs using brake pads. To address this issue, experimental and theoretical research is conducted on AFCs with bonded brake pads made of the non-asbestos material D3923 [3.18, 3.19]. This research aims to answer following questions:

i. What are the hysteresis characteristics of these AFCs?

ii. What is the strength of these AFCs?

iii. What AFC brake pad configuration is best?

iv. What is the effective friction coefficient, it bounds, and strength degradation of these AFCs?

v. What are the design considerations for the strength of these AFCs?

I. MATERIALS AND METHODS

2.1 AFC test specimens with brake pads

A total of 9 AFCs were assembled using brake pads of 4mm - 6mm thickness bonded on the fixed and cap plates instead of shims, and Grade 300 steel plates of 20mm thickness for the fixed, slotted, and cap plates. They were clamped using 2 M16 Grade 8.8 structural galvanized bolts of 110mm length with unthreaded length of 72mm and threaded length of 38mm, as shown in Figures 3.2a – b. Bolts were assembled using a 4mm thick structural washer, a 4mm thick flat washer, and a single Belleville washer of 2.5mm in its fully squashed condition, as shown in Figure 3.1b. Belleville washers were used to reduce bolt clamping force variation due to sliding surfaces degradation [3.1, 3.2]. The bolt grip length measured to the outside of the washers of 78.5mm was due to the three 20mm plates, two 4mm brake pads, 4.0mm structural washer, 4.0mm flat washer, and the 2.5mm flattened Belleville washer. The three configurations considered are shown in Figures 3.2c – d, and defined in Table 3.1. Brake pads were made of non-asbestos friction material D3923 [3.18, 3.19].

The D3923 brake pads, manufactured and distributed by Ferotec Friction Inc [3.18, 3.19] use a flexible, moulded, non-asbestos friction material. They are used in diverse situations, such as automotive brake linings, industrial brake bands, machinery brakes bands, and clutch linings. This non-asbestos friction material is desirable for brake linings applications not only

because of its stability and wear resistant properties, but also because the heat generated in service increases its strength and rigidity [3.18, 3.19]. D3923 is manufactured from non-metallic substances, such as vermiculite (mica), barium sulphate and calcium carbonate. This soft brake pad material is reinforced by the addition of glass and cellulose fibres randomly dispersed to increase the wear resistance [3.18, 3.19]. It is readily available.

Table 3.1. Brake Pad Configurations

	Configuration	Description
A	Bonded on full surface	Brake pads were bonded over the full fixed plate and cap plate surfaces
B	Striped	Brake pads were bonded over the full fixed plate and cap plate surfaces, and then the brake pads were cut and machined so that only one strip of brake pad on each side of each bolt hole remained. This configuration was adapted from [3.17]
C	Striped and recessed	A 2.0mm deep, 170mm wide, and 270mm long recess were made on the fixed plate and cap plate. A 6mm thick brake pad, 170mm wide and 270mm long was fitted and bonded in the 2mm deep recess of the fixed plate and cap plate. It should be noted that after bonding the brake pad on the recess, the full volume of the recess was filled and a brake pad portion of 4mm thick, 170mm wide, and 270mm long projected from the non-recessed surface of the fixed plate and cap plate. Then the projected portion of the brake pad was cut down and machined 4mm, so that only one strip of brake pad on each side of each bolt hole remained. All strips have lateral confinement at their ends in the longitudinal or loading direction, but only the outside of the outer strips have lateral confinement in the width direction. This configuration was adapted from [3.17]

The D3923 brake pads were bonded at one of the surfaces of the fixed and cap plates using the thermosetting adhesive Araldite 64-1 [3.20]. The bonding procedure comprised three stages: i.) degreasing and shot blasting the plate surfaces; ii) applying Araldite 64-1 on the plate surfaces and curing the plate surfaces for 6 hours at 20ºC; and iii) positioning the brake pads on the plate surfaces and clamping the plate – brake pad arrangement with a pressure of 1.0MPa at 150ºC for 30 minutes.

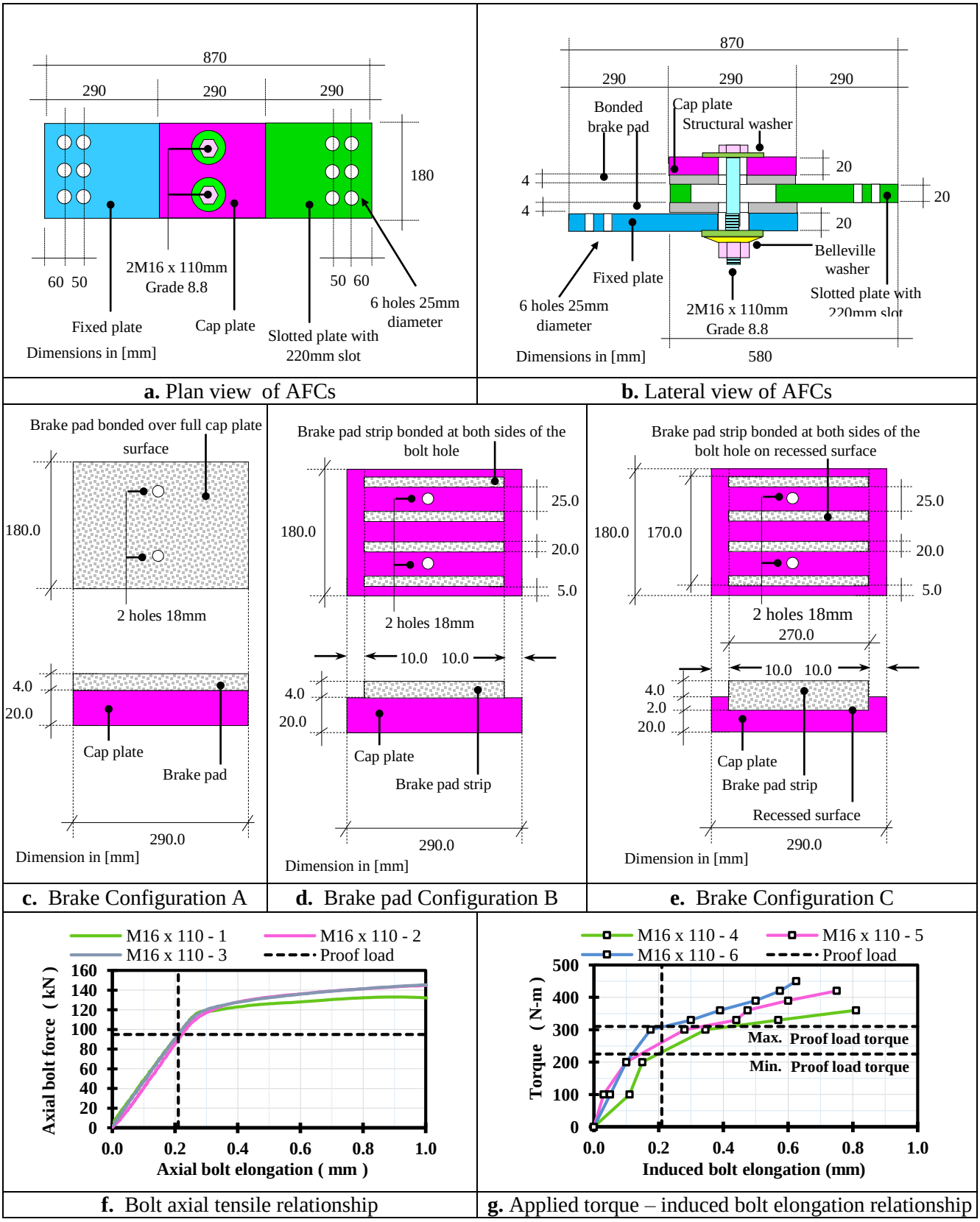

a. Plan view of AFCs

b. Lateral view of AFCs

c. Brake Configuration A

d. Brake pad Configuration B

e. Brake Configuration C

f. Bolt axial tensile relationship

g. Applied torque – induced bolt elongation relationship

Figure 3.2. AFCs assembly, bonded brake pads configurations, assembly relationships (Not to scale)

2.2 AFC assembly

A total of 9 AFCs were assembled and divided into 3 groups of 3 specimens each. The 3 groups of AFCs matched with the 3 brake pad configurations described in Section 2.1. AFCs were assembled by tensioning bolts up to the proof load of 95kN for a Grade 8.8 M16 bolt using the torque control method. In this method, a bolt is gradually tensioned to a torque that develops an axial elongation equivalent to the computed elongation that the bolt develops when it reaches the proof load in axial tensile testing, ignoring bolt torsion. This torque is termed proof load torque. The bolt elongation when it reaches the proof load in axial tensile testing is termed proof load elongation.

The proof load elongation of 0.21mm, which occurred over the grip length measured outside of washers of 78.5mm, was read from an axial tensile testing relationship from 3 bolts using the proof load value, as shown in Figure 3.2f. The proof load torque of 270N-m was assessed as the average of the maximum and minimum torques from a torque - induced bolt elongation relationship for 3 bolts using the proof load elongation value, as shown in Figure 3.2g.

2.3 Quasi-static test procedure

AFCs were quasi-statically tested using a shake table to provide a strictly horizontal input at the required force level, thus minimizing prying effects that reduce AFC strength [3.5, 3.6]. The test setup comprised a fixed bracket attached to a reaction frame bolted to a reaction floor, and a moving bracket attached to a reaction frame bolted to a shaking table. AFCs were connected using 6 M24 Grade 8.8 structural bolts at each end. A load cell was placed between

the fixed bracket and reaction frame, a potentiometer was placed across the connection stroke, and a bolt extensometer was placed across the bolt shank. Details are in Figure 3.3.

The displacement inputs are defined in Figure 3.3 and comprise 21 sinusoidal cycles at the same period with a maximum velocity of 10mm/s and amplitudes varying from 0 to ± 95mm. This amplitude is 95% of the full 200mm slot length. The peak velocity of 10mm/s is slow enough to minimise any potential velocity dependence effects [3.1]. Each AFC was run twice with no bolt re-tensioning and with a 30 minute break to cool down to room temperature after the first run.

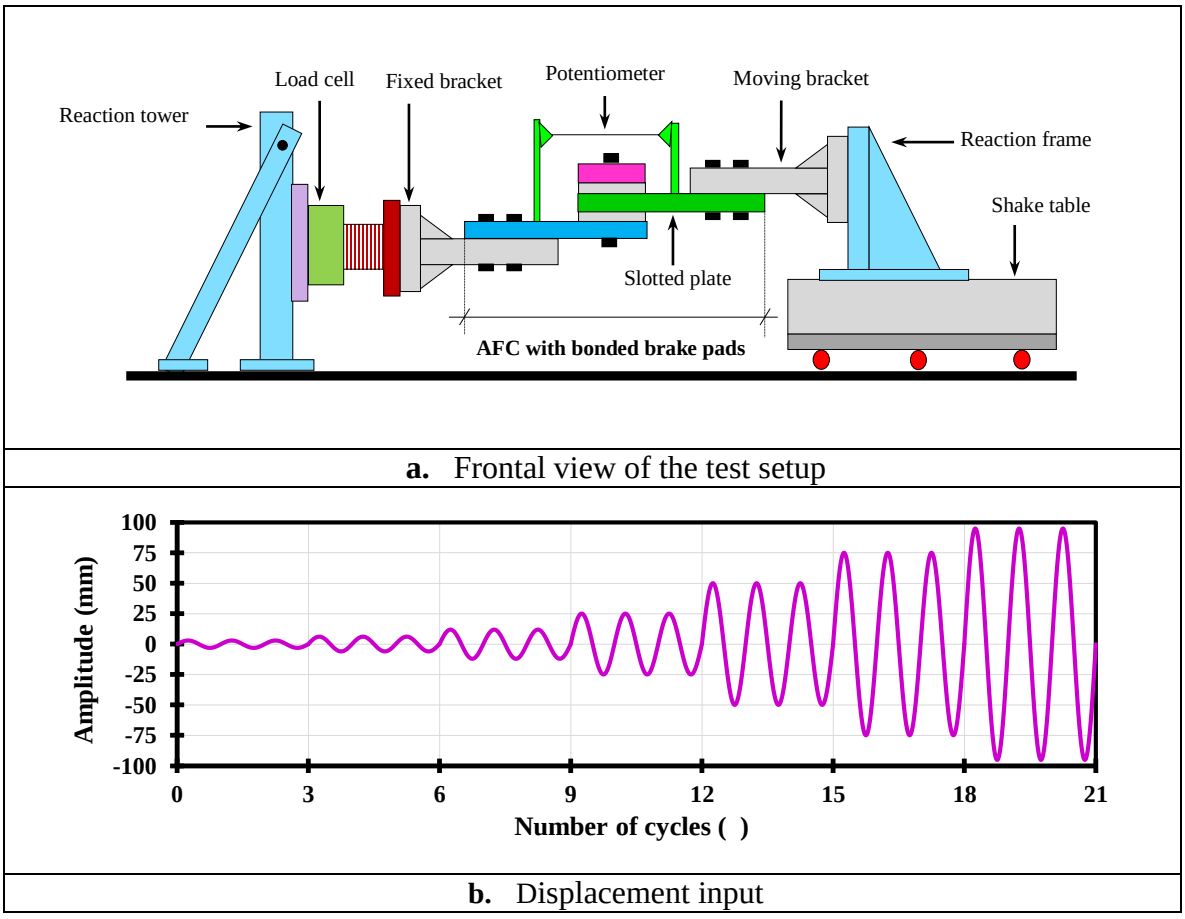

Figure 3.3. Experimental AFC test setup and displacement input (Not to scale)

2.4 Assessment of experimental AFC strength

The experimental AFC strength, *S*, at a given hysteresis loop amplitude for the first and second run was assessed by reading the force values at the four corners and at the two zero displacement points of the hysteresis loop, as shown in Figure 3.4. The average experimental AFC strength, *Sa*, is assessed as the average absolute value of the tension and compression sliding regions of the hysteresis loop, and is defined:

$$Sa = \left[\frac{(LTS + MTS + RTS) + |LBS + MBS + RBS|}{6} \right] \quad (3.1)$$

Where, *LTS*, *MTS*, and *RTS* are the experimental AFC strengths at the tension sliding region of the hysteresis loop, and *LBS*, *MBS*, and *RBS* are the experimental AFC strengths at the compression sliding region of the hysteresis loop. They are all shown in Figure 3.4.

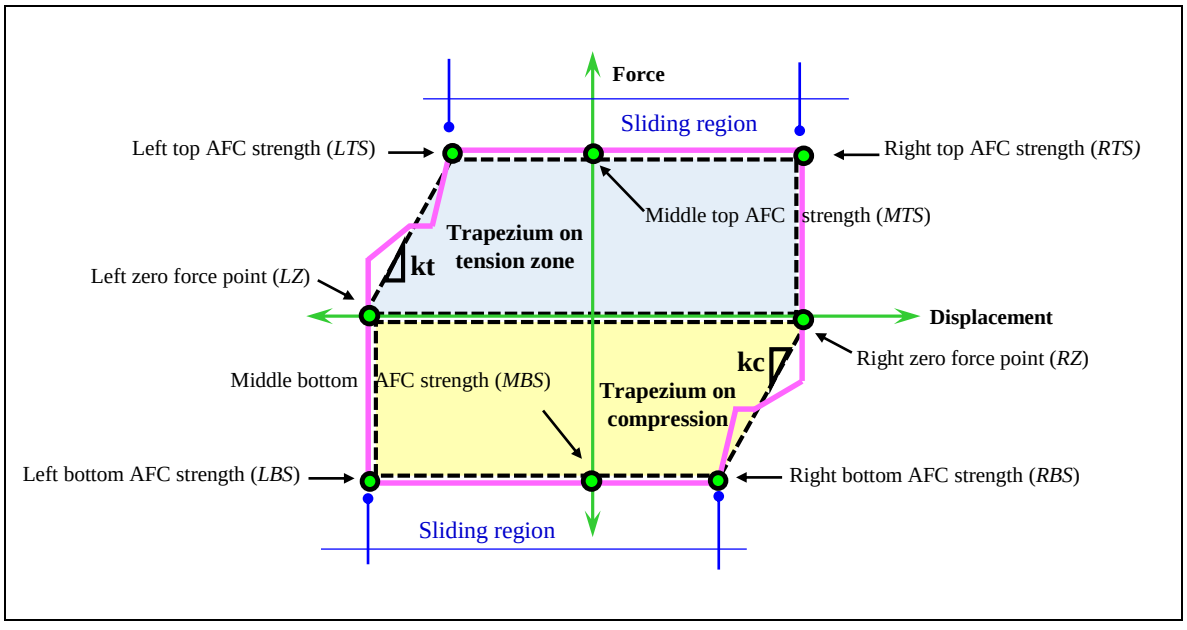

Figure 3.4. Assessment of experimental AFC strength, loading stiffness and energy dissipated at a given hysteresis loop amplitude

2.5 Assessment of the experimental hysteresis loop loading stiffness

The experimental hysteresis loop loading stiffness is defined as the ratio between the force and displacement during the development of the AFC strength. The loading stiffness on the tension side of the hysteresis loop, *kt*, is calculated as the slope of the line connecting the left zero force point, *LZ*, and the left top AFC strength point, *LTS*, as shown in Figure 3.4. The loading stiffness on the compression side of the hysteresis loop, *kc*, is calculated as the slope of the line connecting the right zero force point, *RZ*, and the right bottom AFC strength point, *RBS*, as shown in Figure 3.4. The average loading stiffness at a given hysteresis loop amplitude, *ka*, is calculated as the average of the loading stiffness at the compression and tension sides of the hysteresis loop defined:

$$Ka = \frac{kc + kt}{2} \quad (3.2)$$

2.6 Assessment of energy dissipated by AFCs

The energy dissipated by AFCs, *E*, is defined as the hysteresis loop enclosed area. The energy dissipated at a given hysteresis loop amplitude is calculated by adding the absolute values of the areas of the top trapezium and bottom trapezium fitted on the experimental hysteresis loop, as shown in Figure 3.4. The top trapezium is fitted on the hysteresis loop tension zone and defined by the points *LZ*, *LTS*, *RTS*, and RZ, and the bottom trapezium is fitted on the compression hysteresis loop zone the defined by the points *LZ*, *LTS*, *RTS*, and RZ, *RBS*, *LBS*, and *LZ*, as shown in Figure 3.4.

2.7 Assessment of the effective friction coefficient

The effective friction coefficient is a non-dimensional factor defined as the ratio between the AFC strength and the bolt proof load per bolt on each sliding interface [3.8]. This friction coefficient is termed effective because it is not constant due to the degradation of the AFC sliding surfaces, any surface coating [3.1], and materials used [3.9]. For ease, it is evaluated considering that the clamping force remains constant at the proof load regardless of any degradation of the sliding surfaces. The effective friction coefficient, μ_e, can then be determined:

$$\mu_e = \frac{S}{m \times n \times F_{proof}} \quad (3.3)$$

Where, S is the experimental AFC strength, m is the number of bolts, n is the number of shear planes, and F_{proof} is the proof load per bolt.

2.8 Assessment of strength degradation

Strength degradation, SD, is defined as the reduction in the average AFC strength from the first run to the second run of the displacement input after the AFC was cooled down to room temperature [3.1], and is calculated:

$$SD = \left[1 - \left(\frac{\mu e_{second\ run}}{\mu e_{first\ run}}\right)\right] \times 100\% \quad (3.4)$$

Where, $\mu e_{second\ run}$ and $\mu e_{first\ run}$, are the experimental effective friction coefficients for the first run and second run, respectively.

2.9 Assessment of the bolt rotation angle and the bolt shank horizontal displacement

The bolt rotation angle, θ, and the bolt shank horizontal displacement, Δ, are defined as the angle, and horizontal displacement of the bolt shank over the grip length outside the plates and inside the washers, g, achieved as the bolt slides across the bolt hole. The maximum possible bolt rotation, θmax, and the maximum possible bolt shank horizontal displacement, Δmax, are assessed when the opposite sides of the bolt shank are bearing at the cap plate-top brake pad and fixed plate – bottom brake pad interfaces (bearing points), while the bolt remains straight or without yielding in bending, as shown in Figure 3.5. The maximum possible displacement between the locations of applied force $2P$ is approximately one half of Δmax. Δmax is also the maximum possible displacement on the hysteresis curve between the point of zero force and the maximum force, ignoring the bolt non-rigid body deformation and compression at the corners of the plates.

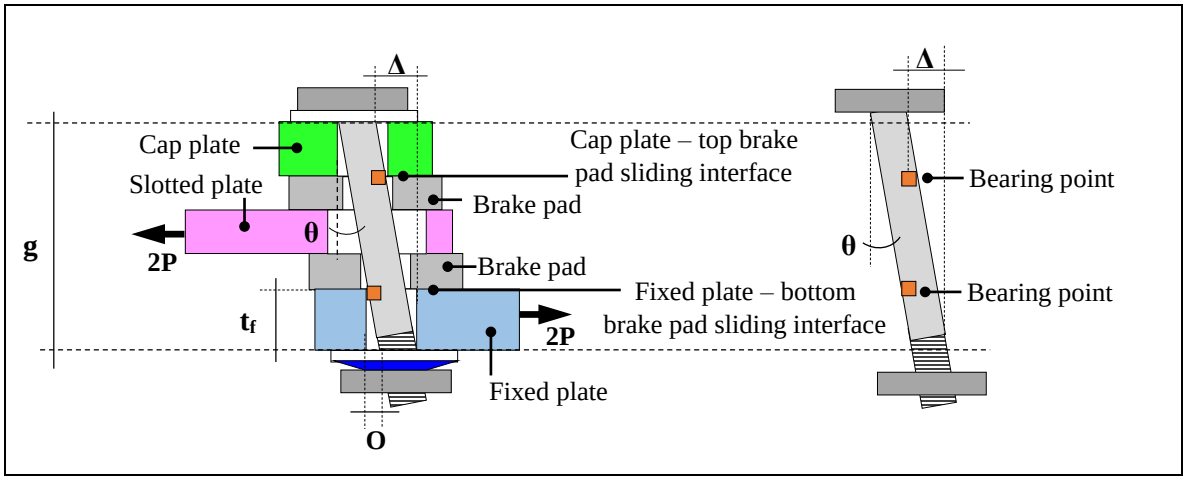

Figure 3.5. Idealized elastic bolt rotation angle and elastic bolt horizontal displacement (Not to scale)

The maximum possible bolt rotation angle and the maximum possible bolt head horizontal displacement in Figure 3.5 are defined:

$\theta max = tan^{-1}\left[\frac{O}{t_f}\right]$	(3.5)
$\Delta max = g \times \frac{O}{t_f}$	(3.6)

Where, O is the bolt hole oversize, t_f is the thickness of the fixed plate, and g is the bolt grip length between the outside of the plates, as shown in Figure 3.5.

II. RESULTS AND ANALYSIS

3.1 Overall behaviour

After testing, all brake pad surfaces were smoother and some brake pad debris had fallen from the AFC specimens. Figures 3.6a-c show brake pad surfaces before and after testing. For all configurations, after testing, brake pad surfaces showed worn areas at both sides of the bolt holes and in the direction of the applied force. Brake pads worn areas were characterized by a dark grey colour and scratches. The dark grey colour on the worn areas is due to friction heat developed during sliding of the slotted plate. More uniform wearing and less deep scratches were observed in Configuration A than those observed in Configurations B and C.

After the first run, in brake pad Configuration B, some brake pad debonding was observed at the ends of the external strips for a distance of about 5mm, the state of the internal strips was not able to be observed. The debonding may be due to the high pressure due to bolt assembly

on the brake pads strips, causing higher debonding shear stresses than in Configuration A. In addition, another possible reason is the strips in Configuration B did not have the confinement provided in Configuration C. After the second run, the delamination in Configuration B did not change from that in the first run.

The hysteresis loops regardless of brake pad configuration, have the same shape, as shown in Figures 3.6d – f. In the first run, AFC strength in the initial sliding cycles was 100kN – 115kN. However, after the initial sliding cycles, it reduced to an average AFC strength, *Sa*, of 77kN – 79kN calculated across the all displacement amplitudes, as defined in Section 2.4, and as shown in Figures 3.6d – f. In the second run, AFC strength was almost constant for all cycles. It was less than recorded in the first run, and the average AFC strength, *Sa*, calculated across the all displacement amplitudes, as defined in Section 2.4, was 48kN – 58kN, as shown in Figures 3.6d - f.

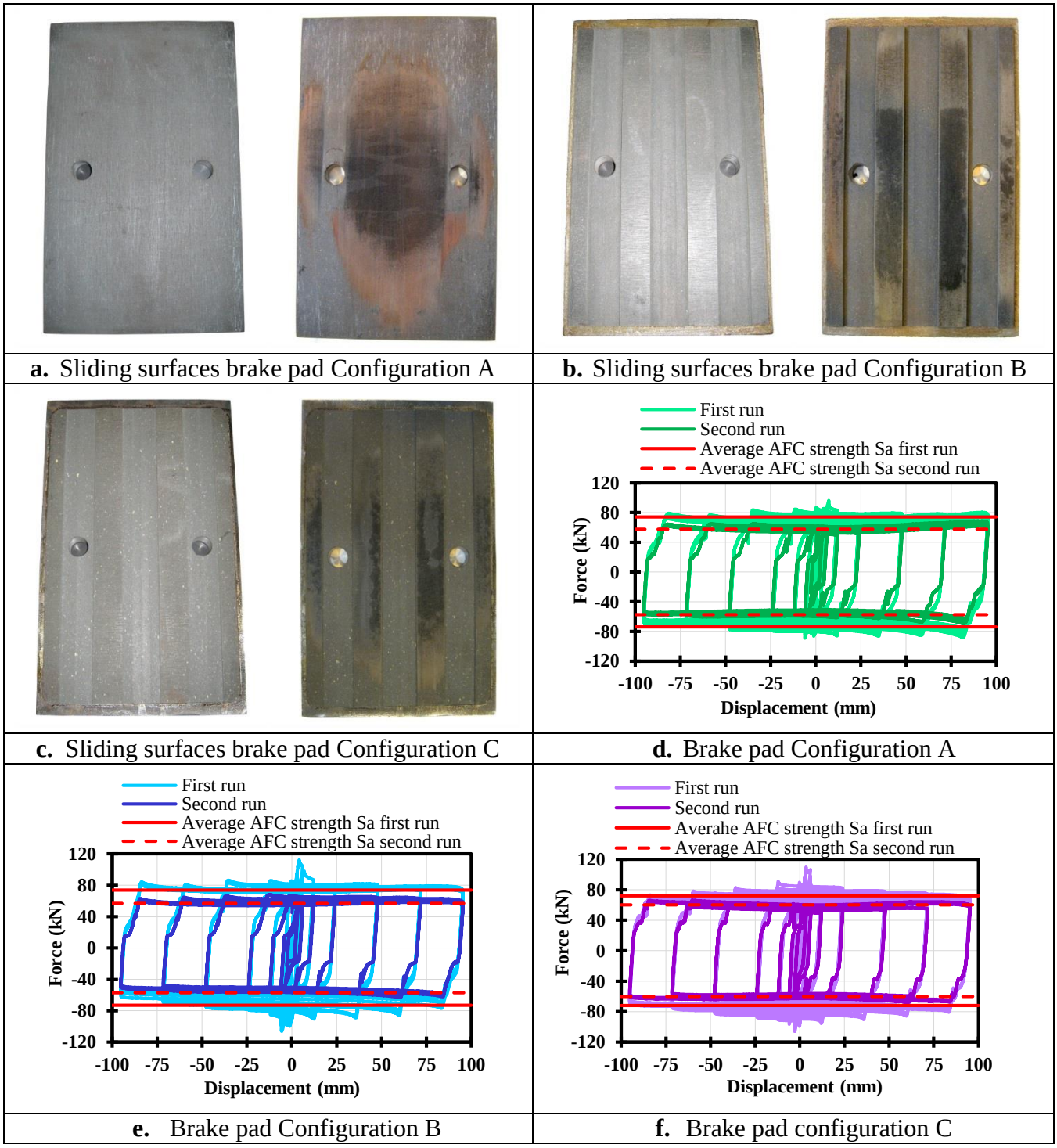

a. Sliding surfaces brake pad Configuration A

b. Sliding surfaces brake pad Configuration B

c. Sliding surfaces brake pad Configuration C

d. Brake pad Configuration A

e. Brake pad Configuration B

f. Brake pad configuration C

Figure 3.6. Brake pad configuration sliding surfaces before and after testing and hysteresis loop of AFCs with bonded brake pads

Hysteresis loop stability is defined as how consistent remain following hysteresis loop variables as the displacement amplitude increases: the average AFC strength, *Sa*, as defined in Section 2.4, the average loading stiffness, *Ka*, as defined in Section 2.5, the unloading stiffness *Ku*, and the energy dissipated, *E*, as defined in Section 2.6. In the first run, *Sa* was almost constant for displacement amplitudes greater than 25mm, as shown in Figure 3.7a, *Ka* was constant for displacement amplitudes greater than 12mm, as shown in Figure 3.7b, *Ku* was constant for all displacement amplitudes, as shown in Figures 3.6d – f, and *E* increased consistently as the displacement amplitude increased, as shown in Figure 3.7c. These results indicate hysteresis loops in the first run were stable for displacement amplitudes greater than 25mm. In the second run, *Sa* and *Ka* were constant for displacement amplitudes greater than 12mm, as shown in Figures 3.7a – b, *Ku* was constant for all displacement amplitudes, as shown in Figures 3.6d – f, and *E* increased consistently as the displacement amplitude increased, as shown in Figure 3.7c. These results indicate hysteresis loops in the second run were stable for displacement amplitudes greater than 12mm. The most stable hysteresis loops, with the least strength degradation between cycles in a run, were exhibited by Configuration C, as shown in Figures 3.6d – f.

Figure 3.7c shows for the first and second runs, energy dissipated, *E*, as defined in Section 2.6, increased consistently with an almost linear trend as the displacement amplitude increased. This indicates the hysteresis loop area increased consistently with the displacement amplitude. Energy dissipated increased with an average ratio of 261kN-mm/mm for the first run, and of 231kN-mm/mm for the second run. The most consistent increase of energy dissipated with the displacement amplitude was exhibited by Configurations A and C.

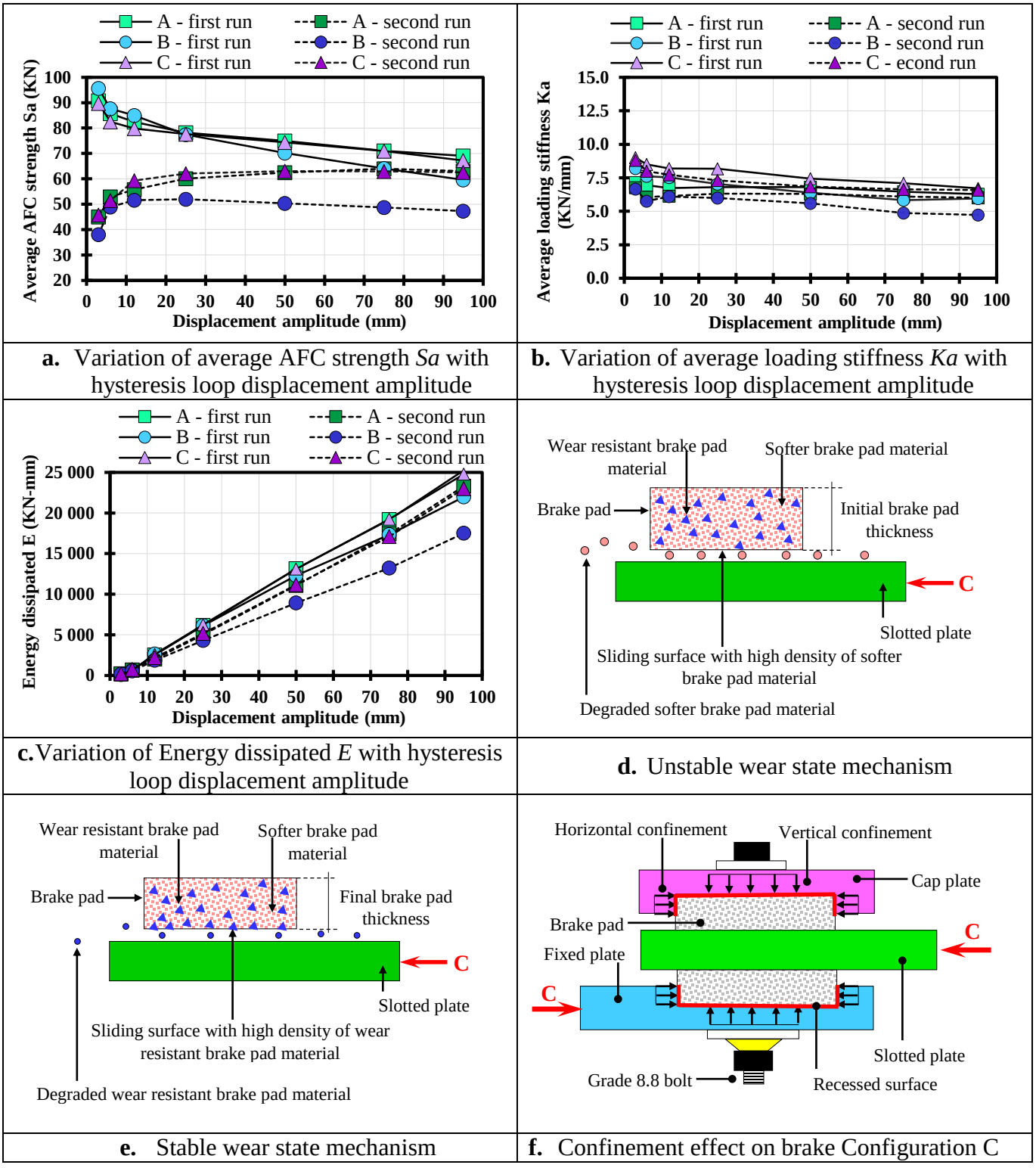

a. Variation of average AFC strength *Sa* with hysteresis loop displacement amplitude

b. Variation of average loading stiffness *Ka* with hysteresis loop displacement amplitude

c. Variation of Energy dissipated *E* with hysteresis loop displacement amplitude

d. Unstable wear state mechanism

e. Stable wear state mechanism

f. Confinement effect on brake Configuration C

Figure 3.7. Variation of average AFC strength, average loading stiffness and energy dissipated with hysteresis loop displacement amplitude in AFCs with bonded brake pads, wear mechanisms in AFCs with bonded brake pads, and confinement effect on brake pad Configuration C

In the first run, the hysteresis loop stability for all three brake pad configurations increased as sliding cycles increased. This result is due to a mechanism termed unstable brake pad wear state [3.21]. This mechanism is developed in brand new or low degraded brake pad sliding surfaces with a high density of soft components and low density of the wear resistant components at the brake pad – slotted plate interfaces, as shown in Figure 3.7d. In this mechanism, as the slotted plate slides, the softer components of the brake pads are primarily removed, significantly increasing the degradation of the brake pad sliding surfaces [3.21], and reducing bolt tension and AFC strength. Hysteresis loop stability in this mechanism increases as the density of the wear resistant components of slotted plate – brake pad interfaces increases as a result of the degradation of the brake pad sliding surfaces. It is noted the degradation of the brake pad sliding surfaces was greater around the bolt holes and reduced with the distance from the bolt holes in the direction of the applied load, as shown in Figures 3.6a-c. This indicates every time the sliding displacement magnitude is increased, a portion of brake pad with low degradation is included in the sliding range. However, the proportion of this low degraded brake pad in the overall sliding magnitude decreases with the larger displacement cycles.

In the second run, the hysteresis loops for the three brake pad configurations are stable due to a mechanism termed stable wear state [3.21]. This mechanism is developed after the brake pad sliding surfaces are degraded and the slotted plate – brake pad interfaces are characterized by high density of the wear resistant components, as shown in Figure 3.7e. In this mechanism, as the slotted plate slides over a high density of wear resistant brake pad components, the degradation of the sliding surfaces reduces significantly [3.21], thus keeping bolt tension almost constant and producing stable hysteresis loops.

The mechanism by which the stable wear state is obtained involves:

i. The surface roughness effect influenced by:

- **a.** A removal of the sharp peaks of the brake pad surface reducing the friction coefficient, and
- **b.** The debris from the peaks moving around on the harder brake pad subsurface below providing a lubrication effect and reducing the friction coefficient, and

ii. The normal force effect is influenced by the two surface roughness effects described above in opposite ways. First, as the peaks are removed, the roughness is decreased and the plates can move together. However, second, as the debris from the removed peaks enters between the sliding surfaces, it can roll around causing the plates move apart. The net result of these effects is the normal force changes due to a change in the bolt tension, and friction forces may be further reduced by reduction in friction coefficient due to smoothing of sliding surfaces.

After a few cycles, the surface roughness effect and the normal force effect stabilise, causing an almost constant bolt tension.

The average AFC strength in the second run divided by the first run average value yields 0.73, 0.62, and 0.75 for Configurations A, B, and C, respectively. The reason that Configuration C, with both stripped and recessed brake pads, had less strength decrease is attributed to the lateral confinement provided by the brake pad recess, particularly on the outside of the outer strips. This lateral confinement was developed when the lateral deformation of the brake pad induced by the compressive force during AFC assembly was restrained by the lateral faces of

the recess, as shown in Figure 3.7f. Under these forces the brake pad is subjected to a biaxial compressive state that limits the debonding of the brake pads observed in the Configurations A and B.

3.2 AFC strength of AFCs with bonded brake pads

AFC strength for each AFC was assessed according to the methodology described in Section 2.4 at each of the 7 displacement amplitudes of 3mm, 6mm, 12mm, 18mm, 25mm, 50mm, 75mm, and 95mm. Thus, AFC strength for each of the 3 brake pad configurations of 3 AFCs is represented by 18 values at displacement amplitude per run, and by 126 values per run when considering the 7 displacement amplitudes, as shown in Figure 3.8. The average of the 18 values of the AFC strength at each displacement amplitude, and the average of the 126 AFC strengths per run across the full displacement range, are also presented in Figure 3.8 for both runs and for the 3 configurations.

In the first run, all three configurations exhibited the greatest AFC strengths in the initial sliding cycles. Thereafter, the AFC strength reduced with the displacement amplitude, as shown in Figure 3.8. During the initial sliding cycles, the AFC strength was 23%, 47%, and 42% greater than the average AFC strength from all cycles and all amplitudes, for brake pad Configurations A, B, and C, respectively, as shown in Figures 3.8a, c, and e. In the final sliding cycles, the AFC strength was 24%, 38%, and 25% less than the average AFC strength from all cycles and all amplitudes, for Configurations A, B, and C, respectively, as shown in Figures 3.8a, c, and e. The increased AFC strength during the initial sliding cycles occurs when the slotted plate is in contact with localized zones of rough virgin brake pad material, which polish the steel sliding surfaces of the slotted plate as sliding occurs. The AFC strength reduced after the initial sliding cycles as the soft brake pad material components are removed

producing loss of bolt tension. This behaviour is linked to the unstable brake pad wear state mechanism described in Section 3.1.

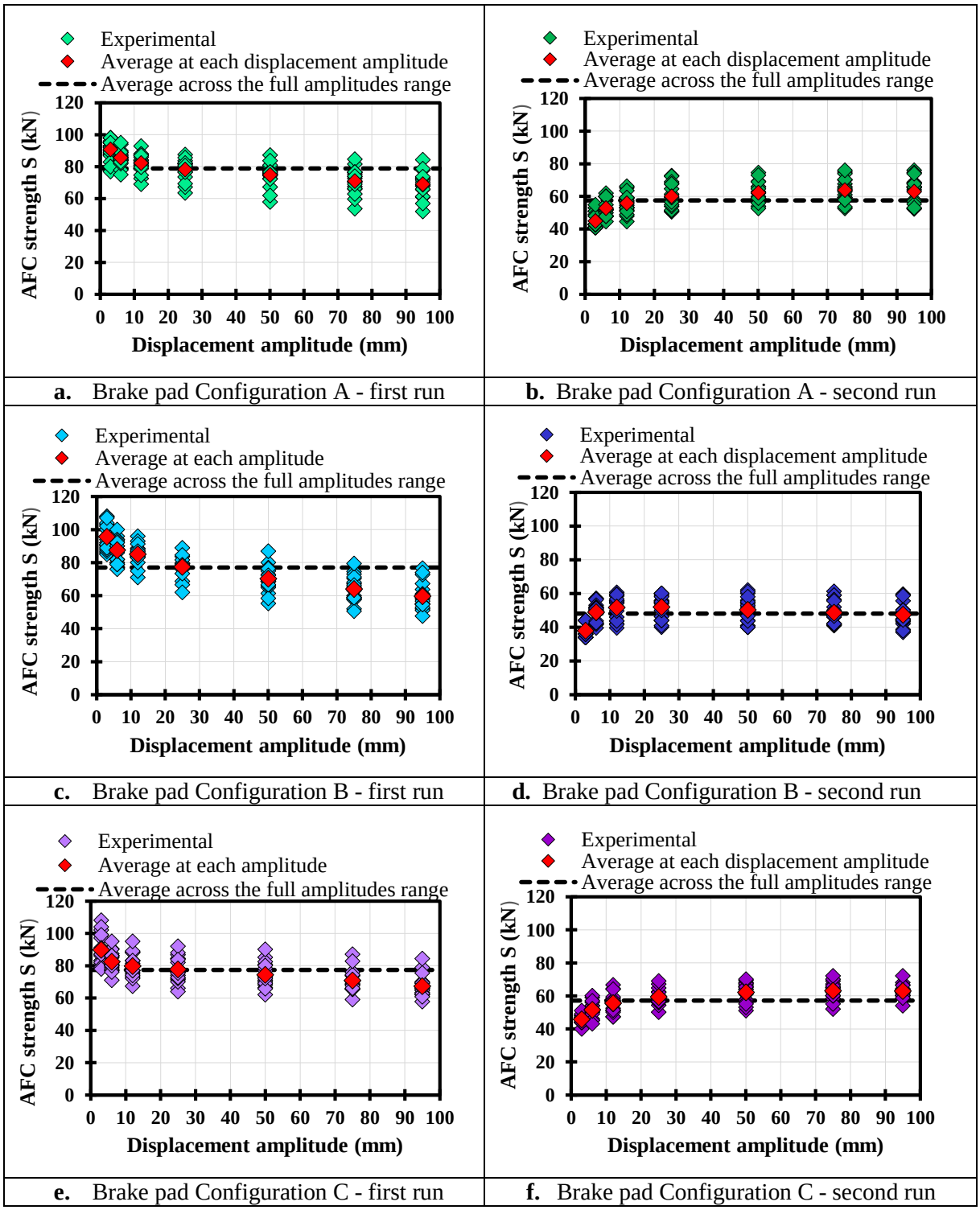

Figure 3.8. AFC strength for AFCs with bonded brake pads

In the second run, all three configurations exhibited the lowest AFC strength in the initial sliding cycles. Then, AFC strength increased as the displacement amplitude increased up to 12mm, and it and was almost constant for displacement amplitudes greater than 12mm, as shown in Figure 3.8. During the initial sliding cycles, AFC strength was 19%, 26%, and 18% less than the average AFC strength from all cycles and all amplitudes, for Configurations A, B, and C, respectively, as shown in Figures 3.8b, d, and f. Reasons for the lower strength are due to the full bolt force not being activated until it is rotated and pulled. Furthermore, the rotated bolt has an axial tension force with a component that directly resists the applied AFC force. After the increase in AFC strength, the AFC strength is almost constant due to the constant friction coefficient and constant bolt tension. This behaviour is linked to the stable brake pad wear state mechanism described in Section 3.1.

Figure 3.8 shows the scatter exhibited by the AFC strength in the first run is greater than that in the second run due to the unstable brake pad wear state mechanism described in Section 3.1.

Results above show variations in AFC strength before becoming constant, are due to either the unstable brake pads wear mechanism or bolt rotation. Other possible cause of AFC strength variation could be related to corrosion for AFCs exposed to corrosive environments. It is expected corrosion may affect variation in AFC strength only in the initial sliding cycles while the corrosive product developed on the external perimeter of the sliding interfaces is removed by the sliding of the slotted plate as observed in testing of corroded AFCs with metallic sliding surfaces [3.22]. In addition, for corroded AFCs with metallic sliding surfaces, after corrosive product was removed in the initial sliding cycles, it was observed AFC strength

was similar to that observed in non-corroded AFCs [3.22]. This indicates the almost constant AFC strength observed as cycles increase in AFCs with brake pads, and resulting from the stable brake pads wear state may be no affected by corrosion.

2.3 Effective friction coefficient, μe, strength degradation, SD

Figures 3.9a - c show that the effective friction coefficient, μe, for each brake configuration at hysteresis loop amplitudes of 3mm – 95mm follow the AFC strength, S, trends described in Section 3.2. This occurs because μe was computed from Equation 3.3 using $m = 2$, $n = 2$, F_{proof} = 95kN, and S as the average of 3 AFCs at each hysteresis loop amplitude following the methodology defined in Section 2.4. In the first run, μe, decreased with the displacement amplitude, going from 0.24, 0.25, and 0.24 down to 0.18, 0.16, and 0.18, for Configurations A, B, and C, respectively. In the second run, μe, at the initial sliding cycles was 0.12, 0.10, and 0.12 and for displacement amplitudes up to 12mm it increased to 0.17, 0.13, and 0.17, for Configurations A, B, and C, respectively. For displacement amplitudes greater than 12mm, μe became almost constant and near the same values as those from the first run at the peak displacement amplitude.

Figures 3.9a-c show the average effective friction coefficient, μea, for all displacement amplitudes in the first run was 0.208, 0.203, and 0.204, and for the second run was 0.151, 0.127, and 0.150 for Configurations A, B, and C, respectively. The average effective friction coefficient for the three brake pad configurations and for all displacement amplitudes, μead, was 0.205 and 0.143 for the first and second runs, respectively. These values were 59% and 41% of the dynamic friction coefficient, μd, of 0.35 suggested by the brake pad manufacturer

[3.18, 3.19]. Differences between μea values and μd are probably due to the AFC testing configuration used in this test, which have been shown to provide significantly lower values than in symmetric friction connections SFCs [3.23]. The peak μe values, obtained in the initial sliding cycles of the first run, were 1.7, 2.2, and 1.9 times μea in the second run, while the lower bound values were 0.71, 0.71, and 0.70 times μea in the second run.

In Figures 3.9a-c the maximum possible displacement, Δmax, of 6.8mm, as defined in Section 2.9 was plotted as a vertical dashed line. It was calculated based on the maximum possible bolt rotation, θmax, as defined in Section 2.9 with Equations 3.5-3.6 for O = 2mm, t_f = 20mm, and g = 68mm. The bolt grip length measured to the outside of the plates, g, of 68mm was due to the three 20mm plates and two 4mm brake pads. In Figures 3.9a-c the effective friction coefficient μe became more uniform/constant after this displacement of Δmax.

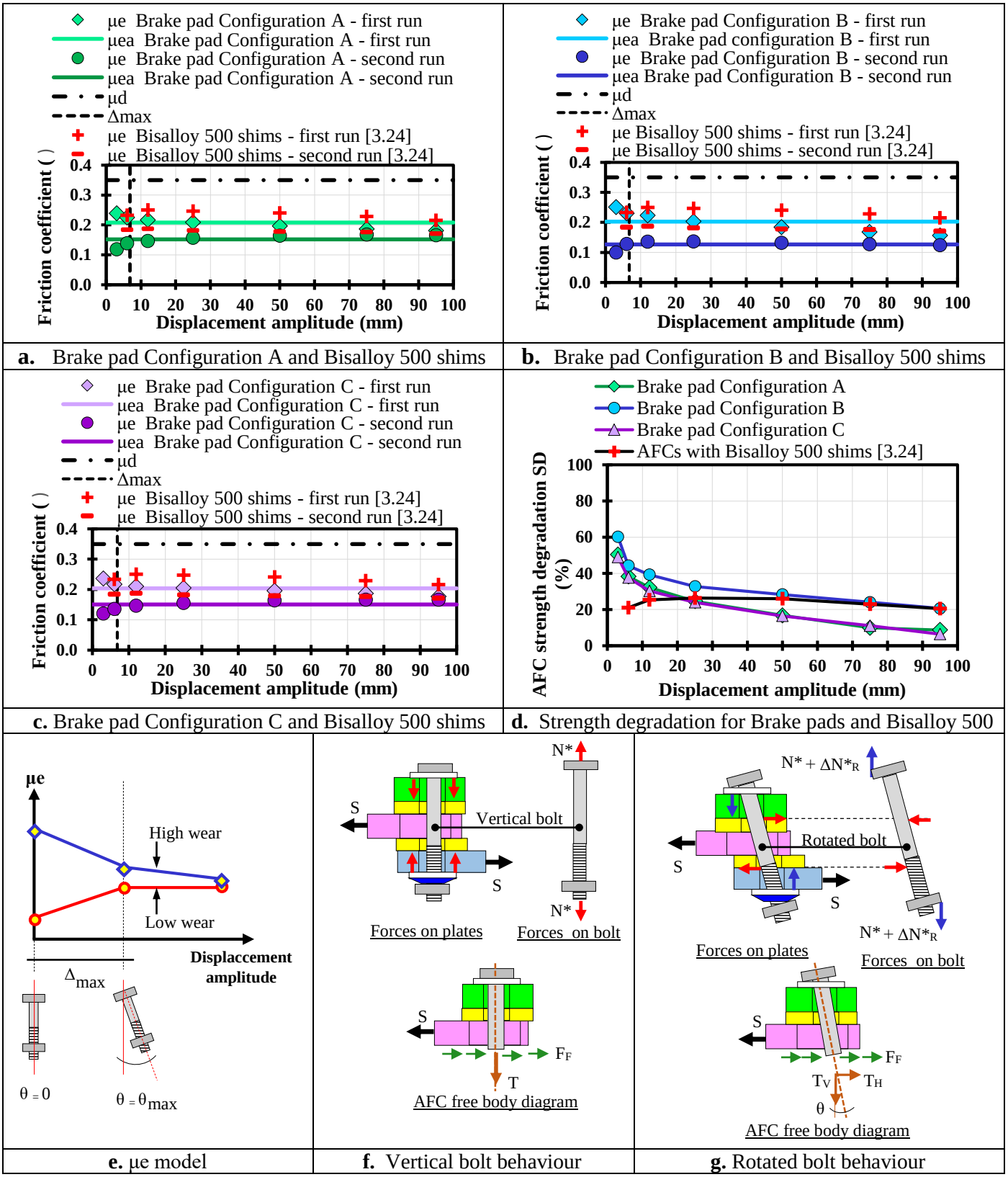

Figure 3.9. Friction coefficient, strength degradation, bolt behaviour, and effective friction coefficient model for AFCs with bonded brake pads and AFCs with Bisalloy 500 shims [3.24]

In the first run, the greatest value of μe occurred in Figures 3.9a-c in the initial sliding cycles at small displacements due to the combined action of the high bolt tension close to the proof load after the bolt assembly, and the high initial roughness of the brand new sliding surfaces of the brake pads. At larger displacements μe decreased due to the unstable wear mechanism described in Section 3.1. The two effects involved are the reduction in friction coefficient as the surface become smoother, and the reduction in bolt tension as the soft brake pad material components are removed. This decreasing trend of μe indicates a high wear of the brake pads, and it reduced as the displacement amplitude increased, as shown in Figure 3.9e.

In the second run, the lowest value of μe occurred in Figures 3.9a-c in the initial sliding cycles. That is because the bolts were nearer vertical and did no undergo any increase in bolt tension due to bolt rotation ΔN^*_R. They were also longer and looser than at the beginning of the first run due to yielding from MPV interaction. The AFC strength corresponds to the friction force, Ff, produced by the vertical bolt axial force N^*, as shown in Figure 3.9f.

In the second run, the increasing μe in Figures 3.9a-c for displacement amplitudes less than Δmax occurs as the bolts rotate from 0 to θmax. Here, there is an increase in bolt tension due to bolt rotation, ΔN^*_R, which increases as the bolt rotation increases, as shown in Figure 3.9g. The increase in bolt tension due to bolt rotation corresponds to an increase in clamping force on the connection plates that makes the sliding surfaces going back in contact after the soft brake pad material components were removed in the first run, as shown in Figure 3.9g. This increase in clamping force on the connection plates is more beneficial for Configuration A than for Configurations B and C. That is because wearing in Configuration A was more uniform and less deep than that observed in Configurations B and C as described in Section

3.1. The AFC strength increase is due to the friction force, *Ff*, produced by the bolt vertical tension component, T_V, (including the ΔN^*_R effect) in addition to the bolt horizontal tension component, T_H, as shown in Figure 3.9g. The almost constant μe for displacement amplitudes greater than Δmax occurs, since further increments on the displacement amplitude do not increase the bolt rotation. Therefore, ΔN^*_R remains constant, which makes the bolt tension, the AFC strength, and μe almost constant. In addition, the surfaces were already smoothed in the first run. Finally, Figure 3.9e indicates that while in the first run the brake pads surface effects dominate due to high wear of the sliding surfaces of the brake pads and polishing of the steel sliding surfaces of the slotted plate, in the second run the bolt rotation effect is significant since the brake pad sliding surfaces and the steel sliding surfaces of the slotted plate had low wear.

Figure 3.9d quantifies for all three configurations the strength degradation, *SD*, associated with the decrease in μe between the first run and second run according to Equation 3.4. Values of *SD* in Figure 3.9d were calculated with values of μe in Figures 3.9a-c. It can be seen in Figure 3.9d that *SD* decreased rapidly for displacement amplitudes less than 25mm, and decreased more slowly thereafter. *SD* was as high as 60% for brake pad Configuration B, but there was less strength degradation up to 50% for brake pad Configurations A and C. Strength degradation was greatest in the initial sliding cycles because μe in the first run was high as a result of the brand new and rough brake pad sliding surfaces before the brake pad sliding surfaces became smooth, and also as result of polishing of the steel sliding surfaces of the slotted plate. Given that the strength degradation for Configuration A is same as that for Configuration C and the hysteresis loop shapes were similar, it is considered that the hysteretic

behaviour of Configuration A is close to that of Configuration C. In practice, Configuration A is easier and faster to assemble than Configuration C.

Figures 3.9a-d compare μe and *SD* for all brake pad configurations with those recorded in similar testing conditions for metallic sliding surfaces of Grade 300 steel – high hardness shims such as Bisalloy 500 [3.24], which are the preferred metallic sliding surfaces for AFCs given the stable and predictable hysteretic performance [3.1, 3.2, 3.8]. In the first run and second run, μe for pad configurations A, B, and C was 0.8 – 1.0, 0.7 – 1.0, 0.7 – 1.0 times μe for Bisalloy 500 shims, respectively. For displacement amplitudes less than 25mm, *SD* for brake pad configurations A, B, and C was 1.3 – 1.8, 1.6 – 2.1, and 1.2 – 1.8 times *SD* for Bisalloy 500 shims, respectively. But for displacement amplitudes equal or greater than 25mm, *SD* for brake pad configurations A, B, and C was 0.4 – 0.9, 1.0 – 1.1, and 0.3 – 0.9 times *SD* for Bisalloy 500 shims, respectively. These results show brake pads developed equal or less friction coefficient than Bisalloy 500 shims. However, after brake pads reached the steady wear state for displacement amplitudes equal or greater than 25mm, they developed same or less strength degradation than Bisalloy 500 shims. This indicates brake pads after reaching the steady wear state may develop similar or more stable and reliable hysteretic performance than that developed by Bisalloy 500 shims.

III. AFC STRENGTH DESIGN CONSIDERATIONS

For design, reliable values of strength, understrength and overstrength values are required. These values must consider the variation associated with bolts tensioning during assembly, the effects of cleanness of sliding surfaces, and the variation of the effective friction with

hysteresis loop amplitude. An understrength factor, γ, and an overstrength factor, β, were defined to account for the likely maximum and minimum average AFC strength, Sa_{min}, and, Sa_{max}, termed understrength and overstrength, respectively. For the three brake pad configurations in both runs, Sa_{min} and Sa_{max} are defined using the dry friction theory of Coulomb from Equation 3.3 and in terms of the μead as defined in Section 3.3:

$Sa_{min} = \gamma \times m \times n \times F_{proof} \times \mu ead$	(3.7)
$Sa_{max} = \beta \times m \times n \times F_{proof} \times \mu ead$	(3.8)

Figure 3.10 compares experimental AFC strength and the predicted average AFC strength, overstrength, and understrength for all three configurations. The experimental AFC strength, for each brake pad configuration comprises the 126 values described in Section 3.2, and the average AFC strength, overstrength, and understrength were predicted using Equations 3.7 – 3.8 using m = 2, n = 2, F_{proof} = 95kN, and μead of 0.205 and 0.143 for the first and second run, respectively from results in Section 3.3. The values of γ = 0.7 and β = 1.4 were adopted from those in current design practice for AFCs with metallic shims [3.25].

It may be seen in Figure 3.10 that the understrength and overstrength envelope 95% of experimental AFC strengths for each brake pad configuration in both runs. These considerations are useful for predicting the average AFC strength for design for this particular material when field conditions approximate laboratory conditions. They thus define a simple bridge to design practice to enable easier uptake and use.

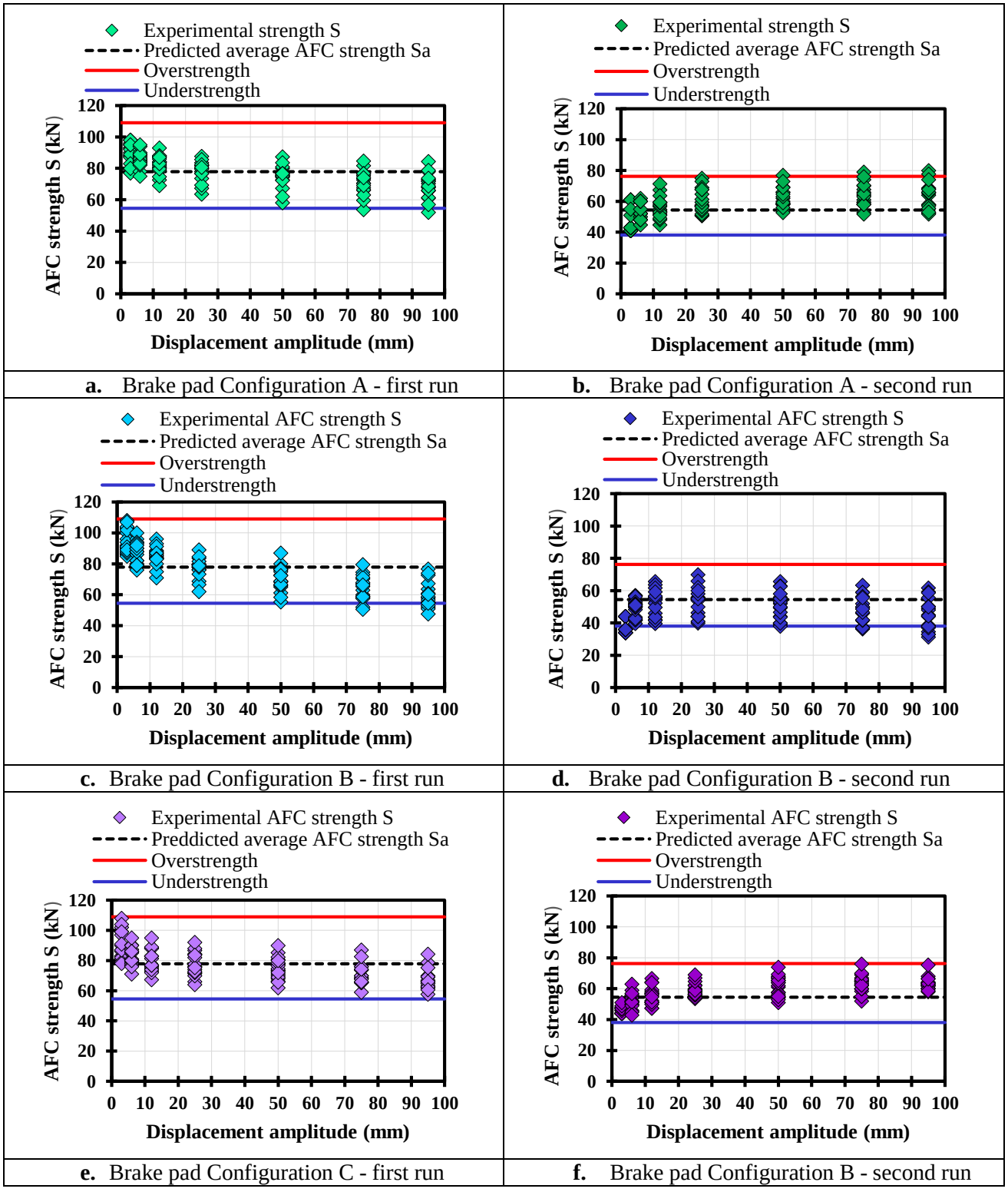

Figure 3.10. Comparison between AFC strength model and experimental AFC strength for AFCs with bonded brake pads.

CONCLUSIONS

This paper describes the hysteretic behaviour of AFCs with bonded brake pads of D3923, it was shown that:

i. The hysteresis loop has the same shape regardless of the brake pad configuration. The hysteresis loop stability increased as the number of cycles increased and the brake pads reached the stable wear state.

ii. AFCs with bonded brake pads on recessed surfaces (Configuration C) had the best performance given their high strength, high hysteresis loop stability within a run, low degradation between runs, and also because in this configuration the brake pads did not undergo debonding. Configuration A could be also used in practice given that this configuration is easy to assemble and hysteretic behaviour is close to that shown by Configuration C.

ii. The greatest AFC strengths occurred in the initial sliding cycles, then AFC strength reduced until becoming almost constant regardless of the brake pad configuration. The AFC strength reduced due to loss of bolt tension that occurs when the soft brake pad components are removed. The AFC strength became constant when sliding occurs over brake pad surfaces with high density of wear resistant components that maintain the bolt tension almost constant.

iii. The steady wear state effective friction coefficient varied in the ranges 0.12 - 0.17, 0.10 - 0.14, and 0.12 – 0.17 with the average values being 0.15, 0.12, and 0.15, for brake pad Configurations A, B, and C, respectively. The peak values, obtained in the initial sliding

cycles were 1.7, 2.2, and 1.9 times the average values, while the lower bound values obtained after many sliding cycles were 0.71, 0.71, and 0.70 times the average values, for brake pad Configurations A, B, and C respectively. Strength degradations were as high as 60% for brake pad Configuration B, but there was less strength degradation up to 50% for brake pad Configurations A and C.

iv. For this particular material and under laboratory conditions, the average AFC strength can be predicted as the product of the total bolt proof load and an average effective friction coefficient of 0.205 and 0.143 for brand new and degraded sliding surfaces, respectively. The maximum and minimum likely average AFC strength can be predicted using understrength and overstrength factors of 0.7 and 1.4, respectively.

ACKNOWLEDGEMENTS

The authors would like to acknowledge funding from MBIE Natural Hazards Research Platform (NHRP), and material donation from John Jones Steel Ltd., for undertaking this research. All opinions expressed remain those of the authors.

REFERENCES

[3.1] Rodgers, GW, Chase, JG, Causse, R, Chanchi Golondrino, J and MacRae, GA (2017). *Performance and Degradation of Sliding Steel Friction Connections: Impact of Velocity, Corrosion Coating and Shim Material*. Engineering Structures, Vol. 141, pp. 292–302. ISSN: 0141-0296. https://doi.org/10.1016/j.engstruct.2017.02.070

[3.2] Khoo, H.H., Clifton, C., Butterworth, J., MacRae, G. and Ferguson, G. (2011). *Influence of steel shim hardness on the Sliding Hinge Joint.* Journal of Constructional Steel Research. Vol 72, May 2012, p 119 – 129. https://doi.org/10.1016/j.jcsr.2011.11.009

[3.3] Clifton, G.C. (2005). Semi-Rigid Joints for Moments Resisting Steel Framed Seismic Resisting Systems. *Published PhD Thesis, Department of Civil and Environmental Engineering.* University of Auckland – New Zealand.

[3.4] Chanchi, J., MacRae, G.A., Chase, J. G., Rodgers, G.W., and Clifton, C.G. (2015). *Clamping force effects on the Behaviour of Asymmetrical Friction Connections (AFCs).* 15th World Conference on Earthquake Engineering – WCCE. Lisbon, Portugal.

[3.5] Borzouie, J, Chase, JG, MacRae, GA and Rodgers, GW (2015). *Experimental Studies on Cyclic Performance of Column Base Weak Axis Aligned Asymmetric Friction Connection*. Journal of Constructional and Steel Research (JCSR), Vol 112, pp. 252-262. https://doi.org/10.1016/j.jcsr.2015.05.007

[3.6] Borzouie, J, Chase, J.G., MacRae, GA, Rodgers, GW and Clifton, C (2016). *Experimental Studies on Cyclic Performance of Column Base Strong Axis Aligned Asymmetric Friction Connections*. ASCE J. Structural Engineering, Vol 142(1), Article 04015078, 10-pages. https://doi.org/10.1061/(ASCE)ST.1943-541X.0001327

[3.7] MacRae, G.A., Clifton, C.G., MacKinven, H., Mago, N., Butterworth, J., Pampanin, S. (2010). *The Sliding Hinge Joint Moment Connection*. Bulletin of the New Zealand Society for Earthquake Engineering. Vol 43, Issue 3, pp. 202-212.

[3.8] Khoo, H.H., Clifton, G.C., MacRae, G.A., Zhou, H., and Ramhormozian, S. (2014). *Proposed design models for the asymmetric friction connection*. Earthquake and Structural Dynamics Journal. Vol 44, Issue 8, p. 1309-1324. https://doi.org/10.1002/eqe.2520

[3.9] Rodgers, G.W., Mesnil, O., Chanchi Golondrino, J., MacRae, G.A. and Chase, J.G. (2014). *Generalised nonlinear modeling of unstable stick-slip force reduction effects in friction energy dissipation devices*. NZSEE Bulletin, Vol 47(3), pp. 217-223, ISSN No. 1174-9857.

[3.10] Rodgers, G.W., Herve, R., MacRae, G.A., Chanchi Golondrino, J., and Chase, J.G. (2017). *Dynamic Friction Coefficient and Performance of Asymmetric Friction Connections.* Structures – Elsevier. Available online 14 September 2017, In Press, Corrected Proof. https://doi.org/10.1016/j.istruc.2017.09.003

[3.11] Grigorian, C.E., Yang, T.S., and Popov, E.P. (1993). *Slotted Bolted Connection Energy Dissipators.* Earthquake Spectra. Vol. 9, No. 3, pp. 491-504. https://doi.org/10.1193/1.1585726

[3.12] Tremblay, R. (1993). *Seismic Behaviour and Design of Friction Concentrically Braced Frames for Steel Buildings.* Unpublished PhD Thesis, Department of Civil Engineering. The University of British Columbia. Vancouver – Canada.

[3.13] Pall, A.S. (1979). Limited Slip Bolted Joints – A Device to Control the Seismic Response of Large Panel Structures. *Unpublished PhD Thesis, Faculty of Engineering.* Concordia University – Canada.

[3.14] Pall, A., Marsh, C., and Fazio, P., (1980). *Friction Joints for Seismic Control of Large Panel Structures.* PCI Journal. Vol. 25 (6), pp. 38 – 61. Doi: 10.15554/pcij.11011980.38.61

[3.15] Tyler, R.G. (1985). Test on Brake Lining Damper for Structures. *Bulletin of the New Zealand Society for Earthquake Engineering.* Vol 18, Issue 3, pp 280-284.

[3.16] Filiatrault, A. (1990). *Analytical Predictions of the Seismic Response of Friction Damped Timber Shear Walls.* Earthquake Engineering and Structural Dynamics. Vol.19, pp. 259 – 273. https://doi.org/10.1002/eqe.4290190209

[3.17] Kim, H.J. (2004). Experimental Characterization of Bolt Stressed Non- Asbestos Organic (NAO) Material-to-Steel-Interfaces. Un*published PhD Thesis, Department of Civil and Environmental Engineering.* University of Toronto – Canada.

[3.18] Ferotec Friction, Inc. (2011). Product Data Sheet – Friction Material Composite D3923.

[3.19] Ferotec Friction, Inc. (2011). Material Safety Data Sheet – Friction Material Composite D3923/ D3924.

[3.20] Huntsman Structural Adhesives. (2004). Brake and Clutch Bonding, Araldite 71 brake and bonding adhesive

[3.21] Erikson, M., Bergman, F., and Jacobson, S. (2002). *On the nature of tribological contact in automotive brakes.* International Journal on the Science and Technology of Friction, Lubrication and Wear. Vol. 252, pp. 26-36. https://doi.org/10.1016/S0043-1648(01)00849-3

[3.22] Chanchí, J., MacRae, G. A., Chase, J. G., Scott, A., Rodgers, G.W., and Clifton, G. C. (2013). *Recent Research on Two Low Damage Dampers Applicable to Steel Framing Systems*. Steel Innovations Conference. Christchurch, New Zealand.

[3.23] Xie, R., Chanchi, J., MacRae, G.A., and Clifton, C.G. (2018). *Braced frame asymmetrical and asymmetrical friction connection performance*. Key Engineering Materials. Vol. 763, pp. 216 – 223. https://doi.org/10.4028/www.scientific.net/KEM.763.216

[3.24] Chanchi, J., MacRae, G.A., Chase, J. G., Rodgers, G.W., and Clifton, C.G. (2015). *Is the Asymmetrical Friction Connection (AFC) a low damage dissipater?* New Zealand Society of Earthquake Engineering Conference. Auckland, New Zealand.

[3.25] MacRae, G.A., and Clifton, C.G. (2015). *Research on Seismic Performance of Steel Structures*. Steel Innovation Conference. Auckland, New Zealand.

Chapter 4

Asymmetric Friction Connections (AFCs) Bolt Lever Arm Effects on Hysteretic Behaviour

Chapter 4

"Asymmetric Friction Connection Bolt Lever Arm Effects on Hysteretic Behaviour"

Jose Christian Chanchi Golondrino [a, b,1*], Gregory Anthony MacRae[b,2], James Geoffrey Chase[c,3], Geoffrey William Rodgers[c,4], George Charles Clifton[d,5]

[a] Universidad Nacional de Colombia – Sede Manizales, Departamento de Ingeniería Civil, Manizales 170004, Colombia.

[b] University of Canterbury, Department of Civil and Natural Resources Engineering, Private Bag 4800, Christchurch 8140, New Zealand.

[c] University of Canterbury, Department of Mechanical Engineering, Private Bag 4800, Christchurch 8140, New Zealand.

[d] The University of Auckland, Department of Civil & Environmental Engineering, Faculty of Engineering, Private Bag 92019, Auckland Mail Centre, Auckland 1142, New Zealand.

[1] jcchanchigo@unal.edu.co, [2]gregory.macrae@canterbury.ac.nz, [3]geoff.chase@canterbury.ac.nz, [4]geoff.rodgers@canterbury.ac.nz, [5]c.clifton@auckland.ac.nz
[*]Corresponding author

Key Words: Asymmetric Friction Connection, Bolt grip length, Bolt grip length to bolt diameter ratio, Loss of bolt tension, Bolt bending, Bolt flexural yielding

ABSTRACT

While Asymmetric Friction Connections (AFCs) have been employed as seismic energy dissipation devices in steel structures, development of design guidance based on robust understanding of their behaviour is required. This paper describes the quasi-static testing of 18 AFCs with Bisalloy 500 shims and 2 M16 Grade 8.8 bolts were tested, to quantify the effect of bolt lever arm to bolt diameter (*l/d*) ratio on the AFC sliding performance. Results show hysteresis loop shape remained similar for all *l/d*. However, increasing *l/d* from 1.38 to 3.88, reduced the average AFC strength by 42% - 47%, reduced the hysteresis loop loading

stiffness by 33% - 47%; and reduced the effective friction coefficient from 0.28 to 0.08. For AFCs with $l/d \geq 3.25$, bolts underwent significant flexural yielding, which reduced their performance in future cycles.

I. INTRODUCTION

Asymmetric Friction Connections (AFCs) are being implemented in steel framed structures in earthquake-prone regions to dissipate seismic energy without damaging the structure. Design requirements for AFCs have been developed based on experimental studies. However, in these experimental studies:

i. AFC strength has been observed to decrease with cyclic loading [4.1, 4.2, 4.3, 4.4]. This reduction in AFC strength has been only attributed to bolt yielding occurring when bolts bend in double curvature while bearing on the connection plates at two points termed bearing points, and

ii. AFC strength reduction has been described as function of the distance between the bolt bearing points, l, divided by the bolt diameter, d, termed bolt lever arm to bolt diameter (l/d) ratio, but tests have been conducted only for a narrow range of l/d [4.2, 4.3, 4.4].

For robust design guidance to be developed for AFCs, there is a need for design procedures and models validated on experimental results over the likely range of l/d used in practice, which also consider the different causes of AFC strength loss. This paper addresses these needs by seeking answers to the following questions via experimental AFC testing:

i. How does the hysteresis loop shape of AFCs change with increasing *l/d*?

ii. How does the hysteresis loop loading stiffness change with increasing *l/d*?

iii. Why does the AFC strength decrease with increasing *l/d*?

iii. When and why do bolts yield in AFCs?

iv. Which values of effective friction coefficient can be used for predicting the strength of AFCs for various *l/d*?

II. PREVIOUS WORK

AFCs are friction bolted connections used as seismic dissipaters. They may be used in moment resistant frames at the beam-column joint or column base connection, in braces of braced frames [4.1], or elsewhere. AFCs have generally been assembled using three Grade 300 steel plates, two thin plates termed "shims" made of high hardness materials (such as Bisalloy 400 or Bisalloy 500), and high strength structural bolts, such as Grade 8.8 bolts to AS 1252. They are generally assembled by tightening bolts up to the proof load.

AFCs dissipate energy via friction between the central slotted plate and the shims placed on either side [4.1, 4.2]. The hysteresis loop sliding force is termed the AFC strength. Quasi-static tests have shown that this strength may be almost constant. The AFC strength is also not sensitive to the bolt tightening force, when the bolt force is greater than the proof load [4.2, 4.3].

AFC strength degrades during cyclic loading. This degradation may result from decrease in compressive force over the surfaces as a result of bolt bending yielding and extension, and/or changes in the properties in the sliding surfaces [4.1, 4.2]. The effect of bolt bending and

yielding increases as the bolt lever arm, *l*, increases [4.3, 4.4, 4.5]. Here, the bolt lever arm, *l*, is defined as the distance between the points where the bolt shank is bearing on the connection plates when bending in double curvature, as shown in Figure 4.1 [4.3, 4.4, 4.5]. Testing of AFCs with Grade 300 steel plates, different shim materials, such as Grade 300 steel, brass, and Bisalloy 400, and M16, M20, M24, and M30 Grade 8.8 bolts with ratios of bolt lever arm, *l*, to bolt diameter, *d*, between 0.9 and 2.29, showed AFC strength decreased as *l/d* increased, regardless of the shim type [4.4,4.5].

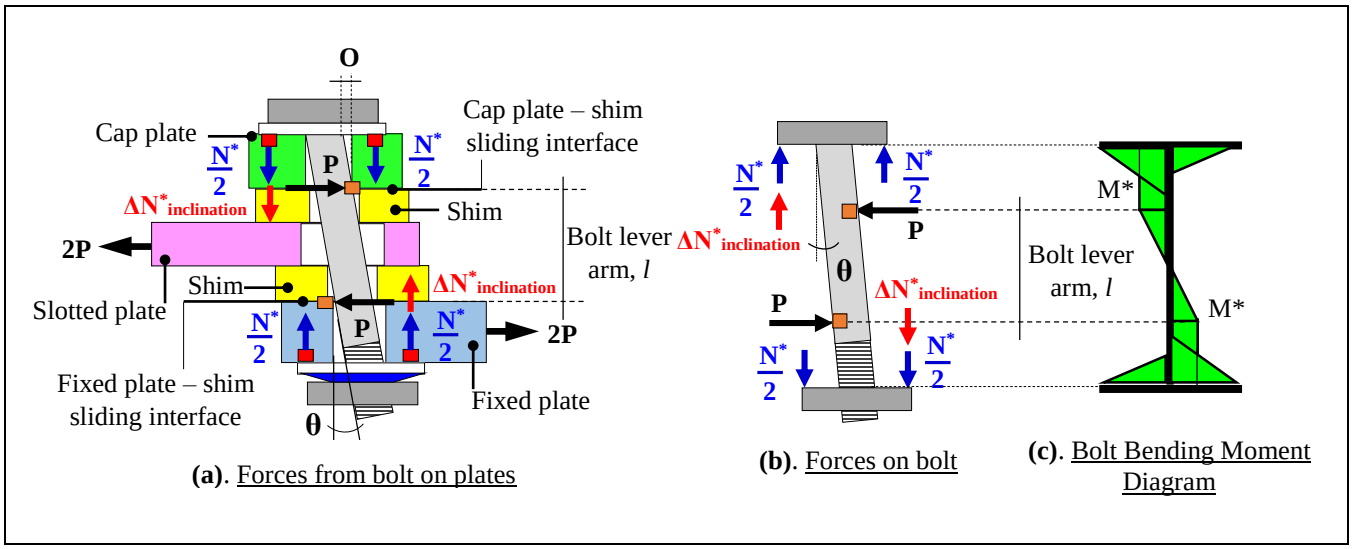

Figure 4.1. Forces on AFCs during sliding of slotted plate, idealized bolt deformation, and bolt bending moment diagram in MPV model [4.3, 4.4, 4.5] (Not to scale)

Models developed considering bolt moment – axial – shear (MPV) interaction in AFC connections indicate strength reduces as *l/d* increases [4.3, 4.4, 4.5]. The moment develops as the bolts incline, bear on the cap plate and on the fixed plate, and bend in double curvature, as shown in Figure 4.1. In this figure, *N** is the bolt axial tension during the sliding and it can be considered to result from:

i. The bolt assembly tension, N^*_A

ii. The effect of MPV interaction, which decreases the bolt tension by ΔN^*_{MPV}, and

iii. The effect of bolt elongation, which increases the bolt tension by $\Delta N^*_{inclination}$ as the bolt inclines during sliding.

The bolt inclination is affected by the amount of friction between the bolt head/nut together with the washer, and the exterior of the plates. The maximum bolt inclination is controlled by the bolt hole oversize, O. At this inclination, no horizontal forces are necessary at the cap plate – structural washer and fixed plate – flat washer interfaces, as shown in Figures 4.1a-b. The increase in bolt tension, $\Delta N^*_{inclination}$, is possible for bolts assembled to less than the bolt ultimate tensile strength. Strain aging can allow additional tension force to be carried.

In existing MPV models [4.2, 4.4, 4.5], AFC strength has been assessed without explicitly considering bolt inclination or the increase in bolt tension, $\Delta N^*_{inclination}$. The bolt design moment – axial – shear (MPV) interaction equation has been defined [4.2, 4.4, 4.5]:

$$\left[\frac{M^*}{M_{rfn}}\right]+\left[\frac{V^*}{V_{rfn}}\right]=I \qquad (4.1)$$

Where, M^* is the bolt moment demand, V^* is the bolt shear demand, M_{rfn} is the nominal bolt moment capacity considering axial force interaction using N^*, V_{rfn} is the nominal bolt shear capacity considering no axial force interaction, and I is the interaction factor. Note, I = 1.0 indicates bolt plastic yielding, while I < 1.0 indicates the bolt has not fully plasticised. The bolt shear demand V^* corresponds to the bearing force from the bolt to the cap plate or to the fixed plate represented by the force P shown in Figure 4.1. This in turn provides the friction force at each of the sliding interfaces. The bolt moment demand M^* corresponds to the

maximum bolt bending moment produced by the force P shown in Figure 4.1. These variables are defined:

$V^* = N^* \times \mu$	(4.2)
$M^* = \frac{N^* \times \mu \times l}{2}$	(4.3)
$M_{rfn} = 0.1665 \times d^3 \times \left[1 - \left[\frac{N^*}{0.56 \times d^2 \times F_{uf}}\right]\right] \times F_{uf}$	(4.4)
$V_{rfn} = 0.62 \times F_{uf} \times 0.56 \times d^2$	(4.5)
$\mu_n = \frac{\mu \times N^*}{F_{proof}}$	(4.6)

Where, μ is the assumed friction coefficient at the sliding interfaces between the slotted plate and the shims, d is the bolt nominal diameter, F_{uf} is the bolt nominal ultimate tensile strength, F_{proof} is the bolt proof load, and l is the bolt lever arm defined as the distance between the cap plate-top shim and fixed plate - bottom shim interfaces, as shown in Figure 4.1.

In this model, the bolt axial tension during the sliding, N^*, considering moment – axial force – shear force (MPV) interaction, can be obtained by solving the quadratic equation resulting from substituting Equations 4.2 to 4.5 into Equation 4.1. The nominal shear sliding strength per bolt and per sliding surface, shown as P for the single bolt connection in Figure 4.1, normalized by the bolt proof load, $F_{proof,}$ is denoted μ_n. It corresponds to a theoretical effective friction coefficient calculated based on the assumed friction coefficient at the sliding interfaces, μ, and on the loss of bolt axial tension due to MPV interaction. This

theoretical effective friction coefficient, μ_n, can then be calculated using Equation 4.6 [4.4, 4.5].

Comparisons between the theoretical friction coefficient, μ_n, predicted with these MPV models and an experimental effective friction coefficient, μ_e, show MPV models can underestimate experimental AFC strengths [4.4,4.5]. The experimental effective friction coefficient, μ_e, is defined as the ratio between the experimental AFC strength and the total nominal bolt proof load. It considers the bolt axial tension during the sliding constant and is equal to the total nominal bolt proof [4.5]. This experimental effective friction coefficient is termed effective because the bolt axial tension is not constant due to loss of bolt tension from either MPV interaction [4.2-4.5] or degradation of the sliding surfaces due to surface coating [4.3], and materials used [4.6]. This experimental effective friction coefficient can be determined [4.5]:

$$\mu_e = \frac{S}{m \times n \times F_{proof}} \quad (4.7)$$

Where, S, is the experimental AFC strength at a given hysteresis loop amplitude, m, is the number of bolts, n, is the number of shear planes, and F_{proof}, is the nominal proof load per bolt. The variation in the experimental AFC strength with increasing l/d for design has been recommended to be taken into account by an understrength factor, α, of 0.7 and an overstrength factor, β, of 1.4 [4.7].

III MATERIALS AND METHODS

3.1 AFC devices

A total of 18 AFCs were assembled using 2 Bisalloy 500 shims with a nominal Brinell Hardness of 477 – 534BH [4.8], Grade 300 steel plates for the fixed, slotted, and cap plates, and clamped using 2 M16 Grade 8.8 structural galvanized bolts assembled with structural washers, flat washers, single Belleville washers, and nuts, as shown in Figure 4.2. The 18 AFCs were divided into 6 groups, varying Grade 300 steel plate thickness and bolt length, as shown in Table 4.1.

Table 4.1. Assembly variables for the 6 groups of AFCs

AFC Group	Grade 300 steel plates thickness	Bolt grip length outside of washers	Bolt size	Bolt shank unthreaded length	Bolt shank threaded length	Bolt lever arm	Ratio of bolt lever arm to bolt diameter	Proof load elongation	Proof load torque	Elongation necessary to yield the bolt in tension	Gain in elongation to yield the bolt in tension
	t	G				l	l/d	δ_{proof}	T_{proof}	δ_y	Δ_y
	mm	mm		mm	mm	mm	mm/mm	mm	N-m	mm	mm
I	10	52.5	M16 x 80	42.0	38.0	22.0	1.38	0.152	245	0.166	0.014
II	16	70.5	M16 x 90	52.0	38.0	28.0	1.75	0.199	265	0.217	0.018
III	25	97.5	M16 x 120	82.0	38.0	37.0	2.31	0.259	310	0.283	0.024
IV	30	112.5	M16 x 140	96.0	44.0	42.0	2.63	0.295	315	0.321	0.027
V	40	142.5	M16 x 180	136.0	44.0	52.0	3.25	0.357	335	0.390	0.032
VI	50	172.5	M16 x 200	156.0	44.0	62.0	3.88	0.433	365	0.472	0.039

The 6 groups of 3 AFCs in Table 4.1 used 2mm bolt hole oversize, shims of 6mm thickness, structural washers of 4mm thickness, flat washers of 4mm thickness, and single Belleville washers beneath the nut with a thickness of 2.5mm at the fully squashed condition. The bolt grip length measured outside of the structural and Belleville washers included the structural washer, the 3 Grade 300 steel plates, the 2 shims, the flat washer, and the fully squashed Belleville washer. The bolt lever arm, *l*, was assessed as the distance from the top shim-cap plate interface to the bottom shim-fixed plate interface, as shown in Figure 4.2c [4.5].

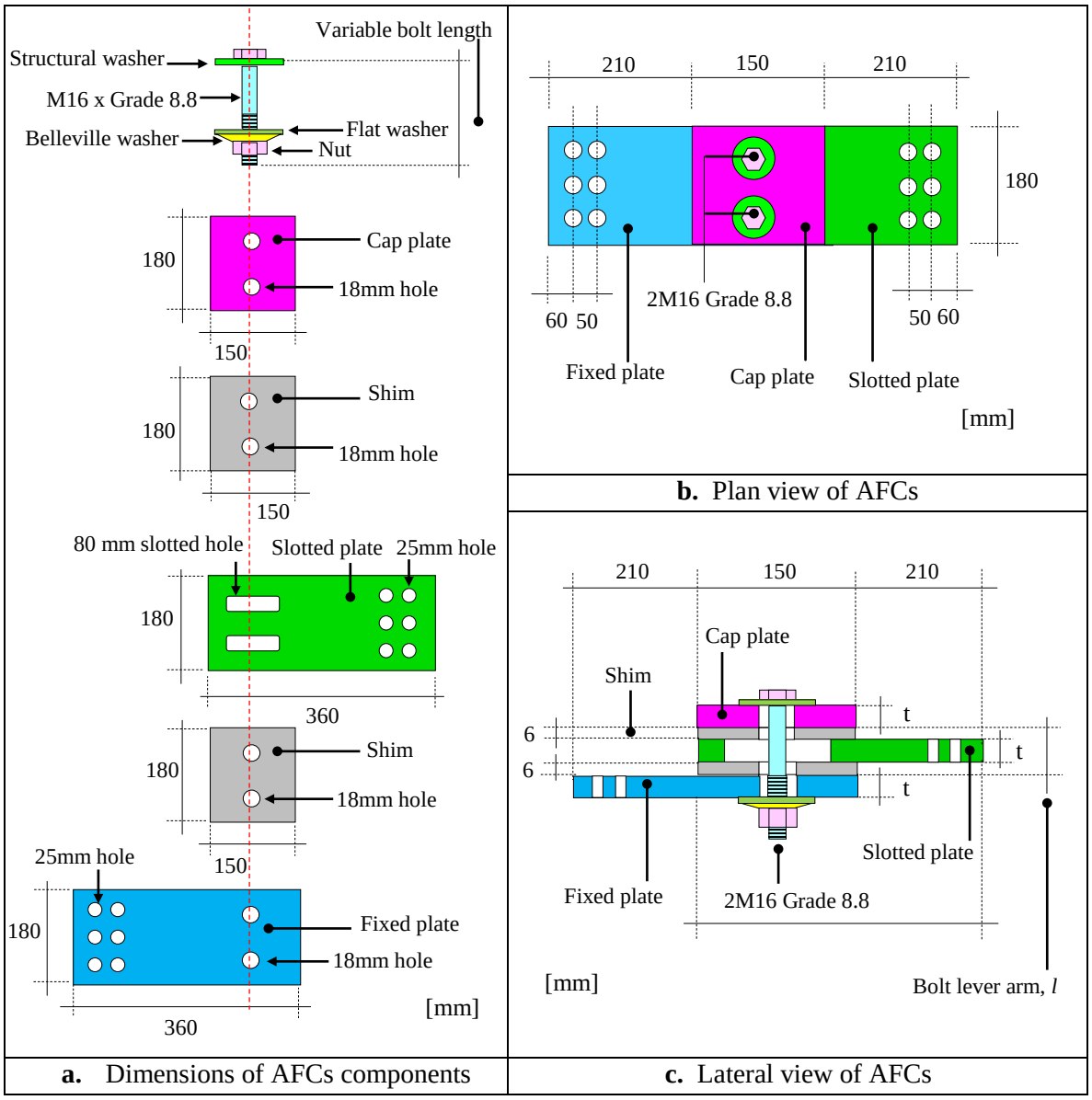

Figure 4.2. Dimensions of AFCs components, plan and lateral view of AFCs (Not to scale)

In Table 4.1 the bolt length for the 6 groups of AFCs was chosen so the ratio of bolt lever arm to bolt diameter, *l/d*, varied from 1.38-3.88. This range also ensures at least one clear thread of bolt projection from the nut, and at least one full thread inside of the bolt grip after bolt tightening, fulfilling the requirements of Clause 4.2.4.1 NZS3404: Part 1: 2009 [4.9].

3.2 AFC device assembly method

Each AFC was assembled by tensioning each of the two bolts in the clamped zone of the connection up to the proof load, F_{proof}, of a Grade 8.8 M16 bolt (95kN) using the torque control method. In this method, a bolt is gradually tensioned to a torque yielding an axial elongation equivalent to the computed elongation the bolt develops when it reaches the proof load in axial tensile testing, ignoring bolt torsion. This torque is termed proof load torque, T_{proof}, and the elongation of the bolt, when it reaches the proof load in axial tensile testing, is termed proof load elongation, δ_{proof}. While this method is standard for bolt tightening [4.9], the actual force in the bolt may be less than the anticipated value due to some bolt torsion allowing greater axial deformation than that due to axial deformation and stresses alone.

Table 4.1 shows the proof load elongation, δ_{proof}, the proof load torque, T_{proof}, the elongation necessary to yield the bolt in tension, δ_y, and the gain in elongation to yield the bolt in tension, Δ_y, defined:

$\Delta y = \delta y - \delta proof$	(4.8)

The proof load elongation, δ_{proof}, was read from an experimental bolt axial tensile relationship using the specified proof load, F_{proof}, for M16 Grade 8.8 bolts. The proof load torque, T_{proof}, was read from an experimental bolt torque - induced elongation relationship using the proof load elongation, δ_{proof}. The elongation necessary to yield in tension the bolt, δ_y, was read from an experimental bolt axial tensile relationship using the force that yields the bolt in

tension (103.6 kN) assessed as the product of a yield strength of 660MPa for Grade 8.8 bolts and a bolt tension area for M16 bolts of 157mm^2.

The experimental bolt axial tensile relationship per AFC group was obtained by tensioning 3 bolts to loads greater than the specified proof load, F_{proof}, for M16 Grade 8.8 bolts, as shown in Figure 4.3. Bolts were axially tensioned in a universal testing machine equipped with a load cell and an extensometer placed across the bolt grip length. The experimental bolt torque - induced elongation relationship per AFC group was obtained by subjecting 3 bolts to torques that increased from the snug tight condition to a torque of 500N-m, as shown in Figure 4.3. Bolts were tensioned using a calibrated torque wrench and the resulting bolt elongations were measured with a micrometer. Both relationships were obtained using a bolt testing length equal to the bolt grip length corresponding to the AFC group defined in Table 4.1. Given the variability in the torque-induced bolt elongation relationships in Figure 4.3**,** the proof load torque, T_{proof}, for each AFC group was assessed as the average of the maximum and minimum torques corresponding to the proof load elongation, as shown in Figure 4.3. Note, the applied torque during the bolt assembly considers the friction under the bolt head and under the nut. Even though the torque control method showed variability on the assembling relationships, this method was preferred in this research work for assembling AFCs since the bolt tension can be systematically controlled during the connection assembly; thus producing resulting bolt tensions close to the proof load.

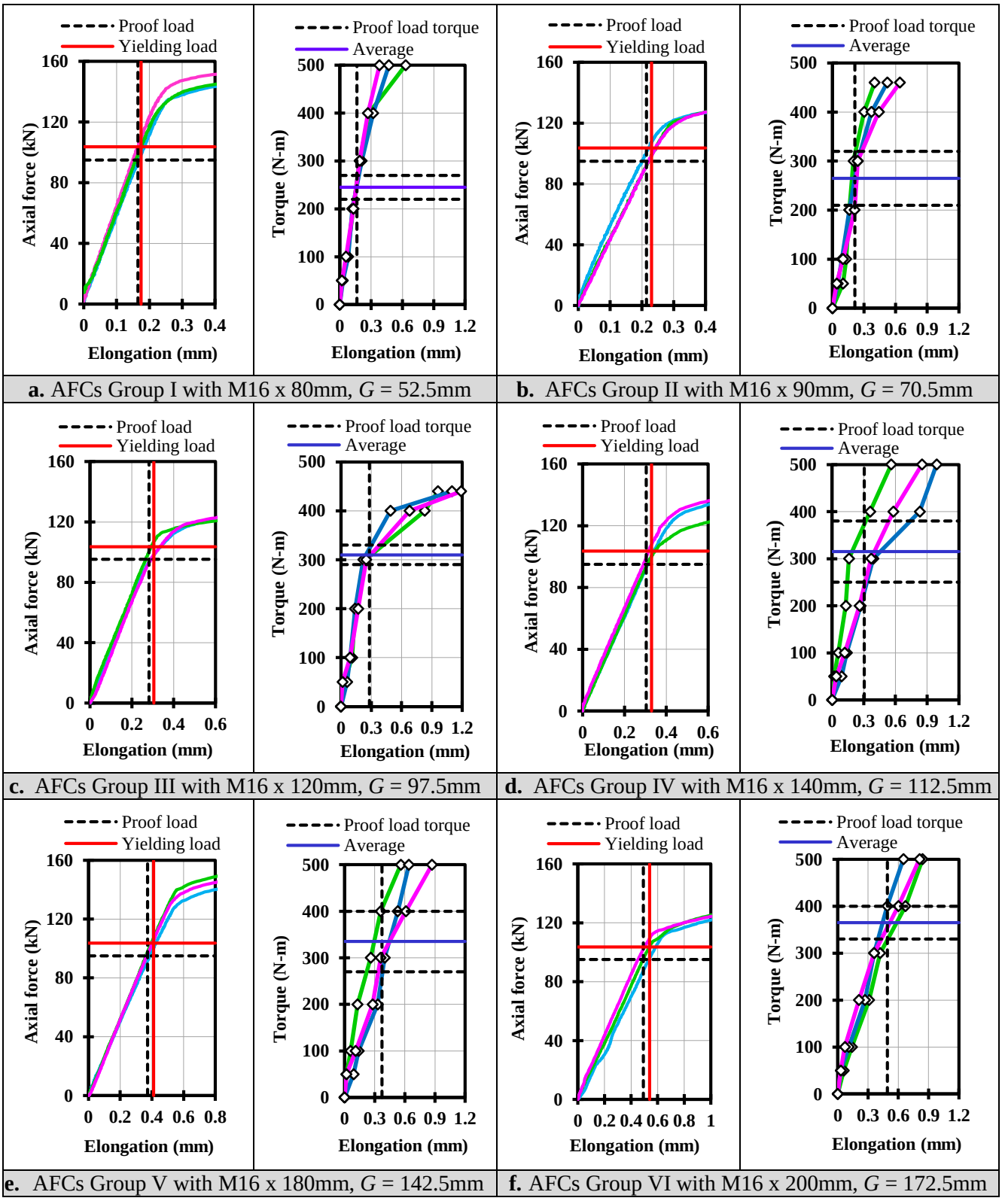

Figure 4.3. Experimental bolt axial tensile relationship and experimental bolt torque - induced elongation relationship for the 6 groups (a-f) of 3 AFCs with different bolt grip lengths, *G*.

3.3 Quasi-static test method

AFCs were quasi-statically tested using a shake table to provide a strictly horizontal input at the required force level, thus minimizing prying effects that reduce AFC strength [4.10, 4.11]. The test setup comprised a fixed bracket attached to a reaction frame bolted to a reaction floor, and a moving bracket attached to a reaction frame bolted to a shaking table. AFCs were connected using 6 M24 Grade 8.8 bolts at each end. A load cell was placed between the fixed bracket and reaction frame, a potentiometer was placed across the connection stroke, and a bolt extensometer was placed across the bolt shank. Details are in Figure 4.4.

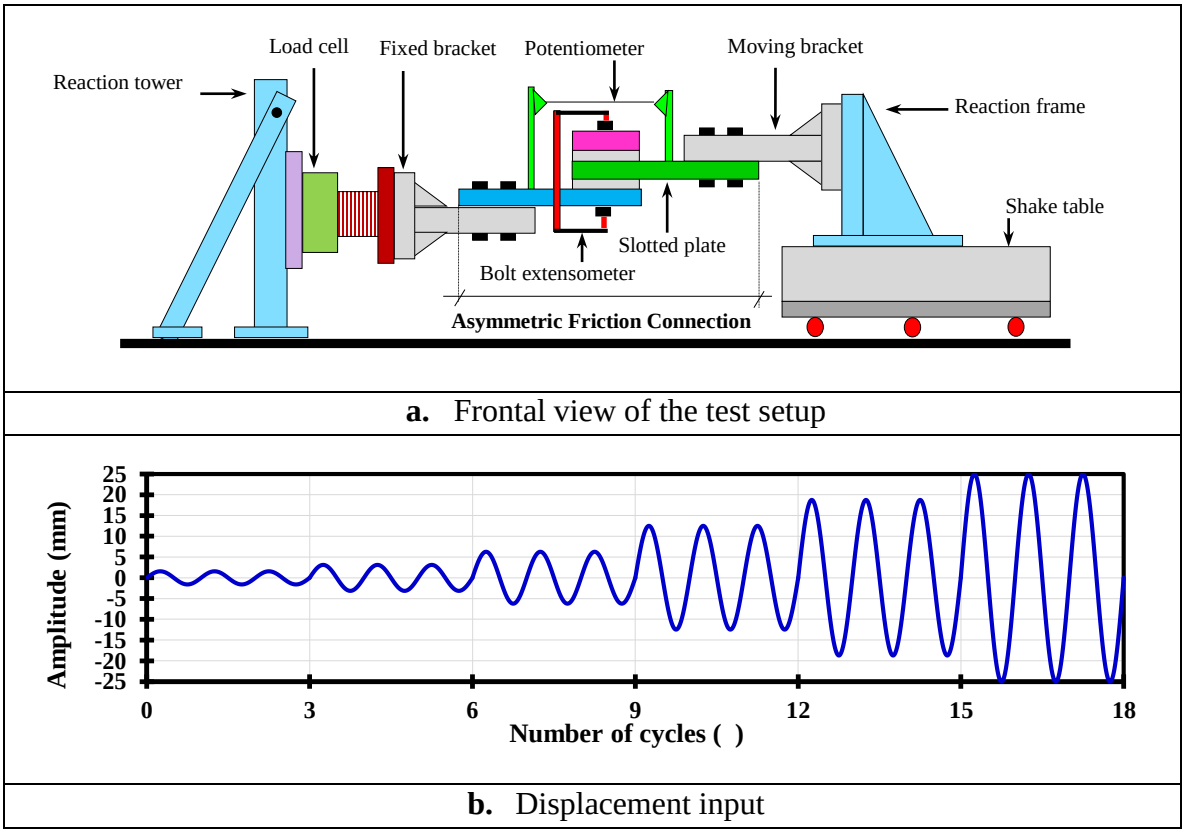

Figure 4.4. Setup of AFCs and displacement input (Not to scale)

The displacement input is defined in Figure 4.4 and comprises 18 sinusoidal cycles with a maximum velocity of 10mm/s and amplitudes varying from 0 to ±25mm. This amplitude is

62.5% of the full 80mm slot length. The peak velocity of 10mm/s is slow enough to minimise velocity dependent effects [4.3]. Each AFC was run twice with no bolt re-tensioning, and with a 30 minute break between runs to cool down the AFC to room temperature, allowing assessment of degradation between multiple events.

3.4 Assessment of experimental AFC strength

The experimental AFC strength, *S*, at a given hysteresis loop amplitude was assessed by reading the force values at the four corners (*LTS*, *RTS*, *LBS*, and *RBS*) and at the two zero displacement points (*MBS* and *RBS*) of the hysteresis loop, as shown in Figure 4.5. The experimental average AFC strength, *Sa*, was assessed as the average absolute value of the tension and compression sliding regions of the hysteresis loop defined:

$$Sa = \left[\frac{\left(LTS + MTS + RTS\right) + \left|LBS + MBS + RBS\right|}{6} \right] \quad (4.9)$$

Where, *LTS*, *MTS*, and *RTS* are experimental AFC strengths in the tension sliding region of the hysteresis loop, and *LBS*, *MBS*, and *RBS* are experimental AFC strengths in the compression sliding region of the hysteresis loop, as shown in Figure 4.5.

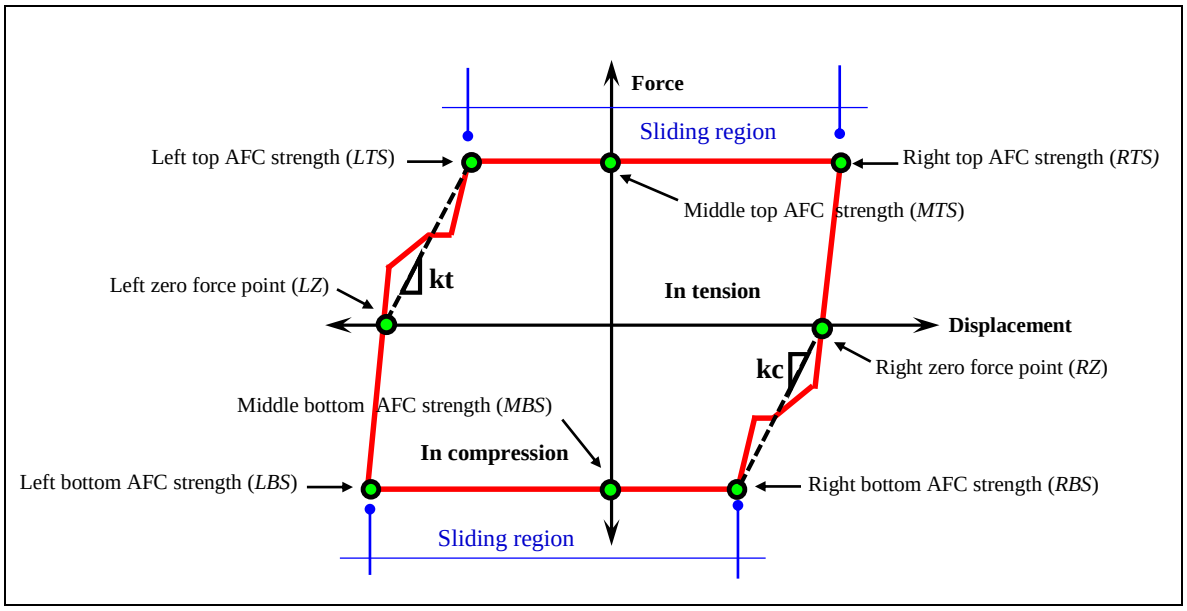

Figure 4.5. Assessment points of experimental AFC strength, and the loading stiffness at a given hysteresis loop amplitude

3.5 Assessment of experimental hysteresis loop loading stiffness

The experimental hysteresis loop loading stiffness is defined as the ratio between the force and displacement during the development of the AFC strength. The loading stiffness on the tension side of the hysteresis loop, *kt*, is calculated as the slope of the line connecting the left zero force point, *LZ*, and the left top AFC strength point, *LTS*, as shown in Figure 4.5. The loading stiffness on the compression side of the hysteresis loop, *kc*, is calculated as the slope of the line connecting the right zero force point, *RZ*, and the right bottom AFC strength point, *RBS*, as shown in Figure 4.5. The average loading stiffness at a given hysteresis loop amplitude, *ka*, is calculated as the average of the loading stiffness at the compression and tension sides of the hysteresis loop, defined:

$$ka = \frac{kc + kt}{2} \qquad (4.10)$$

3.6 Assessment of bolt inclination angle and bolt shank horizontal displacement

The bolt inclination angle, θ, and the bolt shank horizontal displacement, Δ, are defined as the angle, and horizontal displacement of the bolt shank over the grip length outside the plates and inside the washers, g, achieved as the bolt slides across the bolt hole. The maximum possible bolt inclination angle and the maximum possible bolt shank horizontal displacement are assessed when the opposite sides of the bolt shank are bearing at the cap plate-top shim and fixed plate – bottom shim interfaces (bearing points), while the bolt remains straight or without yielding in bending, as shown in Figure 4.6.

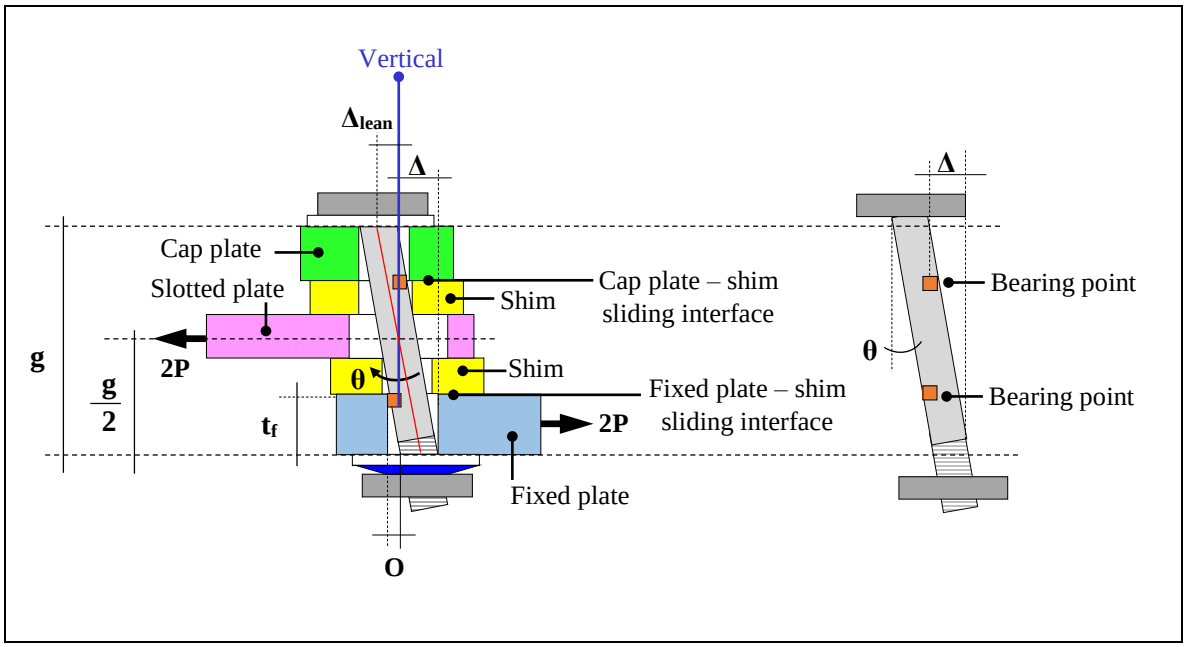

Figure 4.6. Idealized elastic bolt inclination angle and elastic bolt horizontal displacement (Not to scale)

The maximum possible bolt inclination angle and the maximum possible bolt shank horizontal displacement are limited by the bolt hole oversize, and here they are considered as upper bound, according to Figure 4.6 they are defined:

$$\theta_{max} = tan^{-1}\left[\frac{O}{t_f}\right]$$	(4.11)
$$\Delta_{max} = \frac{O}{t_f} \times \left[g - \frac{t_f}{2}\right]$$	(4.12)

Where O is the bolt hole oversize, t_f is the thickness of the fixed plate, and g is the bolt grip length outside of plates. The maximum possible bolt shank horizontal displacement, Δ_{max}, in Equation 4.12 was assessed as twice the maximum horizontal bolt shank displacement from the vertical, Δ_{lean}, shown in Figure 4.6, minus half of the of the bolt hole oversize as the bolt moves from the centre of the bolt hole to the edge of the bolt hole. Equation 4.12 ignores inelastic deformation at the edges of the bolt holes on the fixed and cap plates.

IV RESULTS AND DISCUSSION

4.1 Effects of *l/d* on the hysteresis loop shape

Figure 4.7 shows hysteresis loops recorded in the first and second runs for AFCs with *l/d* = 1.38 – 3.88. For each hysteresis loop the average loading stiffness for the first run, ka_f, and for the second run, ka_s, were assessed as defined in Section 3.5 during the cycle to ± 25mm.

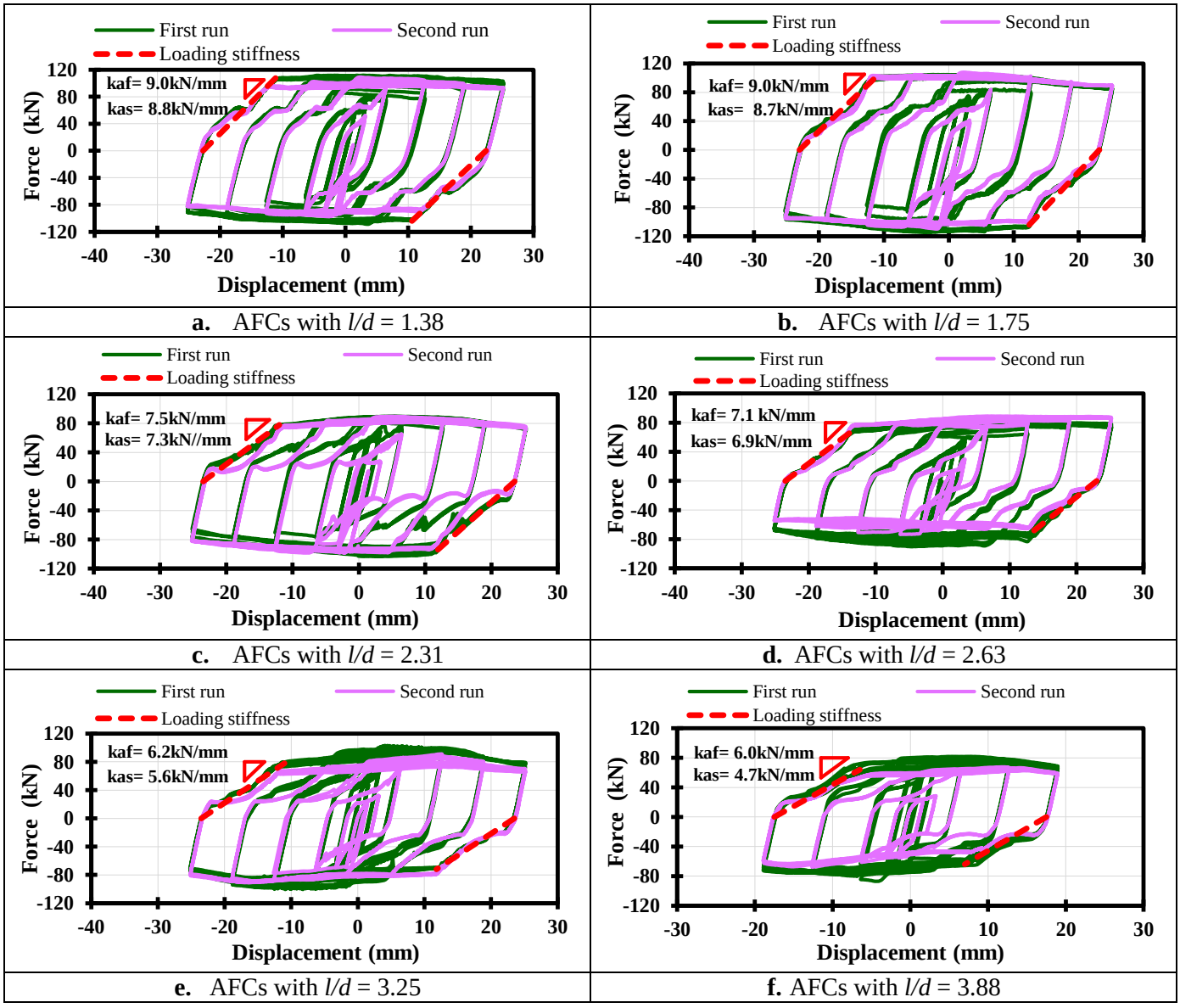

a. AFCs with *l/d* = 1.38 | **b.** AFCs with *l/d* = 1.75

c. AFCs with *l/d* = 2.31 | **d.** AFCs with *l/d* = 2.63

e. AFCs with *l/d* = 3.25 | **f.** AFCs with *l/d* = 3.88

Figure 4.7. AFCs Hysteresis loops with *l/d* of 1.38 – 3.88

Figure 4.7 shows the hysteresis loop shape remains similar regardless of the *l/d* value. The hysteresis loop shape comprises an initial loading stage, where the force increases from zero to the AFC strength representing the case where the slotted plate does not slide, and a sliding stage where the force remains almost constant and equal to the AFC strength representing the case where the slotted plate slides on both interfaces.

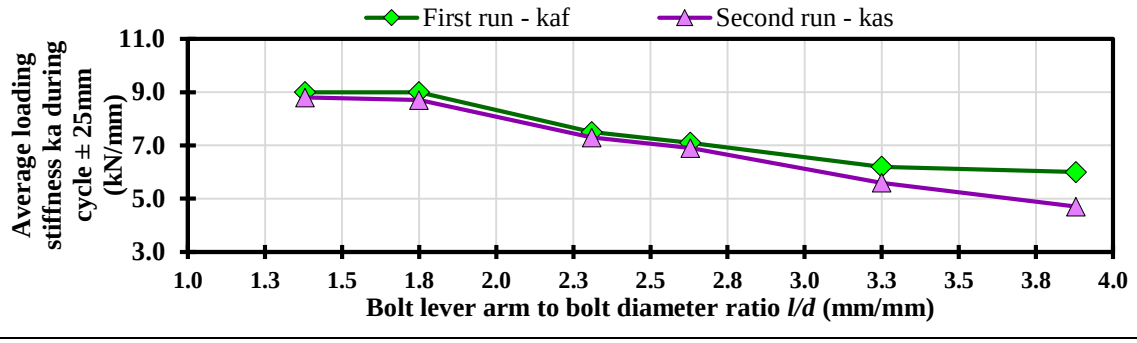

a. Variation of the average loading stiffness with *l/d* in the first and second runs during cycle to ± 25mm

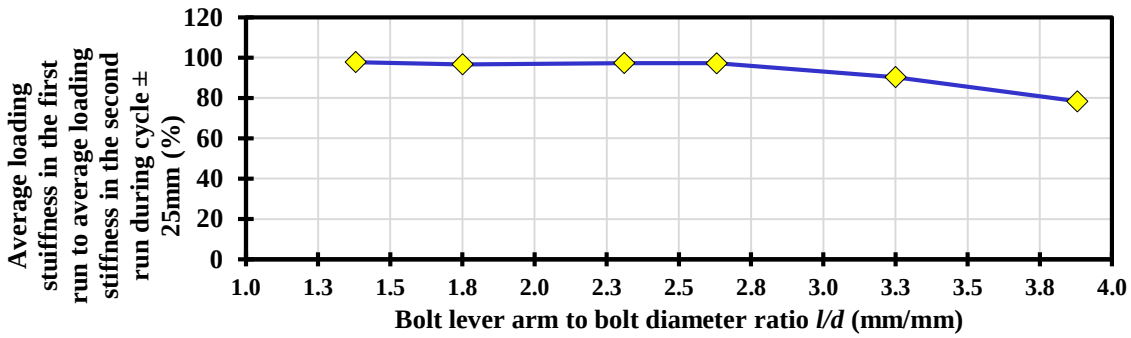

b. Variation of the average loading stiffness in the second run to the average loading stiffness in the first run with *l/d* during cycle to ± 25mm

Figure 4.8. Variation of loading stiffness *ka* for AFCs with *l/d* of 1.38-3.88 in both runs during cycle to ± 25mm

Figures 4.7 and 4.8 show that the average loading stiffness in the first and second runs, ka_f, and, ka_s, decreases with *l/d*. In both runs, while for AFCs with $l/d \leq 1.75$, the loading region of the hysteresis loop is very steep, and *kaf* and *kas* are almost constant, for AFCs with $l/d > 1.75$, *kaf* and *kas* reduced as *l/d* increased. Figures 4.8a-b show *kaf* and *kas* reduced 33% and 47% when *l/d* increased from 1.75 to 3.88, respectively. Figure 4.8b shows for AFCs with

l/d ≤ 1.75 there was almost no variation between *kaf* and *kas*. However, for AFCs with *l/d* > 1.75 *kas* varied between 97.2% and 78.3% of *kaf*, when *l/d* increased from 1.75 to 3.88.

Reductions in *kaf* and *kas*, as well as differences between *kaf* and *kas* for AFCs with *l/d* > 1.75, are due to the increase in length relative to the initial grip length bolts undergo due to MPV interaction. More specifically, the increase in bolt length produced greater plate slip movement until the AFC strength is reached, which in turn reduced *kaf* and *kas*. Increased bolt length is more critical for larger values of *l/d*, where bolts are likely to develop flexural yielding, thus developing plastic hinges and not remaining straight.

4.2 Effect of *l/d* on AFC strength

In Figures 4.9a-b the AFC strength was assessed according to Section 3.4 at the 6 input displacement amplitudes of 1.5mm, 3mm, 6mm, 12mm, 18mm, and 25mm. It is clear AFC strength reduces as *l/d* increases. Average AFC strength decreased 42% and 47% for the first and second runs, respectively, when *l/d* increased from 1.38 to 3.38. Reductions in AFC strength as *l/d* increases are due to material surface modifications between the sliding surfaces, moment-axial-shear interaction (MPV interaction), or both. The material surface effect may occur due to smoothing of the surfaces reducing the friction coefficient, or loss of material between the sliding surfaces causing loss of bolt tension as particles become loose and fall out reducing the bolt elongation, as shown in Figure 4.9c. The MPV interaction effect is developed when bolts incline from the vertical and are transversally loaded by the cap plate and the fixed plate during sliding. This motion causes loss of bolt tension resulting from bolt yielding, as bolts are under combined action of moment, axial force, and shear force, as shown in Figure 4.9d.

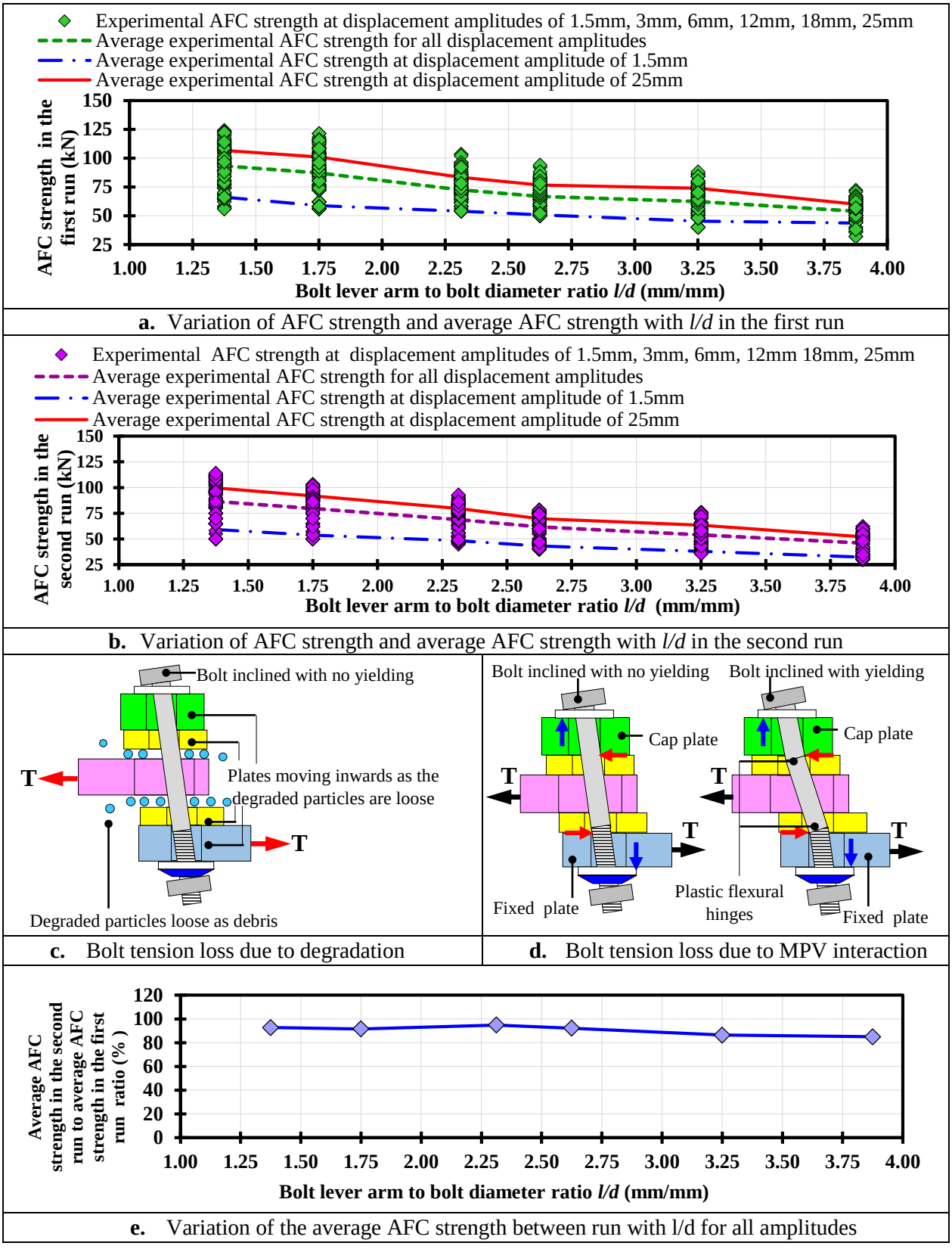

Figure 4.9. Variation of AFC strength for AFCs with *l/d* of 1.38-3.88 in both runs, and bolt tension loss mechanisms

It should be noted that while the material surface effect is independent on *l/d*, the MPV interaction effect is dependent on *l/d*. That is because the increase in bolt lever *l* arm increases only the bolt moment demand, which does not affect the surface degradation but increases the MPV effect.

Figures 4.9a-b show the AFC strength at a cyclic displacement of 1.5mm shown by the dash-dot-dash line, for the first and second runs was 62% - 73% and 59% - 62% of that at 25mm shown by the continuous line, over the range l/d = 1.38 – 3.88, respectively. This difference is likely due to the bolt inclination effect, which may occur due to the bolt inclining more at the larger cyclic displacement and having a larger component of axial tension force in the direction of applied loads, thus increasing the AFC strength. It should be noted the upper bound on the bolt inclination is limited by the bolt hole oversize.

Figures 4.9a – b show the scatter in AFC strength shown by the range of data points, in the first run for small *l/d* is ~ 65kN, rather than for large *l/d* where it is ~ 50kN. Similar behaviour is seen in the second run. The larger scatter may occur because the strength degradation due to the MPV interaction effect, which dominates with high *l/d*, is more reliable and stable than strength degradation associated with material degradation effect. Figure 4.9a – b also shows the scatter is around of a strength range of 2. This strength range was calculated as the ratio between the maximum and minimum recorded AFC strengths for each *l/d* value. This strength range of 2 matches with the ratio of the overstrength factor, β, of 1.4 to the understrength factor, α, of 0.7 that were proposed by MacRae and Clifton [4.7] to account in design the variation in the experimental AFC strength with increasing *l/d*.

In Figure 4.9d, the ratio of the average AFC strength in the second run to that in the first run is calculated. The average AFC strength in the second run varied between 85% and 93% of

that in the first run. For l/d < 2.25 the AFC strength degradation between runs is almost constant. However, it increases slightly with l/d for $l/d \geq 2.25$. This result indicates AFC strength degradation for lower values of l/d is mainly due to material degradation since this effect is independent of l/d, and for larger values of l/d it is mainly due to MPV interaction effect given this effect increases with increasing l/d. The strength degradation from the first run to the second run for larger values of l/d is mainly due to MPV interaction, given that for larger values of l/d bolts undergo flexural yielding producing a significant loss bolt tension, which is likely to occur in the first run; thus in the second run the AFC can not develop same strength as that one developed on the first run.

4.3 Effect of *l/d* on bolt flexural yielding

Bolt flexural yielding occurs during the cyclic performance of the AFCs, and is due to the bolt moment demand, M^*, generated when the bolt inclines and bears at the fixed and cap plates, and bends in double curvature, as shown in Figure 4.1. Bolt flexural yielding is likely when the ratio of the bolt moment demand, M^*, to the bolt nominal moment capacity considering axial force interaction, M_{rfn}, as defined in Equation 4.1, is close to unity. For the 6 groups of AFCs, values of M^*/M_{rfn} were computed by solving Equation 4.1 for an interaction factor I =1, and using Equations 4.2 – 4.6 with a friction coefficient μ = 0.40 for steel - wear resistant sliding surfaces, such as Bisalloy 400 [4.5], and a bolt nominal ultimate tensile strength F_{uf} = 830MPa for Grade 8.8 structural bolts. Values of M^*/M_{rfn} after solving Equation 4.1 are reported in Table 4.2 and are plotted against l/d in Figure 4.10a. Table 4.2 also reports for the 6 groups of AFCs, the ratio of the bolt shear demand, V^*, to the bolt nominal shear capacity considering no axial force interaction, V_{rfn}, resulting after solving Equation 4.1 according to conditions mentioned above.

Table 4.2 and Figure 4.10a show as l/d increases M^*/M_{rfn} increases, thus increasing the likelihood of flexural yielding. For l/d = 3.25 and l/d = 3.88, values of M^*/M_{rfn} of 0.82 and 0.84, and values of V^*/V_{rfn} of 0.18 and 0.16 were obtained, respectively. This result seems reasonable, as greater l gives greater moment, so the sliding shear resistance is decreased. Figure 4.10b shows bolts with l/d of 3.25 and 3.88 show plastic flexural hinges at locations near to the cap plate – top shim and fixed plate – bottom shim interfaces, which are the locations with the greatest bolt moment demand occurs according to Figure 4.1c and Figure 4.10c. Based on the experimental observations it was defined that bolt flexural yielding may occur for $l/d \geq 3.25$, which corresponds to values of $M^*/M_{rfn} > 0.8$ as shown in Table 4.2. Figure 4.10b also shows when $M^*/M_{rfn} \leq 0.8$, which occurred for $l/d < 3.25$, plastic flexural hinges do not seem to occur. It should be noted, Equations 4.1 – 4.6 used to assess values of M^*/M_{rfn} in Table 4.2 do not consider any increase in bolt axial tension or AFC strength due to bolt inclination.

Table 4.2. Assessment of M^*/M_{rfn} and V^*/V_{rfn} for the 6 groups of AFCs using Equation 4.1 with μ = 0.40 and F_{uf} = 830MPa

AFC Group	Bolt lever arm	Ratio of bolt lever arm to bolt diameter	Bolt axial tension during the sliding	Bolt shear demand	Bolt shear capacity considering no axial force interaction	Solved	Bolt moment demand	Bolt moment capacity considering axial force interaction	Solved	Interaction factor
	l	l/d	N^*	V^*	V_{rfn}	V^*/V_{rfn}	M^*	M_{rfn}	M^*/M_{rfn}	I
	mm	mm/mm	kN	kN	kN	----	kN-mm	kN-mm	----	----
I	22.0	1.38	51.91	20.76	73.77	0.28	228.40	319.10	0.72	1.0
II	28.0	1.75	46.20	18.48	73.77	0.25	258.73	346.26	0.75	1.0
III	37.0	2.31	39.82	15.93	73.77	0.22	294.64	376.64	0.78	1.0
IV	42.0	2.63	37.02	14.81	73.77	0.20	311.00	389.92	0.80	1.0
V	52.0	3.25	32.52	13.01	73.77	0.18	338.23	411.33	0.82	1.0
VI	62.0	3.88	29.04	11.61	73.77	0.16	360.04	427.92	084	1.0

Figures 4.10d – g compare the gain in axial elongation necessary to yield the bolt in tension, Δy, as defined in Section 3.2 and calculated in Table 4.1 with the gain in bolt axial elongation, ΔL, recorded during the testing of the 6 groups of AFCs. The gain in axial elongation necessary to yield the bolt in tension, Δy, is plotted on the positive side on Figures 4.10d – g, since this side represents the case where the bolt is under an increase in bolt tension. The gain in bolt elongation, ΔL, was recorded using the bolt extensometer placed across the bolt shank described in Section 3.3. The gain in bolt elongation, ΔL, comprises four components:

i. The increase in bolt axial elongation from degradation of sliding surfaces, ΔL_{DSS}, occurring when degraded particles slide across the clamped zone of the connection and push the AFC plates outwards with a force ΔN^*_{DSS}, as shown in Figure 4.9c,
ii. The increase in bolt axial elongation from bolt inclination, $\Delta L_{inclination}$, produced by the vertical force $\Delta N^*_{inclination}$, generated under the bolt head and nut when bolt inclines, as shown in Figure 4.1b,
iii. The reduction in bolt axial elongation from MPV interaction, ΔL^*_{MPV}, produced by the loss of bolt tension, ΔN^*_{MPV}, resulting from MPV interaction as described in Section II, and
iv. The increase in bolt axial length due to bolt bending, $\Delta L^*_{bending}$, produced by bending of the bolt in double curvature, as shown in Figure 4.10c.

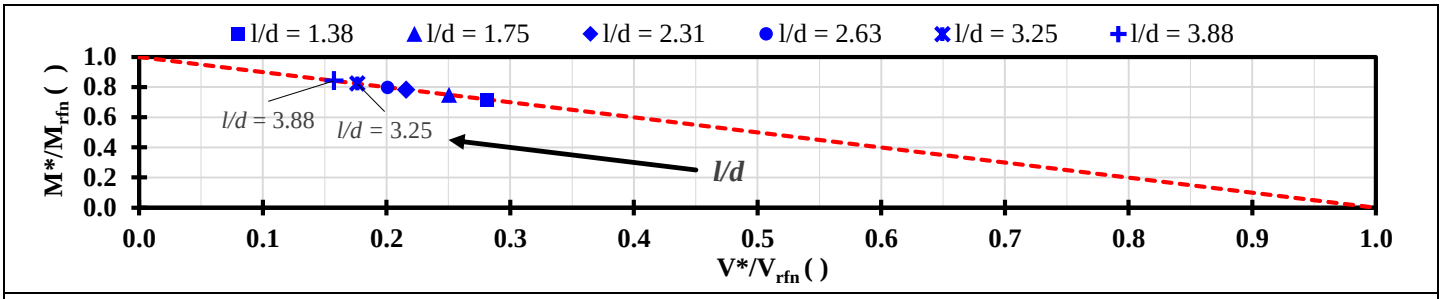

a. MPV interaction for bolts with different *l/d*

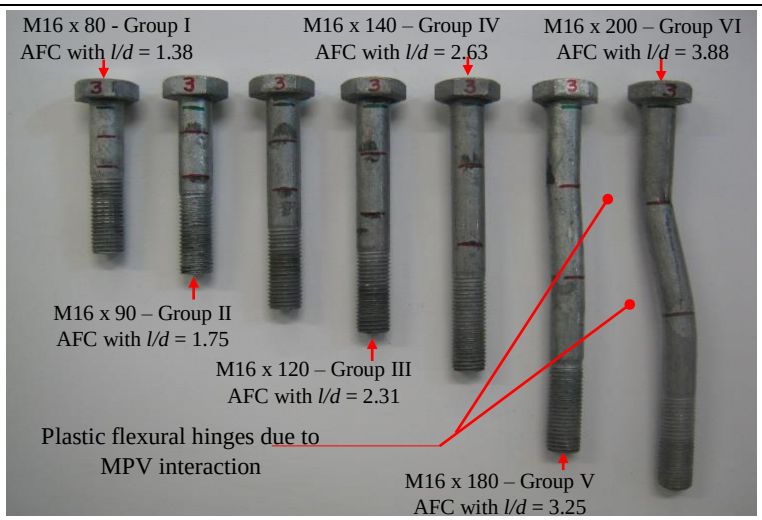

b. Bolts dismantled from the 6 groups of AFCs

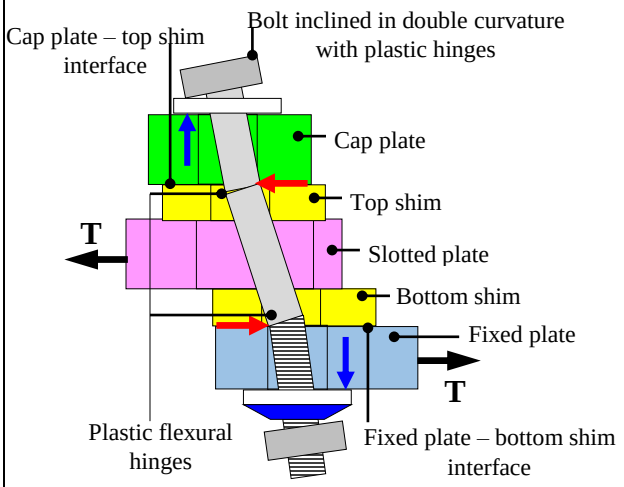

c. Bolt behaviour as sliding occurs

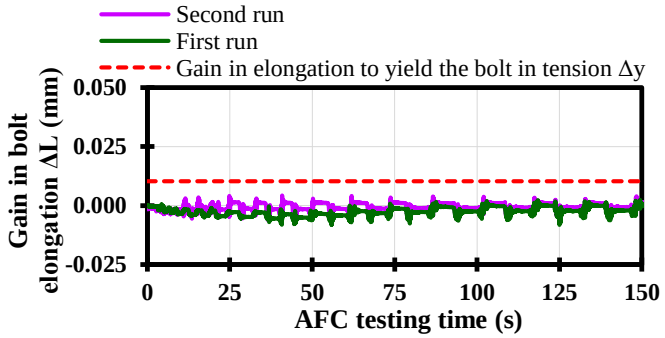

d. Gain in bolt elongation in AFCs with *l/d* = 1.38

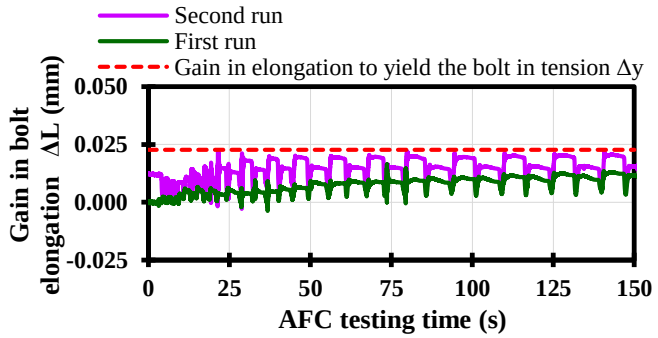

e. Gain in bolt elongation in AFCs with *l/d* = 2.31

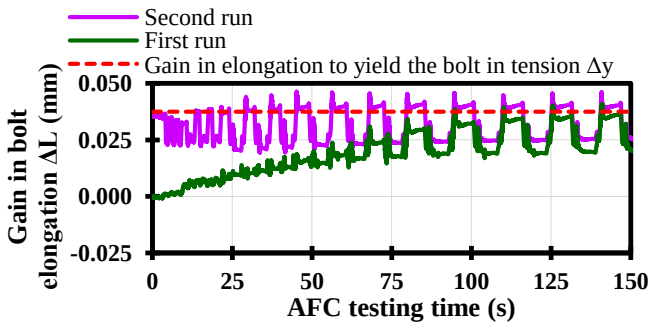

f. Gain in bolt elongation in AFCs with *l/d* = 3.25

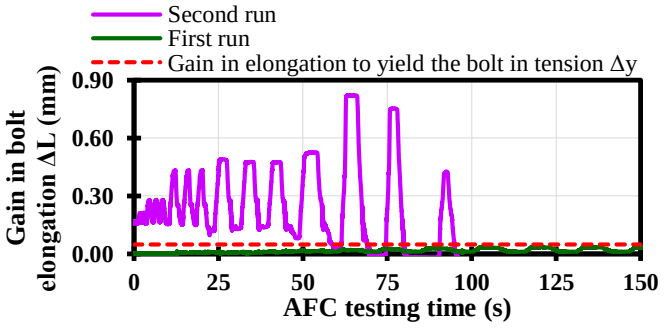

g. Gain in bolt elongation in AFCs with *l/d* = 3.88

Figure 4.10. Gain in bolt elongation for AFC with l/d of 1.88 – 3.88, bolts dismantled from tested AFCs, behaviour of bolts as sliding occurs, and MPV interaction

Figures 4.10d-g show as l/d increases, the gain in bolt elongation, ΔL, also increases, indicating the reduction in bolt axial elongation from MPV interaction, ΔL^*_{MPV}, (Component iii), and the increase in bolt axial length due to bolt bending, $\Delta L^*_{bending}$, (Component iv) dominate, since the increase in bolt axial length due to degradation of the sliding surfaces, $\Delta L^*_{DSS,}$ (Component i) is independent of l/d, and the increase in bolt axial elongation due to bolt inclination, $\Delta L^*_{inclination}$, (Component ii) may reduce as l/d increases given the maximum possible bolt inclination reduces with increasing l/d. Figures 4.10d-g also show for $l/d \geq 3.25$, the gain in bolt elongation, ΔL, is greater than the axial elongation necessary to yield the bolt in tension, Δy. This result indicates for $l/d \geq 3.25$ bolt yielding occurs due to bending. In Figure 4.10g, for $l/d = 3.88$, the gain in bolt elongation, ΔL, for the second run is significant and is represented by a jump after the bolt undergoes flexural yielding. This significant gain in bolt elongation for $l/d = 3.88$ occurs as a result of the accumulation of the plastic deformations due to bolt bending that the bolt undergo at each of the displacements amplitudes of the second run after flexural yielding occurred at the end of the first run.

4.4 Effect of l/d on the effective friction coefficient, μ_e

Figures 4.11a – b show μ_e plotted against displacement amplitudes for the first and second runs, of each of the 6 the groups in Table 4.1. Values of μ_e were assessed with Equation 4.7, using $m = 2$, $n = 2$, $F_{proof} = 95$kN, and S calculated as the average of 3 AFCs assessed according to Equation 4.9. It can be seen μ_e reduces as l/d increases for both runs. For $l/d = 1.38 – 3.88$, μ_e reduced from 0.28 to 0.11 in the first run, and from 0.27 to 0.08 in the second run. Reductions in μ_e with l/d are directly related to the reductions in AFC strength as described earlier.

Figures 4.11a –b show μ_e has two trends regardless of l/d for both runs. An initial trend, where μ_e increases non-linearly, and a final trend where μ_e is almost constant. The initial and final trends converge to displacement amplitudes of 7.5mm for $l/d < 1.75$ and 6.0mm for $l/d \geq 1.75$. These displacements amplitudes match the ranges of the maximum possible bolt shank displacements of 6.5 mm – 7.3mm and 5.5mm – 5.9mm as the bolt moves from one direction to the other direction, which were calculated according to Equations 4.11-4.12 and reported in Table 4.3 for $l/d < 3.25$ and $l/d \geq 3.25$, respectively. This outcome indicates the μ_e trends described above are dependent on the sliding amplitude, and therefore on the bolt inclination angle, θ, and on the bolt shank displacement, Δ.

Table 4.3. Assessment of the maximum possible bolt inclination angle and maximum possible bolt horizontal displacement for the 6 groups of AFCs

AFCs Group	Ratio of bolt lever arm to bolt diameter l/d mm/mm	Plate thickness t mm	Shim thickness t_s mm	Bolt grip length outside of plates g mm	Bolt hole oversize O mm	Maximum bolt inclination angle θ_{max} radians	Maximum Bolt shank horizontal displacement Δ_{max} mm
I	1.38	10.0	6.0	42.0	2.0	0.197	7.3
II	1.75	16.0	6.0	60.0	2.0	0.124	6.5
III	2.31	25.0	6.0	87.0	2.0	0.080	5.9
IV	2.63	30.0	6.0	102.0	2.0	0.067	5.8
V	3.25	40.0	6.0	132.0	2.0	0.050	5.6
VI	3.88	50.0	6.0	162.0	2.0	0.040	5.5

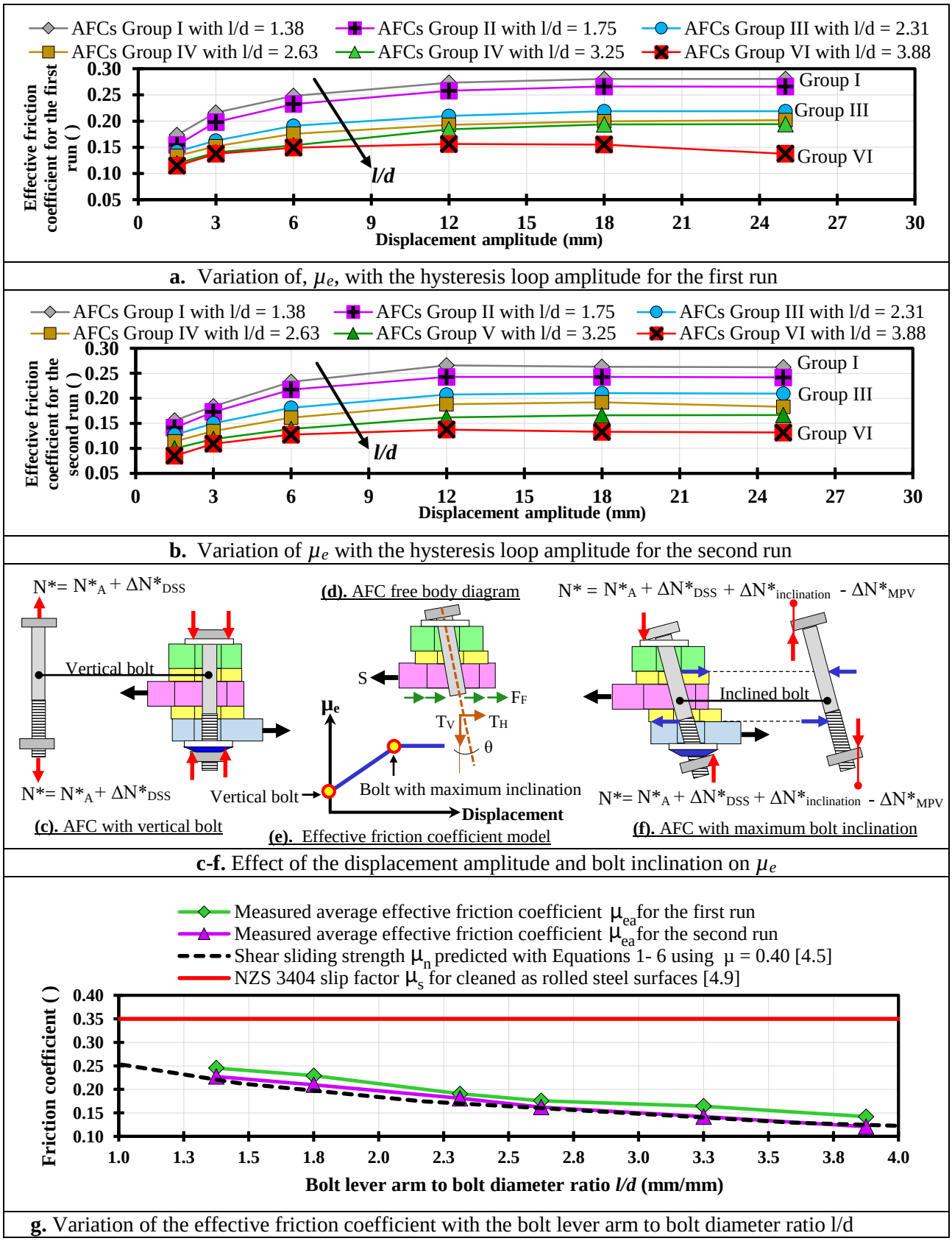

Figure 4.11. μ_e for the first and second run of testing of AFCs with *l/d* of 1.88 – 3.88.

The non-linear increasing μ_e trend occurs for sliding amplitude ranges, where bolts have θ and Δ less than θ_{max} and Δ_{max} as defined in Equations 4.11 – 4.12. Bolt shanks are not bearing at the cap plate – top shim and fixed plate – bottom shim interfaces, and thus bolts are not under significant MPV interaction, as shown in Figure 4.11c. The total bolt axial tension during the sliding, N^*, is the tension due to assembly, N_A^*, as defined in Section II, plus the increase in bolt axial tension due to degradation of the sliding surfaces, $\Delta N^*_{DSS,}$ as defined in Section 4.3, as shown in Figure 4.11d and Equation 4.13. Since bolt inclination angle, θ, increases as the sliding amplitude increases, the horizontal and vertical total bolt tension components, T_H and T_V, shown in Figure 4.11d, increase, thus making the AFC strength and μ_e increase as the sliding amplitude increases, as shown in Figure 4.11e. The minimum AFC strength and μ_e are achieved when bolts are vertical, as shown in Figure 4.11e.

$N^* = N_A^* + \Delta N_{DSS}^*$	(4.13)

The constant μ_e trend occurs for sliding amplitudes, where bolts have θ and Δ equal to θ_{max} and Δ_{max}, as defined in Equations 4.11 – 4.12. Bolt shanks are bearing at the cap plate – top shim and fixed plate – bottom shim interfaces. Thus, bolts are under MPV interaction, as shown in Figure 4.11f. The total bolt axial tension during the sliding, N^*, is the tension due to assembly, N^*_A, as defined in Section II, plus the increase in bolt axial tension due to degradation of the sliding surfaces, $\Delta N^*_{DSS,}$ as defined in Section 4.3, plus the increase in bolt axial tension due to bolt inclination, $\Delta N^*_{inclination}$, as defined in Section 4.3, minus the loss of bolt tension due to MPV, ΔN^*_{MPV} as defined in Section 4.3, as shown in Figure 4.11d and Equation 4.14. At θ_{max}, the horizontal and vertical components of the total bolt tension, TH,

and, *TV*, shown in Figure 4.11c reach the maximum value, additional increments in the sliding amplitude can not increase these components, therefore making the AFC strength and μ_e constant, as shown in Figure 4.11e.

$$N^* = N_A^* + \Delta N_{DSS}^* + \Delta N_{inclination} - \Delta N_{MPV} \quad (4.14)$$

Figure 4.11g shows for the first and second runs the average effective friction coefficient, μ_{ea}, assessed at each value of *l/d* as the average of μ_e values across all displacement amplitudes in Figures 4.11a – b. It can be seen μ_{ea} decreases non-linearly as *l/d* increases. Figure 4.11g compares μ_{ea} with the current in practice NZS3404 slip factor, μ_s, for slip critical friction connections with clean steel as rolled friction surfaces of 0.35 [4.9]. For *l/d* = 1.38 – 3.88, μ_s significantly overestimates μ_{ea} by 42.6% - 146.7% for the first run, and by 53.9% - 190.3% for the second run, and μ_s does not account for the decreasing trend of μ_{ea} with increasing *l/d*. This discrepancy occurs because μ_s was obtained from steel - steel sliding interfaces, which are likely to develop greater strengths than those developed by steel – wear resistant sliding interfaces [1], and also because μ_s was obtained from friction tests in symmetric connections, where the strength is not dependent of MPV interaction. Figure 4.11g also compares μ_{ea} with the shear sliding strength per bolt and per sliding surface normalized by the bolt proof load, μ_n, predicted with the MPV model defined by Equations 4.1 – 4.6 using a friction coefficient, μ = 0.40 for steel - wear resistant sliding surfaces, such as Bisalloy 400 [4.5]. It can be seen μ_n follows the decreasing trend of μ_{ea} with *l/d*. However, μ_n underestimates μ_{ea} by 10.1% - 12.5% for the first run, and by 3.0% - 0.1% for the second run. This result shows the MPV model is consistent with the behaviour with *l/d* recorded for the 6 groups of AFCs.

The MPV model underestimates experimental values because:

i. μ_n was determined for a friction coefficient μ = 0.40, obtained from the calibration of the MPV model for steel – Bisalloy 400 sliding interfaces, rather than for steel – Bisalloy 500 interfaces,

ii. The MPV model was calibrated for *l/d* = 0.9 – 1.9 [4.5], which can be considered limited when compared with the range of *l/d* used in this research,

iii. The MPV model does not consider the increase in AFC strength due to bolt inclination.

Given these discrepancies, it is considered appropriate when using the MPV model for design purposes applying the understrength factor, α, of 0.7 and an overstrength factor, β, of 1.4 suggested by MacRae and Clifton [4.7]. Care should also be given when choosing μ_e for AFCs with Bisalloy 500 shims, and it is recommended to use the available experimental data presented in Figure 4.11.

CONCLUSIONS

This paper describes the hysteretic behaviour of AFCs with two bolts and different bolt lever arm to bolt diameter ratios, *l/d*. It was shown that:

i. The hysteresis loop shape remains similar regardless of the *l/d* value.

iii. The hysteresis loop loading stiffness reduced for *l/d* ≥1.75. When AFCs were cyclically loaded to a displacement amplitude of ± 25mm, and *l/d* increased from 1.75 to 3.88, the

hysteresis loop loading stiffness reduced by about 33% within one test, and 47% after the initial test, cooling and reloading.

iii. The AFC strength decreased approximately linearly with increasing *l/d*. When AFCs were cyclically loaded to a displacement amplitude of ± 25mm, and *l/d* increased from 1.75 to 3.88, the average AFC strength reduced by about 42% within one test, and 47% after the initial test, cooling and reloading. Mechanisms contributing to the reduction in AFC strength are: reduction in friction coefficient due to sliding surface modification and loss of bolt tension due to both MPV interaction and sliding surface modification. While the sliding surface modification does not depend on *l/d*, the MPV interaction effect does.

iv. Bolts underwent flexural yielding for $l/d \geq 3.25$. Bolt flexural yielding is due to MPV interaction. It resulted in significant visible bolt plastic hinges when the ratio between the bolt moment demand and the bolt nominal moment capacity considering axial force interaction (M^*/M_{rfn}) was greater than 0.80. These plastic hinges occurred at the bolt shank locations near to the cap plate – top shim and fixed plate – bottom shim interfaces.

v. The experimental effective friction coefficient, μ_e, reduced as *l/d* increased. It increased as the displacement amplitude and bolt inclination angle increased. For displacement amplitudes generating the maximum bolt inclination angle, μ_e was almost constant. The μ_e of AFCs with Bisalloy 500 shims, Grade 300 steel slotted plates, and with bolts with l/d = 1.88 -3.88 was 0.11- 0.28 for brand new sliding surfaces and 0.08- 0.27 for degraded sliding surfaces. Using a friction coefficient μ = 0.40 with Khoo MPV model [4.5], the decreasing trend of the average experimental effective friction coefficient, μ_e, for AFCs

with Bisalloy 500 shims with l/d = 1.38 - 3.88 was captured. However, for brand new sliding surfaces, μ_e was underestimated by 10% - 13%.

ACKNOWLEDGEMENTS

The authors would like to acknowledge funding from MBIE Natural Hazards Research Platform (NHRP), and material donation from John Jones Steel Ltd., for undertaking this research. All opinions expressed remain those of the authors.

REFERENCES

[4.1] Rodgers, GW, Chase, JG, Causse, R, Chanchi Golondrino, J and MacRae, GA (2017). *Performance and Degradation of Sliding Steel Friction Connections: Impact of Velocity, Corrosion Coating and Shim Material*. Engineering Structures, Vol. 141, pp. 292–302. ISSN: 0141-0296. https://doi.org/10.1016/j.engstruct.2017.02.070.

[4.2] Khoo, H.H., Clifton, C., Butterworth, J., MacRae, G. and Ferguson, G. (2011) *Influence of steel shim hardness on the Sliding Hinge Joint.* Journal of Constructional Steel Research. Vol 72, May 2012, p 119 – 129. https://doi.org/10.1016/j.jcsr.2011.11.009

[4.3] Clifton, G.C. (2005). Semi-Rigid Joints for Moments Resisting Steel Framed Seismic Resisting Systems. *Published PhD Thesis, Department of Civil and Environmental Engineering.* University of Auckland – New Zealand.

[4.4] MacRae, G.A., Clifton, C.G., MacKinven, H., Mago, N., Butterworth, J., Pampanin, S. (2010). *The Sliding Hinge Joint Moment Connection*. Bulletin of the New Zealand Society for Earthquake Engineering. Vol 43, Issue 3, p. 202-212.

[4.5] Khoo, H.H., Clifton, G.C., MacRae, G.A., Zhou, H., and Ramhormozian, S. (2014). *Proposed design models for the asymmetric friction connection*. Earthquake and Structural Dynamics Journal. Vol 44, Issue 8, p. 1309-1324. https://doi.org/10.1002/eqe.2520

[4.6] Rodgers, GW, Mesnil, O, Chanchi Golondrino, J, MacRae, GA and Chase, JG (2014). *Generalised nonlinear modeling of unstable stick-slip force reduction effects in friction energy dissipation devices*. Bulletin of the New Zealand Society for Earthquake Engineering, Vol 47(3), pp. 217-223, ISSN No. 1174-9857.

[4.7] MacRae, G.A., and Clifton, C.G. (2015). *Research on Seismic Performance of Steel Structures*. Steel Innovation Conference 2015. September 3-4, 2015, Auckland, New Zealand.

[4.8] Bisalloy Steels Pty Ltd [2006]. *Bisalloy Technical Manual*, Bisalloy Steels Pty Ltd, Unanderra – Australia.

[4.9] Standards New Zealand. (2009). NZS3404: Part 1: 2009 - Steel Structures Standard. *Standards New Zealand*. Wellington, New Zealand.

[4.10] Borzouie, J, Chase, JG, MacRae, GA and Rodgers, GW (2015). *Experimental Studies on Cyclic Performance of Column Base Weak Axis Aligned Asymmetric Friction Connection*. Journal of Constructional and Steel Research (JCSR), Vol 112, pp. 252-262. https://doi.org/10.1016/j.jcsr.2015.05.007

[4.11] Borzouie, J, Chase, JG, MacRae, GA, Rodgers, GW and Clifton, C (2016). *Experimental Studies on Cyclic Performance of Column Base Strong Axis Aligned Asymmetric Friction Connections*. ASCE J. Structural Engineering, Vol 142(1), Article 04015078, 10-pages. ISSN: 0733-9445. https://doi.org/10.1061/(ASCE)ST.1943-541X.0001327

Chapter 5

Improved Bolt Flexural – Axial Force – Shear Force Interaction Model for Asymmetric Friction Connections (AFCs)

Chapter 5

"Improved Bolt Flexural – Axial Force – Shear Force Interaction Model for Asymmetric Friction Connections (AFCs)"

Jose Christian Chanchi Golondrino [a, b,1*], Gregory Anthony MacRae[b,2], James Geoffrey Chase[c,3], Geoffrey William Rodgers[c,4], George Charles Clifton[d,5]

[a] Universidad Nacional de Colombia – Sede Manizales, Departamento de Ingeniería Civil, Manizales 170004, Colombia.

[b] University of Canterbury, Department of Civil and Natural Resources Engineering, Private Bag 4800, Christchurch 8140, New Zealand.

[c] University of Canterbury, Department of Mechanical Engineering, Private Bag 4800, Christchurch 8140, New Zealand.

[d] The University of Auckland, Department of Civil & Environmental Engineering, Faculty of Engineering, Private Bag 92019, Auckland Mail Centre, Auckland 1142, New Zealand.

[1] jcchanchigo@unal.edu.co, [2]gregory.macrae@canterbury.ac.nz, [3]geoff.chase@canterbury.ac.nz, [4]geoff.rodgers@canterbury.ac.nz, [5]c.clifton@auckland.ac.nz
[*]Corresponding author

Key Words: Energy dissipation, Asymmetric Friction Connections, Force interaction, Bolt tension loss, Bolt bending, Bolt yielding.

ABSTRACT:

Asymmetric Friction Connections (AFCs) are used to dissipate seismic energy via friction. AFC strength is affected by moment–axial force–shear force (MPV) interaction. Current MPV models do not consider the increase in bolt tension due to bolt rotation as bolts are assumed to yield axially during AFC assembly. A MPV model is proposed for AFCs considering the increase in bolt axial tension due to bolt rotation, and elastic or elasto – plastic bolt axial behaviour. A parametric study is presented describing the relative impact and effects of bolt rotation, bolt thread, ultimate strength, friction coefficient at the sliding interfaces, and bolt axial relationship. The predicted AFC strength is validated against

experimental data from 60 tests of AFCs with Grade 8.8 bolts and Bisalloy 400 shims, and 18 experimental tests with Grade 8.8 bolts and Bisalloy 500 shims. The proposed MPV model considering elasto-plastic bolt axial behaviour better matches the experimental data with average absolute errors of 0 - 18% for AFCs with M16, M20 and M24 bolts, and of 55 - 79% for AFCs with M30 bolts.

I. INTRODUCTION

AFCs are friction bolted connections used to dissipate seismic response energy. AFCs are typically assembled using three Grade 300 steel plates, two thin plates, termed shims, made of high hardness materials, such as Bisalloy 400 or Bisalloy 500, and high strength structural bolts, such as Grade 8.8 bolts. AFCs dissipate energy via friction when a slotted plate is forced to slide over the shims [5.1]. The sliding force of the resulting, approximately square hysteresis loop is termed the AFC strength, and quasi-static testing has shown it may be almost constant [5.1, 5.2]. AFCs can be used as seismic dissipaters in moment resistant frames at the beam column joint, or in braced frames [5.3].

However, AFC strength degrades when AFCs are cyclically loaded. This degradation may result from degradation in compressive force over the surfaces as a result of moment – axial force – shear force interaction (MPV interaction), change in the properties in the sliding surfaces [5.2, 5.3], and/or prying effects [5.4,5.5]. The latter two effects relate to device assembly, design and implementation. Overall, MPV interaction is less understood, but is central to device performance.

Models to quantify the AFC strength considering the degradation due to MPV interaction have been developed [5.2, 5.6]. The earliest MPV model was proposed by Clifton [5.2], and

later improved by Khoo [5.6], termed the Clifton model and Khoo model. In these models, AFC strength depends on the bolt tensile ultimate strength, F_{uf}, bolt diameter, d, the friction coefficient at the sliding interfaces of the AFC, μ, and bolt demand during sliding, expressed in terms of the bolt axial force, bolt shear force, and bolt moment [2, 6]. These MPV models assume:

i. Strength degradation is due to loss of bolt tension that occurs when bolts bend in double curvature remaining vertical while the slotted plate slides,
ii. Strength degradation increases as the bolt lever arm increases. Here, the bolt lever arm, l, is defined as the distance between the points where the bolt is on bearing on the connection plates while bending in double curvature, and
iii. Bolt axial force does not increase significantly after installation.

The Clifton model has been compared to AFCs with Grade 300 steel plates, Grade 8.8 bolts, and brass shims [5.7]. The Khoo model has been compared to AFCs with Grade 300 steel plates, Grade 8.8 bolts and Bisalloy 400 shims [5.6]. For brass shims and M24 and M30 bolts, the comparison was performed over a range of bolt lever arm to bolt diameters, l/d, of 0.9 - 1.6, using a friction coefficient, μ, of 0.29, and a bolt lever arm, l, calculated as the thickness of the slotted plate plus the thickness of the two shims plus the 20% of the bolt diameter, as shown in Figure 5.1a [5.7]. For Bisalloy 400 shims and M16, M20, M24 and M30 bolts, the comparison was performed for l/d of 0.9 - 1.9, μ of 0.40, and l calculated as the thickness of the slotted plate plus the thickness of the two shims, as shown in Figure 5.1b [5.6]. These comparisons showed both MPV models followed the decreasing trend of experimental data with increasing l/d, and the MPV models both underestimated the average of the experimental data [5.6, 5.7]. Discrepancies were attributed to the large scatter of the

experimental data due to variations of bolt ultimate strength, sliding surface conditions, installed bolt tension, and reduced experimental data considering combinations of bolt sizes and bolt lever arms [5.7]. To design AFCs considering the Khoo model [5.6], while accounting for these assembly and manufacturing issues, an understrength factor of 0.75 and an over strength factor of 1.4 were suggested. Revised understrength and overstrength factors for design of 0.70 and 1.4, respectively, were proposed in [5.8].

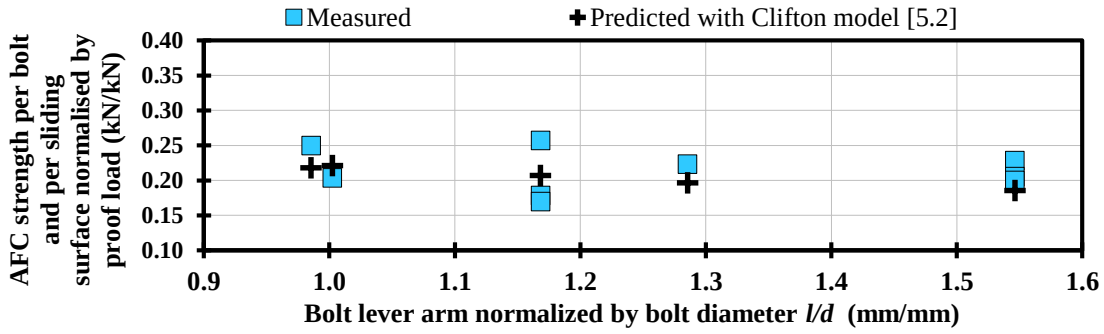

a. Comparison between experimental AFC strength for Brass shims, M24 and M30 Grade 8.8 bolts and theoretical AFC strength predicted with Clifton model based on μ = 0.29 [5.7]

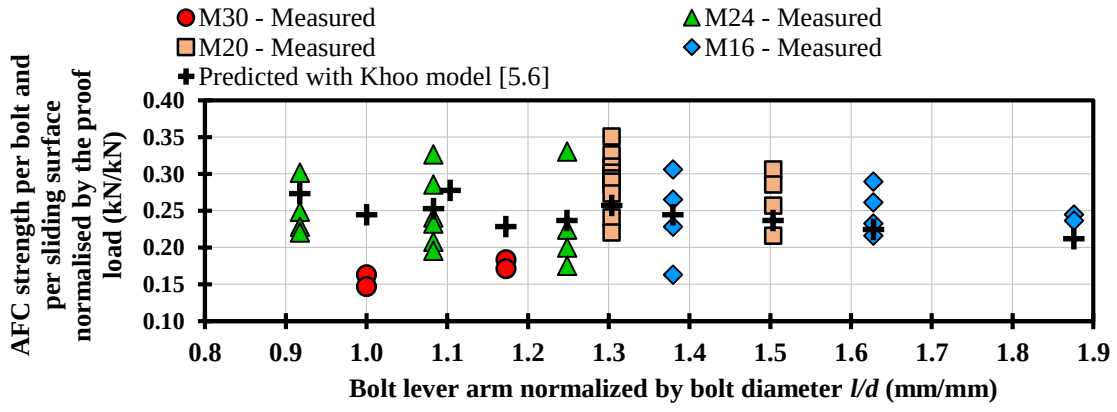

a. Comparison between experimental AFC strength for Bisalloy 400 shims, M16, M20, M24, and M30 Grade 8.8 bolts and theoretical AFC strength predicted with Khoo model based on μ =0.40 [5.6]

Figure 5.1. Comparisons between experimental AFC strength and theoretical AFC strength predicted with Clifton model [5.2] and Khoo model [5.6]

Although efforts have been made to develop a MPV model quantifying AFC strength degradation, the Khoo model [5.6] does not explicitly consider:

i. Kinematic effects on the AFC strength due to the bolt rotation

ii. Effects of bolt ultimate strength and bolt hole oversize

iii. A wide range of bolt lever arm to bolt diameter ratios *l/d*

iv. The use of Bisalloy 500 shims

For design to be conducted with confidence, these parameters, which can affect the sliding behaviour need to be considered. This paper addresses this need by seeking answers to the following questions:

i. Can an improved AFC strength model be developed?

ii. How sensitive is the AFC strength to bolt rotation/inclination during sliding?

iii. How sensitive is the AFC strength to assembly variables such as bolt hole oversize, bolt thread location in the sliding interfaces, the friction coefficient at the sliding interfaces?

iv. How sensitive is the AFC strength to bolt axial behaviour variables such as the bolt tensile ultimate strength, and the bolt axial relationship?

v. What friction coefficient, overstrength, and understrength factors are appropriate to predict the available experimental data with the proposed model?

II. EXPERIMENTAL AND ANALYTICAL METHODS

2.1 AFC devices, assembly, and experimental data

A total of 18 AFCs were assembled using Bisalloy 500 shims and Grade 300 steel for the fixed, slotted and cap plates. Two M16 Grade 8.8 galvanized bolts (d = 16mm) with thread excluded from the sliding interfaces, and assembled with a structural washer, a flat washer, a single Belleville washer in its fully squashed condition, and a nut were used to clamp together shims and plates, as shown in Figures 5.1a-b. Belleville washers were used to reduce bolt clamping force variation due to sliding surfaces degradation [5.1, 5.3]. The 18 AFCs were divided into 6 groups where the slot length was 80mm and the thickness of the shims was 6mm. The thickness of the Grade 300 steel plates and the bolt length varied from group to group, as shown in Table 5.1. In Table 5.1 the bolt lever arm, l, and the bolt lever arm to bolt diameter ratio, l/d, are also presented for each of the 6 groups. The bolt lever arm, l, was calculated as the thickness of the slotted plate plus the thickness of the two shims [5.5].

Table 5.1. Assembling variables for the 6 groups of AFCs

AFCs Group	Grade 300 Steel plates thickness mm	Bolt denomination	Bolt lever arm l mm	Bolt lever arm to bolt diameter ratio l/d mm/mm	Proof load torque N-m
I	10	M16 x 80	22.0	1.38	245
II	16	M16 x 90	28.0	1.75	265
III	25	M16 x 120	37.0	2.31	310
IV	30	M16 x 140	42.0	2.63	315
V	40	M16 x 180	52.0	3.25	335
VI	50	M16 x 220	62.0	3.88	365

Details of the dimensions of the AFCs are presented in Figures 5.2a - b. AFCs were assembled using the torque control method, where the bolts are tensioned up to the proof load by a torque defined experimentally and applied by a calibrated torque wrench [5.9]. Values of the torque used to tension each of the 6 groups of AFCs are reported in Table 5.1.

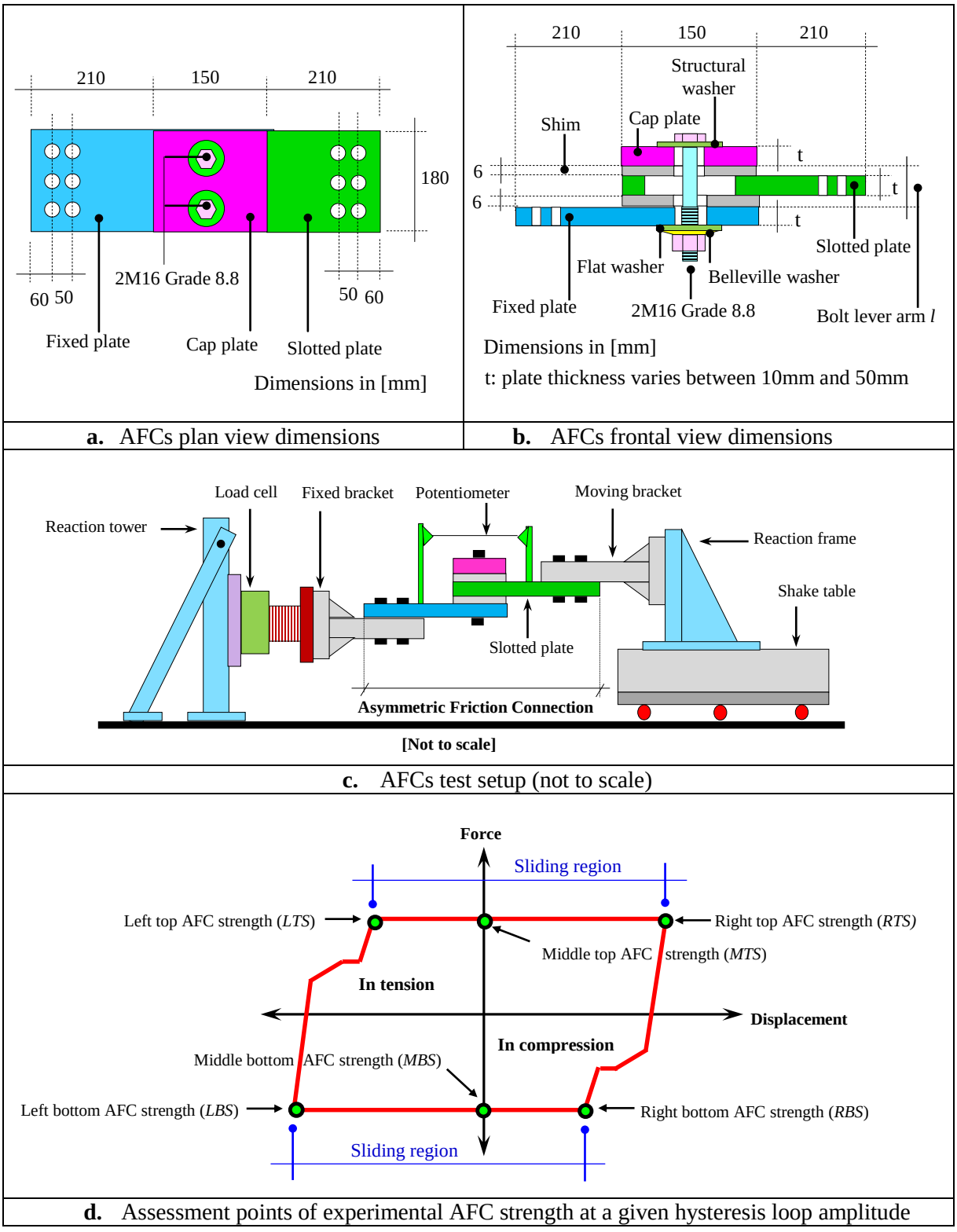

a. AFCs plan view dimensions

b. AFCs frontal view dimensions

c. AFCs test setup (not to scale)

d. Assessment points of experimental AFC strength at a given hysteresis loop amplitude

Figure 5.2. AFC devices dimensions, test setup, and assessment points of experimental AFC strength at a given hysteresis loop amplitude (Not to scale)

AFCs were quasi-statically tested using a shake table to provide the horizontal input, as shown in Figure 5.4c. The test setup comprised one bracket at each end of the AFC, a load cell in series with the brackets, and a potentiometer across the stroke of the AFC. Testing used the shake table to apply a fully horizontal displacement input to avoid prying effects [5.4, 5.5], comprising 18 sinusoidal cycles with a maximum velocity of 10mm/s and amplitudes varying from 1.6mm to 25mm.

2.2 Assessment of experimental AFC strength

Experimental AFC strength in the sliding region of the hysteresis loop in Figure 5.2d, are used to validate the proposed MPV model. Experimental AFC strengths come from the testing undertaken in this research for AFCs with Bisalloy 500 shims, and from the available experimental data for AFCs with Bisalloy 400 shims [5.6]. Experimental data for AFCs with Bisalloy 500 shims correspond to 540 AFC strengths obtained from 18 tests. Each test provides 30 AFC strengths assessed at the two ends points and the zero displacement point of both sliding regions of the hysteresis loop at amplitudes of 1.5mm, 3mm, 6mm, 12mm, and 25mm, as shown in Figure 5.2d. Experimental data for AFCs with Bisalloy 400 shims correspond to 60 AFC strengths obtained from 60 tests of AFCs with *l/d* of 0.90 – 1.90, 4 Grade 8.8 M16, M20, M30, and M36 bolts. Each test provides one AFC strength assessed as the absolute average across the both sliding regions for the initial cycles of loading when a stable AFC strength was first achieved [5.6].

2.3 MPV model basis

The Clifton model [5.2] assumed bolts with the bolt thread excluded from the sliding interfaces. In this model, bolts are assumed to bear on the cap plate and on the fixed plate

bending in double curvature while remaining vertical, during sliding of the slotted plate, as shown in Figure 5.3 [5.2].

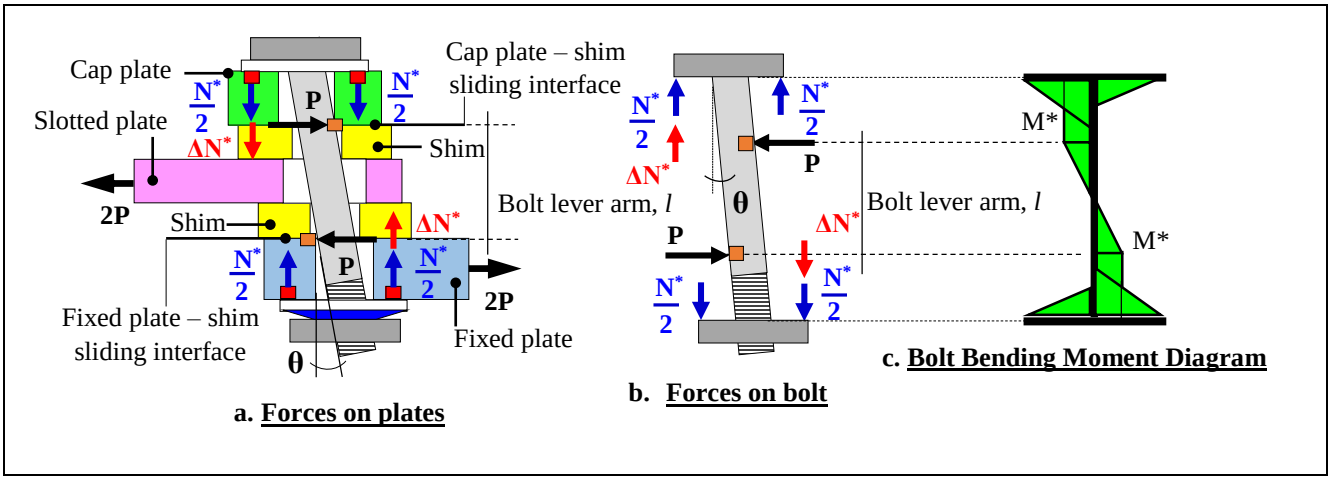

Figure 5.3. Forces on AFCs during sliding of slotted plate, idealized bolt deformation, and bolt bending moment diagram (Clifton MPV model 2005 [5.2]) (Not to scale)

Here, bolts are subjected to an axial tension considering moment – axial force – shear force interaction, N^*, to two opposite horizontal forces equal to the friction force carried by each sliding interface, P, and to an increase in bolt tension resulting from bolt rotation, ΔN^*, which is ignored given the bolts are assumed to yield during assembly, and are not able to carry added axial tension [5.2]. This MPV model was defined:

$\left[\frac{M^*}{M_{rfn}}\right]+\left[\frac{V^*}{V_{rfn}}\right]=1$	(5.1)
$V^* = N^* \times \mu$	(5.2)
$M^* = \frac{N^* \times \mu \times l}{2}$	(5.3)
$M_{rfn} = 0.1665 \times d^3 \times F_{uf} \times \left[1-\left[\frac{N^*}{0.56 \times d^2 \times F_{uf}}\right]\right]$	(5.4)
$V_{rfn} = 0.62 \times F_{uf} \times 0.56 \times d^2$	(5.5)

Where, M^* is the bolt moment demand, V^* is the bolt shear demand, M_{rfn} is the bolt moment capacity considering axial force interaction at the bolt non- threaded zone, and V_{rfn} is the bolt shear capacity considering no axial force interaction at the bolt non- threaded zone. Variables in Equations 5.2 – 5.5 are defined functions of the friction coefficient at the sliding interfaces between the slotted plate and the shims, μ, the bolt nominal diameter, d, the bolt ultimate tensile strength, F_{uf}, the bolt proof load, F_{proof}, and the bolt lever arm, l. The bolt tension, N^*, considering moment – axial force – shear force interaction can be obtained by solving the quadratic equation resulting from the substitution of Equations 5.2 – 5.5 into Equation 5.1.

$$a \times N^{*2} + b \times N^{*} + c = 0 \quad (5.6)$$

The coefficients a, b, and c in Equation 5.6 are functions of F_{uf}, μ, l, and d:

$$a = -2.880 \times \mu \quad (5.7)$$

$$b = \left(1.681 \times \mu \times F_{uf} \times l \times d\right) + \left(1.613 \times \mu \times F_{uf} \times d^2\right) + \left(F_{uf} \times d^2\right) \quad (5.8)$$

$$c = -0.560 \times F_{uf}^2 \times d^4 \quad (5.9)$$

AFC strength, S, considering MPV interaction per bolt and per sliding interface can then be defined:

$$S = \mu \times N^{*} \quad (5.10)$$

The Clifton model [5.2] described above was modified by Khoo [5.6] when considering the effect of bolt thread included in one of the sliding interfaces on the AFC strength. In this case, the Khoo model [5.6] is defined:

$$\left[\frac{2\times M^{*}}{M_{rfn}+M_{rfn-thread}}\right]+\left[\frac{2\times V^{*}}{V_{rfn}+V_{rfn-thread}}\right]=1 \quad (5.11)$$

In Equation 5.11 the bolt moment capacity at the threaded zone, $M_{rfn\text{-}thread}$, and the bolt shear capacity at the threaded zone, $V_{rfn\text{-}thread}$, are defined as function of the bolt diameter at the threaded zone, $d_{thread,}$ yielding:

$$M_{rfn-thread}=0.1665\times d_{thread}^{3}\times F_{uf}\times\left[1-\left[\frac{N^{*}}{0.56\times d_{thread}^{2}\times F_{uf}}\right]\right] \quad (5.12)$$

$$V_{rfn-thread}=0.62\times F_{uf}\times 0.56\times d_{thread}^{2} \quad (5.13)$$

In the Khoo model [5.6], for bolts with threads included in one of the sliding interfaces, the bolt tension, N^{*}, considering MPV interaction can be found using similar process as described earlier for bolts with threads excluded from the sliding interfaces using Equations 5.1-5.10, and the AFC strength can be found using Equation 5.10.

2.4 Mechanics of Proposed MPV model

AFCs are assumed with fixed supports at the ends of both the slotted plate and the fixed plate creating moments M_1 and M_2, as shown in Figure 5.4a. The bolt rotates an angle θ after sliding is activated at the top shim – slotted plate interface and at the bottom shim – slotted plate interface, as shown in Figure 5.4a. Once the bolt rotates, the bolt shank bears horizontally on the fixed plate and cap plate with a force equivalent to half of the AFC strength, *P*, and the bolt head and the nut also provide a compression force on the fixed plate and the cap plate termed tilting force, *A*, as shown in Figure 5.4a. The horizontal forces, *P*, are assumed to be

located at the top shim – slotted plate interface, and at the bottom shim – slotted plate interface at points termed bearing points, located apart a distance equivalent to the bolt lever arm, *l*, as shown in Figure 5.4a. The compression forces, *A*, are assumed to be located on the cap plate and on the fixed plate at points termed tilting points located under the bolt head side and under the bolt nut side in contact with the connection after the bolt rotation occurs, as shown in Figure 5.4a.

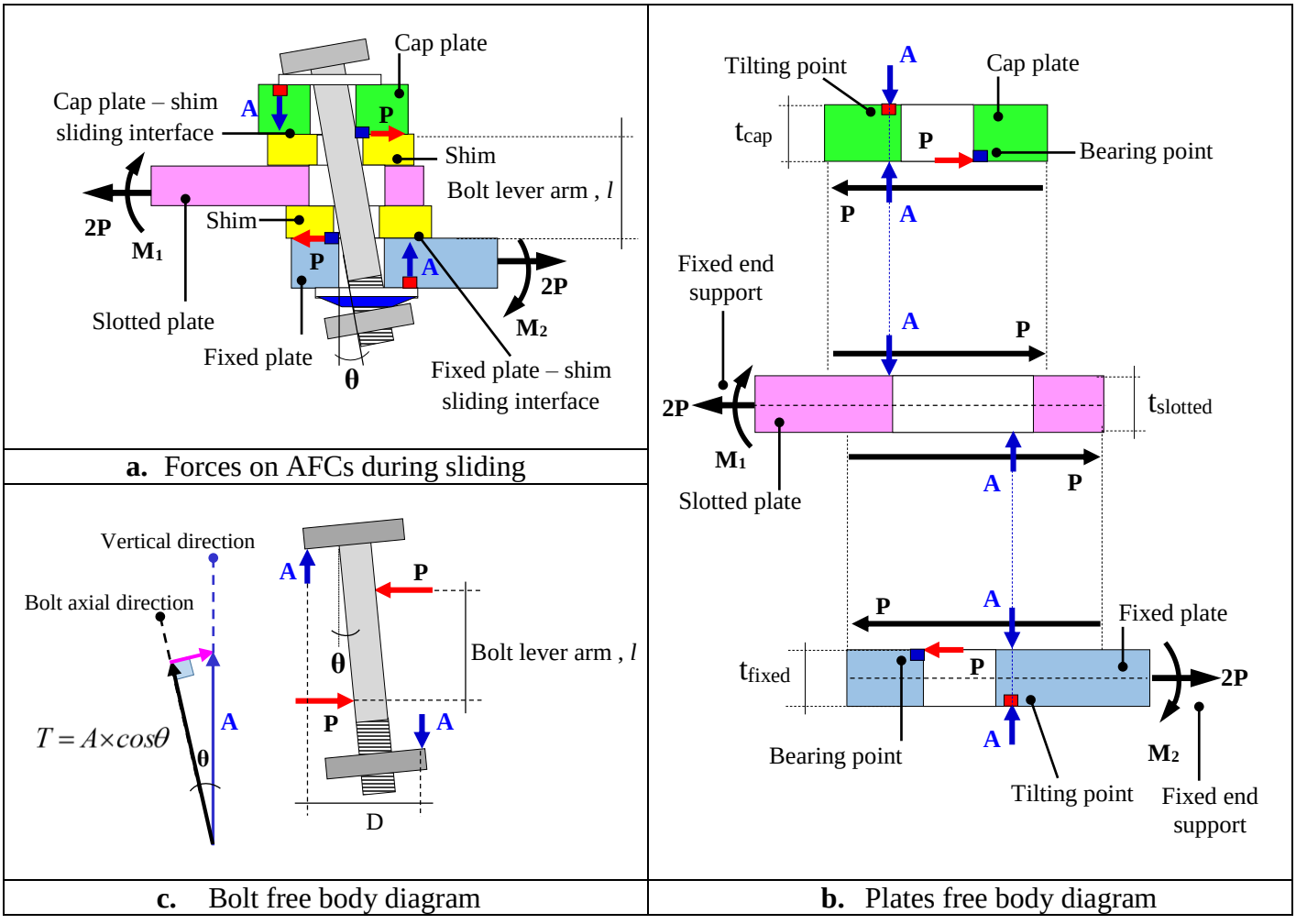

Figure 5.4. Forces on AFCs during sliding, free body diagrams of plates and bolt for proposed MPV model considering AFC with fixed supports at both ends (Not to scale)

It can be seen in Figures 5.4a – b that as a result of the action of the horizontal forces, *P*, and the compressive forces, *A*, on the cap plate and on the fixed plate; the slotted plate, the fixed plate, and the AFC are not in equilibrium, as seen in Figures 5.4a-b. To ensure the individual equilibrium of these plates and the global equilibrium of the AFC, a moment acting on the fixed end of the slotted plate and a moment acting on the fixed end of the fixed plate are required.

Figure 5.4c shows the forces acting on the bolt in the deformed geometry after bolt rotation occurs. The bolt is subjected to two horizontal forces with opposite direction and equivalent to half of the AFC strength, *P*, and to two vertical forces with opposite direction equivalent to the tilting force, *A* acting a distance *D* apart. The component of the tilting force, *A*, in the bolt axial direction corresponds to the bolt tension during the sliding, *T*, as shown in Figure 5.4c. The bolt tension during sliding, *T*, is the resultant of the addition of the bolt tension during the assembly, of the increase in bolt tension due to bolt rotation during the sliding, and of the reduction in bolt tension due to MPV interaction during the sliding.

The bolt axial, shear, and moment demands for the proposed MPV model are presented in Figure 5.5b**,** and expressed as function of the bolt rotation angle, θ, the one half AFC strength, *P*, and the tilting force acting on the bolt, *A*. The maximum possible bolt rotation angle assuming rigid plates, θ, is used, defined as the maximum angle the hole oversize, *O*, and the thickness of the fixed plate, t_{fixed}, allow the bolt shank to horizontally load the fixed plate and the cap plate at only one point during the bolt rotation, as shown in Figure 5.5a, defined:

$\theta = tan^{-1}\left[\frac{O}{t_{fixed}}\right]$	(5.14)

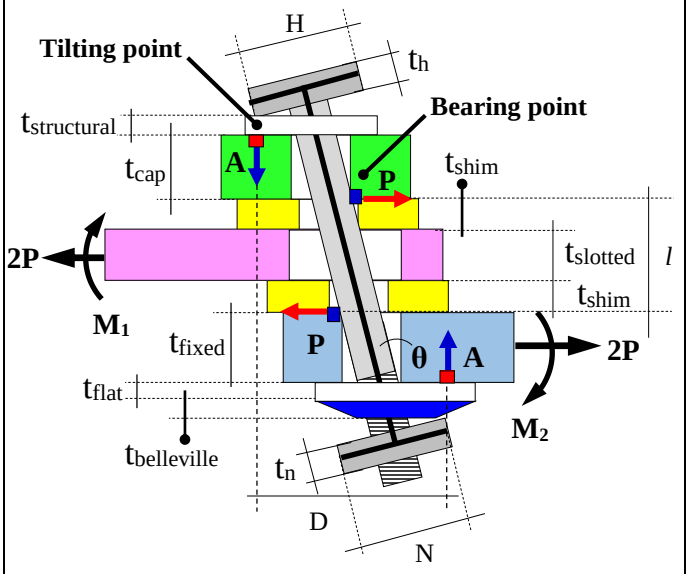

H	:	Width across head flats
t_h	:	Bolt head thickness
N	:	Width across nut flats
t_n	:	Nut thickness
$t_{structural}$	:	Structural washer thickness
t_{cap}	:	Cap plate thickness
t_{shim}	:	Shim thickness
$t_{slotted}$	:	Slotted plate thickness
t_{fixed}	:	Fixed plate thickness
t_{flat}	:	Flat washer thickness
$t_{belleville}$	:	Fully compressed Belleville washer thickness
l	:	Bolt lever arm or distance between bearing points
D	:	Distance between tilting points
θ	:	Bolt rotation angle

a. AFCs during sliding, bolt and plates geometrical variables

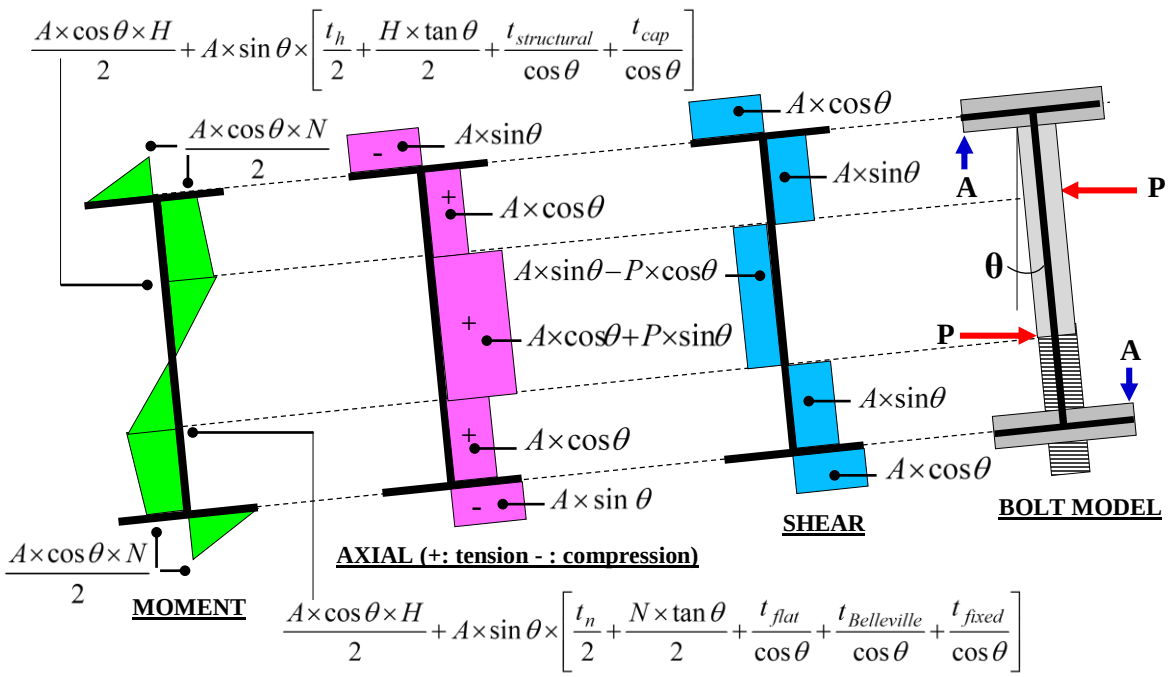

b. Bolt axial, shear, and moment demand

Figure 5.5. Axial, shear, and moment demand of bolt for the proposed MPV models for AFCs with fixed end supports at both ends (Not to scale)

The value of *P* per bolt, which is one half of AFC strength is obtained using Coulomb dry friction theory as the product of the number of sliding interfaces, *n*, corresponding to 2 in AFCs, of the bolt tension during sliding, *T*, and the friction coefficient, μ:

$P = n \times T \times \mu$	(5.15)

The vertical force acting on the bolt, *A*, in Figure 5.5c was obtained by equilibrium on the bolt, and is a function of *P*, the distance between the tilting points, *D*, the bolt grip length outside of washers, *G*, and the distance between the bolt bearing points or bolt lever arm, *l*, yielding:

$A = \frac{P \times l}{D}$	(5.16)

Where *D*, *G*, and, *l* are defined in Figure 5.5a, as:

$D = \frac{\cos\theta}{2} \times (H + N) + \frac{\sin\theta}{2} \times \left[t_h + H \times \tan\theta + t_n + N \times \tan\theta + \frac{2 \times G}{\cos\theta} \right]$	(5.17)
$G = t_{structural} + t_{cap} + 2 \times t_{shim} + t_{slotted} + t_{fixed} + t_{flat} + t_{belleville}$	(5.18)
$l = 2 \times t_{shim} + t_{slotted}$	(5.19)

Equations 5.4-5.5 from the Clifton model [5.2] and Equations 5.11 – 5.13 from the Khoo model [5.6], are used here to develop the proposed improved MPV model for one bolt with thread included in one of the sliding interfaces. By substituting bolt moment capacity with axial force interaction at the non – threaded bolt zone and at threaded bolt zone, M_{rfn}, $M_{rfn\text{-}thread}$, in Equations 5.4 and 5.12, respectively, and the bolt shear capacity without axial force

interaction at at the non – threaded bolt zone and at threaded bolt zone V_{fn}, $V_{rfn\text{-}thread}$ in Equations 5.5 and 5.13,respectively, the maximum bolt moment demand, *M**, the maximum bolt shear demand, *V*,* and the maximum bolt axial demand, *N*,* presented in Figure 5.5b, into Equation 5.11 create the general MPV interaction expression for the proposed model:

$$\left[\frac{T\times K_1}{K_2 - T\times K_3}\right]+\left[\frac{T\times K_4}{K_5}\right]=1 \qquad (5.20)$$

Solving the bolt tension during sliding, *T,* in the proposed MPV model of Equation 5.20 results in the quadratic equation:

$$-\left[K_3\times K_4\right]\times T^2+\left[\left(K_1\times K_5\right)+\left(K_4\times K_2\right)+\left(K_3\times K_5\right)\right]\times T-\left[K_2\times K_5\right]=0 \qquad (5.21)$$

The general expression of the bolt tension during the sliding, *T*, for the proposed improved MPV model is defined:

$$T=\frac{\left[\left(K_1\times K_5\right)+\left(K_4\times K_2\right)+\left(K_3\times K_5\right)\right]-\sqrt{\left[\left(K_1\times K_5\right)+\left(K_4\times K_2\right)+\left(K_3\times K_5\right)\right]^2-\left[4\times K_2\times K_3\times K_4\times K_5\right]}}{2\times K_3\times K_4} \qquad (5.22)$$

Where K_1, K_2, K_3, K_4, and K_5 are defined:

$$K_1=\left[\frac{\mu\times l}{D}\right]\times\left[\frac{H\times\cos\theta}{2}+\frac{\sin\theta\times\tan\theta}{2}\times\left(\frac{t_h}{\tan\theta}+H+t_{structural}+t_{cap}\right)\right] \qquad (5.23)$$

$$K_2=0.17\times F_{uf}\times\left[\frac{d^3+d_{thread}^3}{2}\right] \qquad (5.24)$$

$$K_3=\left[0.30\times\mu\right]\times\left[\frac{d+d_{thread}}{2}\right]\times\left[\frac{l\times\cos\theta}{D}+\sin\theta\right] \qquad (5.25)$$

$K_4 = \left[\frac{\mu \times l \times \sin\theta}{D}\right] - \left[\mu \times \cos\theta\right]$	(5.26)
$K_5 = 0.35 \times F_{uf} \times \left[\frac{d^2 + d_{thread}^2}{2}\right]$	(5.27)

K_1, K_2, K_3, K_4, and K_5 defined above in Equations 5.23- 5.27 are applicable for one bolt with one thread included in one of the sliding interfaces. For one bolt with thread excluded from the two sliding interfaces the bolt diameter at the thread zone, d_{thread}, should be replaced by the bolt nominal diameter, d, for variables K_2, K_3 and K_5 in Equations 5.24-5.25, and 5.27.

The AFC strength per bolt, *S*, considering moment – axial force – shear force interaction and the bolt rotation in the proposed improved MPV model for one bolt with thread included in one of the sliding interfaces or for one bolt with thread excluded from the two sliding interfaces can be assessed as *2P* defined in Equation 5.15, yielding:

$S = 2 \times n \times T \times \mu$	(5.28)

III. RESULTS AND ANALYSIS

Predictions of AFC strength with the proposed MPV model were performed for:

i. A friction coefficient, μ, of 0.25 – 0.40 adopted from values calibrated from experimental results of tests of AFCs with Bisalloy 500 shims [5.3],

ii. A bolt hole oversize, *O*, between 2mm and 3mm adopted from the current in practice site assembly regulations for M16 to M30 bolts [5.9],

iii. A bolt tensile yielding strength, F_y, of 660MPa adopted as the nominal value for Grade 8.8 bolts [5.9], and

iv. A bolt tensile ultimate strength, F_{uf}, of 830 – 996MPa. This range matches with the nominal value of 830MPa [5.9], and the maximum found from axial testing for Grade 8.8 bolts, which is equal to 1.20 times the nominal value [5.2].

3.1 Validation of the proposed MPV model

The proposed MPV model is validated in Figure 5.6 by comparing the experimental AFC strengths described in Section 2.2 with the theoretical AFC strength predicted with the proposed MPV model described in Equations 5.14-5.28. The theoretical AFC strength was predicted for μ = 0.25, O = 2mm, one Grade 8.8 bolt with thread excluded from the two sliding interfaces, F_{uf} = 830MPa, F_y= 660 MPa, and considering:

i. Elastic axial bolt behaviour, where the bolt is assumed linear up to the bolt nominal ultimate strength, and

ii. Elasto-plastic axial bolt behaviour, where the bolt is assumed linear until it yields in tension, and thereafter the strength is assumed to remain constant at the bolt nominal yielding strength. This elasto-plastic axial bolt behaviour is implemented in the proposed MPV model by comparing the bolt tension during the sliding, *T*, calculated from equation 5.22 with the force that yields the bolt in tension, *Ty*, calculated as the product of the nominal yielding strength, *Fy*, and the bolt tension area. For bolts with a resulting bolt tension during the sliding, *T*, greater than the force that yields the bolt in tension, *Ty*, the bolt tension during the sliding, *T*, is assumed equal to the force that yields the bolt in tension, *Ty*.

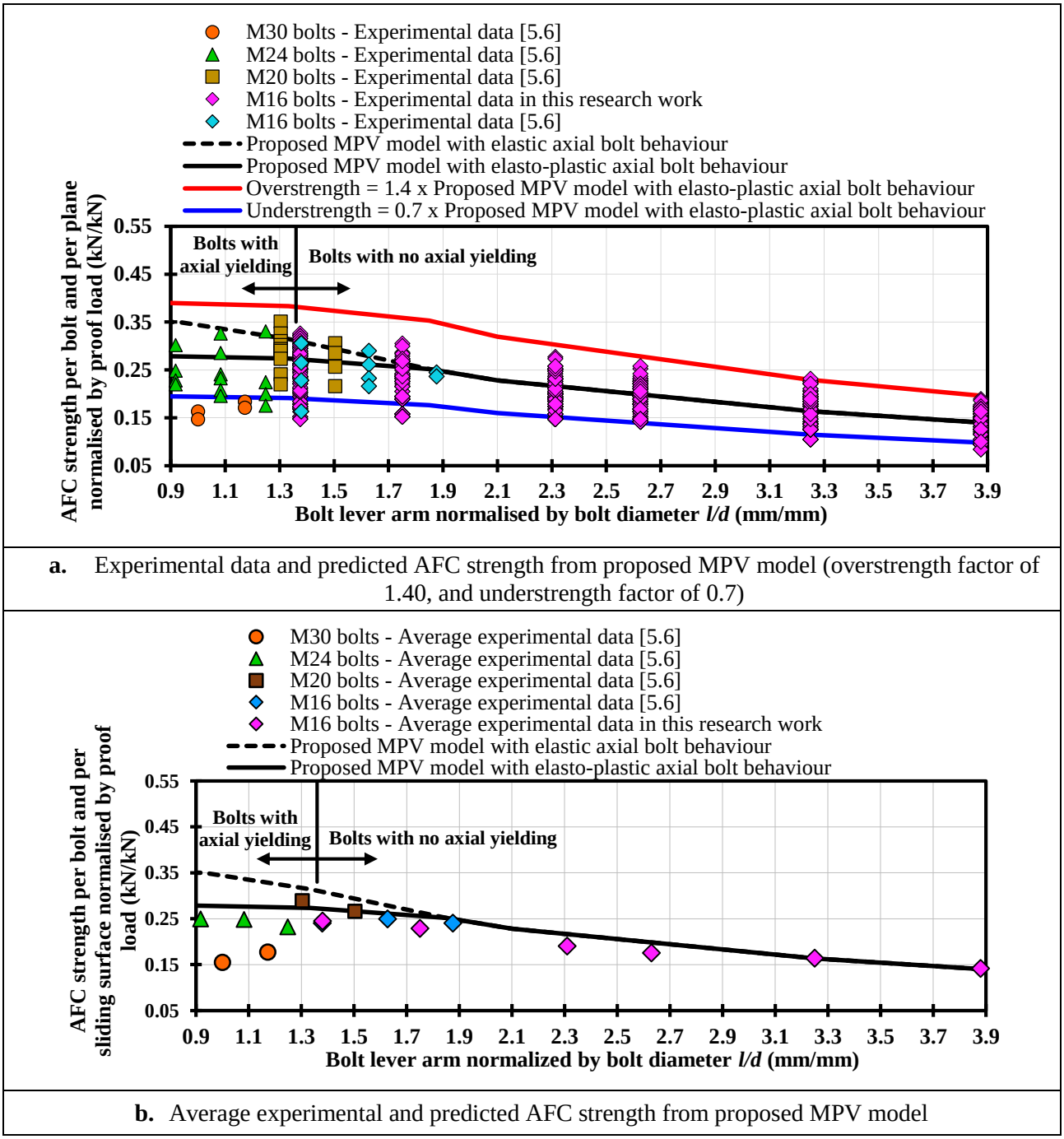

a. Experimental data and predicted AFC strength from proposed MPV model (overstrength factor of 1.40, and understrength factor of 0.7)

b. Average experimental and predicted AFC strength from proposed MPV model

Figure 5.6. Experimental and predicted AFC strength with the proposed MPV model (One Grade 8.8 bolt with thread excluded from the two sliding interfaces, μ = 0.25, O = 2mm, and F_{uf} = 830MPa)

Figure 5.6a shows the proposed MPV model considering elasto-plastic axial bolt behaviour better follows the experimental data than considering only elastic axial bolt behaviour. This

also can be seen in Figure 5.6b, where the theoretical AFC strength predicted considering elasto-plastic axial bolt behaviour agrees well with the almost constant trend, and the decreasing trend of the average experimental AFC with *l/d*. The constant and decreasing trends represent the case where bolts yield axially due to the increase in bolt axial force due to bolt rotation, and the case where the bolt axial behaviour including the increase in bolt axial force due to bolt rotation is elastic, respectively.

In Figure 5.6a to consider the scatter of the experimental AFC strengths due to variability in bolt assembly, bolt mechanical properties, and degradation of the sliding surfaces, the predicted AFC strength considering elasto-plastic axial bolt behaviour is factored by an overstrength factor of 1.40 [5.8] and an understrength factor of 0.7 [5.8]. It can be seen, using these recommended values of overstrength and understrength, the majority of the experimental data is enveloped.

Average experimental strengths were (86-100) %, (96-100) %, (82-89) %, and (21-45) % of those found considering elasto- plastic bolt axial behaviour with the proposed model were obtained for AFCs for AFCs with M16, M20, M24, and M30 bolts, respectively, as shown in Figure 5.6b. The proposed MPV model agrees well with the experimental data for AFCs with M16, M20, and M24 bolts, but does not agree with experimental data for AFCs with M30 bolts, probably due to the lack of experimental AFC strengths for AFCs with M30 bolts, as well as due to the difficulties of reaching the proof load for these bolts during assembly [5.6]. For instance, for M30 bolts only four tests were conducted, two at each of the *l/d* values of 1.0 and 1.17, as shown in Figure 5.6. This sample size does not give a good representation of the behaviour of M30 bolts. Also the disproportionately lower value of the AFC strength

for M30 bolts respect to the predicted AFC strength could be due to the insufficient capacity of the available torque wrench to tension these bolts up to the proof load [5.6].

3.2 Parametric study of the proposed MPV model

The proposed MPV model described in Equations 5.14-5.28 is used to predict the relative impact and effects on the AFC strength on the parameters below:

3.2.1 Effect of bolt model and bolt rotation/inclination on AFC strength prediction

AFC strength is predicted in Figure 5.7 with Khoo model [5.6] and the proposed MPV model considering elasto-plastic bolt axial behaviour as defined in Section 3.1 and O = 2mm. For both MPV models, the AFC strength is predicted for μ = 0.25, one Grade 8.8 bolt with the thread excluded from the two sliding interfaces and F_{uf} = 830MPa.

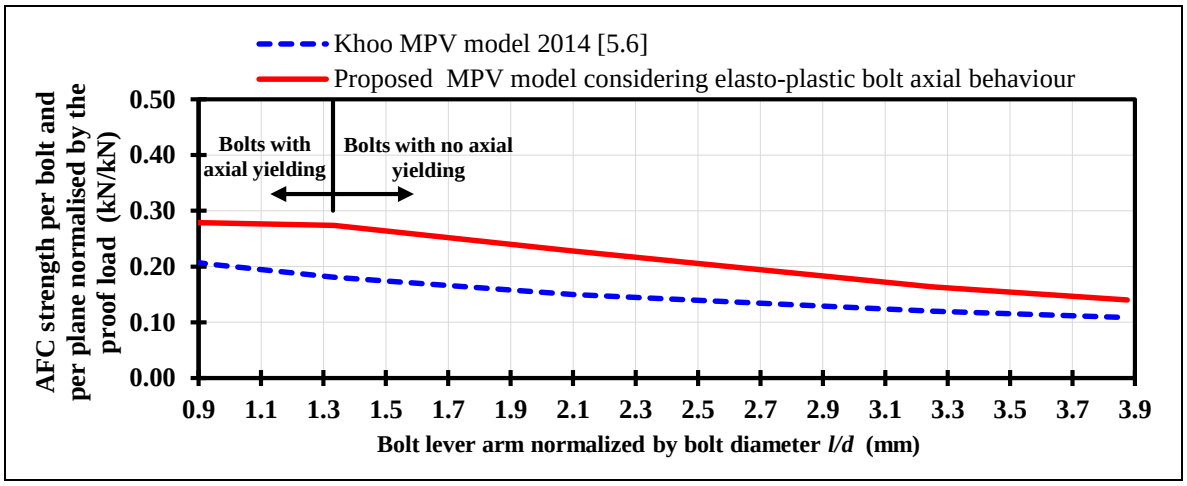

Figure 5.7. AFC strength predictions (One Grade 8.8 bolt with thread excluded from the two sliding interfaces, μ = 0.25 and F_{uf} = 830MPa and O = 2mm)

In Figure 5.7 it can be seen for l/d = 0.90 – 3.9 the AFC strength predicted with the proposed MPV model considering elasto-plastic bolt axial behaviour is 1.2 – 1.5 times greater than the AFC strength predicted by Khoo model [5.6]. This difference is attributed to the increase in bolt axial tension due to bolt rotation considered in the proposed MPV model. For bolts

with no axial yielding, the difference between the predicted AFC strengths reduces as *l/d* increases, since the bolt rotation reduces as *l/d* increases, which in turn reduces the increase in bolt tension due to bolt rotation. For bolts with axial yielding, the difference between the predicted AFC strengths increases as *l/d* increases. That is because once bolts yield, they can not carry the increase in bolt tension due to bolt rotation, and they are subjected only to the reduction in bolt tension due to MPV interaction, which increases with increasing *l/d*. This outcome shows bolt axial tension may increase due to bolt rotation during sliding of the slotted plate, but only if bolts do not undergo axial yielding.

3.2.2 Effect of AFC assembly variables on AFC strength

AFC strength is predicted in Figure 5.8 with the proposed MPV model considering elasto-plastic bolt axial behaviour for one Grade 8.8 bolt, F_{uf} = 830MPa, and F_y= 660 MPa. In Figure 5.8a, AFC strength is predicted for μ = 0.25, O = 2mm, considering the bolt thread *excluded* from the two sliding interfaces, and with the bolt thread *included* in one of the sliding interfaces. It is shown by including the bolt thread in one of the sliding interfaces, AFC strength reduces. For *l/d* = 0.90 – 3.9, reductions in AFC strength up to 17.5% were predicted with the proposed MPV model considering elasto-plastic axial bolt behaviour. Reductions in AFC strength are attributed to reductions in bolt shear capacity and in bolt moment capacity in one of the sliding interfaces resulting from the reduction in diameter due to bolt thread. In practice, the bolt thread *excluded* from the two sliding interfaces, and the bolt thread *included* in one of the sliding interfaces, are both possible for AFCs depending on the plate arrangement thickness. The desirable case corresponds to the bolt thread *excluded* from the two sliding interfaces given that the AFC strength is not reduced by the bolt thread. This case was considered here for assembling the AFCs of this research work.

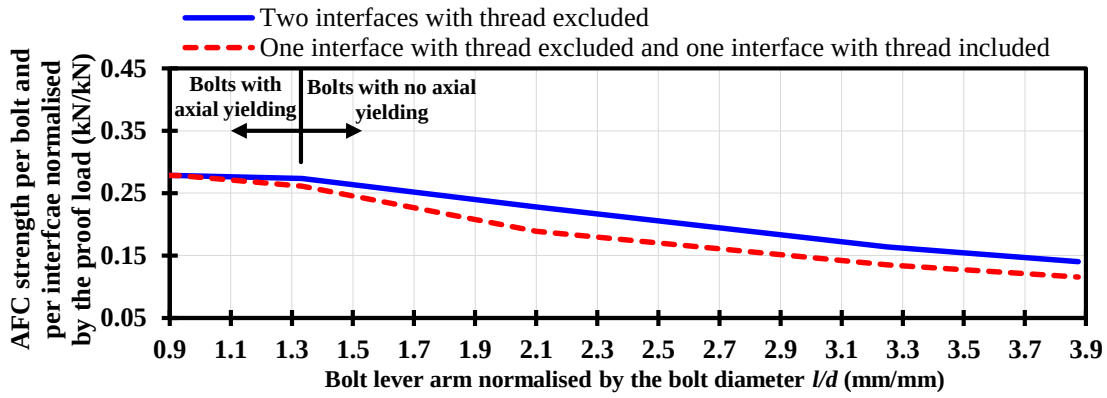

a. Effect of inclusion of bolt thread in the sliding interfaces on AFC strength for one Grade 8.8 bolt, O = 2mm, μ = 0.25, and F_{uf} = 830MPa

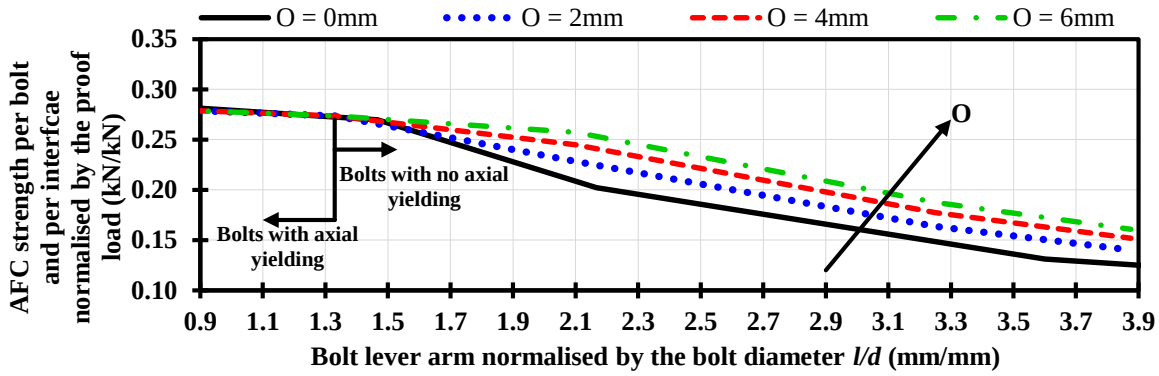

b. Effect of bolt hole oversize, O, on AFC strength for one Grade 8.8 bolt with thread excluded from the two sliding interfaces, μ = 0.25, and F_{uf} = 830MPa

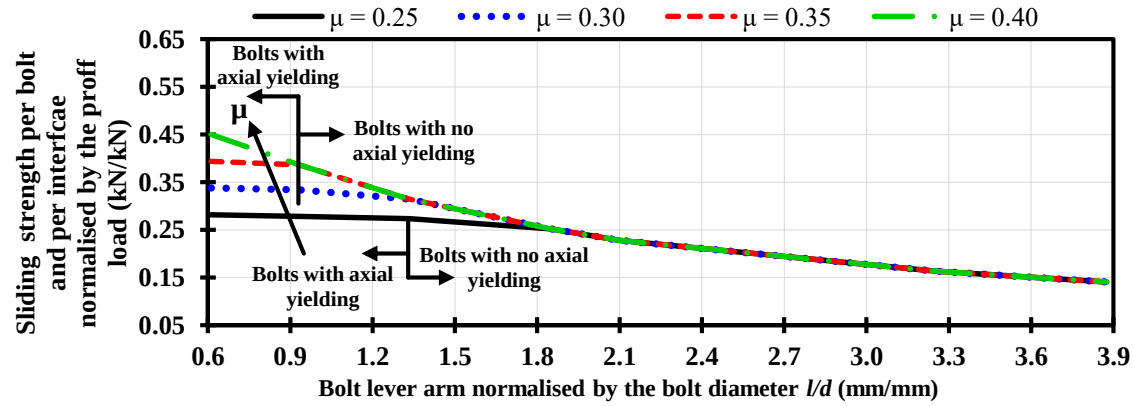

c. Effect of friction coefficient at the sliding interfaces, μ, on AFC strength for one Grade 8.8 bolt with thread excluded from the two sliding interfaces, O = 2mm and F_{uf} = 830MPa

Figure 5.8. Effect of bolt assembling variables on the AFC strength predicted with the proposed MPV model considering bolt elasto – plastic axial behaviour

In Figure 5.8b, AFC strength is predicted for $\mu = 0.25$, considering both bolt threads excluded from the two sliding interfaces, and varying O from 0mm to 4mm. It is shown by increasing O, AFC strength increases. For $l/d = 0.90 – 3.9$ AFC strength increased by 8.4%, and 14.7%, when the standard bolt hole oversize, O, of 2mm is increased to 4mm and 6mm, respectively. This is due to the increase in horizontal component of bolt axial tension when the bolt rotation angle increases with increasing bolt hole oversize. Since increasing the bolt hole oversize increases the bolt rotation angle, and therefore the horizontal component of bolt axial tension, there is not an upper bond on the AFC strength increase with the bolt hole oversize. For O = 0mm, AFCs develop minimum AFC strength, since the bolt remains vertical or with no rotation. Thus, there is no increase in bolt axial tension due to bolt rotation. For design, the New Zealand Steel Structures Standard [5.9] specifies a bolt hole oversize, O, of 2mm for M16, M20, and M24 bolts, and of 3mm for M30 and M36 bolts. Explicit consideration of bolt rotation was not considered in the Clifton and Khoo models [5.2, 5.6].

In Figure 5.8c, AFC strength is predicted for O = 2mm, considering the bolt thread excluded from the two sliding interfaces, and varying the friction coefficient at the sliding interfaces, μ, from 0.25 to 0.40. It is shown by increasing μ AFC strength increases. For $l/d = 0.90 – 3.9$, AFC strength increases up to 20%, 40%, and 60% when μ is increased from 0.25 to 0.30, 0.35, and 0.40, respectively. This occurs because increasing μ increases the friction forces at the sliding interfaces, which in turn increases the AFC strength. Increments in AFC strength due to μ are observed in Figure 5.8b only for $l/d \leq 2.0$. This outcome indicates AFC strength depends on μ only for AFCs when bolt shear demand is significant when compared with bolt moment demand, which occurs for lower values of l/d. Since there is not experimental information supporting this outcome, it is recommended to validate this

outcome by testing AFCs with $l/d > 2.0$ and with different shim materials, so that the friction coefficient at the sliding interfaces varies for recording any gain in AFC strength. Figure 5.8c also shows by increasing μ, bolts undergo axial yielding at a lower values of l/d. This is because the increase in bolt axial force with increasing μ is more significant for AFCs with lower values of l/d, where the bolt rotation is larger.

3.2.3 Effect of bolt axial behaviour variables on AFC strength

AFC strength is predicted in Figure 5.9 with the proposed MPV model for μ = 0.25, O = 2mm, one Grade 8.8 bolt with thread excluded from the two sliding interfaces, F_{uf} = 830MPa, and F_y = 660 MPa.

In Figure 5.9a, AFC strength is predicted considering bolt elasto-plastic axial behaviour and varying the bolt ultimate strength, $F_{uf,}$ from a nominal value of 830MPa to a value of 1.2 times the bolt nominal ultimate strength (1.2 F_{uf} = 996 MPa) [5.2]. It is shown AFC strength increases proportionally with F_{uf}. Increases in AFC strength occur because the bolt shear capacity and the bolt moment capacity increase with F_{uf} allowing the bolt to increase the moment and shear demand, thus increasing the AFC strength.

In Figure 5.9b, AFC strength is predicted considering the increase in bolt axial tension due to bolt rotation is carried by the bolt behaving axially elastic or elasto-plastically as defined in Section 3.1. For $l/d \leq 2.0$ the AFC strength predicted considering bolt elastic bolt axial behaviour is greater than the AFC strength predicted considering elasto-plastic bolt axial behaviour. This result indicates AFC strength is more dependent on the bolt axial relationship for lower values of l/d rather than for larger values of l/d because the bolt axial demand

reduces as l/d increases. For $l/d \leq 1.33$ and $\mu = 0.25$ bolt axial yielding occurs due to the increase in axial force from bolt rotation. As a result of bolt axial yielding, the AFC strength reduces up to 25% for $l/d \leq 1.330$, and this AFC strength reduction decreases rapidly to 0% as l/d increases from 0.94 to 2.0.

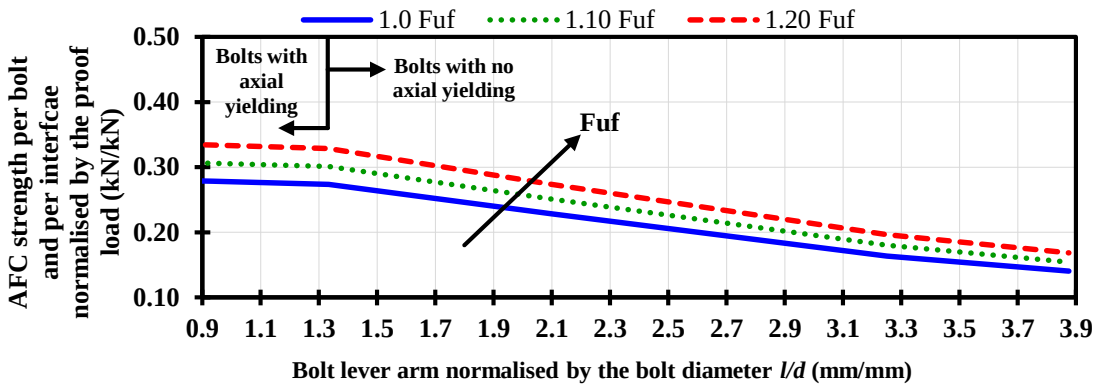

a. Effect of the bolt tensile ultimate strength, F_{uf}, on AFC strength for one Grade 8.8 bolt with thread excluded from the two sliding interfaces, $\mu = 0.25$ and $O = 2$mm

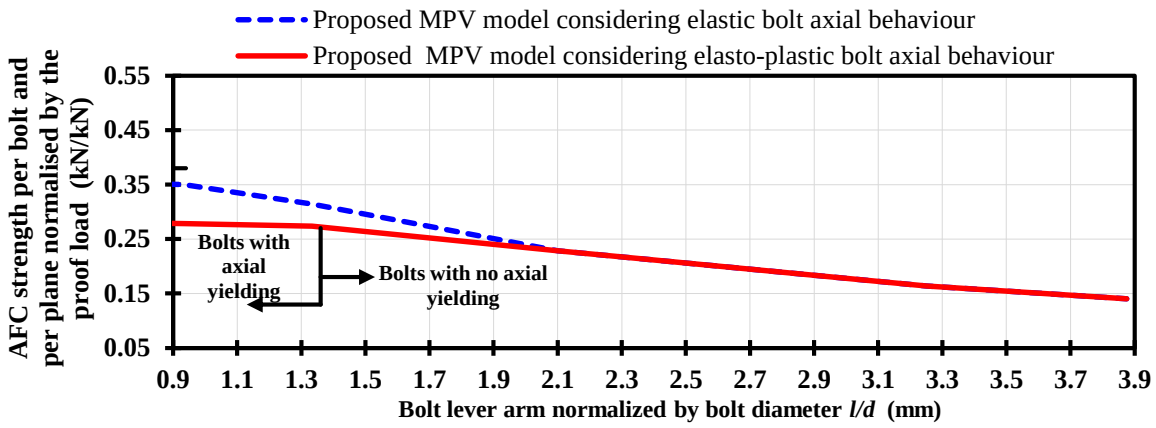

b. Effect of the bolt axial behaviour on AFC strength for one Grade 8.8 bolt with thread excluded from the two sliding interfaces, $O = 2$mm, $\mu = 0.25$ and $F_{uf} = 830$MPa

Figure 5.9. Effect of bolt axial behaviour variables on the AFC strength predicted with the proposed MPV model considering elasto-plastic bolt axial behaviour

Three bolt axial force components take part in the bolt axial yielding:

i. The proof load due to bolt assembly, T_{Proof},

ii. The increase in axial force due to bolt rotation, ΔT_R, and

iii. The reduction in bolt axial force due to MPV interaction, $\Delta T_{MPV.}$

For bolts with $l/d \leq 1.33$, bolt axial yielding occurs when ΔT_R is greater than ΔT_{MPV}. In this case, the resulting force of the two components added to T_{Proof} is greater than the bolt tensile yielding strength. For bolts with l/d >1.33, bolt axial yielding does not occur given ΔT_R is less than ΔT_{MPV}. In this case, the resulting force of the two components added to T_{Proof} generates a bolt axial force less than the bolt tensile yielding capacity. That is because, while the increase in bolt axial tension due to bolt rotation, ΔT_R, is significant for lower for lower values of *l/d*, and it reduces as *l/d* increases, the reduction in bolt axial tension due to MPV interaction, $\Delta T_{MPV,}$ is low for lower values of *l/d*, and it increases as *l/d* increases. This outcome shows the increase in bolt axial force due to bolt rotation, ΔT_R, is critical for bolts with lower values of *l/d*, rather than for bolts with significant values of *l/d*.

CONCLUSIONS

This paper presents a non-linear MPV model for assessing AFC strength considering the bolt rotation and the increase in bolt axial tension due to bolt rotation. It was shown that:

i. A MPV model considering the increase in bolt axial force due to bolt rotation, and the number of threaded/unthreaded bolt regions in the sliding interfaces, was developed.

ii. AFC strength increases with bolt rotation/inclination. This has not previously been explicitly included in previous MPV models.

iii. AFC strength tends to increase with bolt hole oversize and it decreases with bolt threads at the sliding interfaces. Also it increases with greater friction coefficient at the sliding interfaces, but only for bolts with low bolt lever arm to bolt diameter, *l/d*, ratios.

iv. AFC strength increases with bolt tensile ultimate strength. Greater AFC strengths are developed for elastic axial bolt behaviour than for elasto- plastic axial bolt behaviour, but for bolts with low bolt lever arm to bolt diameter, *l/d*, ratios.

v. The proposed MPV model considering an elasto-plastic bolt axial behaviour predicts the average experimental data with accuracies of (86-100)%, (86-94)%, (92-100)%, and (39-59)% for M16, M20, M24, and M30 bolts, respectively. A friction coefficient of 0.25, an overstrength factor of 1.4, and an understrength factor of 0.7 can be used to predict the AFC strength for proof-loaded bolts with Grade 300 slotted plate and Bisalloy 400 or Bisalloy 500 wear resistant shims.

ACKNOWLEDGEMENTS

The authors would like to acknowledge funding from MBIE Natural Hazards Research Platform (NHRP), and material donation from John Jones Steel Ltd., for undertaking this research. All opinions expressed remain those of the authors.

REFERENCES

[5.1] Khoo, H.H., Clifton, C., Butterworth, J., MacRae, G. and Ferguson, G. (2011) *Influence of steel shim hardness on the Sliding Hinge Joint.* Journal of Constructional Steel Research. Vol 72, May 2012, p 119 – 129.

[5.2] Clifton, G.C. (2005). Semi-Rigid Joints for Moments Resisting Steel Framed Seismic Resisting Systems. *Published PhD Thesis, Department of Civil and Environmental Engineering.* University of Auckland – New Zealand.

[5.3] Rodgers, GW, Chase, JG, Causse, R, Chanchi Golondrino, J and MacRae, GA (2017). *Performance and Degradation of Sliding Steel Friction Connections: Impact of Velocity, Corrosion Coating and Shim Material*. Engineering Structures, Vol. 141, pp. 292–302. ISSN: 0141-0296, doi: 10.1016/j.engstruct.2017.02.070.

[5.4] Borzouie, J, Chase, JG, MacRae, GA and Rodgers, GW (2015). *Experimental Studies on Cyclic Performance of Column Base Weak Axis Aligned Asymmetric Friction Connection*. Journal of Constructional and Steel Research (JCSR), Vol 112, pp. 252-262.

[5.5] Borzouie, J, Chase, JG, MacRae, GA, Rodgers, GW and Clifton, C (2016). *Experimental Studies on Cyclic Performance of Column Base Strong Axis Aligned Asymmetric Friction Connections*. ASCE J. Structural Engineering, Vol 142(1), Article 04015078, 10-pages. ISSN: 0733-9445, doi: 10.1061/(ASCE)ST.1943-541X.0001327.

[5.6] Khoo, H.H., Clifton, G.C., MacRae, G.A., Zhou, H., and Ramhormozian, S. (2014). *Proposed design models for the asymmetric friction connection*. Earthquake and Structural Dynamics Journal. Vol 44, Issue 8, p. 1309-1324.

[5.7] MacRae, G.A., Clifton, C.G., MacKinven, H., Mago, N., Butterworth, J., Pampanin, S. (2010). *The Sliding Hinge Joint Moment Connection*. Bulletin of the New Zealand Society for Earthquake Engineering. Vol 43, Issue 3, p. 202-212.

[5.8] MacRae, G.A., and Clifton, C.G. (2015). *Research on Seismic Performance of Steel Structures*. Steel Innovation Conference. Auckland, New Zealand.

[5.9] Standards New Zealand. (2009). NZS3404: Part 1: 2009 - Steel Structures Standard. *Standards New Zealand*. Wellington, New Zealand.

Conclusions

This thesis describes the effects of fire, surface treatments, corrosion, a non-metallic sliding surfaces with brake pads, bolt length, and bolt inclination during sliding on the hysteretic behaviour of Asymmetric Friction Connections (AFCs) with Bisalloy 500 shims. It was shown that:

i. Hysteresis loops of the AFCs heated up to 300°C were stable and the AFC strength was almost constant. Increasing the heating temperature above 150°C reduced the hysteresis loop stability and the AFC strength was not constant. The hardness of Bisalloy 500 shims reduced from 3.0 to 1.1 times the hardness of the Grade 300 steel plates for AFCs heated at temperatures of 300°C - 750°C. Mechanical properties of bolts reduced significantly for AFCs heated at temperatures of 300°C - 750°C. No major changes were observed on the mechanical properties of the Grade 300 steel connection plates of AFCs heated at temperatures up to 750°C.

ii. Hysteresis loop of the AFCs tested with cleaned surfaces were stable. Coating the AFCs surfaces reduced slightly the hysteresis loop stability. The AFC strength increased slightly when surfaces were Sweep Blasted and reduced significantly when surfaces were coated with Alkyd or Zinc.

iii. Regardless of the surface treatment, hysteresis loop of corroded AFCs is similar to that of non-corroded AFCs, except in the initial sliding cycles where corroded AFCs developed increased forces. Increased forces respect to the average AFC strength in the non-corroded

condition of 100%, 120%, 130%, and 50% were developed for the corroded cleaned, sweep blasted, alkyd coated, and zinc coated surfaces, respectively. For severe corrosive environments, regardless of the surface treatment, AFCs developed significant general and crevice corrosion at the external surfaces and slight general and crevice corrosion at the internal clamped surfaces. The most effective surface treatment to delay corrosion was Zinc coated surfaces.

iv. The hysteresis loop of AFCs with bonded brake pads was characterized by increased strengths in the initial sliding cycles. The increased AFC strengths in the initial sliding cycles reduced as the cycles increased, and it became almost constant generating stable hysteresis loops. The hysteresis loop shape was independent on the brake pad configuration and the loop shape was similar to that recorded for AFCs with Bisalloy 500 shims. The most stable hysteresis loop with the least strength degradation was observed for brake pads bonded on recessed holes in the cap and fixed plates.

v. The hysteresis loop of AFCs was almost bilinear for all bolt lengths. Increasing the bolt length reduced AFC strength, hysteresis loop loading stiffness, and hysteresis loop stability. For bolts with significant length, bolt yielding due to bending was observed at bolt shank locations near the cap plate – shim and fixed plate – shim interfaces. Reductions in AFC strength with increasing bolt length were attributed to loss of bolt tension due to either surface degradation or moment – axial force – shear force interaction (MPV interaction). While the loss of bolt tension due to surface degradation did not depend on the bolt length, loss of bolt tension due to MPV interaction did.

vi. The bolt inclination during the sliding increased the bolt axial tension and therefore the AFC strength. This increase in bolt axial tension occurred in the initial sliding cycles until the bolt reached maximum inclination limited by the bolt hole oversize. The increase in bolt tension due to bolt inclination was more critical for bolts with short lengths, where axial yielding was produced. The increase in bolt tension due to bolt inclination increased with bolt hole oversize, bolt ultimate axial strength, friction coefficient at the sliding interfaces and reduced with bolt length.

vii. Models for quantifying the average AFC strength considering effects such as fire, surface treatment, corrosion, and non-metallic sliding surfaces such as brake pads were proposed. These models indicated the average AFC strength can be predicted with the Coulomb dry friction theory using the bolt proof load, number of bolts, number of sliding interfaces and friction coefficients experimentally determined. A model to quantify the reduction in average AFC strength due to moment – axial force – shear force interaction (MPV interaction) considering the bolt inclination during sliding was proposed. In this model the average AFC strength can be also predicted with the Coulomb dry friction, but using the calculated bolt tension during the sliding considering the moment – axial force and shear force bolt demands during the sliding. Models were compared with experimental data, and comparisons showed good agreement between experimental and predicted average AFC strengths. Variations in experimental AFC strengths were accounted in models using overstrength and understrength factors.

APPENDICES

Appendices Summary

Appendices comprise a total of eight conference papers published in different international conferences. Topics of these conference papers were developed along with the topics of the five chapters of this thesis, and they are related to the hysteretic behaviour of Asymmetric Friction Connections (AFCs) and Symmetric Friction Connections (SFCs). Publication details and references of these eight conferences are presented in the list of publications section and in the references section of this thesis. These eight conference papers were organized from Appendix A.1 to Appendix A.8, and their content is summarized below:

i. Appendix A.1 describes the hysteretic behaviour of AFCs using shims *with Brinell hardness (BH)* of 75 – 500. Variation in the hysteresis loop stability and friction coefficient with the shim hardness are discussed.

ii. Appendix A.2 describes the hysteretic behaviour of AFCs with Bisalloy 500 shims assembled with *bolt torques* varying between a torque close to the bolt finger tight condition and a torque close to the bolt failure torque. Variation in the hysteresis loop stability and friction coefficient with the bolt assembly torque are discussed.

iii. Appendix A.3 describes the hysteretic behaviour of AFCs using shims with Brinell hardness (BH) of 75 – 500 and tested with *constant velocities* of 10mm/s and 190mm/s. Boundaries of the friction coefficient at low and high velocities are discussed. A simple model proposed to represent the velocity dependence of AFC strength is discussed.

iv. Appendix A.4 describes the strength degradation of AFCs with Bisalloy 500 shims when cyclic loading displacement is increased. A simple methodology to assess the strength

degradation of AFCs under cyclic loading is proposed. The ability of *reinstating the strength of AFCs by replacing bolts* after cyclic loading is discussed.

v. Appendix A.5 describes the hysteretic behaviour of *SFCs using steel shims with Brinell hardness (BH)* of 150 – 500. Variation in the hysteresis loop stability and friction coefficient with the shim hardness are discussed.

vi. Appendix A.6 describes *possible applications of AFCs* on single, concentrically and eccentrically braced frames. Basic design considerations for braced frames equipped with AFCs, and possible alternatives for computer modelling of these type of frames are discussed.

vii. Appendix A.7 describes the hysteretic behaviour of *braces equipped with AFCs* using Bisalloy 500 shims and placed at one end of the brace (AFC braces). Strength degradation and friction coefficients for AFC braces are discussed. Out of plane AFC braces behaviour and its effects on the brace strength are discussed.

viii. Appendix A.8 describes a *methodology for quantifying the seismic sustainability of steel framed structures*. The most common steel framed structural systems are classified according to their seismic sustainability values in three categories: highly sustainable, semi-sustainable and less sustainable systems.

Future research work will be focussed on developing a hysteresis loop model of AFCs with high hardness shims such as Bisalloy 400 and Bisalloy 500, and also comparing the hysteretic behaviour of AFCs with that of SFCs for steel shims with Brinell hardness (BH) of 150 – 500. This future work will be based on experimental results from Appendices A.1 and A.5.

Appendix A.1

Behaviour of Asymmetrical Friction Connections (AFCs) Using Different Shim Materials

Appendix A.1

Behaviour of Asymmetrical Friction Connections (AFCs) Using Different Shim Materials

J. Chanchí Golondrino

University of Canterbury, New Zealand – National University of Colombia, Colombia

G.A. MacRae, J.G. Chase & G.W. Rodgers

University of Canterbury, New Zealand

C.G. Clifton

University of Auckland, New Zealand

2012 NZSEE Conference

ABSTRACT: Asymmetrical Friction Connections (AFC) have been successfully applied in New Zealand. Testing on small components, and beam column joint subassemblies have demonstrated stable, efficient hysteretic behaviour with almost no damage. This paper reports quasi-static testing of full scale AFC specimens using different shim materials: mild steel, aluminium, brass, bisalloy grades 80, 400 and 500. The assembling process and hysteretic behaviour of the connections are described. Effects of different shim materials on the hysteresis loop stability and on the magnitude of the friction force are also discussed. Results show stable hysteretic behaviour and minimum degradation effects using shim materials with high Brinell hardness values ranging from 300BH to 500BH.

1 INTRODUCTION

Asymmetrical Friction Connections (AFC) were developed by Clifton (2005)**.** Initial development used brass shims following the energy dissipation mechanism proposed by Grigorian and Popov (1994) for slotted bolted connections. Subsequent studies carried out by Mackinven (2006) extended the application of the SHJ concept to mild steel and aluminium shims. Recent studies carried out by Khoo et. al. (2011) introduced the use of bisalloy grades 80 and 400 shims. Although these studies have characterized the hysteresis behaviour using different shim materials, they only validated the concept on subassemblies where displacement demand was less than 50mm. This limitation requires the experimental validation of this concept for superior displacement demands. This paper aims to answer:

i) What is a reliable construction methodology to assemble Asymmetrical Friction Connections?

ii) What is the effect of different shim materials on hysteresis loop stability and friction force?

iii) What is the effect of increasing sliding length on hysteresis loop shape?

2 ASSYMETRICAL FRICTION CONNECTIONS (AFC)

Asymmetrical Friction Connections (AFC) can be described as an arrangement of five plates, three steel plates and two thinner plates termed shims assembled using high strength bolts. Figure 1 show the basic components and assembly of an AFC specimen. Eight AFC specimens divided in two groups were tested, the first group comprised specimens with 80mm slot length using steel and brass shims, and the second group comprised six AFC specimens with 220mm slot length using aluminium, brass, steel and bisalloy grade 80, 400 and 500 shims. Both groups of specimens were assembled using Grade 300 steel plates with 16mm thickness and M16 Grade 8.8 galvanized bolts with 90 mm length. Shim material properties are presented in Table 1.

a. *Right to left: Fixed plate, shim, moving plate, shim, cap plate*

b. *Assembled AFC connection*

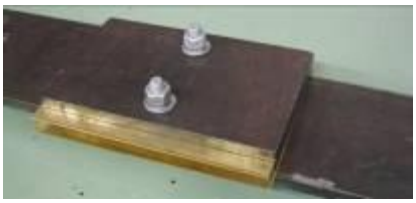

c. *Detail of an AFC joint*

Figure 1. *Components and assembling of Asymmetrical Friction Connections (AFC)*

Table 1. *Summary of materials used for shim plates*

Material	Specification	Brinell Hardness (BH)	Thickness (mm)
Aluminium	5005GP Series Aluminium	75	3.0
Brass	UNS C26000 – ½ Hard Temper	82	3.0
Steel	Cold Rolled Mild Steel	130	3.0
Bisalloy 80	Bisplate 80	255	3.0
Bisalloy 400	Bisplate 400	400	6.0
Bisalloy 500	Bisplate 500	500	6.0

3 EXPERIMENTAL METHODS

Testing was carried out on a DARTEC universal machine using a vertical setup as show in Figure 2. The AFC specimens were connected to two slip critical connections respectively attached to the frame cross head and to the hydraulic ram. These slip critical connections were placed eccentrically in order to allow the asymmetry of the AFC specimens. The setup was instrumented with a load cell connected in series with the moving slip critical connection and the hydraulic ram, and with a potentiometer placed across the stroke of AFC specimen. This vertical setup was later on adapted to a horizontal setup fitted on a shake table due to the reduced availability of the DARTEC universal machine. On the horizontal setup, the slip critical connections at the ends of the AFC specimen were attached to one reaction frame bolted on a shake table and to another reaction frame bolted on a strong floor.

a. *Frontal view*

b. *Lateral view*

c. *AFC on full stroke*

Figure 2. *Setup and testing of AFC connections*

The maximum test sliding length was defined as ± 95 mm. AFC specimens were subjected to 20 sinusoidal cycles divided into six displacement regimes with variable amplitude as shown in Figure 3. Amplitudes were chosen based on increasing the sliding length from 6.25% to 100% of the specimen slot length. The maximum velocity of the sinusoidal cycles was 10mm/s. For this velocity and the different amplitudes, frequencies ranged between 0.017 - 0.27 Hz for specimens with 220mm slot and 0.064 - 1.0 Hz for specimens with 80mm slot.

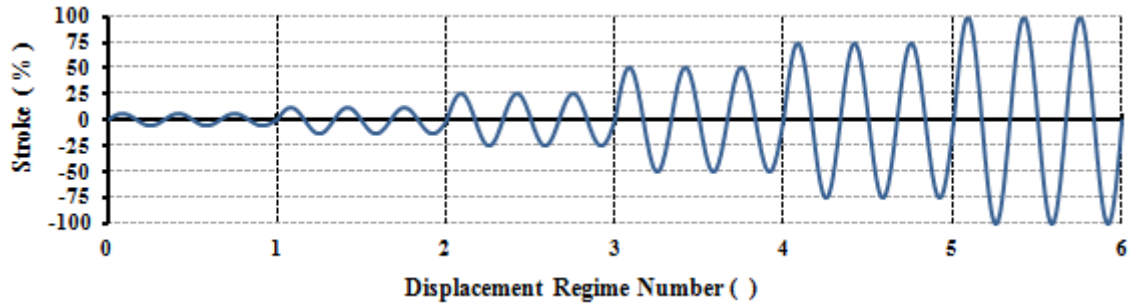

Figure 3. *Imposed displacement regime*

According the New Zealand Steel Construction Standard (NZS 3404, 2009) friction type connections shall be assembled guaranteeing that the minimum tension force per bolt is the proof load. In addition, only the part turn method and the direct tension indication device method are permitted for bolt tensioning purposes. Although, these methods are generally accepted as typical construction practices in New Zealand, they cannot be directly applied to AFC assembly because i) these methods were not developed considering the friction component produced by Belleville washers, and ii) they cannot predict accurately the tension force level on the bolts. Thus, these methods can lead to high variability on the minimum bolt tension force that consequently affects the predicted sliding force. This issue can be seen in the Equation 1 (MacRae et.al. (2010)**)** where, *Fs* is the sliding force, *n* is the number of bolts, μ is the friction coefficient, η is the number of shear planes, and *Ntf* is the proof load per bolt.

$$Fs = n \times \mu \times \eta \times Ntf \tag{1}$$

Alternatively, the torque control method can be used for assembling Asymmetrical Friction Connections. This method is based on tighten the bolts to certain amount of torque defined from an experimentally developed torque – bolt tension relationships. This method is not generally accepted for structural applications according the New Zealand Steel Construction Standard (NZS 3404, 2009*)*. However, it was considered in this research as a first approach to minimize the limitations, and provide a constant bolt tension.

4 RESULTS AND ANALYSIS

4.1 Torque control method for Asymmetrical Friction Connections.

Aiming to assemble Asymmetrical Friction Connections (AFC) using an objective and controllable construction methodology that considers the proof load requirements and the effect of Belleville washers the torque control method was experimentally implemented. Figure 4 shows the data recorded from the axial testing of three bolts and the induced bolt elongation, nut rotation and toque data recorded from assembling five AFC specimens. Results show that the proof load can be reached when the bolt shank elongation is about 0.175mm (Figure 4a). To induce similar bolt shank elongation a torque of 320 - 460N-m should be applied as shown in Figure 4b. According these results a torque value of 390kN-m was recommended for assembling AFC specimens. If the part turn method is used, a nut rotation of 80-115 degrees should be expected (Figure 4c). Thus, an average nut rotation value of

97.5 degrees or close to 1/4 nut rotation was recommended to carry out post assembling controls of AFC specimens. This value disagrees with the 1/2 nut rotation value recommended by the New Zealand Steel Construction Standard (NZS 3404, 2009*)* where a bolt failure due to excessive induced tension is expected (Figure 4c).

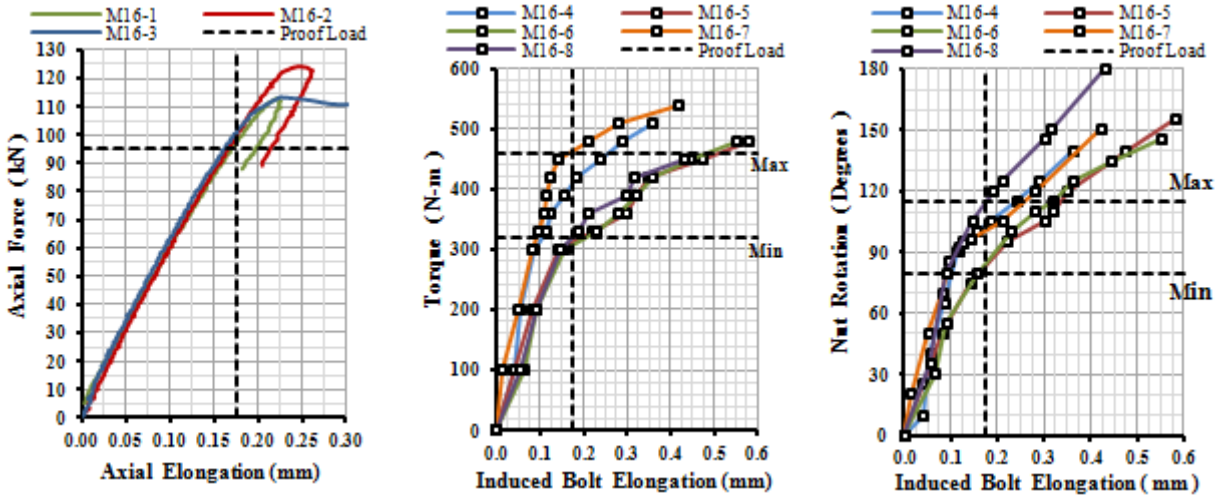

a. *Axial tension bolt testing* ***b.*** *Torque – Induced elongation* ***c.*** *Nut rotation – Induced elongation*

Figure 4. *Torque-control method relationships for AFC specimens using Belleville washers*

4.2 **Sliding length effect on the hysteresis loop shape of AFC specimens**

Previous research works (Clifton (2005), Mackinven (2006), MacRae et.al. (2010), and Khoo et.al. (2011)) reported bilinear hysteresis loop shapes. In contrast, this research shows that the hysteresis loop shape of AFC specimens depends on the sliding length as shown in Figure 5. A bilinear shape was found for sliding lengths less than 50mm and was more accentuated when decreasing the sliding length. However, for sliding lengths of 50-220mm the hysteresis loop shape changes gradually from bilinear to almost square. This change can be attributed to the sliding length required by the connection to move from the first sliding state to the fully activation of the two sliding interfaces (segment *a-b* in Figure 5a). This sliding distance is termed activation length and was found to range from 4mm to 6mm. In the case of connections tested over small sliding lengths the activation length can be considered representative when compared with the hysteresis loop amplitude, thus generating bilinear loop shapes. As the sliding length increases the participation of the activation length over the hysteresis loop amplitude reduces gradually, so that the hysteresis loop can be considered as almost square for sliding lengths bigger than 96mm.

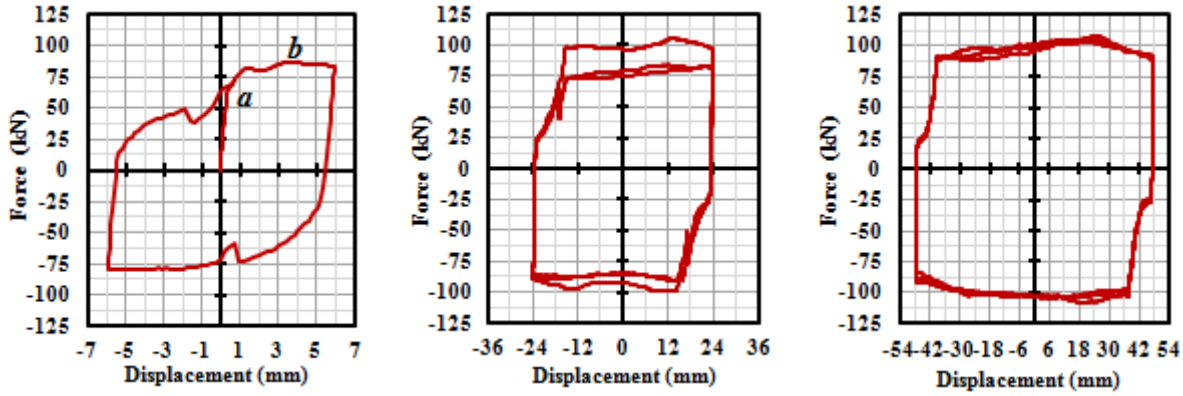

a. *12mm (±6mm) stroke* ***b.*** *48mm (±24mm)stroke* ***c.*** *96mm (±48mm)stroke*

Figure 5. *Hysteresis loop of AFC specimen when testing on different sliding lengths*

4.3 **Shim material effects on the hysteresis loop stability of AFC specimens**

The hysteresis loop stability of AFC specimens can be described considering three groups of shim materials defined according to the Brinell hardness value (BH). The first group correspond to shim materials with low hardness values ranging from 70BH to 100BH, in this group 5005 GP series aluminium and UNS C2600 brass – ½ Hard Temper were tested. Hysteresis loops in this category can be described as moderately stable with slight differences on the dynamic friction force levels when comparing the behaviour of the specimen on small and long sliding lengths as it can be seen in Figures 7a and 7b. The moderate hysteresis loop stability in this group can be attributed to the small amount of wear particles produced during the sliding mechanism. These particles generate minor surface degradation given that they adhere to the sliding surfaces; thus exhibiting an adhesive wear mechanism as defined by Grigorian and Popov (1994). The second group comprises shim materials with medium hardness values ranging from 100BH to 300BH; shim materials such as Grade 300 steel and bisalloy Grade 80 were tested. Hysteresis loops in this category can be considered as unstable; their instability was found to increase with the sliding length. This characteristic is more accentuated for steel shims rather than for bisalloy 80 shims as it can be seen Figures 7c and 7d. The instability of the hysteresis loop in this group can be attributed to the large amount of work hardened wear particles produced during the sliding mechanism. These particles abrade the sliding surfaces in an irregular pattern thus exhibiting a wear abrasive mechanism as defined by Grigorian and Popov (1994) and Khoo et.al. (2011). And the last group correspond to shim materials with high hardness levels ranging from 300BH to 500 BH, shim materials such as bisalloy400 and bisalloy500 shims were tested. Hysteresis loops in this category can be considered as stable, only minor differences on the dynamic force levels were found when comparing the behaviour of specimens on small and long sliding lengths as shown in Figures 7e and 7f. The reason for the stable behaviour in this category is associated to the minimum volume of wear particles produced during the sliding mechanism. These particles either are transferred back to the sliding surfaces or fall out as loose debris producing minimal surface degradation thus exhibiting a slight adhesive wear as defined by Grigorian and Popov (1994).

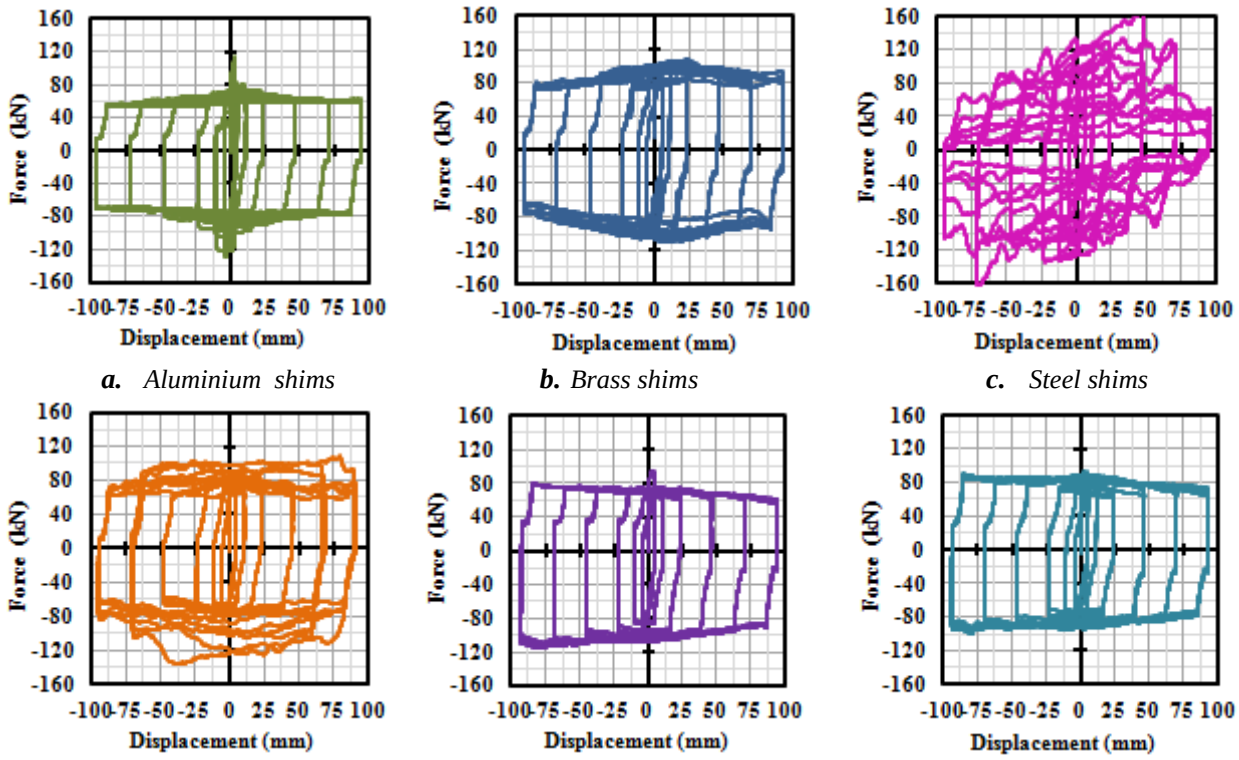

a. *Aluminium shims* ***b.*** *Brass shims* ***c.*** *Steel shims*

d. *Bisalloy 80* ***e.*** *Bisalloy 400* ***f.*** *Bisalloy 500*

Figure 7. *Hysteresis loop shape for different shim materials*

4.3.1 *Shim material effects on the static and dynamic friction force levels*

The static friction force is considered as the maximum force that can be applied on the connection before any sliding occurs. The effect of different shim materials on this value is presented in Figure 8. Results show that higher static friction force levels were exhibited by specimens using aluminium, brass, bisalloy 400 and bisalloy 500 shims, which are respectively characterized with low and high Brinell hardness values and lower levels were exhibited by specimens using steel and bisalloy 80 shims.

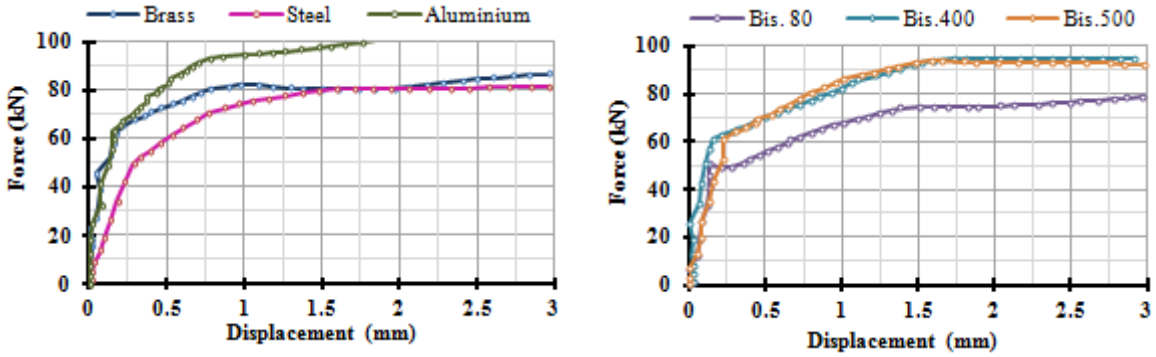

a. *Brass, Steel and Aluminium shim materials* ***b.*** *Bisalloy series shim materials*

Figure 8. *Force-Displacement curve from rest condition to first sliding for different shim materials*

The dynamic friction force can be interpreted as the maximum force level developed by the connection when sliding. The magnitude of this force was calculated as the average value across the hysteresis loop plateau, values for different shim materials are presented in Table 3. Results show that higher dynamic friction force were found for steel and bisalloy 80 shims as a consequence of the dramatic friction force increments associated to wear abrasive mechanisms, and lower levels were found for shim materials characterized by adhesive wear mechanisms, such as aluminium, brass, bisalloy 400 and bisalloy 500.

Table 3. *Friction forces and friction coefficients for different shim materials*

	Static Condition		Dynamic Condition	
Material	**Friction Force (kN)**	**Friction Coefficient ( )**	**Friction Force (kN)**	**Friction Coefficient ( )**
Aluminium	69.5	0.34	70.0	0.18
Brass	65.0	0.37	93.8	0.25
Steel	49.3	0.48	112.5	0.30
Bisalloy 80	50.6	0.47	90.0	0.24
Bisalloy 400	60.9	0.390	88.8	0.23
Bisalloy 500	61.3	0.387	81.3	0.21

The static and friction coefficients per bolt were calculated using Equation 2 considering a proof load of 95kN and two shear planes. Values of the dynamic friction coefficients presented in Table 3 for brass, Grade 300 steel, bisalloy 80, and bisalloy 400 shims agree well with those reported by Clifton (2005) and Khoo et.al (2011). However, the value for aluminium was found to be less than the value reported by MacKinven (2006). Figure 9 presents the variation of the static and dynamic friction coefficients respect to the shim material hardness. It can be seen that the maximum friction coefficients were found for shim materials with medium hardness values ranging from 100BH to 300BH, in this case unstable hysteresis loops were recorded. In contrast, lower friction coefficient values and stable hysteresis loops were found for shim materials with either low hardness values ranging from 70BH to 100BH or high hardness values ranging from 300BH to 500BH.

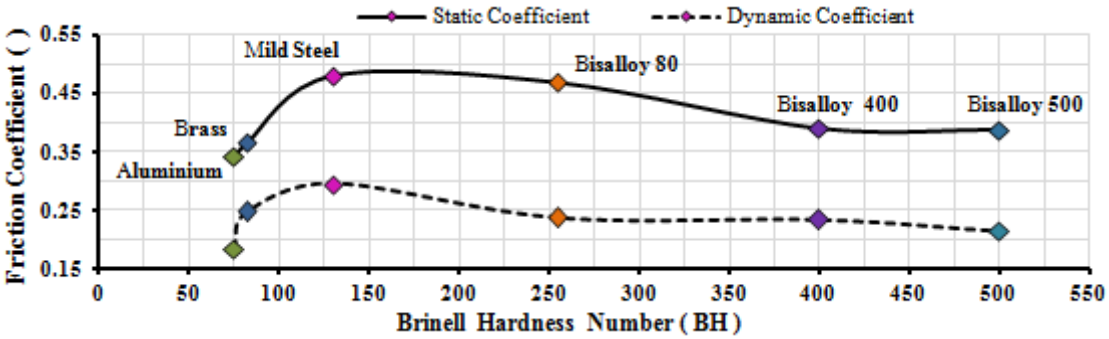

Figure 9. *Variation of the friction coefficient according the shim material Brinell hardness value*

5 CONCLUSIONS

This paper describes the hysteretic behaviour of Asymmetrical Friction Connections using different shim materials. It was shown that:

1. The torque control method can be considered as an objective and controllable methodology for assembling AFC specimens. Torque and nut rotation values for assembling AFC specimens using Belleville washers were suggested.

2. The hysteresis loop shape of Asymmetrical Friction Connections was found to be dependent on the sliding length of the connection. Ranges of sliding lengths where bilinear and almost square hysteresis loop shapes are expected were reported.

3. The stability of the hysteresis loop and the magnitude of the friction forces developed by AFC specimens were found to be directly related to the shim material hardness. Ranges of shim material hardness where stable hysteretic behaviours can be expected were reported.

6 REFERENCES

Clifton, G.C. (2005). Semi-Rigid Joints for Moments Resisting Steel Framed Seismic Resisting Systems. *Published PhD Thesis, Department of Civil and Environmental Engineering.* University of Auckland – New Zealand.

Grigorian, C.E. & Popov, E.P. (1994).Energy Dissipation with Slotted Bolted Connections. *Report UCB/EERC-94/02, Engineering Research Center College of Engineering.* Universityof California at Berkeley – USA.

Khoo, H.H., Clifton, C., Butterworth, J., MacRae, G. and Ferguson, G. (2011) Influence of steel shim hardness on the Sliding Hinge Joint. *Journal of Constructional Steel Research.*

Mackinven, H. (2006). Sliding Hinge Joint for Steel Moment Frames Experimental Testing. *Unpublished ENCI493 Project Report*. *Department of Civil Engineering.* University of Canterbury – New Zealand.

MacRae, G.A., Clifton, C.G., MacKinven, H., Mago, N., Butterworth, J., Pampanin, S. (2010). The Sliding Hinge Joint Moment Connection. *Bulletin of the New Zealand Society for Earthquake Engineering.*

Standards New Zealand. (2009). NZS 3404: Part 1: 2009 – Steel Structures Standard. Wellington – New Zealand.

Appendix A.2

Clamping Force Effects on the Behaviour of Asymmetrical Friction Connections (AFCs)

Appendix A.2

Clamping Force Effects on the Behaviour of Asymmetrical Friction Connections (AFCs)

J. Chanchí Golondrino
University of Canterbury, New Zealand – National University of Colombia, Colombia

G.A. MacRae, J.G. Chase & G.W. Rodgers
University of Canterbury, New Zealand

C.G. Clifton
University of Auckland, New Zealand

SUMMARY
Asymmetrical Friction Connections (AFC) have been recently developed and applied in New Zealand as a low damage damping solution. Research has shown that this connection can be considered as an efficient and economical alternative for dissipating energy on different steel framing systems. This paper reports on the quasi-static testing of Asymmetrical Friction Connections using Bisalloy 500 shims, and assembled with torque levels ranging from 20 to 500 N-m. Effects of increasing assembly torque on the stability of the hysteresis loop and on the sliding force developed by the connection are presented. A simple model to predict the applied bolt tension and the efficiency of the nut rotation method are also discussed. Results show that by developing the proof load on the bolts, stable hysteresis behaviours and approximately 85% of the maximum sliding force of the connection can be achieved, and also that variability in the applied bolt tension should be considered as a part of the design procedure of the connection.

Keywords: Asymmetrical Friction Connections, Clamping Force, Energy Dissipation, Torque Control Method

1. INTRODUCTION

The Asymmetrical Friction Connection (AFC) concept was developed by **Clifton (2005)**. The initial development was based on testing small connection components using brass shims, and beam column subassemblies using this concept as a damping alternative. Research by **Mackinven (2006)**, **Khoo et al. (2011),** and **Chanchí et al. (2012)** have extended the application of this concept to different shim materials, such as aluminium, mild steel and different Bisalloy grades. Results showed that stable and reduced degradation on the hysteretic behaviour of AFC specimens can be achieved by using high hardness shims such as Bisalloy 400 or Bisalloy 500. Although, experiments have been carried out to describe the hysteretic behaviour of the connection, there is a need for developing design and construction guidelines to regulate the application of this technology and ensure predictable performance. For that reason this paper aims to answer:

1. What is the effect of increasing the assembly torque value on the hysteretic behaviour of AFC specimens?
2. What is the assembly torque value required to guarantee stable hysteretic behaviors of AFC specimens?
3. Is the nut rotation method an effective alternative for assembling AFC connections using Belleville washers?
4. Is the sliding capacity of AFC connections influenced by the magnitude of assembly torque?

5. What is the magnitude of the friction coefficient of AFC specimens using Bisalloy 500 shims as a function of assembly torque?

2. ASYMMETRICAL FRICTION CONNECTIONS (AFC)

Asymmetrical Friction Connections can be defined as an arrangement of three steel plates and two thinner plates termed shims, assembled with high strength bolts and Belleville washers. Asymmetrical Friction Connections can be used to dissipate energy on beam-column joints or in braces of different steel framed systems. They are desirable because they can dissipate large amounts of energy with almost no damage in the connection itself or in the structural system (**MacRae and Clifton, 2010**). The Hysteresis loop of the connection can be considered as bilinear for sliding lengths less than 50mm and almost square for sliding lengths near to 220mm (**Chanchí et al. 2012**). This change is due to the sliding length required by the connection to move from the first sliding stage to the fully activation of the two sliding interfaces (*segment a-b Figure1-c*). **Figure 1** presents components, assembly and a hysteresis loop of an AFC specimen using Bisalloy 500 shims.

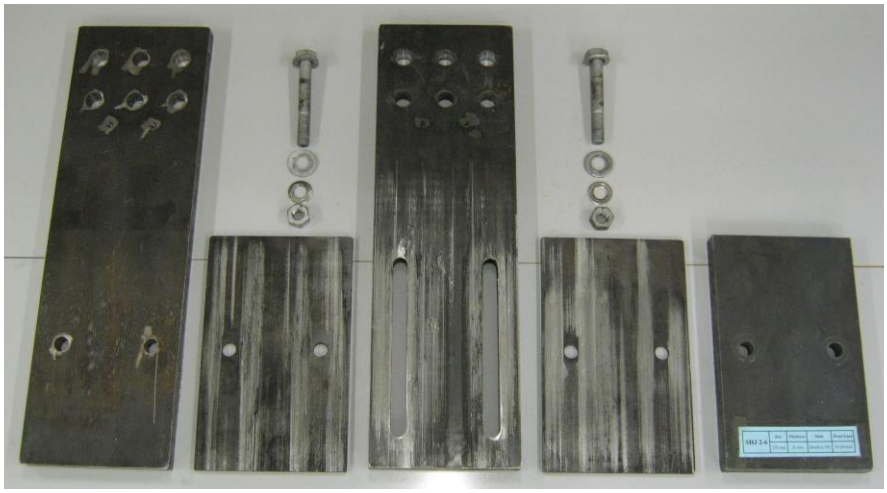

a. Left to right : bottom plate, shim, slotted plate, shim, cap plate

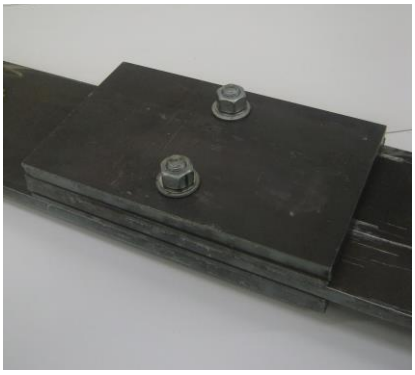

b. AFC assembly

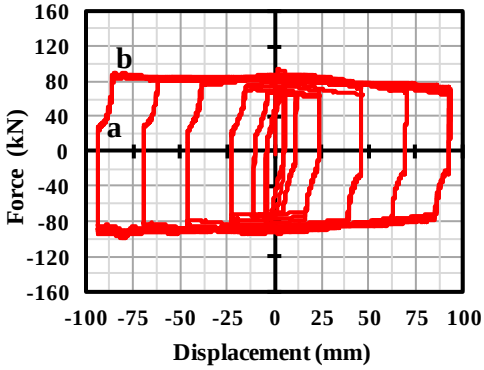

c. Hysteresis loop

Figure 1. AFC using Bisalloy 500 and 2 M16 Grade 8.8 galvanized bolts

3. EXPERIMENTAL METHODS

Twenty one AFC specimens with 220mm slot, Grade 300 steel plates 20mm thickness, Bisalloy 500 shims 6mm thickness, single Belleville washers 1.45mm thickness, and two M16 Grade 8.8 galvanized bolts 110 mm length were tested. Connections were assembled by tensioning bolts to different levels using a calibrated torque wrench (torque control method). Although, the torque control method is not generally accepted for structural applications in the New Zealand Steel Construction

Standard (***NZS 3404, 2009 – clause C.4.2.6.1),*** it was considered in this research as an alternative to systematically control the specimens assembly process. Torque values of 20, 50, 150, 250, 350, 410 and 500 N-m from the finger tighten condition were applied without any lubrication on bolts. At each torque level three connections were considered. Additional requirements related to number of free threads during bolt tensioning were satisfied as described in clause 4.2.4.1.2 (***NZS 3404, 2009)***; for instance, connections were characterized by grip lengths of 72 mm and 7 threads within the grip length when using 110 mm bolt lengths. Testing was carried out on a shaking table using a horizontal setup instrumented with a load cell and a potentiometer across the connection stroke. The sliding mechanism was initiated by applying a displacement regime on the slotted plate connected to the shaking table. The displacement regime comprised 20 sinusoidal cycles with a maximum velocity of 15mm/s and amplitudes varying from 3.13 to 100% of the connection slot. **Figure 2** presents the testing setup and the input displacement regime.

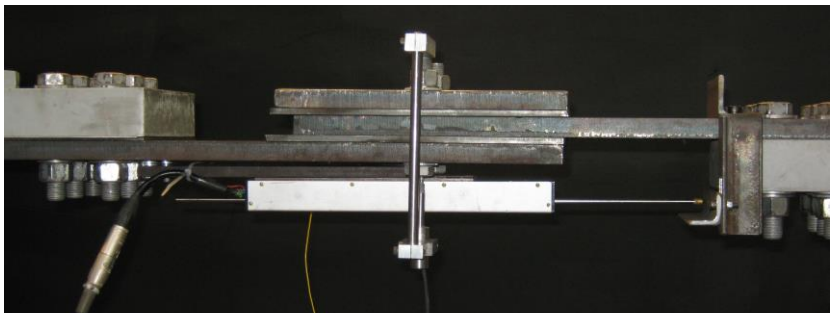

a. Testing setup

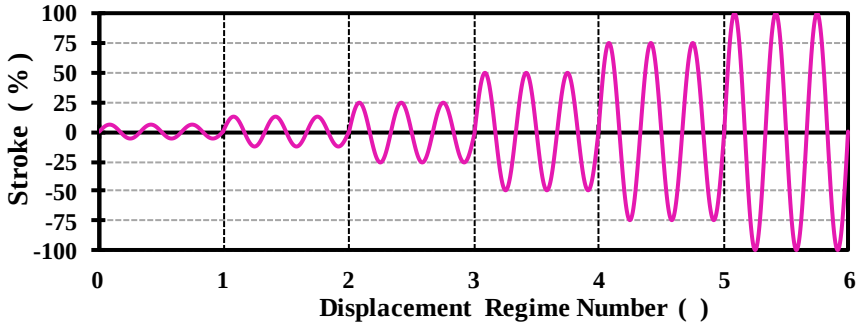

b. Imposed displacement regime

Figure 2. Testing setup of Asymmetrical Friction Connections and input displacement regime

4. RESULTS AND ANALYSIS

4.1. Hysteresis loop shape

Stability and shape of the hysteresis loop of AFC specimens was found to change at different torque levels. Unstable and constricted hysteresis loop shapes were recorded across the total sliding length for torque levels below 50 N-m (**Figure 3a**). At torque values of 50-150 N-m more stable and almost rectangular shapes were found for sliding lengths up to 50mm. However, unstable and partially constricted shapes were kept for sliding lengths between 50 and 220 mm (**Figure 3b**). Stable and almost rectangular shapes across the total sliding length were recorded for torques greater than 350 N-m. AFC specimens exhibited constricted and partially constricted shapes because the bottom plate rotates due to the connection asymmetry. As the bottom plate rotates, the cap plate and the top shim rotate certain amount depending on the bolt tension. This rotation moves apart one end of the top shim from the slotted plate, while the other end gets closer so that the slotted plate surface is not in full contact with shim surfaces. This effect is more accentuated at low torque values, where the bolt tension is not enough to minimize the cap plate and top shim rotation. This effect also causes

differences on the magnitude of the sliding force developed by the connection on the loading and reversal loading conditions. Results show the benefit in terms of stability and hysteresis loop shape when assembling AFC specimens with torque values near to 350 N-m. **Figure 3** shows hysteresis loop shapes for different assembly torque values.

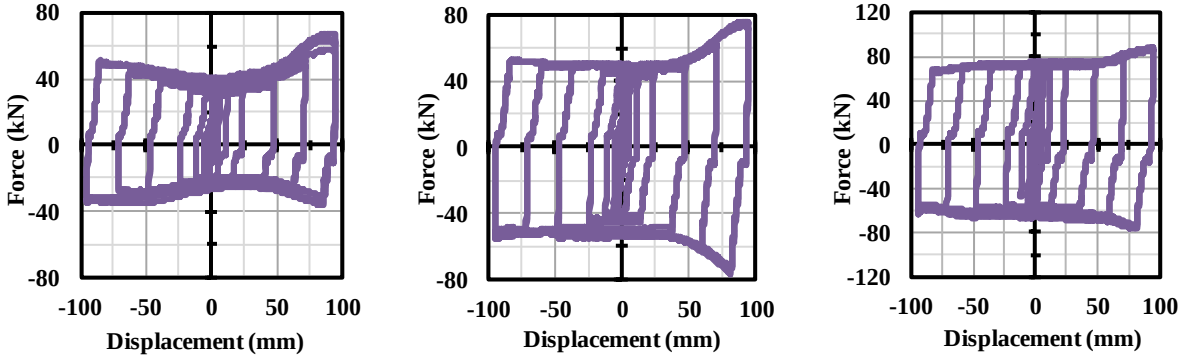

a. Torque 50 N-m **b.** Torque 150 N-m **c.** Torque 250 N-m

Figure 3. Hysteresis loop shapes of AFC connections assembled with different torques values

4.2. Induced bolt elongation during assembling process

Average bolt elongations measured from the finger tighten condition when assembling twenty one AFC specimens using seven torque levels (i.e. three AFC specimens at each torque level) are presented in **Figure 4b.** Although considerable variability in the elongation magnitude was presented as a result of the slight different surface conditions on the threads, three elongations tendencies can be noticed. An initial increasing bolt elongation proportional to the torque value up to 350 N-m, dramatic bolt elongation increments in the range 350 - 410 N-m, and lower bolt elongations than those recorded in the initial range for torque values of 410-500 N-m. These three ranges respectively match with the elastic, yielding, and plastic zones exhibited by bolts when subjected to an axial tension testing (**Figure 4a**),where the bolt grip length was considered as testing length, and the bolt was assembled from the finger tighten condition using a single Belleville washer. Matching elongation values of **Figure 4b and 4a**, it can be predicted that bolts reach the proof load value (95 kN) with a torque value near to 300 N-m, and yield with a torque near to 360 N-m.

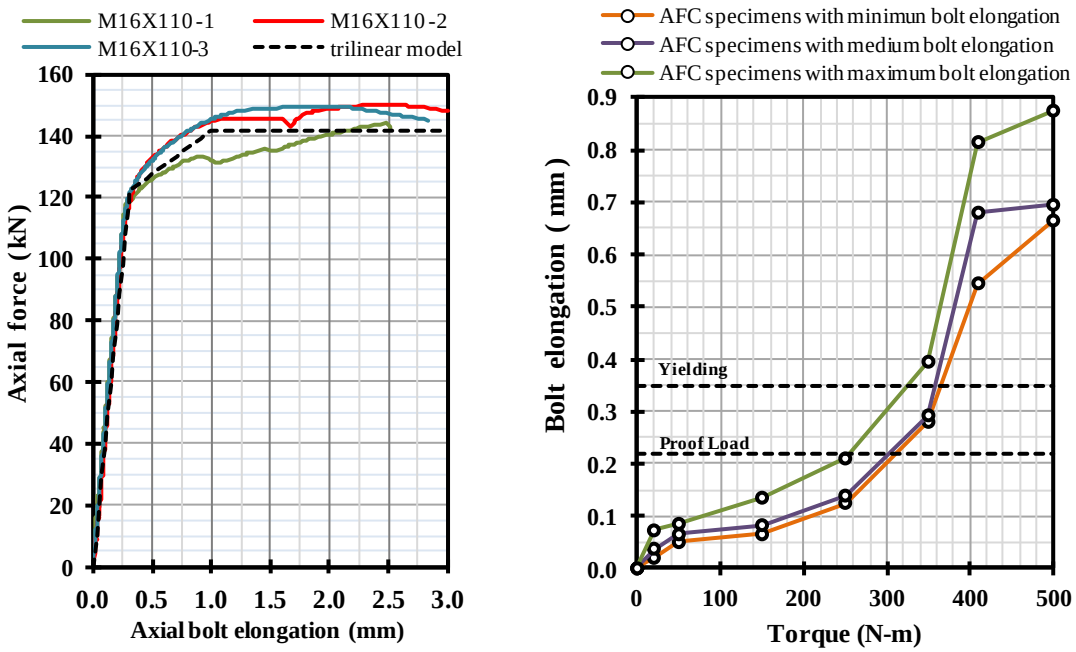

a. Bolt axial testing results **b.** Bolt elongation for different torque levels

Figure 4. Bolt elongation for axial testing and different assembling torques

4.3. Induced bolt elongation during assembling process

Aiming to predict the applied tension on bolts during the assembly process, a similar approach to the one suggested by the Steel Structures New Zealand Standard (**NZS 3404, 2009**) was considered. In this approach the applied bolt tension (T) is predicted considering that the shank and treaded portions of the bolt included in the connection behave as two springs in series (**Figure 5a**), and that the sandwiched plates are rigid and stiff compared to the bolt. This model is represented by **Equation 1,** where δ is the bolt elongation, E is the elasticity modulus calculated using **Equation 2** and the trilinear axial force – bolt elongation model presented in **Figure 4a,** L_1 is the shank length, A_1 is the shank area, L_2 is the threaded length and A_2 is the bolt tension area. Using bolt elongations presented in **Figure 4b,** standard geometrical properties of bolt assembly (nut, washer and Belleville washer), and applying **Equation 1** bolt tension forces for three AFC specimens at each torque level were calculated (**Figure 5b**).

$$T = \frac{\delta \times E}{\frac{L_1}{A_1} + \frac{L_2}{A_2}} \tag{1}$$

$$E = \left[\frac{\Delta T}{\Delta \delta}\right] \times \left[\frac{L_1}{A_1} + \frac{L_2}{A_2}\right] \tag{2}$$

Results presented in **Figure 5b** show a considerable variability on the applied bolt tension when using the torque control method. This variability may be attributed to bolt fabrication issues, and to the low consistency on the bolt torsional behaviour. In addition, it can be noticed that bolts reach the proof load value (95kN) with torque values ranging from 275 to 325 N-m. From these results, an average torque value of 300 N-m from the finger tighten condition is appropriate for these AFC connections using M16 Grade 8.8 galvanized bolts with 110 mm length and Belleville washers. Also, based on these results, to ensure that the proof load is always obtained, a torque of 325 N-m is required.

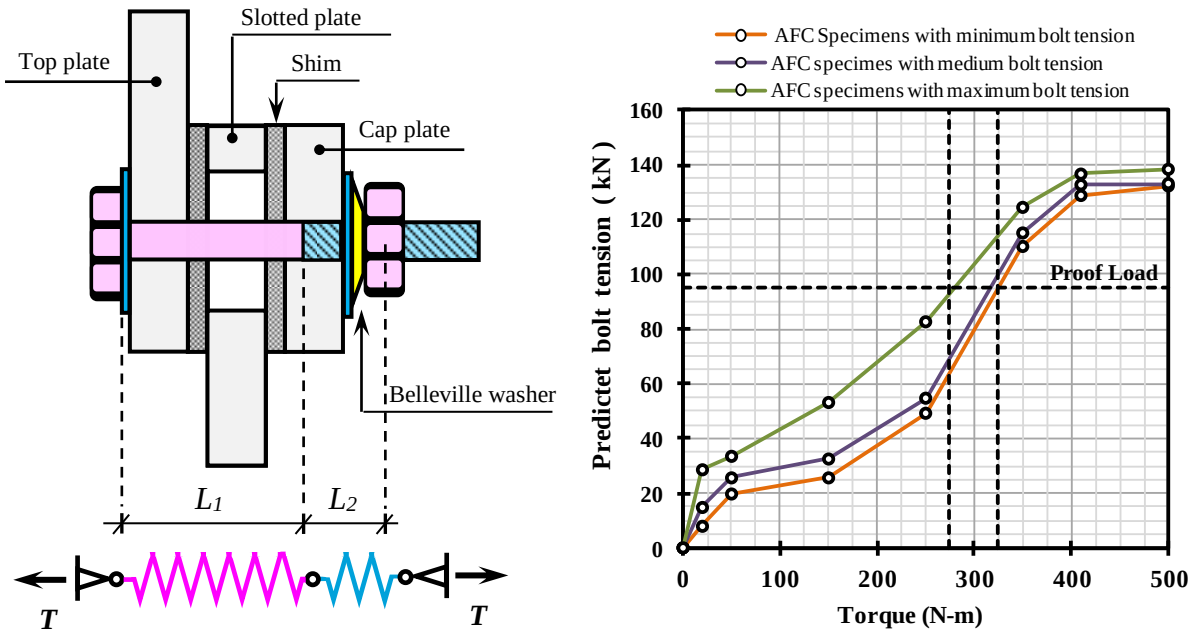

a. Bolt elongation model

b. Predicted bolt tension values

Figure 5. Bolt elongation model and predicted bolt tension forces

4.4. Torque – Nut rotation relationship

Nut rotations calculated as the average of six nut rotations values recorded from the finger and snug tighten condition at each torque level are presented in **Figure 6.**

Average nut rotations calculated as the average of six nut rotations values recorded from the finger and snug tighten condition at each torque level are presented in **Figure 6.**

Average nut rotations measured from the finger tighten condition when assembling twenty one AFC specimens using seven torque levels (i.e. average calculated from six nut rotations corresponding to three AFC specimens at each torque level) are presented in **Figure 6a.**

Results show that the snug tighten (50 N-m) and the bolt yielding condition (350 – 410 N-m) can be respectively reached by applying nut rotations of 1 ¼ and (1 ½ - 1 ¾) turns from the finger tighten condition . In addition, it can be seen in **Figure 6b** that a nut rotation of (1/4 - 1/3) turn is required to reach the proof load condition (300 N-m) from the snug tighten condition. This range is less than the 1/2 turn value suggested for the New Zealand Steel Construction Standard (**NZS 3404, 2009),** this is because the half turn method involves going past the torque required to develop the proof load. Even though, this method guarantees the proof load, the bolt is tensioned near to the ultimate strength, which is not beneficial if the connection is used for seismic purposes. In contrast, application of the torque control method can result in lower bolt tension levels. However, considerable variations on the applied bolt tension can be expected as a result of the variable relationship between torque and bolt elongation for galvanized bolts (**NZS 3404, 2009).** For that reasons further research should be addressed to implement a method to assemble AFC specimens that guarantees consistent and repeatable bolt tension forces.

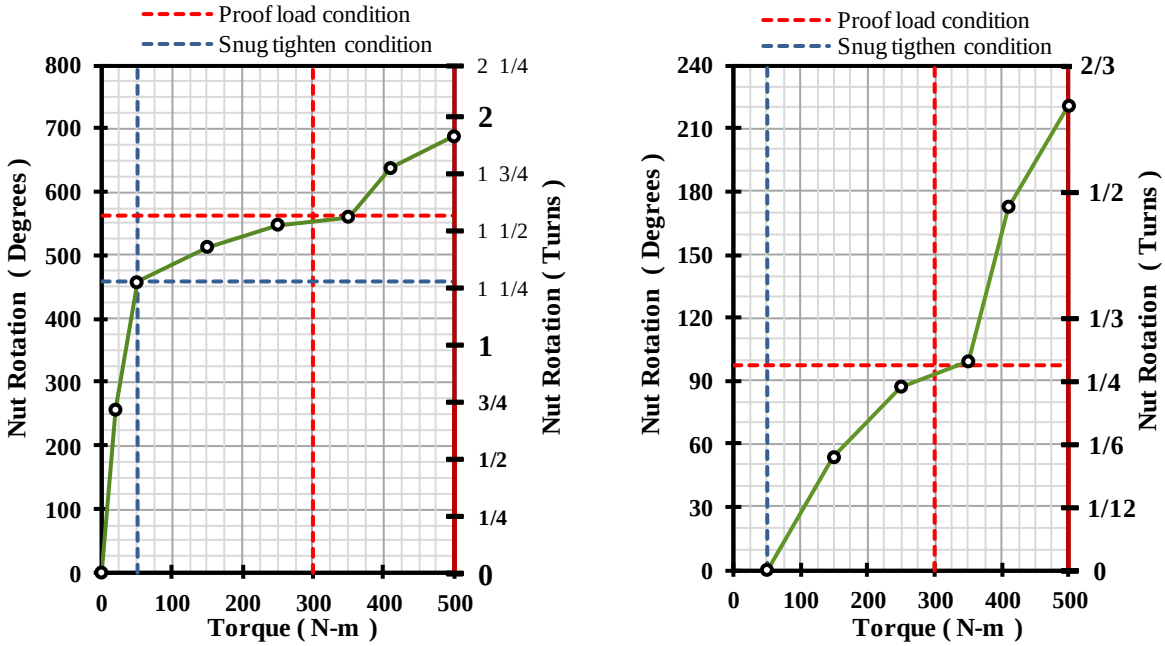

a. From finger tighten condition **b.** From snug tighten condition

Figure 6. Nut rotation values recorded for different torque levels

4.5. Sliding Force

The sliding force is defined as the maximum force developed by the connection when the sliding mechanism is fully initiated. This force level corresponds to the plateau of the hysteresis loop. Average sliding forces calculated from three AFC specimens at each torque level are shown in **Figure 7.** A non linear relationship between sliding force and torque can be noticed, where the sliding force ranges from 10 to 87 kN for assembly torques of 20-500 N-m. This relationship is characterized by dramatic increments on the sliding force for torque values below the torque required to develop the proof load on bolts (proof load torque), and for increment of less than 12.5% of the maximum sliding force for torque values above the proof load torque. In addition, it can be noticed that AFC specimens can develop 50% of the maximum sliding force when they are assembled with torque values corresponding to the snug tighten condition (50 N-m), and that approximately 90% of the maximum sliding force can be developed when assembled with the proof load torque. From these results, a minimum assembling torque of 300 N-m is recommended for AFC specimens using M16-Grade 8.8 galvanized bolts with 110 mm length.

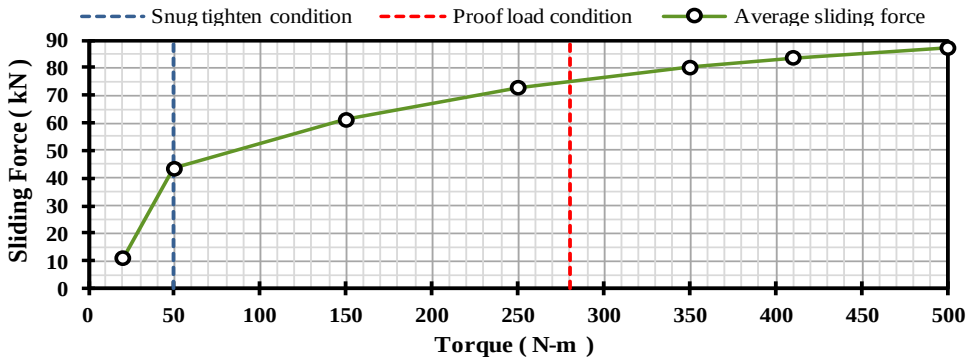

Figure 7. Sliding force values for different torque levels

4.6. Friction Coefficient

Using the predicted bolt tension forces applied during the assembling process, considering minor tension losses during the testing, the friction coefficient (μ) for each AFC specimen was calculated from **Equation 3.** In this equation F_s is the sliding force, n is the number of o bolts, η is the number of shear planes, and T is the tension force per bolt based on the measured bolt elongation at specified torque.

$$\mu = \frac{F_S}{n \times \eta \times T} \tag{3}$$

Average friction coefficients calculated from three AFC specimens at each torque level are presented in **Figure 8**. It can be seen that AFC specimens develop variable friction coefficients when assembled with torques below the proof load torque (300 N-m). This variability was not noticed for connections assembled with torques in the range 350 – 500 N-m, where the friction coefficient value is 0.17. Reasons for this variability at lower torques can be attributed to unstable hysteresis loops, and to the variable behaviour of bolts when subjected to torsion. Considering these results, it can be suggested that a predictable and reliable behaviour of AFC connections can be achieved by using assembly torques in the range 350 – 500 N-m.

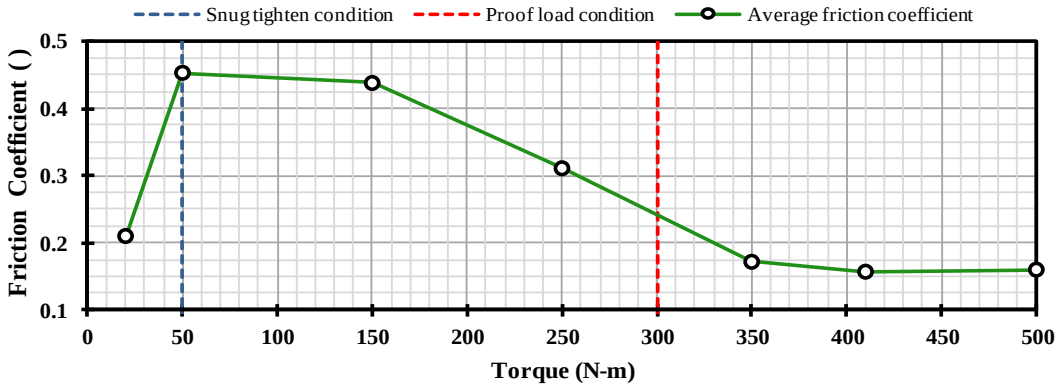

Figure 8. Friction coefficient values for different torque levels

5. CONCLUSIONS

This paper describes the effect of clamping force on the behaviour of Asymmetrical Friction Connections. It was shown that:

1. Stability and shape of the hysteresis loop of AFC specimens across the sliding length was found to be dependant of the assembling torque level. A range of torque values where stable hysteresis loops can be expected was reported.
2. A considerable variability on the applied bolt tension was predicted for AFC specimens assembled with Grade 8.8 galvanized bolts, the effect of this variability should be considered in the design procedure of the connection.
3. The half nut rotation method overestimates the torque value required to develop the proof load on bolts, by using this method applied bolt tensions close to the failure load of the bolt are expected. A range of torque values where applied bolt tensions are close to the proof load was suggested.
4. A noticeable effect of the assembling torque level on the sliding force developed by AFC specimens was found for torque values below the proof load torque. Only minor increments on the sliding force level can be expected for torque values above the proof load condition.
5. Variability of the friction coefficient developed by AFC specimens is influenced by the level of applied bolt tension. Ranges of assembling torques where a considerable variability and constant values of friction coefficients were reported.

REFERENCES

Clifton, G.C. (2005). Semi-Rigid Joints for Moments Resisting Steel Framed Seismic Resisting Systems. *Published PhD Thesis, Department of Civil and Environmental Engineering.* University of Auckland – New Zealand.

Chanchí, J.C., MacRae, G.A., Chase, J.G., Rodgers, G.W., and Clifton, G.C. (2012). Behaviour of asymmetrical friction connections using different shim materials. *Proceedings of the New Zealand Society of Earthquake Engineering- Annual Conference. Christchurch* - New Zealand.

Khoo, H.H., Clifton, C., Butterworth, J., MacRae, G. and Ferguson, G. (2011) Influence of steel shim hardness on the Sliding Hinge Joint. *Journal of Constructional Steel Research.*

Mackinven, H. (2006). Sliding Hinge Joint for Steel Moment Frames Experimental Testing. *Unpublished ENCI493 Project Report*. *Department of Civil Engineering.* University of Canterbury – New Zealand.

MacRae, G.A., Clifton, C.G., MacKinven, H., Mago, N., Butterworth, J., Pampanin, S. (2010). The Sliding Hinge Joint Moment Connection. *Bulletin of the New Zealand Society for Earthquake Engineering.*

Standards New Zealand. (2009). NZS 3404: Part 1: 2009 – Steel Structures Standard. Wellington – New Zealand.

Appendix A.3

Velocity Effects on the Behaviour of Asymmetrical Friction Connections (AFCs)

Appendix A.3
Velocity Effects on the Behaviour of Asymmetrical Friction Connections (AFCs)

Jose C. Chanchi Golondrino*, Gregory A. MacRae, James G. Chase**, Geoffrey W. Rodgers** and George C. Clifton*****

* University of Canterbury - New Zealand, National University of Colombia - Colombia
e-mail: jcchanchigo@unal.edu.co

** University of Canterbury - New Zealand
e-mail: gregory.macrae@canterbury.ac.nz, geoff.chase@canterbury.ac.nz, geoffrey.rodgers@canterbury.ac.nz

*** University of Auckland – New Zealand
e-mail: c.clifton@auckland.ac.nz

Keywords: Asymmetrical Friction Connection, Velocity dependence, Low damage dissipaters, Energy dissipation, Shim materials

Abstract. *This paper reports on the hysteretic behaviour of Asymmetrical Friction Connection (AFC) assembled with different shim materials such as Aluminium, Brass, Mild Steel, Bisalloy 80, Bisalloy 400, and Bisalloy 500 subjected to a cyclic displacement regime applied with a quasi-static velocity and with a high velocity of 10 mm/s and 190mm/s respectively. Results show that at the high velocity regardless of the shim material the hysteresis loop is less stable, and greater forces are required to activate the sliding mechanism of the slotted plate when compared with the hysteresis loop at the low velocity. Boundaries of the effective friction coefficient for the quasi-static and high velocity cases, as well as a model that represents the velocity dependence of AFCs in terms of the effective friction coefficient are presented.*

1 INTRODUCTION

1.1 Asymmetrical Friction Connections (AFC)

AFCs are a type of friction connection assembled with three steel plates and two thin plates termed shims. The three steel plates comprise a bottom plate termed fixed plate, a slotted plate located at the central part of the connection, and a top plate termed cap plate that is attached to the other two plates by means of high strength bolts. The shims are inserted at the interface slotted plate-fixed plate and at the interface slotted plate-cap plate creating a shear plane at each side of the slotted plate (figure 1a). This type of connection can be used to dissipate seismic energy in different structural systems, and energy is dissipated when the slotted plate is forced to slide across the connection by overcoming the friction force generated at both sides of this plate as a result of the clamping force induced by the bolts on the connection. Quasi–static testing of this type of connection have shown that an almost square and stable hysteretic behaviour can be achieved by using shims with a hardness that is lower o greater than the hardness of the slotted plate (figure 1b). For instance the use of Aluminium, Brass, Bisalloy 400, or Bisalloy 500 shims was found to be suitable in terms of hysteretic behaviour of the connection when used on mild steel slotted plates (Chanchi et al. 2012). AFCs can be used as seismic dissipaters in different structural systems such as moment resistant frames (figure 1c) and braced frames (figure 1d). In moment resistant frames the AFC detail is placed at beam column joint where the energy is dissipate as the joint rotates (Clifton 2005), and in

braced frames the AFC detail can be placed at one end of the brace where the energy is dissipated when the brace is elongated (Chanchi et al. 2014).

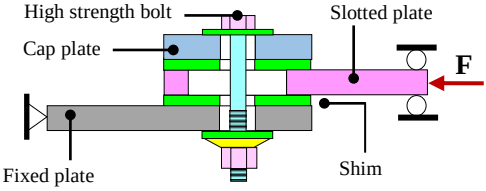

a. AFC components

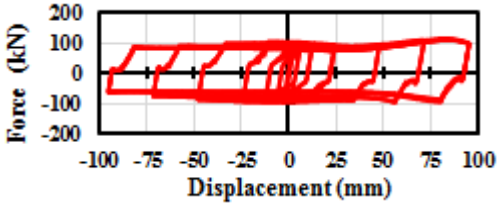

b. Hysteretic loop of AFCs with Bisalloy 500 shims

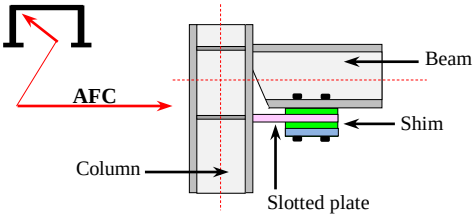

c. AFC on moment resistant frames

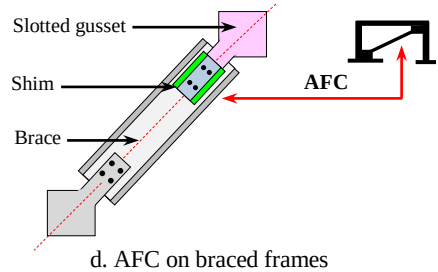

d. AFC on braced frames

Figure 1. AFC components, hysteretic behaviour, and application

1.1 Research background

The concept of the AFC was proposed by Clifton 2005 when considering AFC subassemblies with brass shims tested in quasi-static conditions and over short sliding distances (i.e. up to 50mm). Results showed that by using dissimilar sliding surfaces the hysteretic behaviour of AFCs is stable and can be predicted using a bilinear hysteresis loop. MacRae et al. 2010 carried out quasi-static testing on beam-column joints equipped with AFC details assembled with Aluminium, Brass, and Mild Steel shims. Results confirmed the findings of Clifton 2005 regarding the stability of the hysteretic behaviour of the beam-column joint when using dissimilar sliding surfaces on the AFC detail. However, in the case of sliding Mild Steel slotted plates over Mild Steel shims (i.e. similar sliding surfaces) the behaviour of the beam-column joint was found to be stable when the sliding distances at the AFC detail were less than 50mm. Khoo et al. 2012 replicated the quasi-static testing carried out by Clifton 2005 on AFC subassemblies introducing the concept of using shims with greater hardness than the hardness of the slotted plate. Results showed that by sliding slotted plates of Mild Steel over Bisalloy 400 shims the hysteretic behaviour of the AFC subassemblies is very stable and with low degradation. Chanchi et al. 2012 tested quasi-statically AFC specimens with long slots (i.e. 200mm) with different shim materials such as Aluminium, Brass, Mild Steel, Bisalloy 80, Bisalloy 400, and Bisalloy 500. Results showed that a stable hysteretic behaviour of the AFCs can be achieved by either using shim materials with lower or greater hardness than the hardness of the slotted plate. Results also indicated that the use of Bisalloy 80 and Mild Steel shims on AFCs with Mild Steel slotted plates is not desirable because AFCs with this type of shims exhibited an unstable hysteretic behaviour when tested for sliding distances between 75 and 200mm. From the above research background it can be seen that the hysteretic behaviour of AFCs with different shim materials has been characterized in quasi-static conditions. However, there is no reference of research work quantifying the velocity dependence of AFCs when using different shim materials. For that reason, this paper compares the hysteretic behaviour at low and high velocities of AFCs using Aluminium, Brass, Mild Steel, Bisalloy 80, Bisalloy 400 and Bisalloy 500, and answers these questions:

i) What are the effects of high velocities on the hysteresis loop of AFCs?

ii) Does the velocity change the effective friction coefficient of AFCs?

iii) What are the boundaries values of the effective friction coefficient of AFCs when considering the effect of the velocity?

iv) What is a simple model for representing the effect of the velocity on the effective friction coefficients of AFCs?

2 MATERIALS

AFC specimens were assembled with a fixed, slotted and cap plates manufactured with Grade 300 Mild Steel plates of 20mm thickness, and shims of 6mm thickness manufactured with the materials specified in table 1. The shim materials were chosen in such a way that the ratio between the hardness of the shim material and the hardness of the slotted plate (ρ) varied in the range 0.57 – 3.84 as shown in table 1.

Table 1. Summary of materials used as shims

Material	Specification	Brinell Hardness (BH)	Hardness ratio ρ ( )
Aluminium	5005GP Series Aluminium	75	0.58
Brass	UNS C26000 – ½ Hard Temper	82	0.63
Steel	Cold Rolled Mild Steel	130	1.00
Bisalloy 80	Bisplate 80	255	1.96
Bisalloy 400	Bisplate 400	400	3.08
Bisalloy 500	Bisplate 500	500	3.85

Two galvanized bolts of Grade 8.8 (i.e. 800 MPa ultimate strength) with 16mm diameter and 110mm length were used to clamp together the three steel plates and the two shims. The bolt assembly comprised a structural washer placed under the bolt head, a flat washer and a Belleville washer placed under the bolt nut (figure 2b). The AFC specimen was characterized by a slot of 200mm, a clamped zone of 180mm width and 290mm long with a grip length of 72mm, and two unclamped zones of 180mm width and 290mm long located at both sides of the clamped zone. At both ends of the AFC specimen six holes of 26mm diameter were drilled to attach the connection on testing rig (figure 2a).

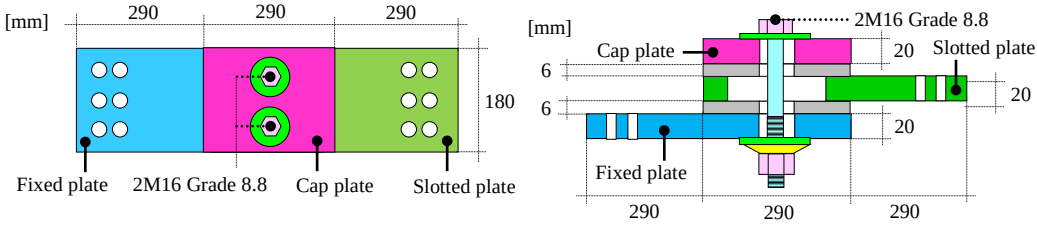

a. Plan view b. Lateral view

Figure 2. Configuration of an AFC specimen with 200mm slot and using two Grade 8.8 M16x110 bolts.

3 TESTING METHODS

3.1 AFC assembling procedure

Four AFC specimens were assembled at each type of shim material, so that a total of twenty four AFC specimens were considered in this research work. Each AFC specimen was assembled using the torque control method based on finding experimentally a torque that develops the proof load on the bolts (proof load torque).

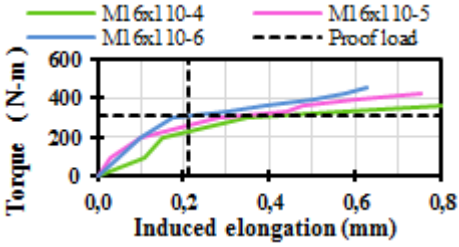

a. Torque – induced elongation relationship

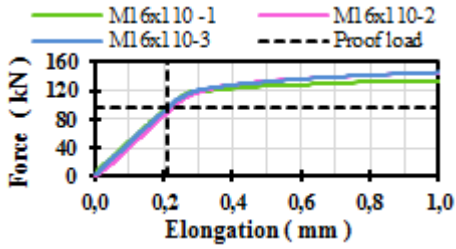

b. Tensile testing relationship

Figure 3. Assembling relationships for an AFC specimen with two M16 X110 Grade 8.8 bolts.

The proof load torque was extrapolated from a relationship between torque and induced bolt elongation obtained from two bolts with a grip length equal to the grip length of the AFC specimens (i.e. 72mm). This torque – induced bolt elongation relationship was developed by gradually increasing the torque on the three bolts up to the failure torque, and by recording at each torque the elongation of the two bolts (figure 3a). The bolt elongation used to extrapolate the assembling torque from the torque-induced bolt elongation relationship was defined as the elongation exhibited by three bolts when reaching the proof load on a tensile testing (figure 3b). Using the above methodology a torque value of 300N-m from the finger tight condition was defined as proof load torque.

3.2 Testing setup

AFC specimens were tested in a setup horizontally arranged and constituted by a fixed and a moving support. The fixed support was assembled with a bracket bolted on a reaction frame and termed fixed bracket, and the moving support with a bracket attached to a frame bolted on a shaking table and termed moving bracket. Slip critical connections with six Grade 8.8 M24x120mm bolts were used to bolt the fixed and slotted plates of the AFC specimen onto the fixed and moving brackets of testing setup. By attaching the slotted plate onto the moving bracket, the shaking table was able to drive the slotted plate of the AFC specimen to target displacement and at pre-defined velocity (figure 4a).

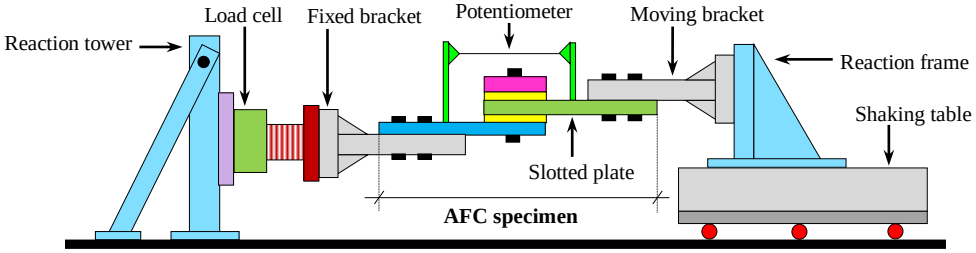

a. Lateral view of the AFC specimens testing setup

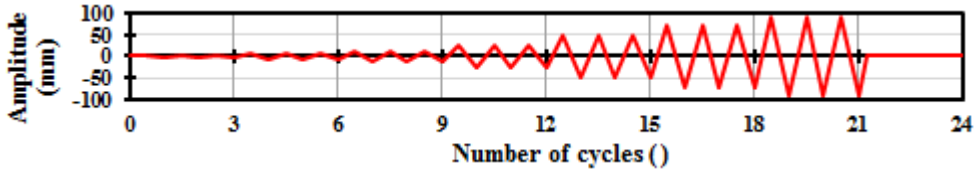

b. Displacement regime applied at constant velocities of 10 and 190 mm/s

Figure 4. Testing setup and displacement regime used on the testing of AFC specimens.

This setup was instrumented with a load cell placed in series with the fixed bracket, and with one extensometer placed horizontally across the AFC specimen. Testing of AFC specimens was carried out by running the shaking table with a controlled displacement regime with a constant velocity. Half of the AFC specimens were tested by running the displacement regime at a constant quasi-static velocity of 10mm/s, and the other half of the specimens by running the displacement regime at a constant high velocity of 190mm/s. The displacement regime comprised 20 sawtooth cycles with amplitudes between 3 and 90% of the total slot length of the AFC specimen (i.e. 200mm) as shown in figure 4b.

4 RESULTS AND ANALYSIS

4.1 Effects of the velocity on the hysteresis loop

Hysteresis loops recorded at quasi-static and high velocities (i.e. 10mm/s and 190mm/s) for AFCs assembled with different shims materials are presented in figure 5.

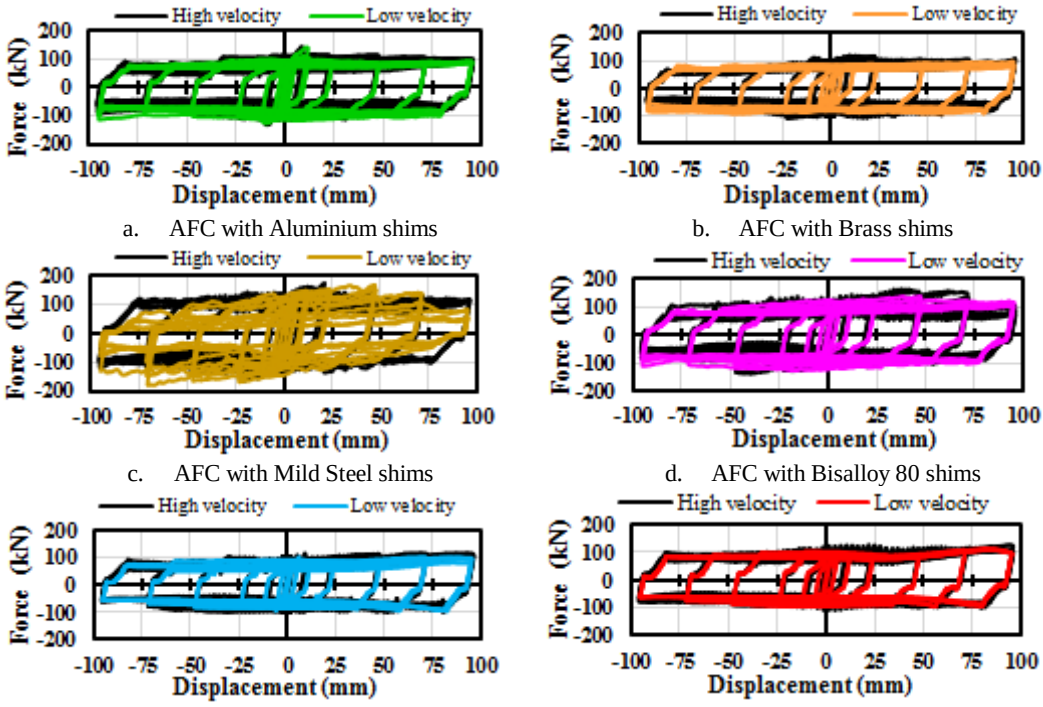

a. AFC with Aluminium shims

b. AFC with Brass shims

c. AFC with Mild Steel shims

d. AFC with Bisalloy 80 shims

e. AFC with Bisalloy 400 shims

f. AFC with Bisalloy 500 shims

Figure 5. Hysteresis loop of AFCs with different shim materials

When comparing the hysteresis loops recorded at low and high velocities, two effects of increasing dramatically the testing velocity on the hysteresis loop can be observed: i) the post-yielding zone at high velocities is less stable than at low velocities, and ii) forces across the post-yielding at high velocities are greater than those recorded at low velocities. Both effects are more accentuated for shim materials with hardness similar to the hardness of the slotted plate (i.e. Mild Steel and Bisalloy 80 shims), rather than for shim materials where the shim hardness is either lower or greater than the hardness of the slotted plate. These two effects are linked to the development of an abrasive sliding mechanism where the significant

amount and size of the degraded particles degrading the sliding surfaces and observed at low velocities is significantly increased at high velocities.

4.2 Effects of the velocity on the effective friction coefficient

The effective friction coefficient (equation 1) was calculated as the ratio between the average force across the post-yielding zone of the hysteresis loop ($F_{sliding}$) and the product of the number of bolts (i.e. 2), the number of shear planes (i.e. 2), and the bolt proof load (i.e. 95kN). Figure 6 presents the average effective friction coefficient calculated from two AFC specimens at each group of shims for the low and high velocity testing cases and at different sliding distances.

$$\mu_{effective} = \frac{F_{sliding}}{2 \times 2 \times 95} \tag{1}$$

In Figure 2 it can be seen that for whole shim materials the effective friction coefficient at high velocity is greater than the effective friction coefficient at low velocity across the full sliding distance of the connection. It can also be seen that as the ratio between the hardness of the shim material and the hardness of the slotted plate material increases (ρ) the effective friction coefficient at high velocities y closer to the effective friction coefficient at low velocities. This proximity between the effective friction coefficient at high and low velocities is attributed to adhesive sliding mechanisms typical of hardness ratios (ρ) greater than 3 (Chanchi et al. 2012) where the amount and size of degraded particles is minor, so that as the degraded particles slide at high velocities there is minor increment on the friction force.

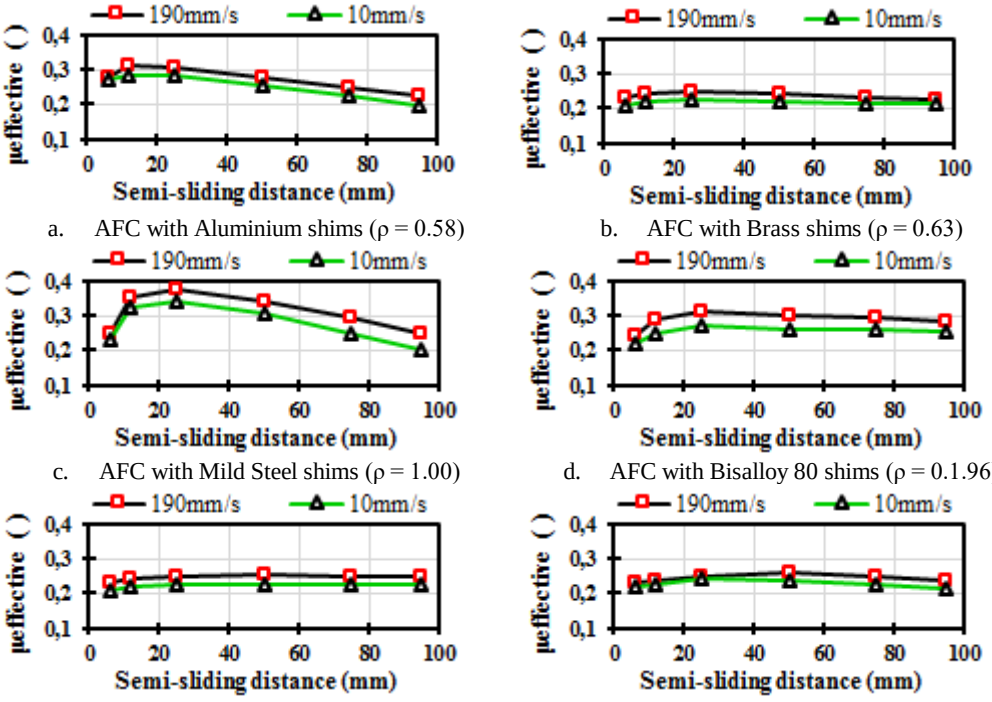

a. AFC with Aluminium shims (ρ = 0.58)
b. AFC with Brass shims (ρ = 0.63)
c. AFC with Mild Steel shims (ρ = 1.00)
d. AFC with Bisalloy 80 shims (ρ = 0.1.96)
e. AFC with Bisalloy 400 shims (ρ = 3.08)
f. AFC with Bisalloy 500 shims (ρ = 3.85)

Figure 6. Effective friction coefficient ($\mu_{effective}$) of AFCs with different shim materials.

4.3 Effect of the shim hardness on the effective friction coefficient

The boundaries of the effective friction coefficient for low and high velocities for different shim materials were calculated as the average across the post-yielding zone from two AFC specimens at each testing velocity **(**figure 7). Figure 7 shows that al low and high velocities the effective friction coefficient of AFC varies in the ranges 0.22 – 0.27 and 0.24 – 0.31 respectively.

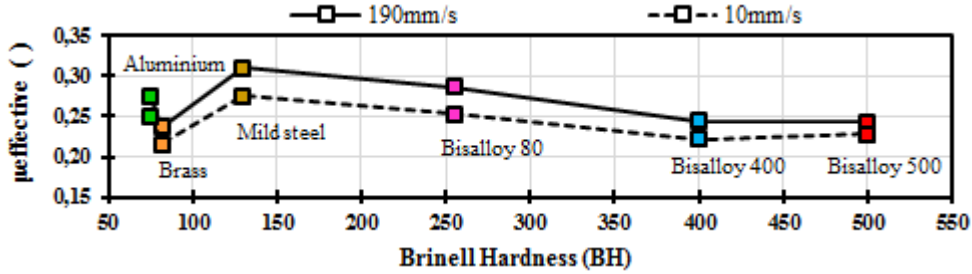

Figure 7. Effective friction coefficient ($\mu_{effective}$) of AFCs with different shim material hardness.

Figure 7 also shows that the maximum effective friction coefficients with the greatest velocity dependence can be achieved by using hardness ratios of unity (i.e. Mild steel slotted plates sliding over Mild steel shims). However in this case the hysteretic behaviour of the AFC specimen is unstable. In contrast, minimum effective friction coefficients with the lowest velocity dependence and stable hysteretic behaviours can be achieved by using hardness ratios greater than 3.0 (i.e. Mild Steel slotted plates sliding over Bisalloy 400 or Bisalloy 500 shims).

4.4 Velocity model

In order to quantify the velocity dependence of AFC specimens, they were assumed to behave as viscous dampers, where the force that activates the sliding of the connection (F) is proportional to a coefficient that depends on the geometrical configuration of the connection (C), to the testing velocity (V), and to an exponent (α) that represents the magnitude of velocity dependence of the connection as shown in equation 2 (Peckan et al. 1995).

$$F = C \times V^{\alpha} \tag{2}$$

$$F_h = F_q \times \left[\frac{V_h}{V_q}\right]^{\alpha} \tag{3}$$

$$\mu_h = \mu_q \times \left[\frac{V_h}{V_q}\right]^{\alpha} \tag{4}$$

Using equation 2 for both the quasi-static case (10mm/s) and the high velocity case (190mm/s), and equating the connection coefficient (C), an expression that correlates the force at high velocity (F_h), the force at quasi-static velocity (F_q), the quasi-static velocity (V_q), the high velocity (V_h), and the velocity dependence exponent (α) was found (equation 3). This equation can be extended to the effective friction coefficient as shown in equation 4, and by using the boundaries of the effective friction coefficients found in section 4.3 the velocity dependence exponent (α) was quantified for different shim materials in figure 8. It can be seen that the velocity dependence exponent for AFC specimens varies in the range of 0.020 to

0.045 and the maximum and minimum values are presented for Mild Steel slotted plates sliding over Mild Steel shims and Bisalloy 400 or Bisalloy 500 shims respectively.

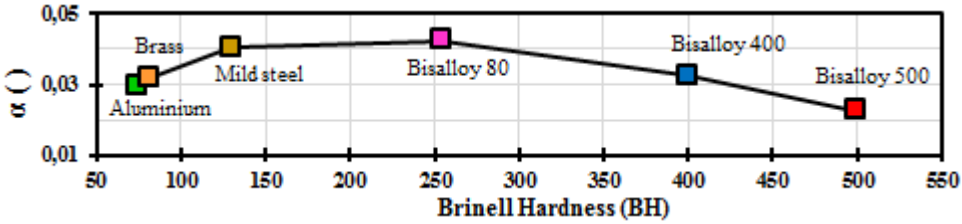

Figure 8. Velocity dependence exponent (α) of AFCs with different shim materials.

5 CONCLUSIONS

This paper describes the velocity effects on the AFC using different shim materials. It is shown that:

i) At high velocities the hysteresis loop of AFCs loses stability, and greater forces are required to activate the sliding mechanism when compared with the forces required in quasi-static conditions.

ii) The effective friction coefficient of AFCs increases with increments on the velocity. Magnitude of the increments on the effective friction coefficient depends on the ratio between the hardness of the shim material and the hardness of the slotted plate.

iii) For ratios between the hardness of the shim material and the hardness of the slotted plate (hardness ratio) varying on the range 0.58-3.85, the effective friction at low and high velocities vary in the ranges 0.22-0.27 and 0.24-031 respectively.

iv) The effective friction coefficient at high velocities can be quantified as the product between the effective friction coefficient at low velocities and the ratio between the high and low velocity raised to the power of an exponent that varies in the range of 0.020 - 0.045.

REFERENCES

[1] Chanchi, J.C., MacRae, G.A., Chase, G., Rodgers, G, and Clifton, C. (2012). Behaviour of asymmetrical friction connections using different shim materials. *New Zealand Society for Earthquake Engineering Conference.*

[2] Clifton, G.C. (2005). Semi-Rigid Joints for Moments Resisting Steel Framed Seismic Resisting Systems. *Published PhD Thesis, Department of Civil and Environmental Engineering.* University of Auckland – New Zealand.

[3] Chanchi, J.C., Xie R., MacRae, G.A., Chase, G., Rodgers, G, and Clifton, C. (2014). Low damage brace using Asymmetrical Friction Connections. *New Zealand Society for Earthquake Engineering Conference.*

[4] MacRae, G.A., Clifton, C.G., MacKinven, H., Mago, N., Butterworth, J., Pampanin, S. (2010). The Sliding Hinge Joint Moment Connection. *Bulletin of the New Zealand Society for Earthquake Engineering.*

[5] Khoo, H.H., Clifton, C., Butterworth, J., MacRae, G. and Ferguson, G. (2011) Influence of steel shimhardness on the Sliding Hinge Joint. *Journal of Constructional Steel Research.*

[6] Pekcan, G., Mander, J. B., M. Eeri, and Chen, S. S. (1995). The Seismic Response of a 1:3 Scale Model R.C. Structure with Elastomeric Spring Dampers. *Earthquake Spectra*, Vol. 11, No. 2, pp 249 – 267.

Appendix A.4

Is the Asymmetrical Friction Connection (AFC) a Low Damage Dissipater?

Appendix A.4

Is the Asymmetrical Friction Connection (AFC) a Low Damage Dissipater?

2015
NZSEE
Conference

J. Chanchi Golondrino

University of Canterbury - New Zealand, National University of Colombia, Colombia

G.A. MacRae, G. Chase & G. Rodgers

University of Canterbury - New Zealand

C. Clifton

University of Auckland - New Zealand

ABSTRACT: Asymmetrical Friction Connections (AFC) are used in structures in earthquake zones to dissipate energy without causing major damage to the structural members. This means that the structure itself does not require replacement after a major seismic event. Testing of these connections has been undertaken and degradation in strength has been observed. However, (i) reasons for this degradation have not been clear, (ii) a means of assessing the strength degradation has not been available, (iii) the importance of the strength degradation (which is related to the amount of strength degradation) has not been described, (iv) the ability to reinstate the joint using new bolts is not known, and (v) effective friction factors for the connection after connection reinstatement are not known. This paper describes the testing of AFC specimens with high hardness shims (i.e. Bisalloy 500) under increasing cyclic displacements to address the issues stated above. Tests were conducted twice with the same setup. In the second test, the change in performance as a result of the first test was able to be observed. Then the bolts were replaced and tests were conducted twice more.

1 INTRODUCTION

Asymmetrical Friction Connections (AFC) have been recently proposed and applied as seismic energy dissipaters in several structural systems in New Zealand. Testing of AFC components and beam column joints equipped with this type of dissipater demonstrated stable hysteretic behaviour, and the ability to absorb a significant amount of seismic energy with low damage (Clifton 2005). Testing aiming to describe the behaviour of AFCs considering different assembling methods, different surface conditions, as well as long term effects such as corrosion have been also undertaken by Chanchi et al. 2013. Results show that by assembling AFCs either with high or low hardness sliding surfaces, and using Grade 8.8 bolts (i.e. 660 MPa yield strength) tensioned up to the proof load, a predictable hysteretic behaviour can be achieved. Applications of AFCs on different braced framing systems where AFCs act as fuses protecting the structural system by imitating the amount of seismic force that the system can absorb were also proposed by MacRae 2008, and these applications are under experimental research at University of Canterbury – New Zealand (Chanchi et al. 2014). AFCs have been qualitative categorized by several researchers as a promising low damage dissipater that can be applied in different structural systems (Clifton 2005, MacRae 2008, Chanchi et al. 2013). However, to date there is no study that quantifies the strength degradation that this dissipater undergoes under cyclic load. For that reason, this paper aims to propose a simple methodology to quantify the strength degradation of AFCs, and answers following questions:

1. What is the strength degradation of AFC specimens using Bisalloy 500 shims when subjected to cyclic load?
2. What is the effect of bolt replacement on the strength degradation of AFC specimens using Bisalloy 500 shims and subjected to cyclic load?
3. What is a simple methodology to assess the degradation of AFC specimens?

4. Can an AFC be regarded as a low damage dissipater?

2 ASYMMETRICAL FRICTION CONNECTION (AFC)

AFCs are a type of friction connection comprising three steel plates, and two thinner plates termed shims. This connection is assembled by placing the shims at both sides of a slotted plate, and by sandwiching this shims-slotted plate arrangement between a short plate termed cap plate, and a long plate termed fixed plate (Figs. 1a, b). High strength bolts tensioned up to 70% of the ultimate strength (proof load) and assembled with structural, flat, and Belleville washers are used to clamp together plates and shims. AFCs can be used to dissipate seismic energy in different structural systems; energy is dissipated when the slotted plate is forced to slide across the connection arrangement and the force is transmitted via shear forces (Fig. 1c). By using Bisalloy 500 shims (Chanchí et al. 2013) an almost square and stable hysteretic behaviour can be achieved (Fig. 1d).

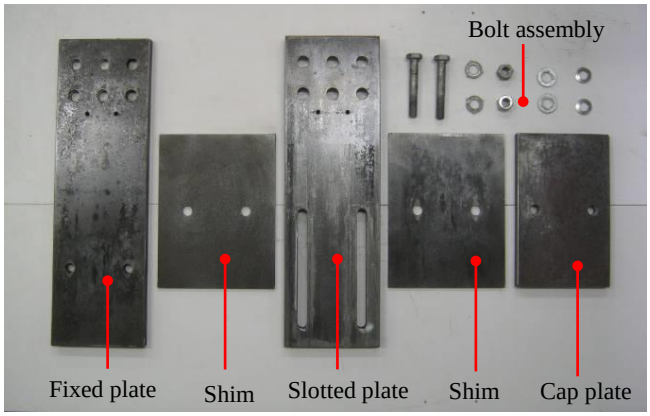

a. AFC components

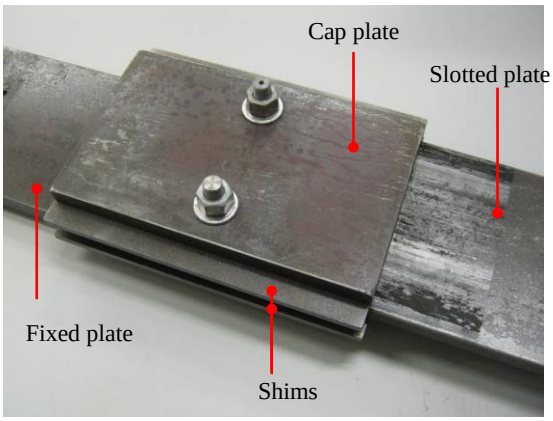

b. AFC assembly

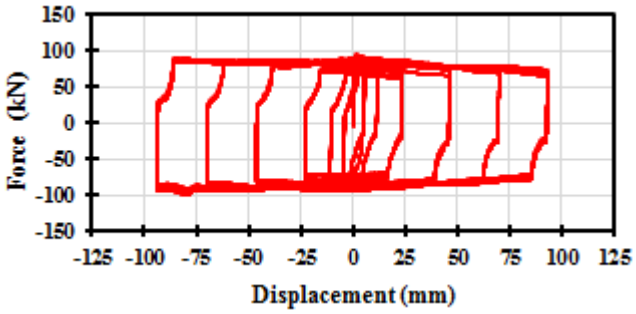

d. Hysteresis loop of AFC with Bisalloy 500 shims

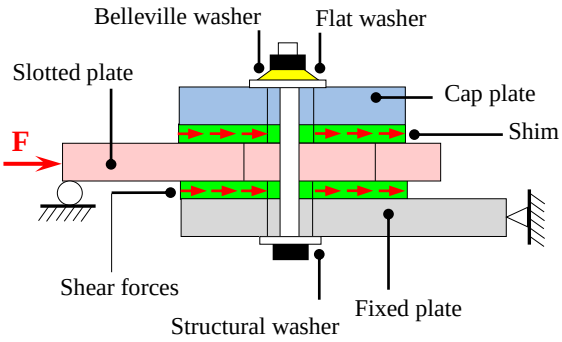

c. Mechanism of force transmission in AFCs

Figure 1. Assembly and behaviour of AFCs

3 APPLICATIONS OF AFC

AFCs can be used to dissipate seismic energy in framed or rocking wall based structural systems (Fig. 2). In framed systems the AFC detail can be placed in beam column joints where dissipation occurs when the beam rotates (Clifton 2005), or within braces where dissipation occurs when the brace elongates (MacRae 2008; Chanchí et al. 2014). In the case of rocking wall systems, AFC details can be placed at both sides of the wall on the base connection following configurations suggested by Bora et al. 2007. In this configuration, dissipation occurs as the wall experiences rocking or uplifting. Applications of AFC details are desirable not only because assembling process and cost are similar to traditional bolted connections; but also because components are replaceable, and the capacity of the connection can be accurately controlled by using high or low hardness shims (Chanchi et al. 2013).

Another significant advantage in the case of braces equipped with AFC details is that they can be assembled in the shop, so reducing the erection time and improving quality control on site.

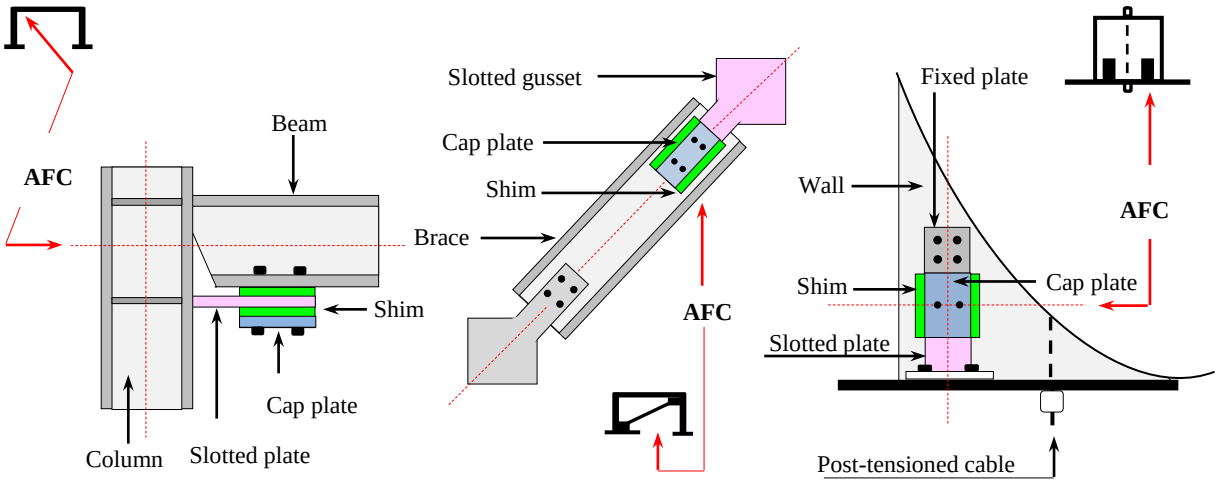

a. AFC on beam-column joints **b.** AFC on braces **c.** AFC on rocking walls

Figure 2. Applications of AFCs on different structural systems

4 MATERIALS

Two AFC specimens with 200mm slots were assembled using 20mm thick Grade 300 steel plates, 6mm thick Bisalloy 500 shims, and two M16 x 110mm Grade 8.8 galvanized bolts with 72mm shank. Surfaces of plates and shims were used as bare condition, and impurities of sliding surfaces were removed by using a thin layer of acetone applied with a rag. Bolts were assembled with structural, flat, and single Belleville washers; structural washers were located under bolt heads and Belleville and flat washers under nuts (Fig. 3a). A calibrated torque wrench was used to tension bolts up to the proof load; in the pre-assembling stage the single Belleville washers were not flat, and they became flat at tensioning forces well below the bolt proof load.

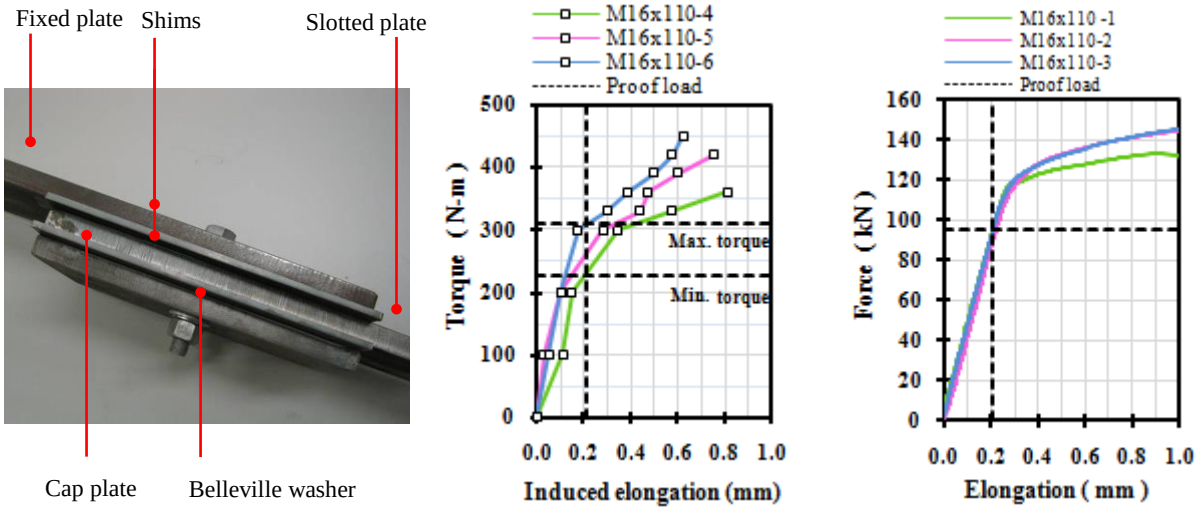

a. AFC assembly **b.** Torque relationship **c.** Tension relationship

Figure 3. AFC assembly and assembling relationships

Assembling procedure of AFC specimens was based on using a torque that tensions bolts up to the proof load (proof load torque). This torque was defined by developing a relationship between torque

and induced bolt elongation on three bolts using similar assembly as that one used in AFC specimens, and where the torque was gradually increased from the finger tight condition to the bolt failure (Fig. 3b). In this relationship, the proof load torque was considered as the torque that induces a bolt elongation similar to that one recorded in a tension test when bolts reach the proof load (Fig. 3c). Using these relationships a torque of 300N-m was chosen as the assembling torque; this value corresponds to nut rotations of 1/4 –1/2turn.

5 TESTING METHODS

Testing of SFC specimens was conducted using a vertical setup in a Dartec 10MN axial testing machine. Setup was constituted by a moving bracket attached to a servo-controlled actuator, and a fixed bracket attached to a rigid crosshead. The slotted and fixed ends of specimens were respectively connected to the moving and fixed bracket by means of slip critical connections assembled with 6 M20 Grade 8.8 bolts. This setup was instrumented with a load cell placed in series with the brackets, and a potentiometer placed across the connection stroke (Fig. 4). Sliding of the slotted plate was induced by imposing a displacement regime comprised of 18 sinusoidal cycles with maximum amplitudes in the range of 6.25 -100 % of the specimen effective stroke (±95mm), and ran to a maximum velocity of 10mm/s.

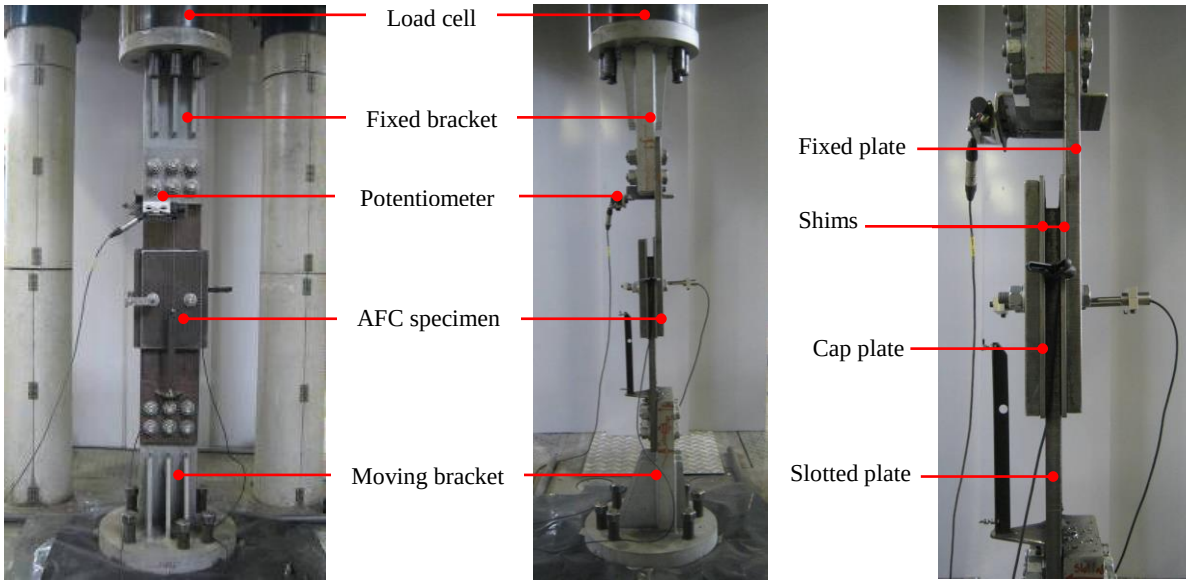

a. Frontal and lateral view of testing setup **b.** AFC specimen

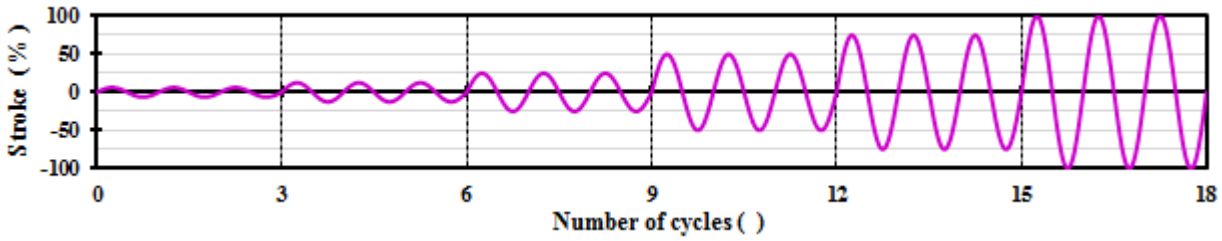

c. Displacement regime

Figure 4. AFC testing setup and displacement regime

Two AFC specimens were tested with no replacement of plates or shims; each specimen was subjected to four runs of the displacement regime. Between runs a time of 15 minutes was used to allow connection components to cool down to room temperature. Initial two runs were carried out on both AFC specimens without bolt replacement, no bolt re-tensioning between the first and second run was applied. Final two runs were carried out on same AFC specimens with a new set of bolts tensioned up

to the proof load; no re-tensioning between the third and fourth run was applied.

6 RESULTS AND ANALYSIS

6.1 Qualitative assessment of strength degradation

Hysteresis loop of AFC specimens is almost rectangular; the post-yielding zone is non-horizontal due to the development of prying forces between the slotted plate and shims. These prying forces are developed as a result of the secondary bending that the connection undergoes when the driving force on the slotted plate is transmitted to the fixed plate. When comparing hysteresis loops recorded in the first and second run (i.e. brand new sliding surfaces and brand new bolts) of the displacement regime for both AFC specimens (Fig. 5a, 5b), it can be seen that the force that activates the sliding mechanism of the slotted plate (sliding force) reduces as sliding distance and number of cycles increase. This strength reduction is due to loss of bolt tension presented as sliding surfaces degrade not only as a result of the sliding mechanism, but also because prying forces loosen bolts. Hysteresis loops recorded in the third and fourth run (i.e. degraded sliding surfaces and brand new bolts) of the displacement regime for both AFC specimens exhibited a similar trend on strength reduction as that one observed on the first and second run (Fig. 5c, 5d). It can be also seen that by replacing bolts the strength of AFC specimens was fully restored. However, increased forces at the initial cycles were developed as result of the degradation that the zone around the bolt hole undergoes due to the clamping stress concentration. These increased forces were reduced at further cycles when AFC specimens experienced loss of bolt tension. From the above results, it can be stated that by retensioning the original bolts and using degraded sliding surfaces the strength of the AFC specimen can be fully restored. The appropriate amount of bolt retension should be that one that restores the bolt tension to the proof load.

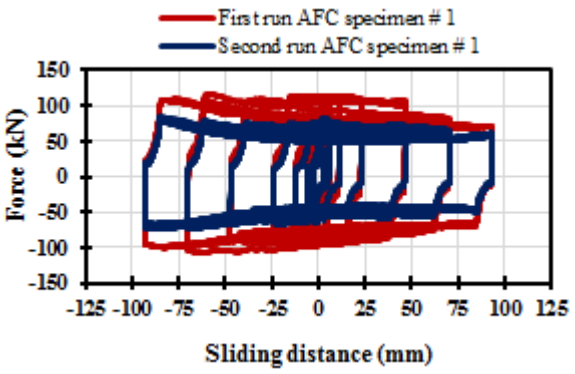

a. AFC specimen # 1 with brand new sliding surfaces and brand new bolts

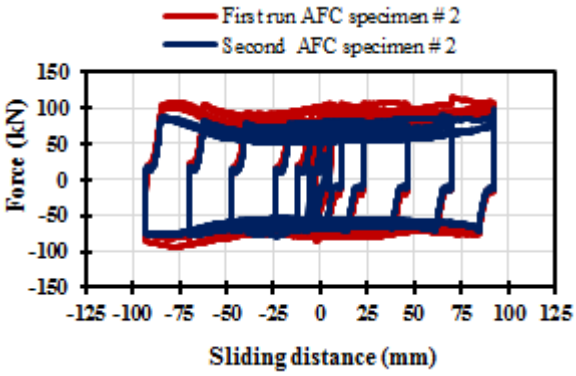

c. AFC specimen # 2 with brand new sliding surfaces and brand new bolts

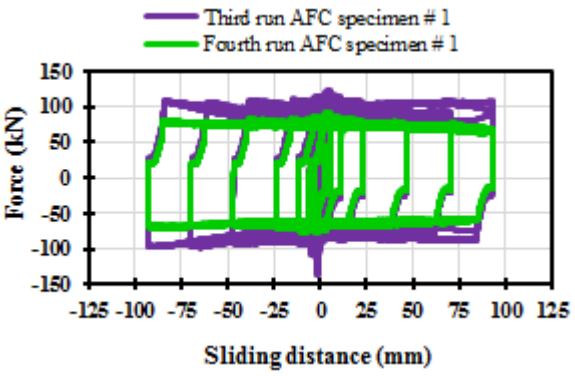

b. AFC specimen # 1 with degraded sliding surfaces and brand new bolts

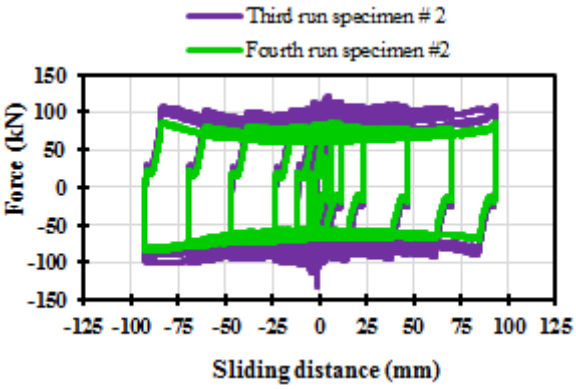

d. AFC specimen # 2 with degraded sliding surfaces and brand new bolts

Figure 5. Hysteresis loops of two AFC specimens with brand new and degraded surfaces.

6.2 **Qualitative assessment of strength degradation**

The effective friction coefficient (Equation 1) was calculated as the ratio between the total sliding force ($F_{sliding}$) from the two bolts considering the two shear planes and the bolt proof load (F_{proof}).

$$\mu = \frac{F_{sliding}}{2 \times 2 \times F_{proof}} \tag{1}$$

The effective friction coefficient was calculated at different sliding distances for the four runs of the displacement regime in both tests of AFC specimens. At each sliding distance, the sliding force in Equation 1 was considered as the average sliding force of both specimens and assessed across the tensile and compressive post-yielding zones. It can be seen that the effective friction coefficient varies with the sliding distance, and this variation is more accentuated for sliding distances less than 24mm (Fig. 6).

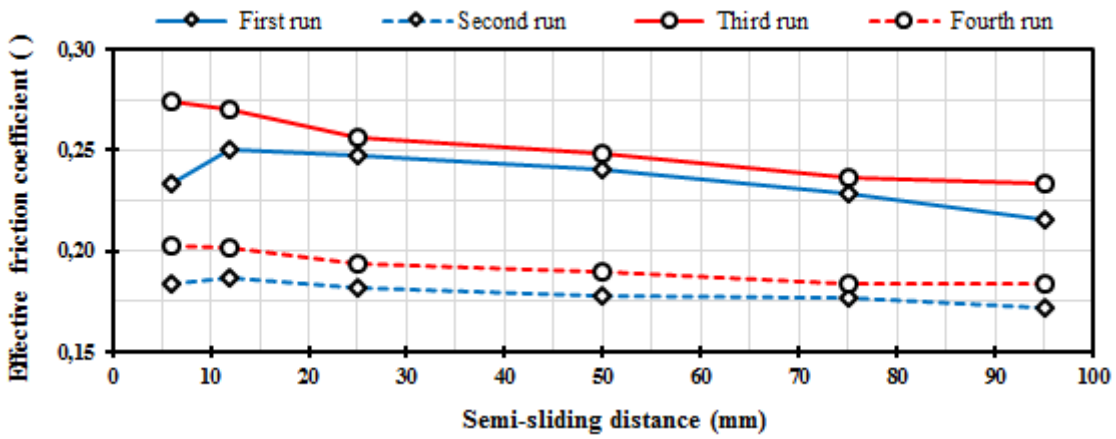

Figure 6. Average effective friction coefficient from two AFC specimens for first, second, third and fourth run.

The greatest values of effective friction coefficients were exhibited at those runs where bolts were brand new (first and third run), and ranged from 0.22 to 0.27. Lowest and less variable effective friction coefficients were exhibited for cases where no bolt replacement was made (third and fourth run). In this case the effective friction coefficient ranged from 0.17 to 0.20, and stability of the effective friction coefficient is attributed to the reduced influence of prying forces when bolts underwent loss of tension.

6.3 **Quantitative assessment of strength degradation**

Strength degradation (*sd*) of AFC specimens was quantified as function of the degradation index (Equation 2). The degradation index was defined as the ratio between the residual effective friction coefficient exhibited on a second run of the displacement regime by an AFC specimen with no bolt replacement ($\mu_{residual}$), and the initial effective friction coefficient ($\mu_{initial}$) exhibited on the first run of the displacement regime.

$$sd = 1 - \frac{\mu_{residual}}{\mu_{initial}} \tag{2}$$

Strength degradations from the first to second run, and from the third to fourth run of the displacement regime were calculated using the average effective friction coefficients of both AFC specimens (Fig.

7a). It can be seen that strength degradation varies with sliding distance, and this variation is more noticeable in brand new surfaces (first to second run) rather than in worn out surfaces (third to fourth run). When calculating the average degradation of both AFC specimens exhibited in the four runs of the displacement regime it can be seen that the strength degradation varies in the range 21- 26% (Fig. 7b). Given that displacement regime used in this research is more rigorous than the one reported by Grigorian & Popov 1994 as maximum expected in structural systems using friction connections when subjected a severe seismic movement; it can be argued that AFCs are not only a low damage solution but also a sustainable dissipater that only require bolt replacement to restore the full strength.

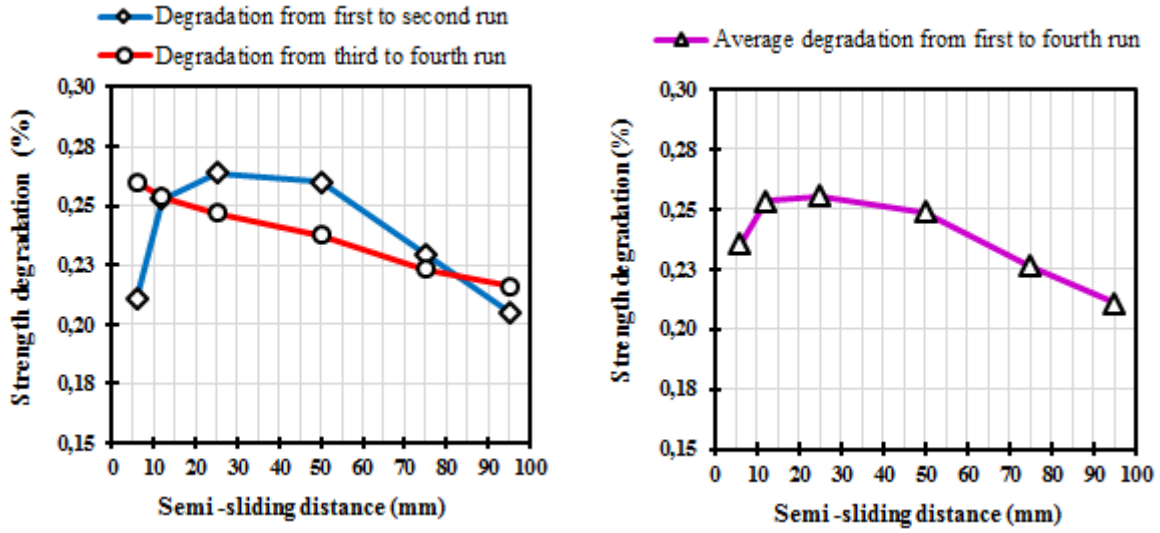

a. Average strength degradation from first to second run (brand new sliding surfaces and brand new bolts), and from third to fourth run (degraded sliding surfaces and brand new bolts)

b. Average strength degradation from first to fourth run (from brand new sliding surfaces with brand new bolts to degraded sliding surfaces with brand new bolts)

Figure 7. Assessment of degradation for brand new and degraded sliding surfaces.

7 CONCLUSIONS

This paper describes and quantifies the strength degradation of Asymmetrical Friction Connections using Bisalloy 500 shims and subjected to cyclic load; it was shown that:

1. Strength degradation is due to loss of bolt tension, and it is associated with the degradation that sliding surfaces undergo as result of the sliding mechanism and prying forces resulting from secondary bending effects in the connection.
2. A simple methodology to assess the strength degradation of AFCs under cyclic load can be based on quantifying the reduction of effective friction coefficient across the sliding distance of the connection.
3. Strength degradation varies with the connection sliding distance. Strength degradations of 21-26% can be considered as upper degradation boundary when estimating the residual capacity of AFC specimens exposed to a severe seismic event.
4. By replacing bolts, the strength of connections with degraded surfaces can be fully restored. However, increased forces at the initial sliding cycles can be developed as consequence of the localized degradation exhibited on the zone around bolt holes where clamping stresses are concentrated. Since the strength can be restored, AFCs can be qualified as a low damage and sustainable dissipaters that can be applied in different structural systems.
5. The effective friction coefficient varies with the connection sliding distance. Effective friction

coefficients of 0.22-0.27 can be considered as upper boundary to estimate the strength of AFC specimens as function of the bolt proof load.

8 REFERENCES

Bora, C., M. Oliva, S. Nakaki, & R. Becker. (2007). "Development of a unique precast shear wall system with special code acceptance". *PCI Journal*. 52(1). 122-135.

Chanchí, J.C., MacRae, G.A., Chase, J.G., Rodgers, G.W., & Clifton, G.C. (2013). "Recent research on two low damage dampers applicable to steel framing systems". *Steel innovations conference.* New Zealand.

Chanchí, J.C., Xie, R., MacRae, G.A., Chase, J.G., Rodgers, G.W., & Clifton, G.C. (2014). "Low damage braces using Asymmetrical Friction Connections (AFC)" *NZSEE - annual conference.* New Zealand.

Clifton, G.C. (2005). Semi-Rigid Joints for Moments Resisting Steel Framed Seismic Resisting Systems. *Published PhD Thesis, Department of Civil and Environmental Engineering.* University of Auckland – New Zealand.

Grigorian, C.E. & Popov, E.P. (1994). *Experimental and Analytical Studies of Steel Connections and Energy Dissipaters. Report UCB/EERC-95/13, Engineering Research Center.* San Francisco (USA).

MacRae, G. A. (2008). "A New Look at Some Earthquake Engineering Concepts". *M. J. Nigel Priestley Symposium* Proceedings, IUSS Press, 2008.

Appendix A.5

Hysteretic Behaviour of Symmetrical Friction Connections (SFCs) Using Different Steel Grade Shims

Appendix A.5

Hysteretic Behavior of Symmetrical Friction Connections (SFCs) Using Different Steel Grade Shims

J. Chanchí Golondrino
University of Canterbury, New Zealand – National University of Colombia, Colombia
jose.chanchigolondrino@pg.canterbury.ac.nz

G.A. MacRae; J.G. Chase; G.W. Rodgers
University of Canterbury, New Zealand
gregory.macrae@canterbury.ac.nz; geoff.chase@canterbury.ac.nz; geoff.rodgers@canterbury.ac.nz

G.C. Clifton
University of Auckland, New Zealand

Abstract

Symmetrical Friction Connections can be considered as an efficient means to dissipate energy because they are characterized by stable hysteretic behavior, low strength degradation and assembling cost comparable to conventional construction. Stability and low degradation on the hysteretic behaviour of this connection type can be achieved by providing dissimilar hardness friction surfaces. This paper reports on the quasi-static testing of symmetrical friction connections using steel shims of different hardness such as mild steel, Bisalloy 80, Bisalloy 400 and Bisalloy 500. Effects of increasing the shim material hardness on the hysteresis loop stability, and on the connection effective friction coefficient are discussed. Results show that shim materials with hardness values greater than 2.5 times the connection material hardness generate stable hysteretic behaviour with low variability on the effective friction coefficient.

1. Introduction

Symmetrical Friction Connections (SFC) were initially proposed as a means to prevent damage in large panel precast concrete structures subjected to seismic excitations (Pall; 1979). In these studies, testing of SFC specimens using different surface treatments such as sand blasting, zinc based coatings, polyethylene based coatings and brake pads were undertaken. Results showed that by using heavy duty break lining pads inserted between the sliding surfaces a reliable, repeatable and square hysteresis loop can be achieved. Later studies introduced the concept of using SFC specimens equipped with mild steel and brass thin plates (shims) inserted between the sliding surfaces of the specimen (Grigorian and Popov; 1993). Results showed that SFC specimens using steel shims exhibited an undesirable hysteretic behaviour characterized by spiky forces; in contrast, the use of brass shims was recommended given the stability on the specimen hysteresis response. From these studies it can be noticed that the inclusion of dissimilar sliding surfaces in SFC can lead to a suitable hysteretic behavior. For that reason, this paper aims to describe the influence of increasing the hardness of steel shims on the hysteretic behaviour of SFC, shim materials such as Cold-rolled mild steel, Bisalloy 80, Bisalloy 400 and Bisalloy 500 are considered.

2. Symmetrical Friction Connections (SFC)

2.1. Concept

SFC can be defined as an arrangement of three steel plates and, two thinner plates termed shims and placed at both sides of the slotted plate (Figure 1). Plates and shims are clamped together by means of high strength bolts assembled with structural, flat and Belleville washers; and tensioned up to a force around 70% of the bolt ultimate strength (proof load). This type of connection can be used to dissipate energy via friction by applying a force on the slotted plate until sliding is reached. If the shim material is properly chosen, this connection can dissipate energy with stable forces and with low material degradation.

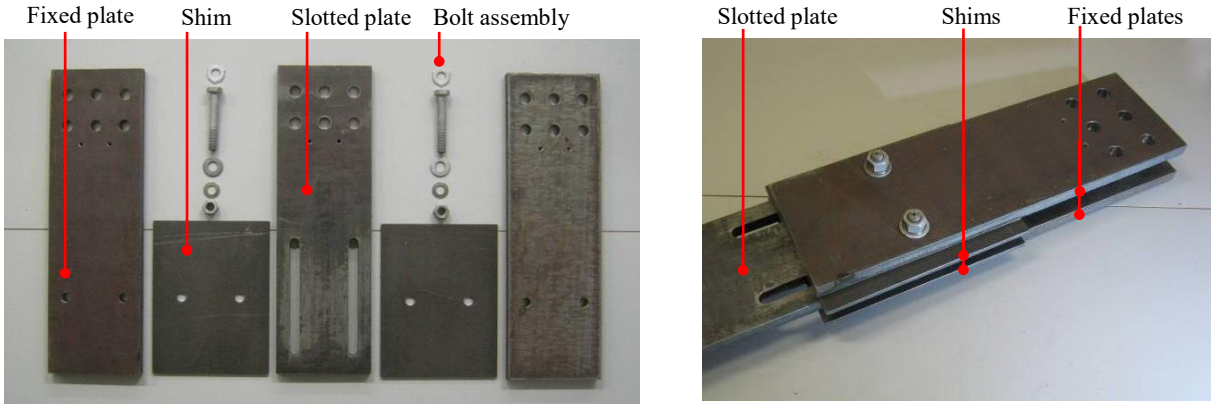

1.a Connection components **1.b Connection assembly – 3D view**

Figure 1: SFC components and assembly

2.2. Applications

SFC can be used to dissipate seismic energy in different structural systems (Pall, 1979; Popov, 1993). In the case of moment resisting frames they can be either placed near to the beam bottom flange in beam-column joints similar to the Asymmetrical Friction Connection (AFC) configuration proposed by Clifton, (2005) or within braces in the case of braced configurations (Pall and Marsh, 1982; Popov, 1993); footing configurations and rotational links are also possible. In beam-column joints the SFC detail dissipates energy against beam rotations and in braces against brace elongations (Figure 2). In both cases the SFC detail is designed to activate the sliding mechanism before any frame component yields, thus protecting the structural system.

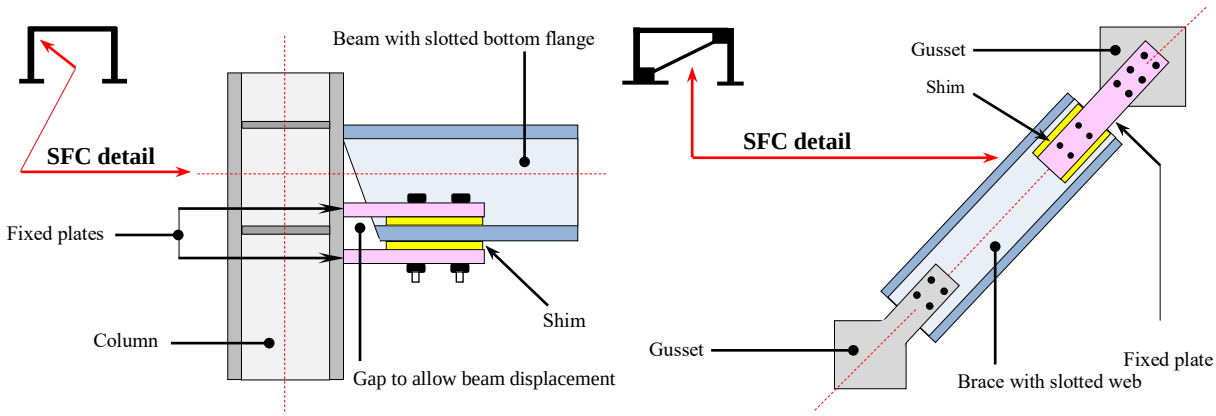

2.a Beam – Column joint configuration **2.b Brace configuration**

Figure 2: Application of SFC on moment resisting frames

3. Materials and Experimental Methods

3.1. Materials

SFC specimens were assembled using 20mm thick Grade 300 steel plates, and two M16 x 110mm Grade 8.8 galvanized bolts with 72mm shank using structural, flat and single Belleville washers. Four types of shim materials were considered as described in Table 1. For each type of shim, three SFC specimens with slot length of 200mm were assembled.

Table 1: Summary of materials used as shims

Material	Specification	Brinell Hardness* (BH)	Thickness (mm)
Steel	Cold Rolled Mild Steel	150	6.0
Bisalloy 80	Bisplate 80	255	6.0
Bisalloy 400	Bisplate 400	400	6.0
Bisalloy 500	Bisplate 500	500	6.0

***** Typical values

3.2. Assembling procedure

SFC connections were assembled using a calibrated torque wrench; the assembling torque was defined as the torque that induces a bolt elongation similar as that one recorded in a tension test when bolts reach the proof load (Figure 3a). Using this definition, a relationship between torque and induced bolt elongation was developed for three bolts where the torque was gradually increased from the finger tight condition to the failure torque (Figure 3b). From this relationship a torque of 300N-m was chosen as assembling torque, this value corresponded to nut rotations of 1/4 –1/2turn.

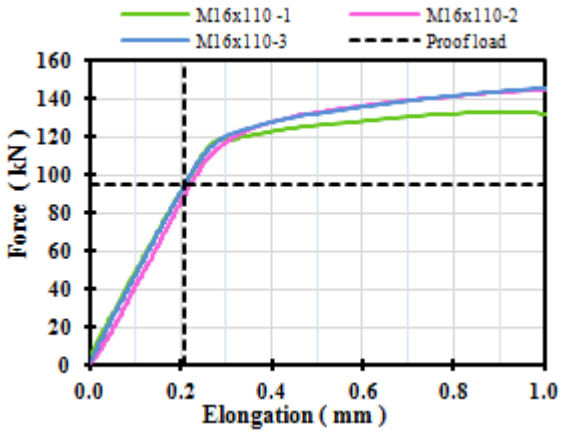

3.a Force – elongation from axial test

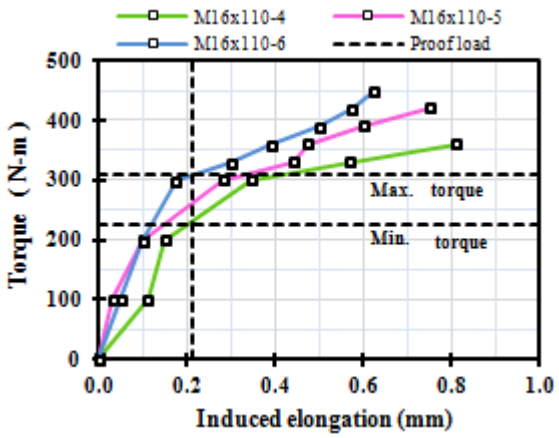

3.b Torque – induced bolt elongation

Figure 3: Assembling relationships for bolts M16 x 110 mm Grade 8.8, using a single Belleville washer and with 70mm grip length.

3.3. Experimental Setup and Displacement Regime

Testing of SFC specimens was conducted using a vertical setup in the Dartec 10MN axial testing machine. Setup comprised of a moving bracket attached to a servo-controlled actuator, and a fixed bracket attached to a rigid crosshead. The slotted and fixed plates of specimens were connected to the moving and fixed bracket respectively by means of 6 M20 Grade 8.8 bolts. This setup was instrumented with a load cell placed in series with the brackets, and a potentiometer placed across the connection stroke (Figure 4). Sliding of specimens was induced by imposing a displacement regime on the moving end of the setup. Displacement regime comprised 20 sinusoidal cycles with maximum amplitudes in the range of 6.25 -100 % of the specimen effective stroke (±95mm) and maximum velocities of 10mm/s.

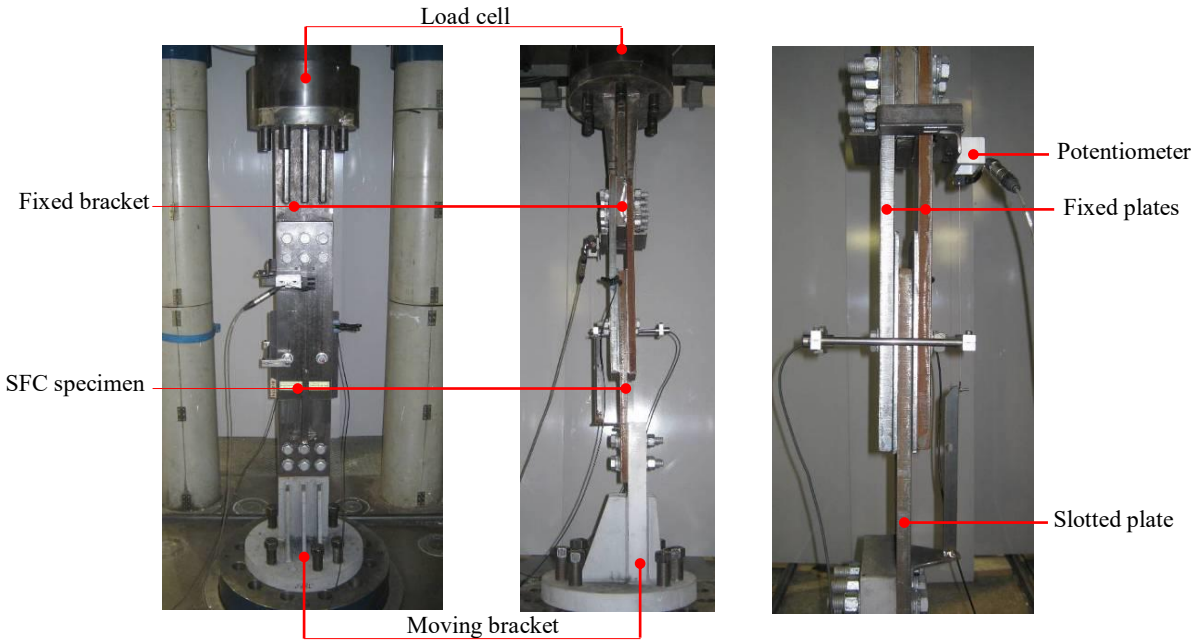

4.a Setup frontal view **4.b Setup lateral view** **4.c SFC on loading**

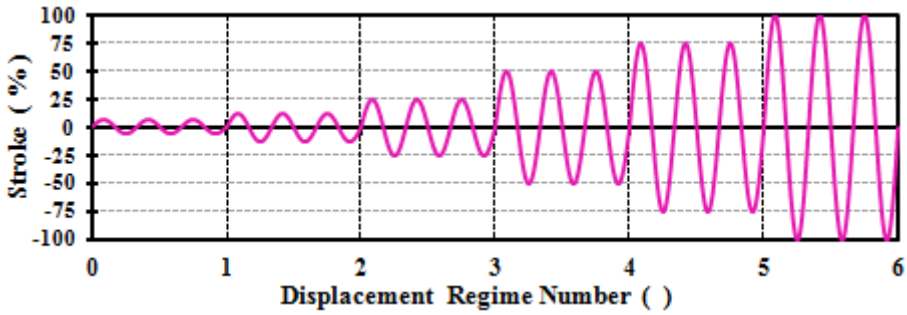

4.d Imposed displacement regime

Figure 4: Testing setup and displacement regime

4. Results and discussion

4.1. Hysteresis loop

Hysteresis loop of Symmetrical Friction Connections can be described as almost rectangular. Loading and reversal loading stages are characterized by a very stiff initial load –

displacement relationship followed by a post-yielding zone with stability dependent on the hardness dissimilarity between the connection plates and the shim material. It can be seen that by increasing this dissimilarity the stability and smoothness of the hysteresis loop are increased (Figure 1). Hysteresis loop of specimens using cold rolled mild steel shims are characterized by post-yielding zones that were stable at the initial cycles and became unstable as the sliding distance was increased (Figure 1a). This instability is due to the development of large volumes of work hardened particles that abraded the sliding surfaces and produced loose of bolt tension when they fell out as debris. A less accentuated abrasive mechanism was noted in specimens using Bisalloy 80 shims; in this case specimens developed hysteresis loops with increased forces up to 25% of the average sliding force at cycles with amplitudes near the full connection stroke (Figure 1b). In contrast, hysteresis loops with stable post-yielding zones across the full connection stroke were developed by specimens using Bisalloy 400 and Bisalloy 500 shims (Figure 1c and 1d). This hysteresis loop stability is attributed to the noticeable difference in hardness between the sliding surfaces that generates small volumes of debris that either adheres to the sliding surfaces or is loose as debris.

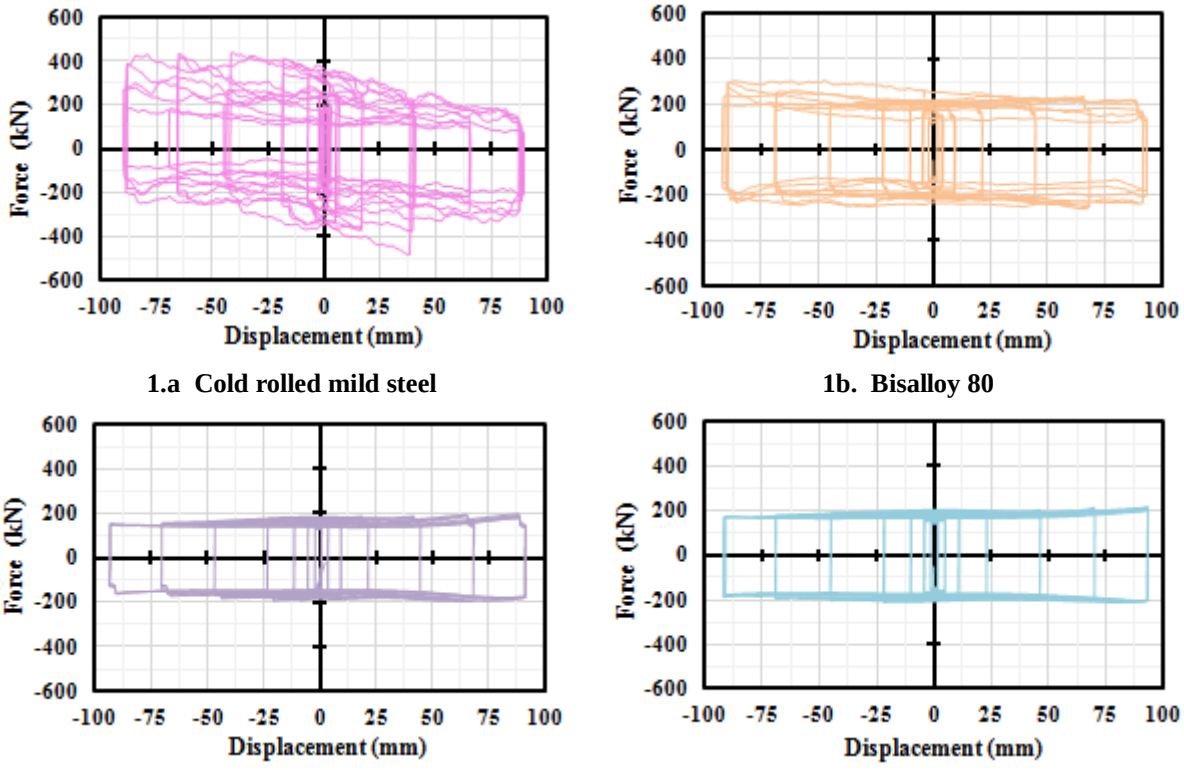

1.a Cold rolled mild steel **1b. Bisalloy 80**

1c. Bisalloy 400 **1d. Bisalloy 500**

Figure 5: Hysteresis loops of SFC using different steel grade shims and 2M16x110mm galvanized bolts

4.2. Effect of hardness on the effective friction coefficient

The effective friction coefficient, defined as the average of the sliding forces developed across the full connection stroke on both shear planes for each bolt, and divided by the proof load was calculated for three specimens at each shim material category (Figure 6). It can be seen that the highest effective friction coefficients are developed when the ratio between the shim hardness and the connection plates hardness is in the range (1-1.7). In this case, the effective friction coefficient is also variable as a result of the hysteresis loop instability

associated with abrasive sliding mechanisms. Lower and less variable values of effective friction coefficients can be developed by using shims materials with hardness values greater than 2.5 times the hardness of the connection plates. This low variability on the effective friction coefficient is associated with the development of adhesive wear sliding mechanisms where only minimum degradation of the sliding surfaces is exhibited. The use of shim materials such as Bisalloy 400 or Bisalloy 500 are recommended given the repeatability and smoothness of the hysteresis loop. Average effective friction coefficients of 0.42 and 0.49 can be considered to predict sliding force of Bisalloy SFC details respectively.

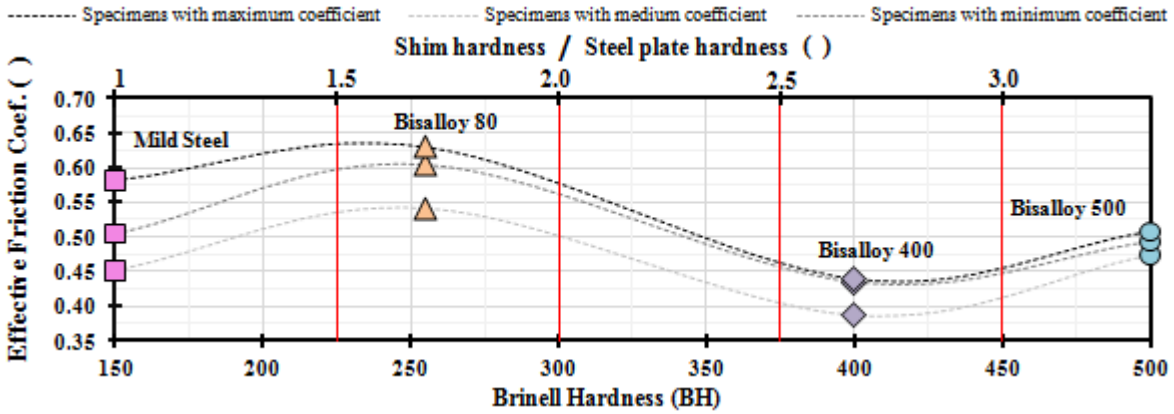

Figure 6: Variation of the effective friction coefficient with the shim material hardness

5. Conclusions

This paper described the hysteretic behaviour of Symmetrical Friction Connections, it was shown that:

i. The hysteresis loop of SFC is almost rectangular and stability of the post-yielding zone depends on the shim material hardness.

ii. Abrasive and adhesive sliding mechanisms were related to the cases where the shim hardness is similar to, and significantly different than, the connection plates hardness respectively. Abrasive sliding mechanisms can be associated with unstable hysteresis loops and adhesive with stable and smooth hysteresis loops.

iii. Magnitude and variability of the effective friction coefficient depends on the ratio between the shim hardness and steel plate hardness. Hardness ratios larger than 3 are recommended to achieve low variability on the effective friction coefficient and stable hysteretic behaviours.

iv. Materials such as Bisalloy 400 or Bisalloy 500 can be considered as alternatives to steel for SFC as reliable and low damage dissipators. Effective friction coefficients of 0.42 and 0.49 can be considered to estimate sliding forces respectively.

6. References

Clifton, G.C. (2005). *Semi-Rigid Joints for Moments Resisting Steel Framed Seismic Resisting Systems. Published PhD Thesis, Department of Civil and Environmental Engineering.* University of Auckland – New Zealand.

Grigorian, C.E. & Popov, E.P. (1994). *Experimental and Analytical Studies of Steel Connections and Energy Dissipaters. Report UCB/EERC-95/13, Engineering Research Center.* San Francisco (USA).

Pall, A.S. (1979). *Limited Slip Bolted Joints – A Device to Control the Seismic Response of Large Panel Structures. Unpublished PhD Thesis, Faculty of Engineering*. Concordia University – Canada.

Pall, A.S. & Marsh, C. (1982). *Response of friction Damped Braced Frames*. *Journal of the Structural Division.* Vol.108 (6), pp 1313 – 1323

Appendix A.6

Design Considerations for Braced Frames with Asymmetrical Friction Connections (AFCs)

Appendix A.6

Design Considerations for Braced Frames with Asymmetrical Friction Connections (AFCs)

J. Chanchí Golondrino
University of Canterbury, New Zealand – National University of Colombia, Manizales - Colombia.

G.A. MacRae, J.G. Chase, G.W. Rodgers & A. Mora Muñoz
University of Canterbury, New Zealand.

G.C. Clifton
University of Auckland, New Zealand.

ABSTRACT: Friction connections are efficient seismic energy dissipaters because they are cheap, easy to build and can dissipate a significant amounts of energy keeping the remainder of the building within the elastic limits. One of the promising applications of this technology is the Asymmetrical Friction Connection concept originally developed and applied in New Zealand. This paper presents an overview of Asymmetrical Friction Connections and possible applications on single, concentrically and eccentrically braced frames. Basic design consideration and possible alternatives for computer modelling of frames applying this concept are also presented. Results from a single braced frame case of study show that the force-displacement response of the frame is bilinear when the connection properties are bilinear. Finally, ongoing research at the University of Canterbury as well as recommendations to promote further research and application of Asymmetrical Friction Connections are proposed.

1 INTRODUCTION

Several studies have been carried out exploring the possibility of applying friction connections as energy dissipaters in structural systems. Analytical results of Pall and Marsh (1982) show that steel braced frames including sliding friction devices have superior seismic performance compared with conventional steel framing systems. Experimental and analytical results carried out by Tremblay (1993) and Grigorian & Popov (1994) on symmetrical friction connections with slotted holes revealed that a stable response can be achieved by providing and adequate sliding material and a defined level of clamping force; furthermore, friction applications on braced frames were found to be an effective alternative for seismic energy dissipation, cost effective and easy to be applied in practice when compared with conventional braced frame systems (Tremblay 1993).

Another alternative of applying friction connections as energy dissipaters is the concept of Asymmetrical Friction Connections, initially developed to be applied in moment resistant steel frame connections by Clifton (2005) and later on improved by MacRae (2010). These studies show that asymmetrical friction connections generate a stable hysteretic response, self-centering properties and minimal damage on the tested subassemblies. For these reasons asymmetrical friction connections were categorized as a low damage alternative for dissipating seismic energy on steel beam-column joints. The same concept has been proposed to be applied in braced frames by Butherworth(1999) and MacRae (2008, 2010). Analytical results show that by placing the connection within braces the frame is enabled to dissipate a significant amount of energy and minimal damage is expected in the structure after a major earthquake. Given that no experimental testing has been carried out on brace connections, research at University of Canterbury is addressing this issue. In relation to this, this paper is written to answer the following questions:

i) Which are the potential advantages of using Asymmetrical Friction Connections in braced frames?

ii) What are some possible configurations of Asymmetrical Friction Connections on conventional braced systems?

iii) Which are the design parameters of Asymmetrical Friction Connections?

iv) What are the basic considerations for design and modeling of braced frames with Asymmetrical Friction Connections?

v) Which is the main research topic of the ongoing research on Asymmetrical Friction Connections at University of Canterbury?

2 ASYMMETRICAL FRICTION CONNECTIONS

Asymmetrical Friction Connections - AFC can be built with three plates and two shims connected by means of high strength bolts as shown in Figure 1. The top plate is provided with standard holes; the central plate is the bottom plate provided with slotted holes to allow its relative movement respect to the arrangement. The bottom plate is A cap plate with standard holes. This plate is a floating plate because is connected to the arrangement through the bolts only. Between top, bottom and cap plate shims with standard holes are placed.

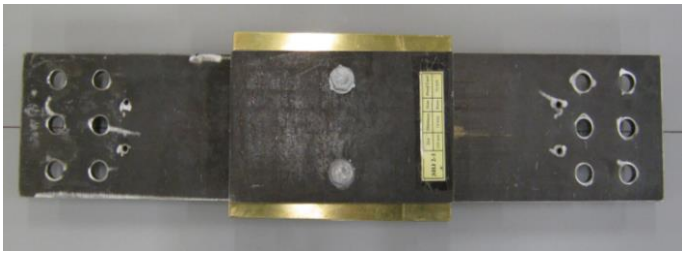

a. Plan view of Asymmetrical Friction Connection

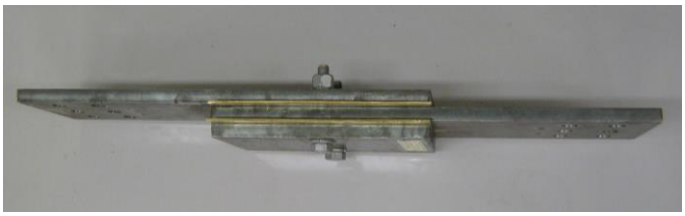

b. Frontal view of Asymmetrical Friction Connection

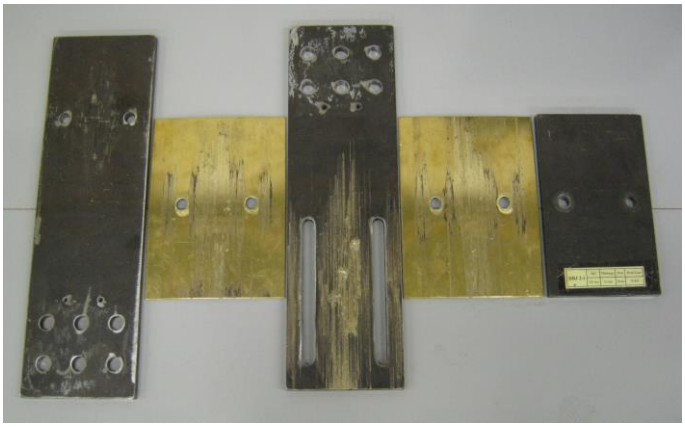

c. Top, bottom, cap plate and brass shims

Fig 1. Tested AFC with brass shims and M16 bolts

Movement in asymmetrical friction connections can be generated by applying a driving force in the central plate, once the sliding mechanism is initiated, friction forces of one half of the magnitude of the driving force are developed in the two interfaces between the central plate and the shims, these forces are transferred to the top and cap plate by shearing and deforming the bolts in double curvature. Hysteresis loop generated by the cyclic mechanism described above has been found on the ongoing research carried out at University of Canterbury to be rectangular when using shims of different materials such as brass, mild steel, aluminium and bisalloy of different grades. Figure 2 presents a hysteresis loop for a 220mm slot asymmetrical friction connection with 2 M16 Grade 8.8 bolts and brass shims.

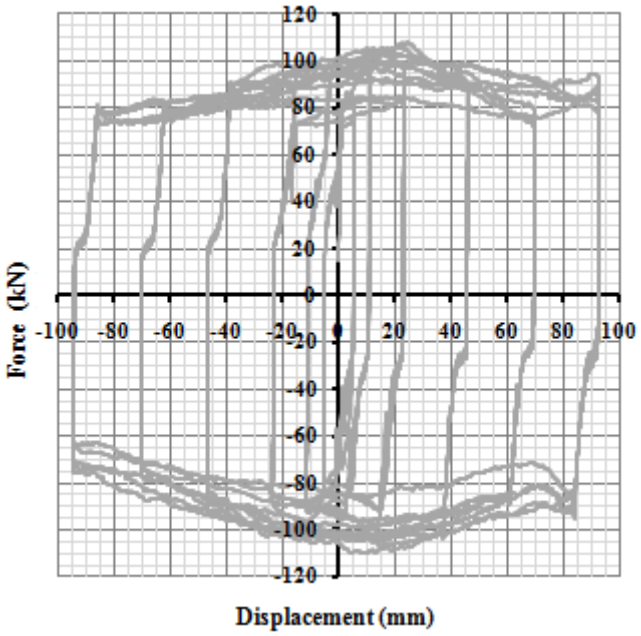

Fig 2. Hysteresis loop for AFC with brass shims and 2 bolts M16 grade 8.8

3 APPLICATION ON BRACED FRAMES

Conventional braced frames are structural systems based on dissipating energy by yielding localized components of the structural system. In order to reduce the damage level of these systems it is proposed the use of Asymmetrical Friction Connections at specific locations of the frame providing following advantages: i) the deformation capacity of the system can be increased by using long slotted holes, ii) the strength of the brace can be controlled easily by using different number and size of bolts, iii) no damage is expected in the frame and low damage is expected in the connection itself, and most importantly iv) thecost of construction is similar as conventional steel construction. Several applications of Asymmetrical Friction Connections for steel braced frames have been proposed by MacRae & Clifton (2010) and Butterworth (1999). Some of them are currently under experimental research at University of Canterbury and are described below.

3.1 *Single Braced Frames*

For single braced frames the Asymmetric Friction Connection can be placed at the end of the brace where the gusset has slotted holes and is bolted to the beam column joint as presented in Figure 3a. This disposition is suitable for any replacement required if the gusset undergoes severe damage. Another possibility is to consider the brace divided in two components bolted to the gussets at the ends and

joined by the Asymmetrical Friction Connection detail as presented in Figure 3b. This configuration can generate a lighter design given the short span covered by the AFC detail.

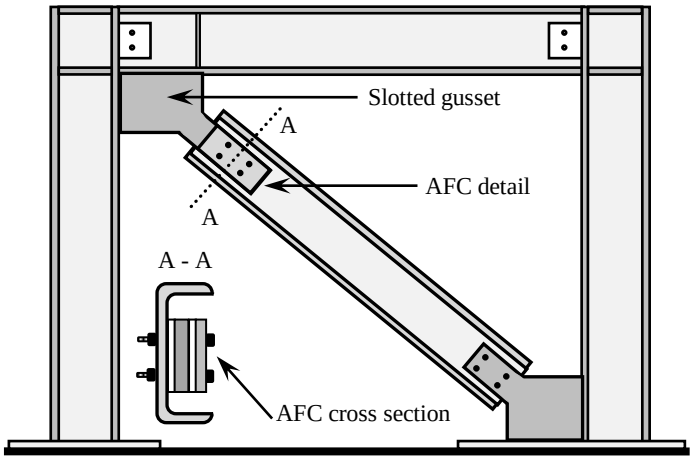

a. AFC detail placed at the end of the brace

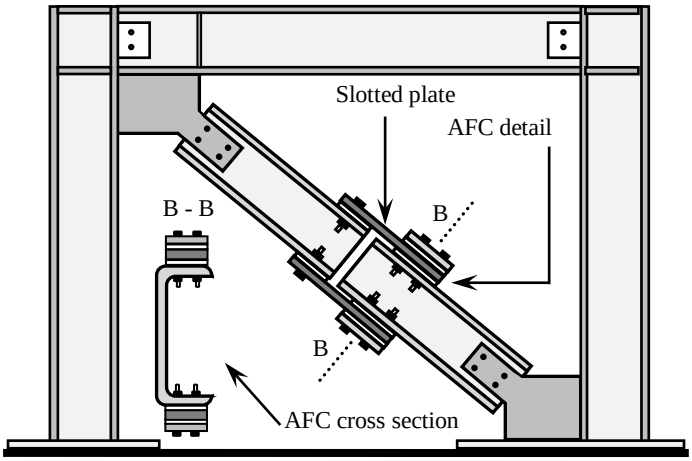

b. AFC detail placed within brace

Fig 3. AFC detail on single braced frames

3.2 *Two brace concentrically braced frames*

Three possibilities can be considered for concentrically braced frames with two braces per bay, the first possibility considers the AFC detail in a vertical arrangement placed below the beam bottom flange as presented in Figure 4a; in this configuration a slotted gusset is bolted or welded to the beam bottom flange, braces are connected to a plate with standard holes located behind the gusset and the cap plate is floating in front of the gusset. Figure 4b presents the second possibility where the AFC detail is placed in a horizontal arrangement, in this configuration the beam bottom flange is slotted and braces can be welded or bolted to a vertical plate welded to a horizontal plate located below the beam; two cap plates are required to be placed above the beam bottom flange. The third possibility is a similar configuration as that one described for single braced frames using the AFC detail within the braces as presented in Figure 3a or 3b. It can be seen that the first and second configuration are based on sliding the beam forward and backward respect to the plate attached to the braces while the third configuration uses sliding in each brace at the same time.

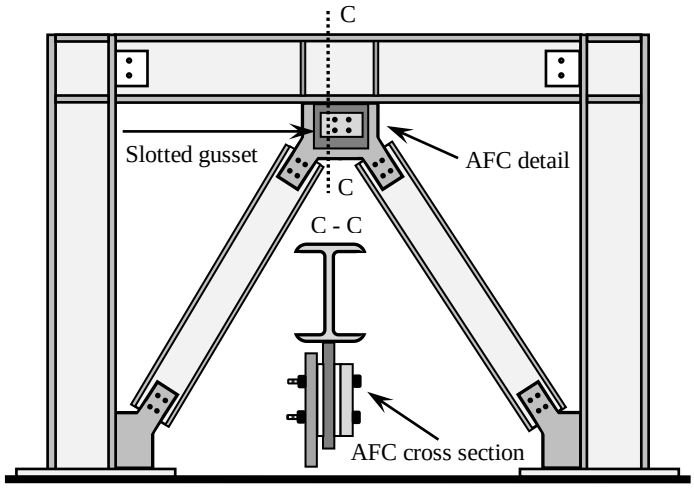

a. AFC detail placed on a vertical arrangement

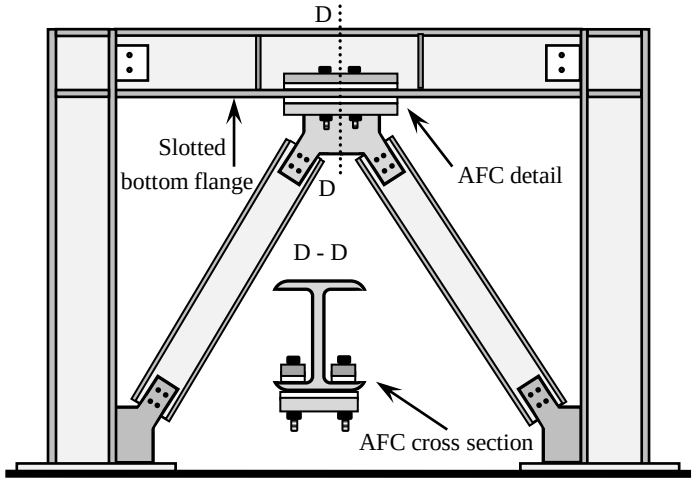

b. AFC detail placed on a horizontal arrangement

Fig 4. AFC detail on two brace concentrically braced frames

3.3 *Eccentrically braced frames*

For eccentrically braced frames the AFC detail is placed within braces following same principle applied for single braced frames as shown in Figure 4. In this configuration it is expected that both AFC details slide at the same time, this condition is difficult to be achieved because the presence of issues such as construction tolerance and variability on bolt tension and friction coefficients values. As a consequence the beam will be subjected to an additional vertical force generated by the brace without sliding; therefore special design requirements should be considered when designing the beam for this frame configuration.

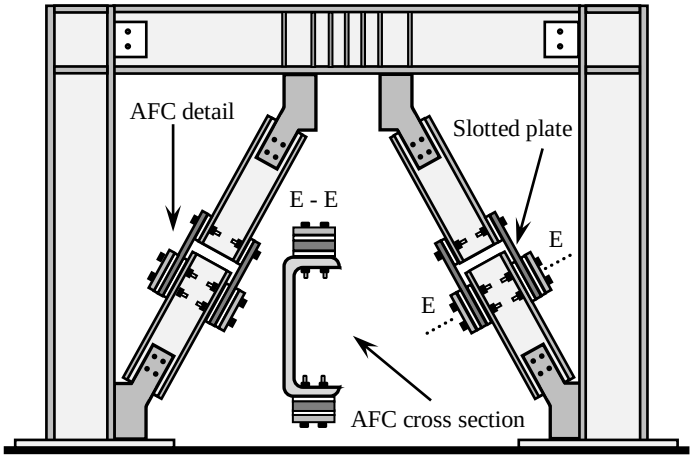

Fig 5. AFC detail on eccentrically braced frames

4 DESIGN OF AFC CONNECTION AND BRACE

4.1 *Slot Length*

For AFC details attached to beam bottom flanges the slot length, L, can be calculated using Equation 1, where Δ is the maximum horizontal displacement of the frame at the level where the connection is located, d is the standard hole diameter for the bolt size used in the connection, and ϕs is an oversize factor (>1.0) to avoid any localized yielding at the ends of the slot caused by bolt bearing. Equation 1 can be also applied for AFC details placed within braces if the maximum horizontal displacement Δ is replaced by the brace elongation, *db*, instead. Equation 2 presents a conservative approach to calculate the brace elongation from considering an elastic single braced frame pinned in the base subjected to horizontal load with span, S, height, H, brace length, B, and maximum horizontal displacement, Δ.

$$L = \phi s \times (2\Delta + d) \quad (1)$$

$$db = \sqrt{H^2+(S+\Delta)^2} - B \quad (2)$$

4.2 *Sliding Force*

Following a similar approach to MacRae (2010), the sliding force Fs can be expressed in terms of the number of shear planes n, the proof load per bolt N_{tf} and the friction coefficient between steel and the shim material μ as shown in Equation 3. In this equation the number of shear planes should be considered as two, values of the proof load for bolts Grade 8.8 are recommended by New Zealand Standard, and values of friction coefficient has been reported by MacRae et al (2010) to be in the range 0.21 to 0.22 for steel and brass shims; however, values of 0.26 have been recently found for brass shims in the ongoing research on real scale asymmetrical friction connections tested by the authors at University of Canterbury.

$$Fs = \mu \times n \times Ntf \quad (3)$$

4.3 *Hysteresis Loop*

Recent ongoing research at the University of Canterbury on real scale Asymmetrical Friction Connections has shown that the hysteresis loop is almost rectangular in component tests to larger displacements. This is contrast with the bilinear loop shape from previous work on small subassemblies and beam column joint configurations carried out by Clifton (2005) and MacRae et al (2010). Considering this disagreement a first approach to the model of the hysteresis loop can be made by considering a rectangular shape with a maximum force level equal to the sliding force magnitude and with amplitude equal to the slot length of the connection. Figure 6 shows a hysteresis loop model for an asymmetrical friction connection with 2 M16 grade 8.8 bolts, brass shims and 220 mm slot.

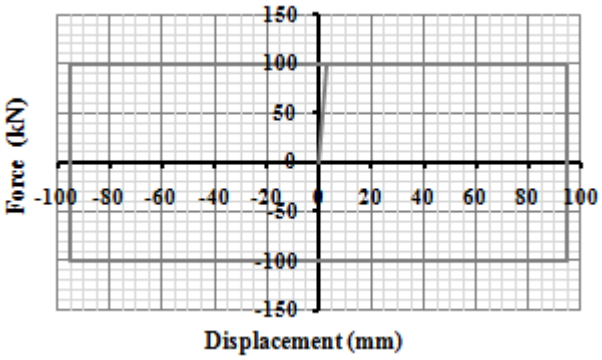

Fig 6. Hysteresis loop model for AFC with 2 bolts M16 Grade 8.8, brass shims and 220 mm slot

5 BASIC DESIGN CONSIDERATIONS FOR FRAMES WITH AFC DETAILS

Design of AFC frames follows similar steps to those used for conventional braced frames. However; some special considerations should also be taken into account when modeling the frame, and designing and detailing braces. A general overview of these considerations is presented below.

5.1 *Overstrength factor*

An overstrength factor (>1.0) should be included in the design process of the frame in order to consider any variability of the sliding force magnitude of the connection due to uncertainties on friction coefficients or on bolt tensioning force levels.

5.2 *Design and detailing of braces*

The design criteria of braces is based on providing a cross section that allows sliding on the Asymmet-

rical Friction Connection prior to the brace reaching a limit state of strength such as yielding or buckling (Tremblay 1993). The limit state of deformation can be controlled by sizing adequately the length of the slot according the expected drift limits of the frame using a simple approach as that one defined by Equation 2. Given that the energy dissipation mechanism of Asymmetrical Friction Connections is based on axial and shear forces, an adequate brace detail satisfying the transmission of these forces and minimizing any moment transmission from the beam- column joint should be provided. According to the Uniform Force Method (AISC 2005), this condition can be achieved by choosing the geometry of the end brace connection so that the axes of the brace, column and beam intercept at the geometrical centre of the panel zone as shown in Figure 7. In addition, the end brace connection should be designed as pinned so that brace alignment issues do not cause second order effects.

5.3 *Structural Analysis Modelling*

Modelling of AFC frames can be carried out using software such as SAP2000 (Computer and Structures Inc. 2008). In order to develop a frame model consistent with the design considerations describe above, brace elements must be modeled realising the internal moments at the ends; thus, braces are allowed to transmit axial and shear forces only. Asymmetrical Friction Connections can be modeled as nonlinear links with elasto- plastic hysteresis loops defined by the sliding force and the effective slot length. A first approach to the force displacement behaviour of the frame can be obtained through a static non linear pushover analysis or alternatively a more detailed approach can be made by carrying out a time history analysis.

5.4 *Single braced frame case of study*

To illustrate the performance of a single AFC braced frame a simple model with a 3.0 m bay and 2.50 m story height was subjected to static non linear pushover analysis. A 200UC59.5 section was used for beam and column elements and a channel section 250PFC for the brace, both sections with a nominal yield stress of 300 MPa. Connections in the frame model were defined as pinned in the base and rigid between the column and the stub beams, additional pinned connections were defined between the stub beams and the remaining beam segment as shown in Figure 7. The Asymmetrical Friction Connection with an slot of 220 mm and within the brace follows the model presented in Figure 3a, using the Equation 4 and considering brass shims with a friction coefficient of 0.26 and four M16 grade 8.8 bolts tensioned to a proof load per bolt of 95 kN the sliding force of the connection is 200 kN. Applying the design and modeling considerations described above the pushover curve presented in Figure 7 was obtained. It can be seen that the maximum response of the frame in terms of lateral displacements and base shear can be controlled easily by the sliding force magnitude of the Asymmetrical Friction Connection, furthermore, the force – displacement response can be described as the superposition of a steep segment generated before the sliding mechanism occurs and a flat segment generated once the sliding mechanism is activated.

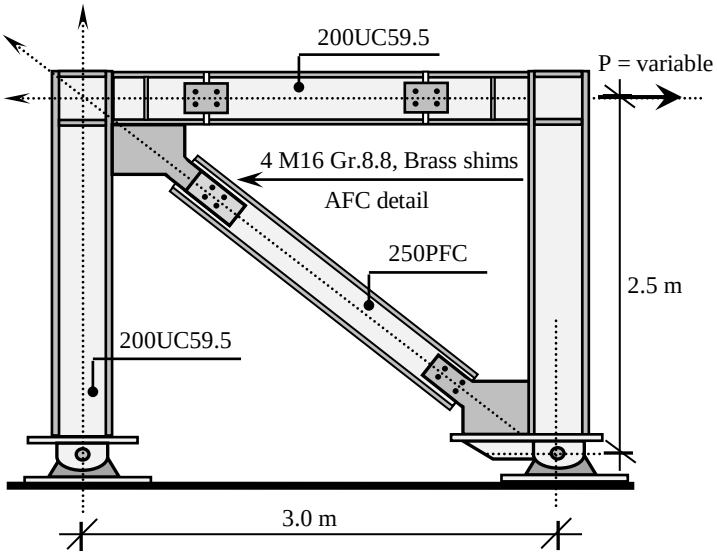

a. Configuration of AFC single braced frame

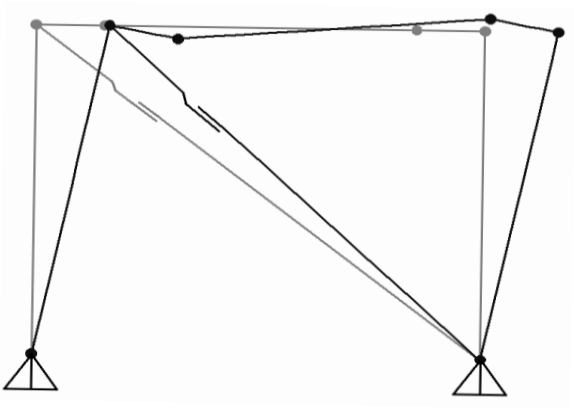

b. Model of AFC single braced frame

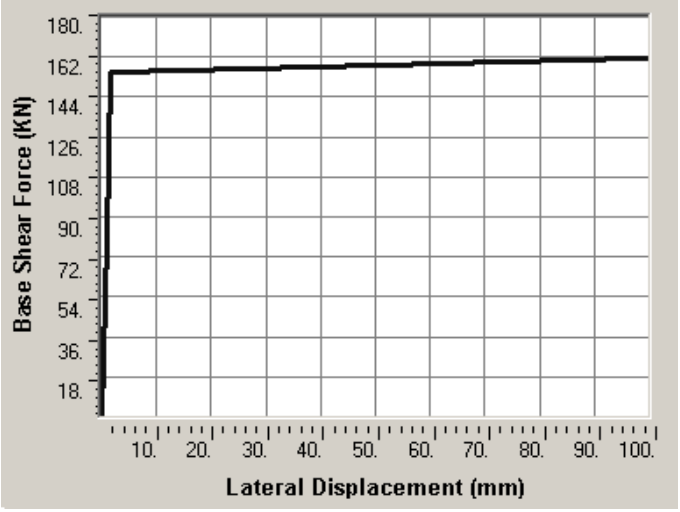

c. Pushover curve of single braced frame

Fig 7. Model and results of AFC frame case of study

6 ONGOING RESEARCH

Given the potential advantages of the AFC structural system, research work continues at University of Canterbury in order to validate its application as a low damage alternative for seismic active regions. Ongoing research is addressed to describe the behaviour of asymmetrical friction connections considering 500 and 750 grade bisalloy shims, high velocity load regimes, post-fire and corrosion effects; furthermore, a full scale frame including AFC details as that one presented in Figure 7 using single, concentrically and eccentrically brace configurations and without braces is planned to be tested in order to quantify the brace effect and to develop design regulations for braced systems applying this concept.

7 CONCLUSIONS

This paper describes possible applications and design regulations of asymmetrical friction connections (AFC) on conventional braced frames. It was shown that:

i. Among the potential advantages that AFC systems offer over conventional steel framed construction are: i) by using long slots large deformation capacities can be achieved, ii) the strength of the brace can be controlled through number and size of bolts, and importantly, iii) no major damage is expected in the connection; while some bolts may be affected they can easily be replaced.

ii. Asymmetrical friction connections can be used on different conventional braced frames configurations, for example, on single braced frames and on eccentrically braced frames they can be placed either at the end of the brace or at any place within the brace, and for concentrically braced frames they can be placed in a link below the beam or in the bottom flange of the beam.

iii. The design process of Asymmetrical Friction Connections is based on strength and deformation demand requirements. The strength of the connection is governed by the friction factor developed between shims and steel components as well as by the size and number of bolts. Deformation demand is based on the expected frame drift; it can be controlled by giving the connection an adequate slot length. Simple expressions to quantify connection strength, deformation demand and the overstrength factor for frame design pursposes were presented.

iv. The design of AFC frames is similar to that for conventional braced frames, special considerations on design, detailing and modeling were presented. A single braced frame case of study including design values and results from a static non linear pushover analysis were also presented. Results show that the force- displacement response of the frame can be described as bilinear with an initial steep segment followed by a flat segment with a force level around to the sliding force of the asymmetrical friction connection.

v. Ongoing research at University of Canterbury is focussed to further insight into the behaviour of Asymmetrical Friction Connections (AFC) considering 500 and 750 grade bisalloy shims, high velocities, post-fire and corrosion effects; as well as on the quasi-static cyclic behaviour of full scale AFC braced models.

8 REFERENCES

AISC. (2005). *Steel Construction Manual.* American Institute of Steel Construction. 13th Edition, Chicago – USA.

Butterworth, J. W. (1999). Seismic Damage Limitation in Steel Frames Using Friction Energy Dissipators. *6th International Conference on Steel and Space Structures* -September 1-2. Singapore.

Clifton, G.C. (2005). Semi-Rigid Joints for Moments Resisting Steel Framed Seismic Resisting Systems. *Unpublished PhD Thesis, Department of Civil and Environmental Engineering.* University of Auckland – New Zealand.

Grigorian, C.E. & Popov, E.P. (1994). Experimental and Analytical Studies of Steel Connections and Energy Dissipaters. *Report UCB/EERC-95/13, Engineering Research Center.* San Francisco – USA.

MacRae, G. A. (2008). A New Look at Some Earthquake Engineering Concepts. *M. J. Nigel Priestley Symposium Proceedings*, IUSS Press, 2008.

MacRae, G.A., Clifton, C.G., MacKinven, H., Mago, N., Butterworth, J., Pampanin, S. (2010). The Sliding Hinge Joint Moment Connection. *Bulletin of the New Zealand Society for Earthquake Engineering*, 43(3), 202 -212.

MacRae, G.A & Clifton, G. C. (2010). New Technology Applications, Recent Developments and Research Directions for Seismic Steel Structures in New Zealand. *Asia Conference on Earthquake Engineering*, Bangkok, Thailand, 1-3 December.

Pall, A.S. & Marsh, C. (1982). Response of friction Damped Braced Frames. *Journal of the Structural Division*. Vol.108 (6), pp 1313 – 1323.

Computer and Structures Inc. (2008). Analysis Reference Manual for SAP2000. Berkeley, California, United States of America.

Tremblay, R. (1993). Seismic Behaviour and Design of Friction Concentrically Braced Frames for Steel Buildings. *Unpublished PhD Thesis, Department of Civil Engineering.* University of British Columbia – Canada.

Appendix A.7

Low Damage Braces Using Asymmetrical Friction Connections (AFCs)

Appendix A.7

Low Damage Braces Using Asymmetrical Friction Connections (AFCs)

J. Chanchi Golondrino

University of Canterbury, New Zealand – National University of Colombia, Colombia

R. Xie, G. MacRae, G. Chase, & G. Rodgers

University of Canterbury, Christchurch, New Zealand

C. Clifton

University of Auckland, Auckland, New Zealand

2014 NZSEE Conference

ABSTRACT: Braces equipped with Asymmetrical Friction Connection (AFCs) details, assembled with Bisalloy 500 shims and placed at one end of the braces, have been tested quasi-statically. It is shown that braces equipped with AFC details are characterized by a repeatable hysteretic behaviour with strength degradations up to 10%. This degradation corresponds to the case where braces are subjected up to 40 cycles across the effective stroke of the connection with no components replaced or bolts re-tensioning. Also, out-of-plane brace deformation slightly causes a change in strength with axial displacement. Effective friction coefficients ranging between 0.16 and 0.20 were obtained for AFC braces.

1. INTRODUCTION

The concept of Asymmetrical Friction Connections (AFC) was recently developed and applied as energy dissipater in steel moment resisting frames systems in New Zealand (Clifton 2005). Testing of the connection subassembly as well as beam-column joints equipped with this type of connection have demonstrated that this technology can be considered as a reliable means of dissipating energy and controlling the level of damage of structural systems subjected to severe seismic events (MacRae et al. 2010) . The initial development and applications of this technology was based on placing AFC details in beam-column joints, where energy is dissipated as the beam rotates and overcomes the friction resulting from the total clamping force provided by bolts in the AFC detail (Clifton 2005). Another configuration that has been proposed by several researchers is based on placing the AFC detail at the end or within braces, where energy is dissipated as the brace experiences axial elongations (Butterworth 1999, MacRae 2008, Chanchi et al. 2012). This configuration can be used in different structural systems such as single, concentrically and eccentrically braced or it can be also used to retrofit existing buildings. The brace configuration can be considered more versatile than the beam-column configuration not only because offer more possibilities of placing AFC details according the structural needs; but also because braces using this type of technology can be assembled on the shop, which enhances the quality control of the assembling process and reduces the erection time of the structural system. To date there are no details of any experimental programme showing the behaviour of braces equipped with AFC details; for that reason this paper aims to describe the quasi-static hysteretic behaviour of braces equipped with AFC details at one end of the brace (brace-gusset connection type).

2. CONCEPT

AFC braces are braces equipped with an Asymmetrical Friction Connection detail (AFC) that can be either placed at one end of the brace or within the brace. In this type of braces the AFC detail is considered as an energy dissipater that absorbs energy via friction, and protects the brace from any limit state such as yielding or buckling. Friction in AFC braces is developed when a slotted plate attached to one end of the brace is pulled or pushed across two shear planes generated by two shims

placed at both sides of the slotted plate and that are clamped to the brace section by means of high strength bolts and a cap plate (Fig. 1).

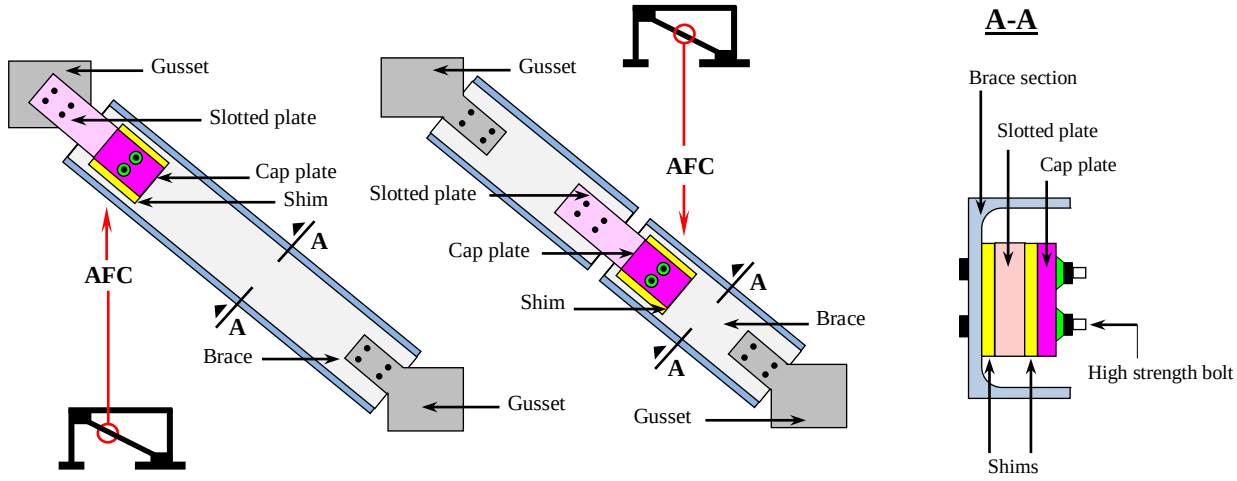

a. AFC braces longitudinal view **b.** AFC detail cross section

Figure 1. Possible configurations of AFC braces

3. APPLICATIONS

AFC braces can be considered as a passive damping solution to dissipate seismic energy in braced frames. Structural systems with single, concentrically, and eccentrically brace configurations can be implemented using AFC braces (Fig. 2). In these systems, AFC braces dissipate seismic energy as the structural systems deform laterally and induce axial forces that trigger the sliding mechanism in the AFC details (Butterworth 1999, MacRae 2009, Chanchi et al. 2012). Once the sliding mechanism is activated, braces act as fuses that allow the slotted plate to slide at a constant load; thus limiting the amount of seismic force that the structural system can absorb during a seismic event. The design methodology for this type of structural systems is based on considering the load that activates the sliding mechanisms on AFC braces for computing the structural system load demand, and for designing the different structural members. By doing that, no limit stage is reached before or when the sliding mechanisms are activated; so that the structural system can deform at a predefined load with no structural damage.

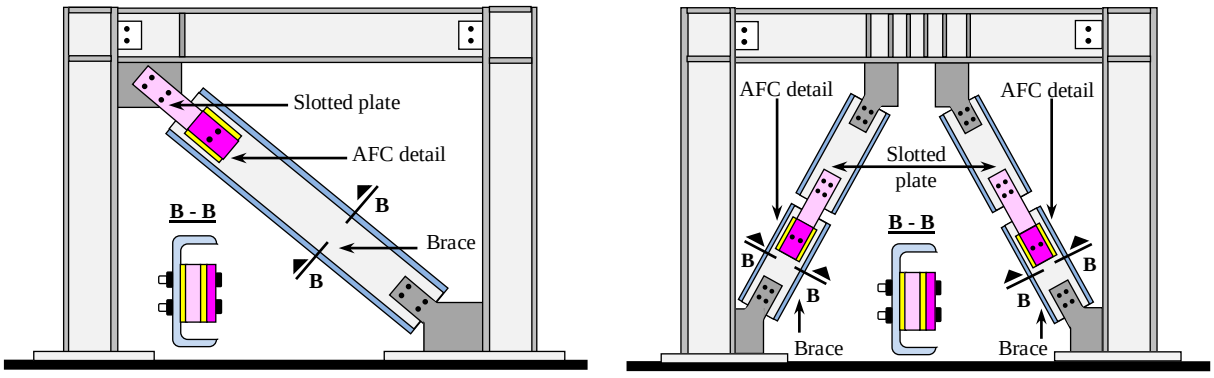

a. Single braced system with AFC brace **b.** Eccentrically braced system with AFC braces

Figure 2. Application of AFC braces in braced structural systems

AFC braces are desirable not only because the force that triggers the sliding mechanism can be accurately predicted when using high hardness shims such As Bisalloy 400 or Bisalloy 500 **(**Chanchi 2012); but also because the assembling process as well as pricing are similar to conventional bracing systems.

4. MATERIALS

Braces were assembled using Grade 300 steel hot rolled profiles with parallel flange channel section (250PFC). At one end of braces the channel web was used as fixed plate to assemble the AFC detail; at the opposite end of braces as well as at the end of slotted plates, slip critical connections of 6 M24 Grade 8.8 bolts were used (Fig. 3a). The AFC detail was characterized by a 200mm slot, 6mm thick Bisalloy 500 shims, and 2 M16 Grade 8.8 bolts of 130mm length (100mm grip length) with single Belleville washers. The slotted and cap plates were assembled using Grade 300 steel plates of 40mm and 16mm thickness respectively. To avoid bearing failure of the channel web due to the force transmitted by bolts at the AFC detail location, the web of the channel was strengthen by welding a 16mm thick Grade 300 steel plate (Fig. 3b).

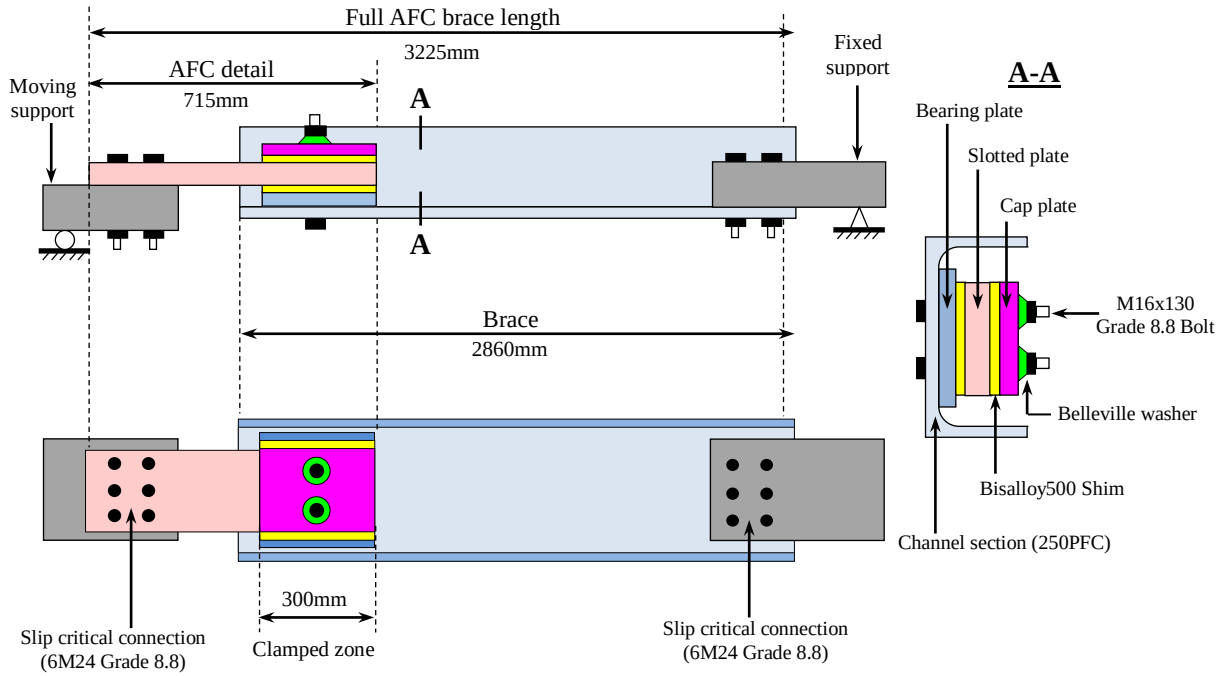

a. AFC brace longitudinal brace configuration **b.** Cross section at the AFC detail

Figure 3. AFC brace specimen configuration

5 METHODS

5.1 Assembling Methods

Assembling of the AFC detail was carried out using a calibrated torque wrench. The torque required to tension the bolts up to the proof load (proof load torque) was extrapolated from a relationship between torque and induced bolt elongation. This relationship was developed by increasing the torque and recording the bolt elongation on two bolts with same assembling configuration as that one used in the brace (Fig. 2a). The bolt elongation used to extrapolate the assembling torque was defined as the elongation exhibited by two bolts when reaching the proof load from tensile testing (Fig. 2b). Using the above methodology a torque value of 310N-m from the hand tight condition was defined as proof load torque. This torque value corresponds to a nut rotation between 1/4 and 1/2 turn when using the nut rotation method.

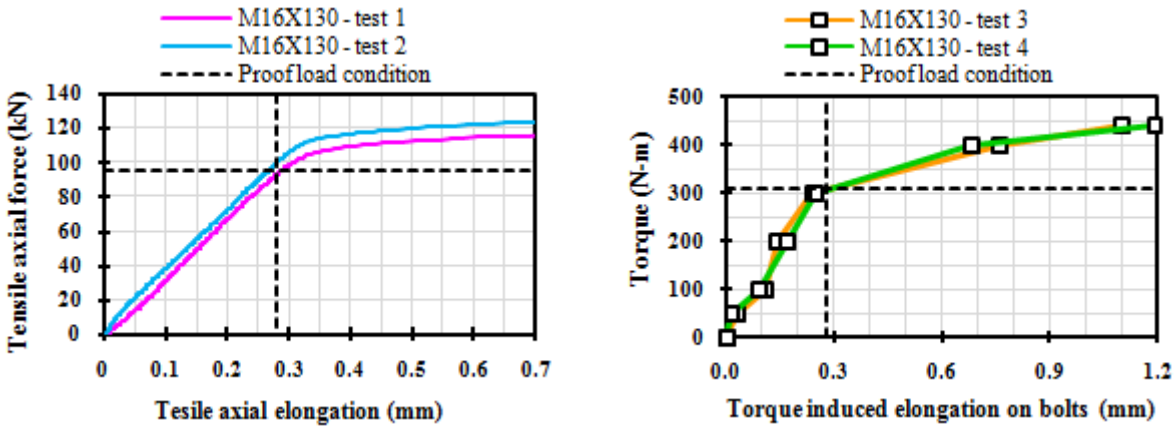

a. Tensile testing relationship **b.** Torque – induced bolt elongation relationship

Figure 4. Relationships used for assembling AFC details

5.2 Testing Methods

Braces were tested in a horizontal setup constituted by a fixed and a moving support. The fixed support was assembled with a bracket bolted on a reaction frame, and the moving support with a bracket attached to an actuator bolted on a reaction tower. Ends of the braces were bolted on the fixed and moving support by using slip critical connections. The ends of braces with AFC detail were bolted on the moving support, so that forces imposed by the actuator could drive the slotted plated as the stroke of the actuator is developed; the other end of the brace was bolted to the fixed support. This setup was instrumented with a load cell in series with the actuator, one extensometer placed horizontally across the brace length, and four extensometers placed vertically at each quarter of the brace length (Fig. 5a).

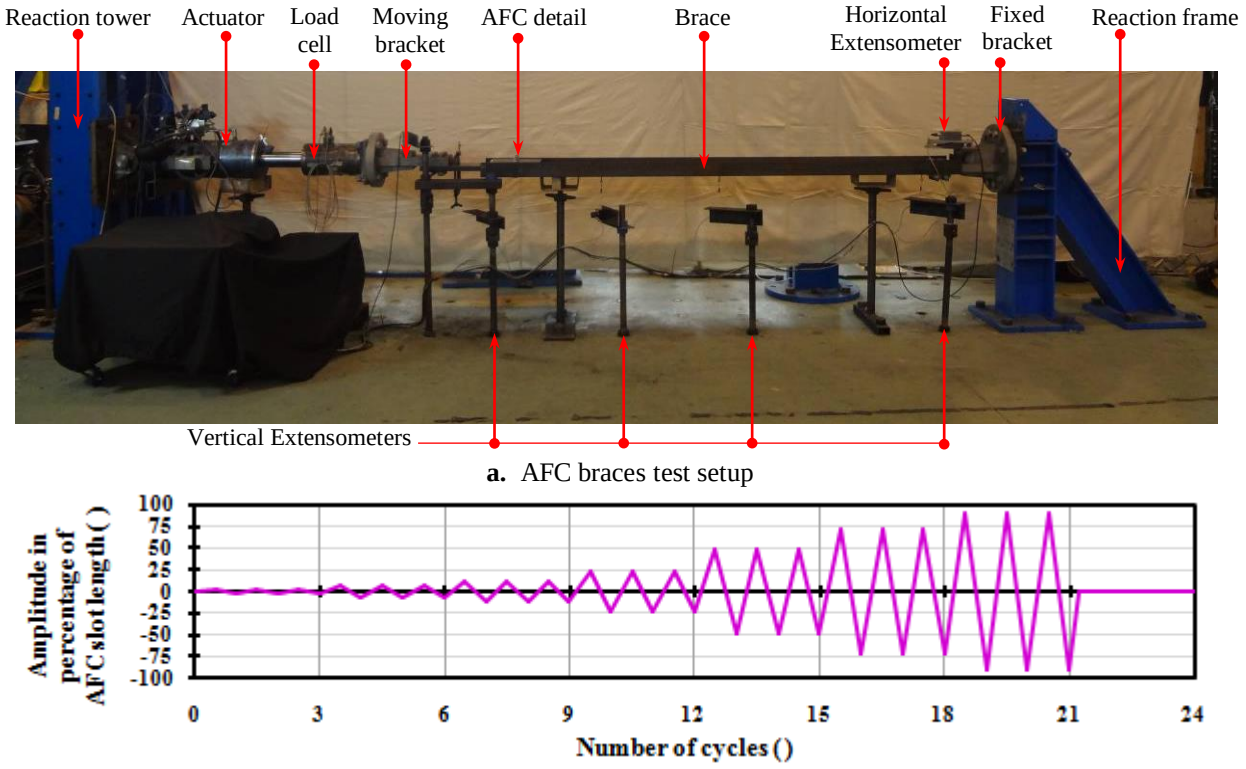

a. AFC braces test setup

b. Displacement regime

Figure 5. AFC braces test setup and imposed displacement regime

Two tests were conducted keeping the initial brace, and at each test the slotted plate, shims, cap plates, and bolts were changed. Testing of each specimen was carried out by applying on the actuator two runs of a controlled displacement regime. No bolt re-tensioning was applied after the first run of the displacement regime, so that the degradation of sliding surfaces and loss of bolt tension can be indirectly observed when comparing hysteresis loops of the first and second run. The displacement regime was applied to a constant velocity of 3mm/s, and it comprises 20 sawtooth cycles with amplitudes between 3 and 90% of the slot length of the AFC detail (Fig. 5b).

6 RESULTS

6.1 Hysteresis loop

Hysteresis loop of AFC braces is almost rectangular, and is characterized by four stages where the stiffness of AFC braces change from a very steep tendency to an almost horizontal tendency (Figs. 6a, b). In the initial stage AFC braces exhibited a very steep stiffness due to the elastic stiffness contribution of the brace and the AFC detail components. No apparent sliding of any of the AFC detail components is presented in this stage (Fig. 6c). In the second stage, the slotted plate partially slides dragging the cap plate and both shims; which in turn push and displace bolts for a distance equal to the construction tolerance of the holes on the web channel section (Figure 6d). Given that slotted plate, cap plate, shims and bolts freely displace with no restriction until bolts reach the edge of the holes on the web channel section, AFC braces exhibit a loss of stiffness. In the third sage, bolts come into bearing with the web channel section; thus rapidly increase the stiffness of AFC braces. Bolts behave as cantilever beams supported on the web of the channel section and transversely loaded by shims and cap plate (Figure 6e). The stiffness exhibited by braces in this stage is less than the initial stiffness; that is because the initial stiffness of the AFC detail is reduced by the influence of the flexural stiffness of bolts. The fourth stage is termed post-yielding zone given that the sliding mechanism of the slotted plate is fully activated and the slotted plate can be driven to different sliding distances. In this stage the stiffness of AFC braces adopts an almost horizontal tendency as the slotted plate slides (Figure 6f).

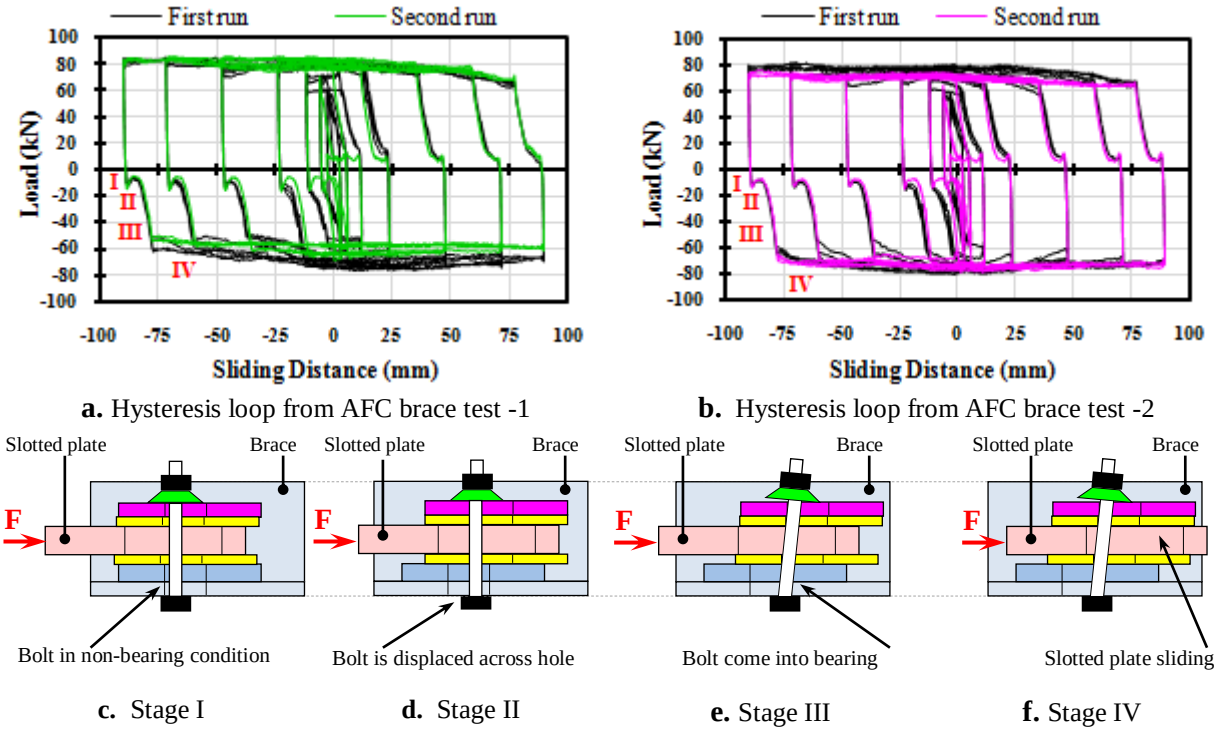

a. Hysteresis loop from AFC brace test -1 **b.** Hysteresis loop from AFC brace test -2

c. Stage I **d.** Stage II **e.** Stage III **f.** Stage IV

Figure 6. Hysteretic behaviour of AFC braces and development of sliding mechanism in compression

The force that fully activates the sliding mechanism of AFC braces is termed sliding force, and values exhibited on the tension side of the hysteresis loop (top side) are 10% bigger than those on the

compression side. This difference is attributed to bending issues of the non-clamped zone of the slotted plate, and that are caused by the asymmetry of the connection that transfers the load from the actuator to the slotted plate.

6.2 Strength Degradation

When comparing hysteresis loops obtained on the first and second run of the displacement regime for two tests of AFC braces; it can be seen that sliding forces in the second run range between 90 and 95% of the sliding forces recorded in the first run. These reductions on sliding forces are attributed to the loss of bolt tension presented as the surfaces of the slotted plate and shims degrade. Degraded material can be described as fine debris that can be associated with adhesive sliding mechanisms. In this type of sliding mechanism the product of degradation either adheres to the sliding surfaces or it is pushed out of the clamped zone producing loss of bolt tension (Grigorian & Popov 1994, Chanchi et al. 2011). Given that the strength degradation that AFC braces exhibited for a total of 40 cycles distributed across the effective slot of the AFC detail was only up to 10%, and considering that the adopted displacement regime is characterized by a cumulative travel that is approximately 150 times of that referenced by Grigorian & Popov 1994 as the maximum observed in structural systems using braces with slotted bolted connections subjected to severe earthquakes; it can be argued that AFC braces are a low damage solution that can be implemented in new structural systems to dissipate seismic energy, or as a possible solution to upgrade the seismic strength of existent structural systems.

6.3 Effective Friction Coefficient

The effective friction coefficient (Equation 1) is defined as the ratio between the total sliding force ($F_{sliding}$) from the two bolts considering the two shear planes and the minimum specified assembling force represented by the bolt proof load (F_{proof}).

$$\mu_{effective} = \frac{F_{sliding}}{2 \times 2 \times F_{proof}} \tag{1}$$

The effective friction coefficient was calculated at different sliding distances for the first run of the displacement regime in both tests of AFC braces. For each sliding distance, the sliding force in Equation 1 was considered as the average sliding force assessed across the tensile and compressive post-yielding zones of the respective hysteresis loop. In both tests it can be seen that the effective friction coefficient varies with the sliding distance, and this variation is more accentuated for sliding distances less than 24mm (Fig. 7a).

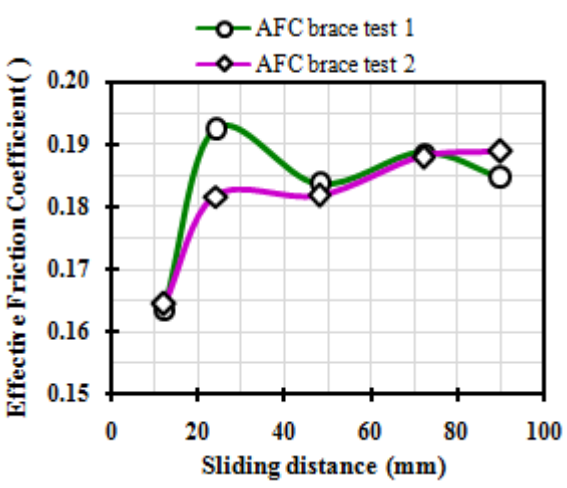

a. Effective friction coefficient

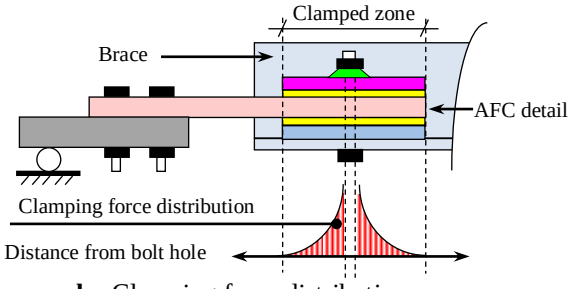

b. Clamping force distribution

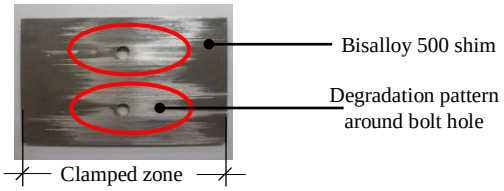

c. Degradation on sliding surfaces

Figure 7. Effective friction coefficient, clamping force distribution and sliding surface degradation

This sliding distance dependence of the effective friction coefficient is attributed to the degradation of the sliding surfaces, and also to the real distribution of the clamping force across the sliding distance. Variation of the effective friction coefficient shows that clamping forces are more heavily concentrated around the bolt hole and decrease as distance increases from the bolt hole (Fig. 7b). This clamping force distribution can be confirmed when observing a similar pattern on the degradation of the sliding surfaces as noted in Figure 7c. For practical applications a range of values of the effective friction coefficient requires to be defined, so that the strength of AFC braces can be quantified as function of the assembling force (proof load). This range can be defined as 0.16 – 0.20 according to Figure 7a , and by using the upper limit of this range variations of the clamping force can be ignored for design purposes.

6.4 Out of plane brace behaviour

Vertical deflections of AFC braces recorded from three extensometers placed along the brace span were plotted for the case where the AFC detail develops the full stroke (± 90mm) in compression and tension (Figs. 8a, b). For both AFC braces it can be seen that maximum deflections are presented at the AFC detail location, and at both sides of the AFC detail deflections reduce with distance towards the fixed or moving supports of the brace (Fig. 9). Maximum deflections are exhibited at the AFC detail location not only because the abrupt change in stiffness when comparing the flexural and axial stiffness of the channel with those of the slotted plate; but also because the load transferred from the slotted plate to the channel is eccentric, thus the brace is subjected to a moment that produces bending around of one of the principal axis of the brace (Fig. 9). Magnitude of this moment depends on the total clamping force used to assemble the connection, on the effective friction coefficient, and on the distance between centroids of the slotted plate section and the brace section. As a result of this bending moment, the non-clamped zones of the slotted plate and the brace bend, so that when the sliding mechanism is activated the slotted plate slides prying the shim close to the channel when in compression and the shim close to the cap plate when in tension. Prying forces may increase the magnitude of sliding forces; for that reason the post-yielding zone of the hysteresis loop is not perfectly flat as expected in friction devices (Figs. 6a,b). Out-of-plane behaviour of AFC braces cannot be avoided given eccentric nature of AFC details. However, these issues can be minimized by providing a stiff slotted member with minimum eccentricity from the brace section. When designing AFC braces care should be given on checking and matching the flexural and axial capacity of the brace and slotted members. A good design practice can be based on considering the member effective length factor as 2 for the slotted member (i.e. cantilever member), and of unity for the brace member.

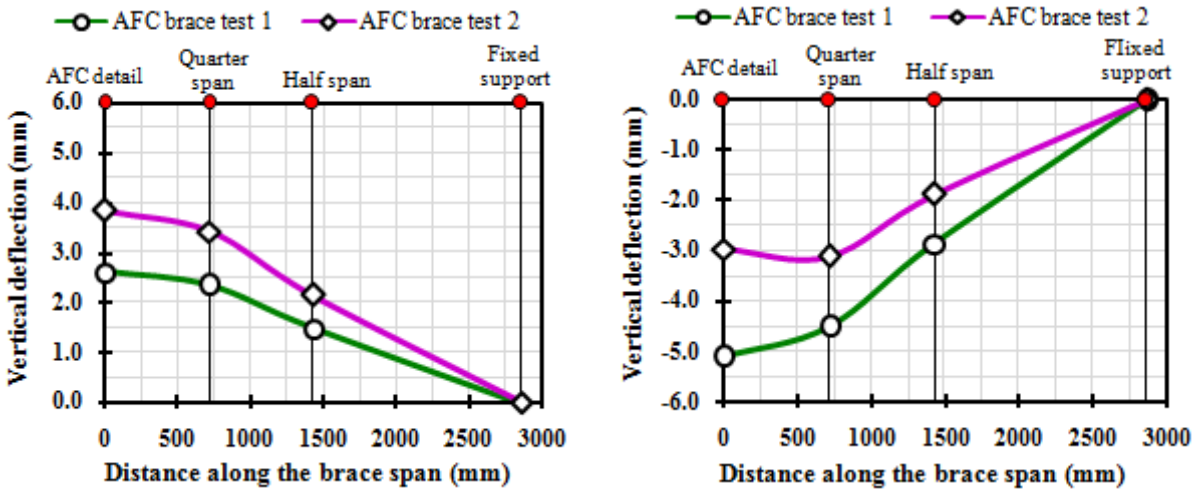

a. Vertical deflections of braces in tension for a sliding distance of 90mm

b. Vertical deflections of braces in compression for a sliding distance of 90mm

Figure 8. Vertical deflections in AFC braces in tension and compression

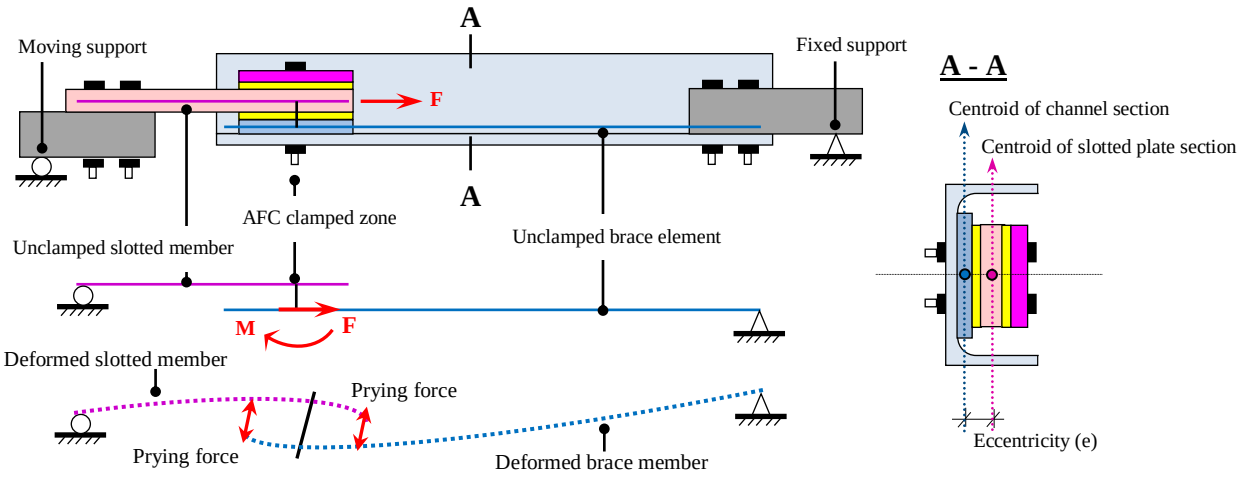

Figure 9. Vertical deflections and prying forces in AFC braces in compression

7 CONCLUSIONS

This paper describes the behaviour of AFC braces using Bisalloy 500 shims, it was shown that:

i) The hysteresis loop of AFC braces is approximately rectangular and stable. Sliding forces developed by AFC braces when in tension are different from those when in compression by 10%. This difference is attributed to prying forces developed as a result of the eccentricity between the slotted plate and the brace section.

ii) Strength degradation of AFC braces was estimated as 10%, for the case where no change of the AFC components or bolt re-tensioning was made after subjecting braces up to 40 cycles distributed across the full stroke of the connection. Reduction in strength is attributed to loss of bolt tension presented as sliding surfaces degrade. This was exacerbated by prying.

iii) The effective friction coefficient is variable with the sliding distance due to the distribution of the clamping force across the AFC detail. Effective friction coefficient ranged from 0.17 to 0.20.

iv) AFC braces underwent out-of-plane deflections as a result of bending moments generated in the load transfer mechanism from the slotted plate to the brace member. Maximum out-of-plane deflections occurred at the AFC location, causing prying forces that increase with slid.

REFERENCES:

Butterworth, J. W. (1999). Seismic Damage Limitation in Steel Frames Using Friction Energy Dissipators. *6th International Conference on Steel and Space Structures* - September 1-2. Singapore.

Chanchí, J.C., MacRae, G.A., Chase, J.G., Rodgers, G.W., Clifton, G.C, & Munoz, A. (2012). Design considerations for braced frames with asymmetrical friction connections (AFC). *STESSA 2012, Santiago de Chile*, January.

Chanchí, J.C., MacRae, G.A., Chase, J.G., Rodgers, G.W., & Clifton, G.C. (2011). Behaviour of Asymmetrical Friction Connections (AFC) using different shim materials. *NZSEE - annual conference.* New Zealand.

Grigorian, C.E. & Popov, E.P. (1994). *Experimental and Analytical Studies of Steel Connections and Energy Dissipaters. Report UCB/EERC-95/13, Engineering Research Center.* San Francisco (USA).

Clifton, G.C. (2005). Semi-Rigid Joints for Moments Resisting Steel Framed Seismic Resisting Systems. *Published PhD Thesis, Department of Civil and Environmental Engineering.* University of Auckland – New Zealand

MacRae, G. A. (2008). A New Look at Some Earthquake Engineering Concepts. M. J. *Nigel Priestley Symposium* Proceedings, IUSS Press, 2008.

MacRae, G.A., Clifton, C.G., MacKinven, H., Mago, N., Butterworth, J., Pampanin, S. (2010). *The Sliding Hinge Joint Moment Connection. Bulletin of the New Zealand Society for Earthquake Engineering.* Vol.43, No 3, September.

Appendix A.8

Methodology for Quantifying Seismic Sustainability of Steel Framed Structures

Appendix A.8

Methodology for Quantifying Seismic Sustainability of Steel Framed Structures

J. Chanchí Golondrino
University of Canterbury, New Zealand – National University of Colombia, Manizales - Colombia.

G.A. MacRae, J.G. Chase & G.W. Rodgers
University of Canterbury, New Zealand

C.G. Clifton
University of Auckland, New Zealand

ABSTRACT: Seismic sustainability is directly related with the capability of the system to survive against any severe seismic event without requiring major repair or replacement. This paper presents a qualitative methodology to assess the seismic sustainability of steel framed structural systems in terms of four parameters: drift damage, element replaceability, floor damage and permanent displacement. Results show that conventional framed systems such as moment resistant frames, concentrically and eccentrically braced frames are less sustainable than those framed systems equipped with devices for dissipating energy with almost no damage in the structure. Finally, conclusions and recommendations about future considerations on seismic sustainability of steel framed systems are presented in order to promote the adoption of this concept in design practice.

1 INTRODUCTION

The sustainability concept of structural systems is directly associated to environment, social and economic impacts resulting from any activity associated with construction, occupancy and maintenance processes developed during the lifespan of the system (ASCE 2005); in that sense, the role that the structural engineer plays on a sustainable design is not only specifying reusable materials, or an efficient structural system, but also choosing a level of acceptable damage that the structural system can undergo as a result of the likelihood of any major loading event (Hays and Cocke 2009).

According this definition it can be argued that the seismic sustainability of any structural system can be evaluated by predicting the expected level of damage of the structural system after a major earthquake. Application of this methodology over different structural systems requires the definition of a group of parameters influencing the level of damage. These parameters are termed damage indicators and they should be rated on a numerical scale using a rational understanding of the energy dissipation mechanism of the assessed structural system. The development of a simple methodology incorporating the general ideas described above will enable engineering practitioners to easily asses the seismic sustainability of any structural system and more importantly, to choose the most sustainable option.

It can be seen that it is important to develop a methodology to quantify the seismic sustainability of steel earthquake resistant structural systems. This paper does this by answering the following questions:

i) What are the most common steel framed systems and how do they behave inelastically due to earthquake?

ii) What are the main parameters that influence the seismic sustainability of steel framed systems?

iii) What is a simple rating system to assess the seismic sustainability of steel framed systems?

iv) What is the classification of the steel framed systems in terms of seismic sustainability?

v) What are some possible directions for future research on seismic sustainability of steel structures?

CLASSIFICATION OF SYSTEMS

In order to assess the seismic sustainability of the most common steel structural systems, they have been classified in three categories according the en-

ergy dissipation mechanism and the level of damage after a major earthquake.

1.1 *Traditional Systems*

This category comprises systems of conventional construction with or without different brace dispositions where the energy dissipation mechanism is based on yielding at specific locations.

1.1.1 *Moment Resisting Frames – MRF*

MRF systems consist of beams rigidly connected to columns as shown in Fig1a; their lateral resistance is developed from shear forces and bending moments in joints and members (Bruneau et al. 1998). The most desirable inelastic mechanism is associated with hinges at the beam ends and at the columns bases; structural and non-structural damage is expected as a consequence of the highly ductile performance.

1.1.2 *Eccentrically Braced Frames – EBF*

EBF systems consist of frames and braces non-concentrically placed so that generating a segment of beam termed link as shown in Fig 1b; their lateral resistance is developed by inelastic action in the links and elastic action on the surrounding frame (Chen & Scawthorn 2003). The inelastic mechanism is based on yielding of the link. As a result, significant structural damage is expected around the link zones.

1.1.3 *Concentrically Braced Frames – CBF*

CBF systems consist of frames and braces concentrically placed at each level of the frame as shown in Fig 1c; their lateral resistance is developed by axial forces and small flexural actions in whole members (Feeney & Clifton 1995). The inelastic mechanism is based on tension yielding and post buckling behaviour of braces; significant permanent displacements on braces and large inelastic rotations in connections are expected.

1.1.4 *Buckling Restrained Frames – BRB*

BRB systems consist of frames and braces assembled from a steel core placed inside of a tubular member that laterally supports the core as shown in Fig 1d; their lateral resistance is developed by inelastic action in braces and elastic action in beam and columns (Iwata et al 2000). The inelastic mechanism is based on yielding the braces in tension and compression; large permanent drifts are expected because the low post-yielding stiffness of the braces.

1.1.5 *Plate Shear Walls – PSW*

PSW systems consist of steel panels surrounded by beams and columns as shown in Fig 1e; lateral resistance is developed by generating a tension field in the steel panel after being subjected to an early shear buckling stage. (Dastfan & Driver 2009). The desirable inelastic mechanism is associated with yield of the panels and the development of hinges at beam ends columns bases (Berman & Bruneau 2003).

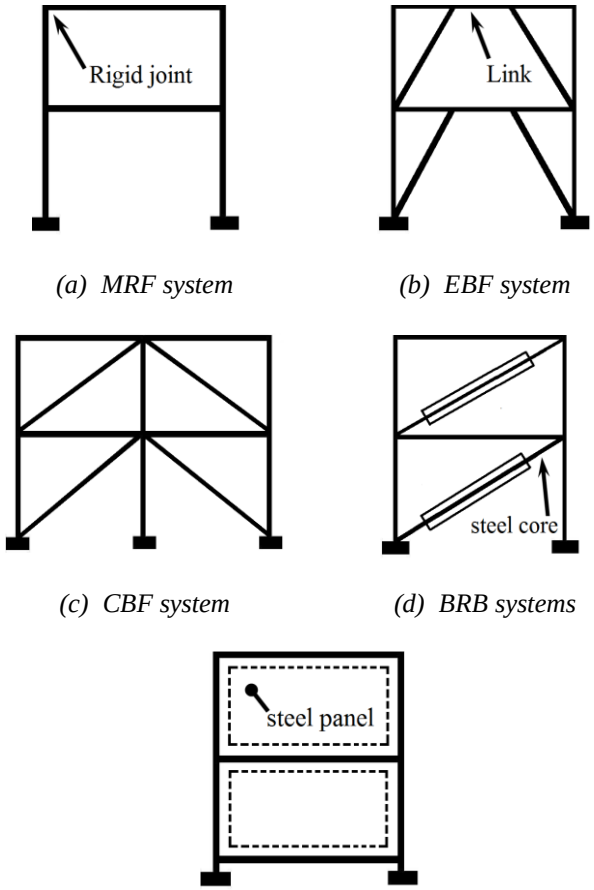

(a) MRF system *(b) EBF system*

(c) CBF system *(d) BRB systems*

(e) PSW system

Fig.1. Traditional steel systems

1.2 *Improved Joint and Element Systems*

This category comprises traditional systems where elements or joints have been modified to improve their seismic performance. The energy dissipation mechanism is mainly based on yielding components that can be easily replaced if any damage occurs.

1.2.1 *Reduced Beam Sections – RBS*

RBS systems consist of frames where beams have trimmed flanges in short segments away from the column faces as shown in Fig 2a. Their lateral resistance is developed in a similar way as moment resisting frames; however, a superior inelastic behaviour is expected (Chen et al 1996). The inelastic mechanism is based on forcing the formation of plastic hinges in the weakened segments of the beams. As a result, large inelastic rotations are expected.

1.2.2 *EBF with Replaceable Links – EBFRL*

These systems consist of EBF frames equipped with ductile and replaceable links placed within beams as shown in Fig 2b; their lateral resistance is developed in a similar way as eccentrically braced frames; however, a superior inelastic behaviour is expected (Mansour et al. 2006). The inelastic mechanism is based on yielding links through high shear forces, as a consequence high inelastic shear deformations and inelastic drifts are expected.

1.2.3 *Post – Tensioned Steel Frames – PTSF*

PTSF systems consist of MRF frames with beams and columns placed in contact by post-tensioned high-strength strands; additional bars at the beam-column connections are incorporated for energy dissipation purposes as shown in Fig 2c; their lateral resistances is developed through moment and shear forces in joints and members. Inelastic mechanism is based on yielding axially the energy dissipation bars after gap openings at the beam-column interfaces are activated (Christopoulos et al. 2002). Large inelastic deformations without any residual drift are expected.

1.2.4 *Rocking Frames – RF*

RF systems consist of CBF frames with post-tensioned strands lined with the columns and discontinuities at the column bases to allow columns uplifting at the foundation as shown in Fig 2d; their lateral resistance is based on developing a rocking mode that counteract seismic forces by the rotational inertia of the system (Sause et al. 2006). The inelastic mechanism is based on keeping frame member elastics and yielding the post-tensioned strands; no structural damage or residual drift are expected.

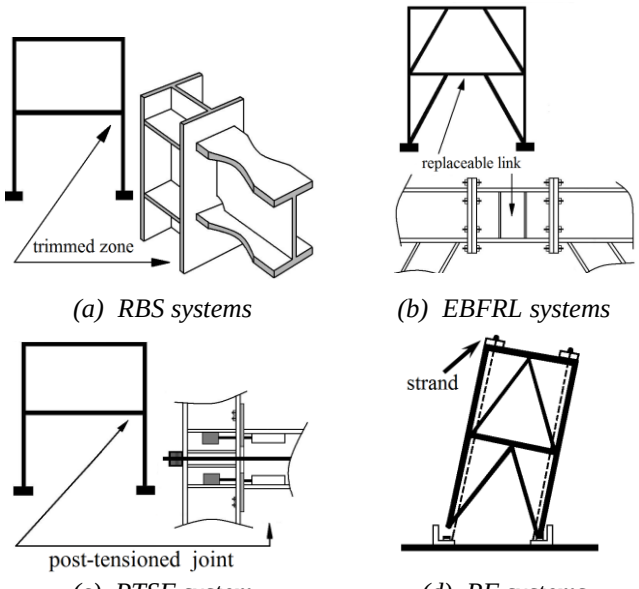

(a) RBS systems *(b) EBFRL systems*

(c) PTSF system *(d) RF systems*

Fig.2. Improved joint or element steel systems

1.3 *Low Damage Systems*

This category comprises traditional systems equipped with special devices that provide supplementary damping to the system. The energy dissipation mechanism is based on activating the devices at certain force level defined in such as way that the main structural members remain elastic and only minimal damage is expected in the structural system as well as in the devices.

1.3.1 *Lead Extrusion Dissipaters – HF2V*

These systems are based on MRF frames equipped with lead extrusion dissipaters – HF2V below the beam bottom flanges, gaps are provided at the beam-column interfaces and angle brackets to attach beams to columns as shown in Fig 3a. Their lateral resistance is developed through moment and shear forces in connections and frame members. The inelastic mechanism is based on activating the lead extrusion process in the HF2V device as the joint opens and closes (Mander 2009); thus providing energy dissipation and avoiding yielding of any frame member. Large drifts can be achieved without any structural damage.

1.3.2 *Sliding Hinge Joint Systems – SHJ*

These systems are based on MRF frames with asymmetrical friction connections details placed on the web and below the bottom flange of beams. Beams are placed away from columns by gaps and attached at the beam top flanges as shown in Fig 3b. Their lateral resistance is developed through moment and shear forces in connections and frame members. The inelastic mechanism is based on activating a friction mechanism as the beam column joint rotates (MacRae 2008). This dissipates energy and keeps frame members within elastic range. Only minor damage to the asymmetrical connection bolts are expected.

1.3.3 *Asymmetrical Friction Connections – AFC*

These systems are based on conventional braced frames with asymmetrical friction connections details placed within braces or below the beam bottom flange as shown in Fig 3c. Their lateral resistance is developed according the brace configuration of the system. The inelastic mechanism is based on activating the friction mechanism as the frame laterally deforms (MacRae and Clifton 2010). By sliding the asymmetrical friction detail frame members are maintained in the elastic range and protected from any yielding or buckling limit state. Large drifts can be achieved with only minor damage on the asymmetrical connection bolts.

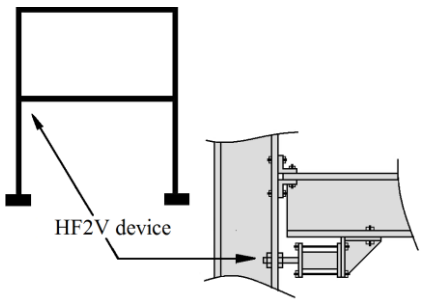

(a) HF2V systems

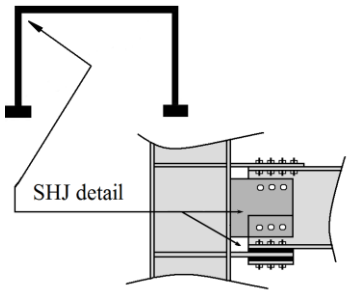

(b) SHJ systems

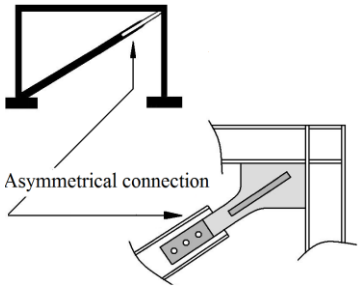

(c) AFC systems

Fig. 3 Free damage steel systems

2 DAMAGE INDICATORS

The seismic sustainability of steel framed structural systems is developed here from Chanchí et al (2010). Four parameters influencing the expected level of damage are considered. These parameters are termed damage indicators and can be used for assessing subjectively the likelihood of damage on the structural system as described below.

2.1 *Element Replaceability [ER]*

Conventional steel framed structural systems dissipate energy through yielding specific locations of one or several frame members. Although the structural system dissipates energy satisfactorily, the resulting structural damage can be difficult, time consuming and expensive to repair (Mander et al. 2009). Replaceable energy dissipating elements such as yielding, friction or other elements allow component replacement. The damage indicator for element replacebility *ER* was defined. To rate this indicator a numerical scale varying from 0 to 3 was defined, where 0 corresponds to systems with high likelihood of replacing damaged elements without major economic or time disruptions effects, and 1 corresponds to low or non likelihood of replacements without major economic or time disruption effects.

2.2 *Floor Damage [ER]*

During seismic excitations floor slabs systems of conventional steel framed systems may exhibit severe damage at the beam hinge zones given the deformation incompatibilities between the floor slab and frame beams (Sasikumar & Mitra 2009). Furthermore, inelastic action generates larger deformations on beam hinged zones causing the growth of beams; as a result major tensile stresses are presented on the floor slabs causing severe local damage (Umarani & MacRae 2007). This beam growth phenomenon not only occurs on conventional steel framed systems but also on improved joint or element systems; thus making them susceptible to produce severe floor damage (Umarani & MacRae 2007). For this reason implementation of damage free systems where the seismic incompatibilities between the floor slab and structural system are minimized are beneficial. To assess subjectively the likelihood of any floor damage level resulting from the seismic performance of the steel structural system the floor damage indicator *FD* was defined. This indicator is rated on a numerical scale varying from 0 to 2, where 0 corresponds to structural systems with no likelihood of floor damage especially those with damage free solutions, and 2 corresponds to structural systems with high likelihood of floor damage, especially those with beam growth effects.

2.3 *Drift Damage [DD]*

Energy dissipation mechanisms of conventional framed steel structural systems are based on providing horizontal displacement capacity through localized inelastic ductile action (Christopoulus et al 2008), as a result these structural systems undergo high inter-story drift levels during a major earthquake; thus generating high structural and non structural damage. In contrast, modern structural systems involving supplemental damping components such as friction, metallic yielding, or viscous – elastic devices are characterized by dissipating energy through the devices thus keeping the structural system in the elastic range (Pekcan et al. 1995) and consequently reducing the inter-story drift and damage level. In order to subjectively assess the level of damage generated on the structural system as a result of the inter-story drift demand, the damage indicator drift

damage *DD* was defined. A numerical scale varying from 0 to 3 was defined, where 0 corresponds to systems characterized by low drift demand such as those systems equipped with any damper, and 3 to systems with ductile inelastic response involving high drifts demands as those exhibited by conventional systems.

2.4 *Permanent Displacement [PD]*

After a major earthquake structural systems may be left with permanent displacements, which can make the system unusable, unsafe or difficult to repair (MacRae and Kawashima 1997). The magnitude of the permanent displacements depends on factors such as the intensity of the ground motion, structural characteristics and the characteristic hysteresis loop shape of the system (MacRae and Kawashima 1997). In that sense, aiming to assess subjectively the level of damage associated with the permanent displacements of any steel framed structural system, the damage indicator for permanent displacement *PD* was defined in terms of the three idealized hysteresis loops presented in Figure 4.

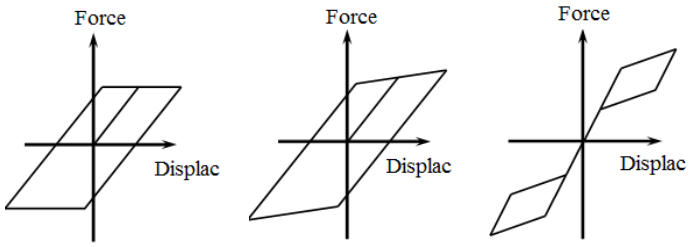

(a) Elasto - Plastic *(b) Bilinear* *(c) Flag Shaped*

Fig.4 Idealized hysteresis loops

Elasto - plastic loops represent systems where energy is dissipated through yielding frame members and large permanent displacements are expected, bilinear loops represent may represent conventional or improved systems with hysteresis loops with post-elastic stiffness and no major permanent displacements and flag shaped loops represent systems with improved joints or equipped with dampers characterized by self-centering properties and minimum permanent displacements. To rate this indicator a numerical scale varying from 0 to 2 was defined, where 0 corresponds to systems with flag shaped or minimum permanent displacements hysteresis loops and 2 to systems with elasto-plastic or large permanent displacement hysteresis loops.

3 QUANTIFICATION OF SUSTAINABILITY

Given that the seismic sustainability of any structural system is associated to the expected level of damage that the system will undergo after a major earthquake, the seismic sustainability can be found by rating subjectively the likelihood of any damage on each of the four damage indicators described above according their respective range, the addition across the four parameters is a numerical representation of the total expected damage on the structural system. Considering that each of damage indicators has similar influence on the total damage and assuming for simplicity that the relationship between damage and sustainability is linear, the seismic sustainability can be found through Equation 1.

$$Sustainability = 9 - \Sigma\,(damage\ indicator)_i \qquad (1)$$

To illustrate the application of Equation 1, the seismic sustainability of moment resisting frames MRF was assessed in Table 1. It can be seen that except for the floor damage indicator all the indicators were rated with maximum scores, therefore resulting with a high expected level of damage and a low sustainability value. This assessment can be explained considering that the system has a ductile behaviour based on yielding the beam ends, large lateral displacements, large inelastic drifts and severe damage on structural and non structural elements. For that reasons this system should not be considered as an economic alternative for seismic actives zones.

Table 1. Seismic sustainability assessment of MRF

Damage Indicator		Scale	Damage
Element Replaceability	*[ER]*	[0 - 2]	2
Floor Damage	*[FD]*	[0 - 2]	1
Drift Damage	*[DD]*	[0 - 3]	3
Permanent Displacement	*[PD]*	[0 - 2]	2
	Total Damage		8
	Sustainability		1

4 SUSTAINABILITY SUMMARY CHART

Following the methodology described above the seismic sustainability of the different steel framed structural system described in this paper was calculated as shown in Table 2, where *ER*, *FD*, *DD*, and *PD*, respectively are the damage indicators: element replaceability, floor damage, drift damage and permanent displacement. Using results from Table 2,

the structural systems were classified according seismic suitanability values as shown in Table 3.

Table 2. Seismic sustainability assessment of most common steel framed structural systems

CATEGORY	SUBCATEGORY	ER	FD	DD	PD	Damage	Sustainability
		[0 – 2]	[0 – 2]	[0 – 3]	[0 – 2]	[0 – 9]	[0 – 9]
Traditional Systems	Moment Resisting Frames – *MRF*	2	1	3	2	8	1
	Eccentrically Braced Frames – *EBF*	2	1	2	2	7	1
	Concentrically Braced Frames – *CBF*	2	0	2	2	6	3
	Buckling Restrained Frames – *BRB*	0	0	3	2	5	4
	Plate shear walls – *PSW*	1	1	2	1	5	4
Improved Joint or Element Systems	Reduced Beam Section – *RBS*	2	1	3	2	8	1
	EBF with replaceable link – *EBFRL*	0	1	2	1	4	5
	Post-Tensioned Steel Frames – *PTSF*	1	1	2	0	4	5
	Rocking Frames – *RF*	1	1	2	0	4	5
Damage Free Systems	Lead Extrusion Dissipators – *HF2V*	0	0	0	1	1	8
	Sliding Hinge Joint – *SHJ*	0	0	1	1	2	7
	Asymmetrical Friction Connections – *AFC*	0	0	1	1	2	7

Table 3. Classification of most common steel framed structural systems according seismic sustainability

Structural System	Lead Extrusion Dissipators Sliding Hinge Joint Asymmetrical Friction Connections	Buckling Restrained Frames Plate Shear Walls EBF- with Replaceable Link Post-Tensioned Steel Frames Rocking Frames	Moment Resisting Frames Eccentrically Braced Frames Concentrically Braced Frames Reduced Beam Section
Main Damage Indicator	DD, PD	FD, DD	ER,FD,DD,PD
Sustainability	High [6 – 9]	Medium [4 – 5]	Low [0 – 3]

5 DISCUSSION OF RESULTS

Considering results presented in Table 2, it is possible to regroup the assessed structural systems in three main categories.

The first category corresponds to highly sustainable systems with sustainability values ranging from 6 to 9. These structural systems are characterized for dynamical self centering properties, high possibility to replace elements, minor floor damage and their damage level is mainly influenced by the drift and permanent displacement indicators.

The second category comprises structural systems with seismic sustainability values ranging from 4 to 5, thus being considered as semi-sustainable systems. Their expected level of damage is mainly influenced by indicators such as drift and floor damage and their energy dissipation mechanism is based on generating damage at localized elements that can be replaced without incurring major cost.

The final category comprises the less sustainable structural systems with sustainability values ranging from 0 to 3. Structural systems in this category are characterized for ductile energy dissipation - mechanisms based on yielding elements that are difficult to replace, thus generating costly and disruptive repair or replacement processes. Their expected level of damage is influenced for medium of high scores on whole damage indicators. Table 3 presents the classification described above.

6 FUTURE RESEARCH DIRECTIONS

Further research and development should be made in two main directions. Firstly, on the development of a more objective and sophisticated methodology to assess seismic sustainability. Methods of this type, considering initial cost are being developed using loss-based methodology at the University of Canterbury. Secondly, improved techniques are required to improve seismic sustainability.

7 CONCLUSIONS

This paper presents a simple methodology to assess the seismic sustainability of steel framed systems. It was shown that:

i) Steel framed structural systems were classified in three categories: traditional systems, improved joint or element systems, and low damage systems. This classification is based on the energy dissipation mechanism and the level of damage that the structural systems can undergo after a major earthquake.

ii) The damage indicators used to quantify seismic sustainability were: element replaceability, floor damage, drift damage and permanent displacement.

iii) A qualitative methodology to assess the seismic sustainability of any steel framed structural system was proposed. This methodology is based on rating subjectively the expected level of damage on each of the damage indicators using numerical scales varying from 0 to 3. For simplicity, a linear relationship between sustainability and the total expected level of damage was considered.

iv) Steel framed structural systems were classified according their seismic sustainability values in three categories: highly sustainable, semi-sustainable and less sustainable systems.

v) Further research should develop a rigorous method to assess seismic sustainability. Also improved structural systems with high sustainabilities should be developed.

8 REFERENCES

American Society of Civil Engineers (2004). Sustainable Engineering Practices: An Introduction. *ASCE- Committee on Sustainability*. Reston, Virginia, United States of America.

Berman, J. and Bruneau, M. (2003). Plastic Analysis and Design of the Steel Plate Shear Walls. *Journal of Structural Engineering*, 129(11), 1448-1456.

Bruneau, M., Uang, C. M., and Whittaker, A. (1998). Ductile Design of Steel Structures. *McGraw-Hill*, New York, United States of America.

Chanchi, J., MacRae, G.A., Chase, J.G. and Clifton, C.G. (2010). Quantifying Seismic Sustainability of Steel Framed Structures. *Steel Structures Workshop – Research Directions and Priorities for Steel Structures.* Christchurch, New Zealand, April 13-14.

Chen, S. J., Chu, J.M. and Chou, Z.L. (1997). Dynamic Behaviour of Steel Frames with Beam Flanges Shaven around Connection. *Journal of Constructional Steel Research*, 42(1), 49 -70.

Chen, W.F., and Scawthorn, C. (2003). Earthquake Engineering Handbook. *CRC Press*. Boca Raton, Florida, United States of America.

Christopoulus, C., Filiatraut, A., Uang, C.M., and Folz, B. (2002). Posttensioned Energy Dissipating Connections for Moment- Resisting Steel Frames. *Journal of Structural Engineering*, 128(9), 1111-1920.

Christopoulus, C., Tremblay, R., Kim, H.J. and Lacerte. (2008). Self-Centering Energy Dissipative Bracing System for the Seismic Resistance of Structures: Development and Validation. *Journal of Structural Engineering*, 134(1), 96-107.

Dastfan, M., and Driver, R.G. (2009). Investigation on the Effect of Frame Member Connection Rigity on the behaviour of Steel Plate Shear Walls Systems. *Behaviour of steel structures in Seismic Areas, STESSA 2009*, Philadelphia, Pennsylvania, United States of America.

Feeney, M. J. and Clifton, G.C. (1995). Seismic Design Procedures for Steel Structures .*HERA Report R4-76*. First edition. New Zealand.

Hays, B., and Cocke, D. (2009). Missed Opportunities in Structural Sustainability. *Structure Magazine*, April 2009.

Iwata, M., Kato, T., and Wada, A. (2000). Buckling –restrained braces as Hysteretic Dampers" *Behaviour of steel structures in Seismic Areas, STESSA 2000*, Balkelma, Rotterdam.

MacRae, G. A., and Kawashima, K. (1997). Post-Earthquake Residual Displacement of Bilinear Oscillators. *Earthquake Engineering and Structural Dynamics.* 26(7), 701-716

MacRae, G. A. (2008). A New Look at Some Earthquake Engineering Concepts. M. J. *Nigel Priestley Symposium Proceedings*, IUSS Press, 2008.

MacRae, G.A & Clifton, G. C. (2010). New Technology Applications, Recent Developments and Research Directions for Seismic Steel Structures in New Zealand. *Submitted to ACEE journal.*

Mander T.J., Rodgers G.W., Chase J.G., Mander J.B., MacRae G. A. & Dhakal R. (2009). A Damage Avoidance Design Steel Beam-Column Moment Connection Using High-Force-To-Volume Dissipators. *Journal of Structural Engineering.* 135 (11), 1390 – 1397.

Mansour, N., Christopoulus, C., and Tremblay, R. (2006). Seismic Design of EBF Steel Frames using Replaceable Nonlinear Links. *Behaviour of steel structures in Seismic Areas, STESSA 2006*, Yokohama, Japan.

Pekcan, G., Mander, J. B., Eeri, M., and Chen, S. S. (1995). The Seismic Response of a 1:3 Scale Model R.C. Structure with Elastomeric Spring Dampers. *Earthquake Spectra*, 11(2), 249 – 267.

Sasikumar, R., and Mitra, D. C. (2009). Linear and Nonlinear Dynamic Response of Chevron Type EBF. *10th National Conference on Technological Trends (NCTT09)*, 6-7 November 2009.

Sauce, R., Ricles, J.M., Roke, D., Seo, C.Y., and Lee, K.S. (2006). Design of Self Centering Steel Concentrically Braced Frames. *4th International Conference on Earthquake Engineering*, Taipei, Taiwan, October 12-13.

Umarani, C. and MacRae, G. A. (2007). A New Concept for Consideration of Slab Effects on Building Seismic Performance. *Journal of Structural Engineering.* (34), 1, 25-32.

References

References for thesis introduction:

[1] Clifton, G.C. (2005). Semi-Rigid Joints for Moments Resisting Steel Framed Seismic Resisting Systems. *Published PhD Thesis, Department of Civil and Environmental Engineering.* University of Auckland – New Zealand.

[2] MacRae, G.A., Clifton, C.G., MacKinven, H., Mago, N., Butterworth, J., Pampanin, S. (2010). *The Sliding Hinge Joint Moment Connection*. Bulletin of the New Zealand Society for Earthquake Engineering. Vol 43, Issue 3, pp. 202-212.

[3] Khoo, H.H., Clifton, C., Butterworth, J., MacRae, G. and Ferguson, G. (2011). *Influence of steel shim hardness on the Sliding Hinge Joint.* Journal of Constructional Steel Research. Vol 72, May 2012, p 119 – 129. https://doi.org/10.1016/j.jcsr.2011.11.009

[4] Rodgers, GW, Chase, JG, Causse, R, Chanchi Golondrino, J and MacRae, GA (2017). *Performance and Degradation of Sliding Steel Friction Connections: Impact of Velocity, Corrosion Coating and Shim Material*. Engineering Structures, Vol. 141, pp. 292–302. ISSN: 0141-0296. https://doi.org/10.1016/j.engstruct.2017.02.070

[5] Khoo, H.H., Clifton, G.C., MacRae, G.A., Zhou, H., and Ramhormozian, S. (2014). *Proposed design models for the asymmetric friction connection*. Earthquake and Structural Dynamics Journal. Vol 44, Issue 8, p. 1309-1324. https://doi.org/10.1002/eqe.2520

[6] MacRae, G.A., and Clifton, C.G. (2015). *Research on Seismic Performance of Steel Structures*. Steel Innovation Conference. Auckland, New Zealand.

[7] Borzouie, J, Chase, JG, MacRae, GA and Rodgers, GW (2015). *Experimental Studies on Cyclic Performance of Column Base Weak Axis Aligned Asymmetric Friction Connection*. Journal of Constructional and Steel Research (JCSR), Vol 112, pp. 252-262. https://doi.org/10.1016/j.jcsr.2015.05.007

[8] Borzouie, J, Chase, J.G., MacRae, GA, Rodgers, GW and Clifton, C (2016). *Experimental Studies on Cyclic Performance of Column Base Strong Axis Aligned Asymmetric Friction Connections*. ASCE J. Structural Engineering, Vol 142(1), Article 04015078, 10-pages. https://doi.org/10.1061/(ASCE)ST.1943-541X.0001327

[9] Xie, R., Chanchi, J., MacRae, G.A., and Clifton, C.G. (2018). *Braced frame asymmetrical and asymmetrical friction connection performance*. Key Engineering Materials. Vol. 763, pp. 216 – 223. https://doi.org/10.4028/www.scientific.net/KEM.763.216

References for published or submitted journal papers in this thesis:

[10] Chanchí Golondrino, J.C., MacRae, G.A., Chase, J.G., Rodgers, G.W, Abu, A.K., Clifton, G.C. (2018). *Asymmetric friction connections post-heating behaviour.* Journal of Constructional Steel Research. Vol. 149, Oct. 2018, pp. 119 – 129. https://doi.org/10.1016/j.jcsr.2018.07.018

[11] Chanchí Golondrino, J.C., MacRae, G.A., Chase, J.G., Rodgers, G.W, Scott, A.C., Clifton, G.C. (2018). *Steel Building Friction Connection Seismic Performance – Corrosion Effects*. Structures – Research Journal of the Institution of Structural Engineers. Vol. 19, Jun. 2019, pp. 96 – 109. https://doi.org/10.1016/j.istruc.2018.11.008

[12] Chanchí Golondrino, J.C., MacRae, G.A., Chase, J.G., Rodgers, G.W, Clifton, G.C. (2018). *Hysteretic Behaviour of Asymmetric Friction Connections Using Brake Pads of D3923.* Structures – Research Journal of the Institution of Structural Engineers. Vol. 16, Nov. 2018, pp. 164 – 175. https://doi.org/10.1016/j.istruc.2018.09.012

[13] Chanchí Golondrino, J.C., MacRae, G.A., Chase, J.G., Rodgers, G.W, Clifton, G.C. (2018). *Asymmetric Friction Connection Bolt Lever Arm Effects on Hysteretic Behaviour.* Submitted to Journal of Earthquake Engineering.

[14] Chanchí Golondrino, J.C., MacRae, G.A., Chase, J.G., Rodgers, G.W, Clifton, G.C. (2018). *Asymmetric Friction Connection (AFC) design for seismic energy dissipation*. Journal of Constructional Steel Research - Elsevier. Vol. 157, Jun. 2019, pp. 70 – 81. https://doi.org/10.1016/j.jcsr.2019.02.027

References for published conference papers in this thesis:

[15] Chanchí Golondrino, J.C., MacRae, G.A., Chase, J.G., Rodgers, G.W, Clifton, G.C. (2012). *Behaviour of Asymmetrical Friction Connections using different shim materials.* New Zealand Society for Earthquake Engineering Conference - NZSEE 2012. Christchurch, New Zealand. 13- 15 April 2012.

[16] Chanchí Golondrino, J.C., MacRae, G.A., Chase, J.G., Rodgers, G.W, Clifton, G.C. (2012). *Clamping Force Effects on the Behaviour of Asymmetrical Friction Connections (AFC*). 15th World Conference on Earthquake Engineering - WCEE 2012. Lisbon, Portugal. 24-28 September 2012

[17] Chanchí Golondrino, J.C., MacRae, G.A., Chase, J.G., Rodgers, G.W, Clifton, G.C. (2015). *Velocity Effects on The Behaviour of Asymmetrical Friction Connections (AFC).* 8th International Conference on Behaviour of Steel Structures in Seismic Areas. Shanghai, China. 1-3 July 2015

[18] Chanchí Golondrino, J.C., MacRae, G.A., Chase, J.G., Rodgers, G.W, Clifton, G.C. (2015). *Is the Asymmetrical Friction Connection (AFC) a low damage dissipater?* New Zealand Society for Earthquake Engineering Conference - NZSEE 2015. Christchurch, New Zealand. 10 – 12 April 2015.

[19] Chanchí Golondrino, J.C., MacRae, G.A., Chase, J.G., Rodgers, G.W, Clifton, G.C. (2013). *Hysteretic Behaviour of Symmetrical Friction Connections (SFC) Using Different Steel Grade Shims.* The Pacific Structural Steel Conference - PSSC 2013. Singapore, 8 – 11 October 2013.

[20] Chanchí Golondrino, J.C., MacRae, G.A., Chase, J.G., Rodgers, G.W, Mora Muñoz, A., Clifton, G.C. (2012). *Design considerations for braced frames with asymmetrical friction connections – AFC.* Behaviour of Steel Structures in Seismic Areas - STESSA 2012. Santiago, Chile. 9 – 11 January 2012.

[21] Chanchí Golondrino, J.C., Xie, R., MacRae, G.A., Chase, J.G., Rodgers, Clifton, G.C. (2014). *Low Damage Braces using Asymmetrical Friction Connections (AFC)*. New

Zealand Society for Earthquake Engineering Conference - NZSEE 2014. Chistchurch, New Zealand. 21- 23 March 2014.

[22] Chanchí Golondrino, J.C., MacRae, G.A., Chase, J.G., Rodgers, G.W, Clifton, G.C. (2012). *Methodology for quantifying seismic sustainability of steel framed structures.* Behaviour of Steel Structures in Seismic Areas - STESSA 2012. Santiago, Chile. 9 – 11 January 2012.